RELATIVE ORIENTATION WITH LIMITED CONTROL IN CLOSE RANGE PHOTOGRAMMETRY

H. RÜTHER

Presented to the University of Cape Town
in fulfilment of the requirements for
the Degree of Doctor of Philosophy

Cape Town
1982

Thus problems, even practical problems, are always theoretical. Theories on the other hand can only be understood as tentative solutions of problems, and in relation to problem situations.

Karl Popper

ACKNOWLEDGMENTS

I have been most fortunate in the encouragement and advice I have received from Professor L.P. Adams of the Department of Surveying at the University of Cape Town who inspired this thesis through his interest and research in close-range photogrammetry.

I am also deeply indebted to Professor Benjamin Shmutter (Technion, Haifa) who, as a visiting lecturer at the University of Cape Town, gave me invaluable advice on some of the mathematical aspects of this thesis.

I am also most grateful to Dr Antony Hall-Martin of the National Parks Board of Trustees S.A. for his guidance in the work with elephants at close range and for his dedication to the elephant research project. I also wish to express my appreciation to S. le Brun for his design of the camera frame and for his help in the execution of the elephant photography. To Dr Ian Douglas-Hamilton (Kenya) I owe the inspiration to apply photogrammetry to shoulder height measurements of African elephants.

My colleague, Herman van Gysen, deserves special thanks for reading this thesis and helping me to overcome some of the problems I encountered in expressing my thoughts in a language the subtleties of which I have difficulty in mastering.

I thank Ruby MacDonald, Velma Vulliamy and Christine Langley on whom fell the burden of typing the text and in particular the complex equations. Credit is due to Alice Akhurst for drawing the numerous diagrams and to Sidney Smith for his assistance in the photographic laboratory.

Finally I should especially like to thank my wife, Lynn, for her understanding, patience and assistance during the time I spent completing this thesis.

August 1982 Heinz Rüther

ABSTRACT

In close-range photogrammetry, situations can arise in which it is difficult or impossible to establish a network of control points as required for a conventional absolute orientation procedure. The thesis investigates the replacement of the traditional control network by a few control distances measured between well-defined artificial markers or natural feature points. The measured distances must then serve to reduce deformations suffered by the photogrammetric model in the orientation procedures. All investigations are based on analytical rather than analogue photogrammetry.

After a review of the concepts of rotation matrices, least squares adjustment and the generation of synthetic image co-ordinate observations, the study is executed in three major steps.

A test field of high precision is established by means of space intersection and a camera calibration method for close-range cameras is developed which combines perspective projection with geodetic observations of the lens system parametres. Thus a problem inherent in many camera calibration methods, namely the exact determination of the perspective centre, is largely overcome.

Deformation characteristics related to error in elements of interior and relative orientation are determined by the controlled introduction of errors into these elements. The deformations are presented in tabular and diagrammetrical form. An analysis of the deformation leads to the conclusions of theoretical and practical relevance for close-range photogrammetry.

As a result of the deformation analysis mathematical models are introduced which utilise the measured distances for the reduction of model deformations. The efficiency of homogeneous scaling, affine scaling and convergency correction, as applied individually and in various combinations, is tested. A mathematical formulation of the converging correction as a restraining condition in a least squares adjustment is developed for this purpose. It is shown that a convergency error is less relevant to close-range photogrammetry than generally assumed and that characteristic model deformations in close-range photogrammetry have the character of affine scale errors.

Throughout the thesis algorithms are developed which make it possible to execute all computations on computers with limited memory capacity. A program sample for the relative orientation adjustment is given in Appendix IV to demonstrate the memory saving techniques.

Finally the results of the investigation are applied to the survey of shoulder height of African elephants in their natural habitat. Equipment and field work are described and results reported.

CONTENTS

	Page
ACKNOWLEDGMENTS	ii
ABSTRACT	iii
NOMENCLATURE	vii
1. INTRODUCTION AND PRINCIPLES OF THE INVESTIGATION	1
1.1 Introduction	1
1.2 Methods and principles of the investigation	5
2. OUTLINE OF THE STRUCTURE OF THE INVESTIGATION	9
3. MATHEMATICAL METHODS	12
3.1 Rotation matrices	13
3.2 Least squares adjustment	25
3.3 The synthetic photograph	33
3.4 Computer generated normally distributed random numbers	39
3.5 Space intersection	43
3.6 Transformation of observed plate co-ordinates to image co-ordinate system	54
4. EQUIPMENT	58
4.1 Tektronix 4050 mini computer system	58
4.2 Topocart stereo plotter Carl Zeiss Jena	60
4.3 Stereo comparator STEKO 1818	62
4.4 Universal measuring cameras UMK 10/1318	63
5. CLOSE-RANGE PRECISION TEST FIELD	68
6. PHOTOGRAMMETRIC ORIENTATION	77
6.1 The principle of photogrammetric orientation	77
6.2 Classification of mathematical models for analytical photogrammetric orientation	80
6.2.1 The "Grand" solution and reduced grand solution	81
6.2.2 Projective transformation	84
6.2.3 Double point space resection	86
6.2.4 Sequential solution	90

Page

7. INNER ORIENTATION AND RELATIVE ORIENTATION 93

7.1 Inner orientation 93

7.2 The historical development of relative orientation 104

7.3 Choice of mathematical model for relative orientation 113

7.4 The least squares model of relative orientation 117

7.5 The weight model of the relative orientation adjustment 128

7.6 Optimum number of image points for a relative orientation adjustment 130

7.7 Comparison of combined case and quasi-parametric case in the relative orientation adjustment 134

7.8 Model co-ordinates 136

7.9 Error theory of the relative orientation adjustment 144

7.9.1 Standard deviation of unit weight 144

7.9.2 Standard deviation a priori of an observation 145

7.9.3 Standard deviation of an unknown 145

7.9.4 Standard deviation of model co-ordinates 146

7.9.5 Standard deviation of a distance in model space 147

7.10 Convergency correction 148

7.11 Homogeneous and affine scaling 165

8. MODEL DEFORMATIONS 167

8.1 The principles of model deformations and a method of deformation analysis 167

8.2 Model deformations in normal oriented one-camera photogrammetry 171

8.3 Design of test cases for the analysis of model deformations and model control methods 176

8.4 Presentation of test results 184

8.5 Point configurations for deformation tests 195

8.6 Analysis of individual cases 197

8.7 Affine scales in model deformation 219

Page

8.8 Real photography tests 220

8.9 Summary of conclusions derived from the analysis of model deformations 227

9. OVERALL SUMMARY AND CONCLUSIONS 236

Fold-out Tables 8-1 to 8-4 240

10. THE PHOTOGRAMMETRIC MEASUREMENT OF SHOULDER HEIGHTS OF AFRICAN ELEPHANTS IN THEIR NATURAL HABITAT 247

10.1 The significance of shoulder height measurements in research on African elephant (Loxodonta africana) 247

10.2 Equipment 249

10.3 Field work 251

10.4 Evaluation of photographic images 257

10.5 Results 257

REFERENCES 261

APPENDICES 271

I Standard deviation of model co-ordinates 271

II Derivation of a condition equation for a measured control distance in object space 281

III Derivation of an algorithm for the incorporation of a control distance condition equation into the relative orientation adjustment 287

IV Program documentation: least squares adjustment of relative orientation 298

BASIC Program for least squares adjustment of relative orientation 308

NOMENCLATURE

$\underline{\ }$	small letters with an underbar represent vectors, capital letters matrices
', "	the symbol ' is associated with the left image of a stereographic pair, the symbol " with the right image
a_i	coefficients of observations in condition equation (first equation of system)
	also: transformation coefficient
a_{ij}	elements of rotation matrix
	also: coefficients of observations in adjustment of space intersection
A_a, A_b	coefficients of an unknown in a condition equation (first and second equation of system)
$\underline{A}$	matrix of coefficients of the unknowns
b	base length
b_i	coefficients of observations in condition equation (second equation of system)
b_{ij}	transformation coefficients for projective transformation
	also: coefficient for observations for space intersection
	also: elements of rotation matrix for right perspective centre
B_a, B_b	coefficients of an unknown in a condition equation (first and second equation of system)
$\underline{B}$	matrix of coefficients of observation
c_i	transformation coefficient
$\underline{D}$	auxiliary matrix used in derivations only
e_i	expected frequency in class i
$\underline{E}$	auxiliary matrix used in derivations only
f	degree of freedom
$\bar{f}$	principal distance
f_i	principal distance equivalent, rectified
$\underline{f}$	vector of the partial derivatives of a function with respect to the observations

$\underline{\bar{f}}$ vector of the partial derivatives of a function with respect to the unknowns

F represents the expression for an entire function to simplify derivations

h_{ij} elevation angle from point P_i to point P_j

$\underline{I}$ identity matrix

k counter, indicating number of summations in the generating of normally distributed random variables

also: number of classes (χ^2 test)

$\underline{k}$ vector of Lagrange multipliers

ℓ observed quantity

$\underline{\ell}$ vector of discrepancies between provisional and observed values in the parametric case

ℓ_{ij} length of the vector between theodolite and space point in the space intersection adjustment

n number of observations

o_i actual frequency of computer generated observations in class i

P weight of an observation

$\underline{P}$ weight matrix

P_a weight of observation pertaining to the first observation equation in (3.2.1) and subsequent equations

P* quasi-weight

$\underline{P}^*$ quasi-weight matrix

P.P. principal point

P.D. principal distance

P.C. perspective centre

Q_{FF} weight coefficient of a function of unknowns and/or observations

Q_{xx} element of variance matrix pertaining to unknown x

$\underline{Q}$ variance matrix

r number of condition equations

r_i coefficients of observations in condition equation (last equation of system)

r_i also: uniformly distributed random values

r_{ij} elements of rotation matrix

$\underline{R}$ general rotation matrix

$\underline{R}_{x,\alpha}$ rotation matrix describing a single rotation by an angle α about the x axis

$\underline{R}_x$ rotation matrix describing a single rotation about the x axis

s_i normally distributed random values

s_i' first approximation for s_i

u number of unknowns

v_i corrections to observations

$\underline{v}$ vector of corrections

V_i^* quasi-corrections

$\underline{V}^*$ vector of quasi-corrections

w_a discrepancy term in condition equation

$\underline{w}$ discrepancy vector

$\underline{x}$ vector of unknowns

$\bar{x}$ mean value of a sample

$\bar{x}_o, \bar{y}_o$ principal point co-ordinates

$\bar{\bar{x}}_i, \bar{\bar{y}}_i$ image point and fiducial mark co-ordinates in comparator system

$\bar{\bar{x}}_o, \bar{\bar{y}}_o$ principal point position in comparator system

$\bar{x}_i, \bar{y}_i, \bar{f}=\bar{z}$ image (or plate) co-ordinates and principal distance

$\bar{x}_i^*, \bar{y}_i^*, \bar{f}_i^*$ corrected image co-ordinates and principal distance

X_i, Y_i, Z_i model co-ordinates

also: co-ordinates of test field points

X_o, Y_o, Z_o perspective centre position in terms of model co-ordinates

also: perspective centre position in test field co-ordinates

α,β,γ	general rotation angles
α_{ij}	horizontal direction from point P_i to point P_j
δ	orientation unknown
$\delta x,\delta y$	deviation of principal point from the position indicated by the fiducial marks
$\varkappa,\bar{\varkappa}$	rotation angle about z axis
$\varphi,\bar{\varphi}$	rotation angle about y axis
$\omega,\bar{\omega}$	rotation angle about x axis
λ	scale factor
ξ	mean value of distribution
σ	standard deviation
σ^2	variance
σ_0	standard deviation of unit weight
σ_i	standard deviation of an observation a priori
σ_x	standard deviation of an unknown
σ_F	standard deviation of a function of unknowns and/or observations
Φ	represents the expression for an entire function to simplify derivations

1. INTRODUCTION AND PRINCIPLES OF THE INVESTIGATION

1.1 INTRODUCTION

Photogrammetry is generally associated with the mapping of topographical features using cameras mounted either on airborne platforms or on the ground. These two applications, normally referred to as aerial and terrestrial photogrammetry respectively can also be classified as long-range and medium-range photogrammetry. At the turn of the century, another field of application emerged with the introduction of architectural photogrammetry at close-range (Meydenbauer 1894). Subsequently, close-range photogrammetry as a measuring or mapping tool has found its way into a wide range of disciplines and today there is hardly any scientific discipline in which an attempt has not been made to obtain necessary metric information from photographs.

The range of applications of close-range photogrammetry is so vast that only a brief cross section can be given here:

The proceedings of the first International Symposium on Photogrammetric Surveys of Monuments and Sites, Athen (Badekas, 1974) reflects the worldwide application of close-range photogrammetry to historical sites and archaeological monuments. Scogings (1978) reports a further application to archaeology in the very-close-range mapping of petroglyphs resulting in a 0,5 mm contour map.

In a combination of zoology and engineering, Adams (1980) mapped the beak of a Shoebill for subsequent structural analysis and a large range of biological and medical uses of photogrammetry are reported by Herron (1972). Höhler (1971) and McNeil (1969) describe the survey

of underwater objects and application to shipbuilding are discussed by Kenefik (1977), Oshima (1976) and Newton (1974 and 1975). Purely analytical methods are employed in the monitoring of particle tracks in bubble chambers by Garfield (1964) and in the real time digital processing of single camera data for the simulated retrieval and deployment of payloads by the NASA orbital Space Shuttle (Kratky 1979).

Deformation surveys were carried out by Danphin and Torlegård (1977) and by Erlandson and Veress (1975). Abdel-Aziz reports the application of photogrammetric techniques without photographs to building constructions (1979). In geology and geomorphology, Münzer (1979) uses close-range photography to survey geological objects in alpine areas and Collins and Moon (1979) monitor stream bank erosion.

An example for industrial applications is Singh's (1971) paper on "Welding Defects", Shmutter's and Etrog's calibration of storage tanks (1971), and Faig's (1971) work on "Shapes of Thin Soap Membranes". The use of non-metric cameras and movie cameras in close-range applications is of special interest for the non-photogrammetrist and numerous publications recognize the importance of non-metric equipment in close-range photogrammetry (for example, van Wijk and Ziemann (1976), Kölbl (1976), Abdel-Aziz and H. Karara (1974), Adams (1978), Welch and Dikkers (1978), Renner (1977) and Beattie and Lozowski (1976).

Reviews of the field of close-range photogrammetry are given by Torlegård (1976) in a paper to the XIII Congress of the International Society

of Photogrammetry and in two books "Handbook of Non-Topographical Photogrammetry" (Karara, 1979) and "Development in Close-Range Photogrammetry-1" (Atkinson 1980). Both analogue and analytical methods are employed in close-range photogrammetry. The literature survey revealed a tendency in later publications to move away from sophisticated analogue instrumentation, whenever possible, in favour of analytical equipment in the form of stereo comparators, digitisers and electronic computers, which do not require highly skilled operators once a routine has been established and a computer program is provided.

In the analytical approach a variety of traditional and newly developed relative and absolute orientation models (discussed in Chapter 6) as well as the projective transformation are employed. It is characteristic for these techniques, that they rely on a three-dimensional control network comprising of premarked and geodetically surveyed control points for the restitution of an object in space.

Besides these mathematically rigorous or near-rigorous methods there is a second group of techniques, frequently employed by the photogrammetrically inexperienced scientist of non-technical disciplines. These ad hoc methods are generally based on simple perspective projection theories often neglecting fundamental photogrammetric concepts, such as model deformations and image distortions. In these cases the potential of photogrammetry is not fully realised and inferior accuracies are accepted.

An extreme but characteristic example for this category is the standard archaeological recording technique in which a scale is

placed close to the object and dimensions are derived from a single photograph. A similar method is applied by Groze (1972) for the determination of body dimensions of elephants. However, often the "ad hoc" solution is the only possible technique, - even if more sophisticated methods and equipment are at hand, - when control points in the conventional sense cannot be established or when field conditions prohibit the use of complex equipment.

The writer encountered such a situation when he was asked to determine, with an accuracy of a few centimetres, the shoulder height of wild African elephants in their natural habitat. During field experiments it soon became obvious that the elephants could not be photographed within the confines of a previously surveyed control point network. Postmarking and fixing of control points was rejected as impractical and established control methods could not therefore be employed.

On the other hand, make-shift solutions, which had previously been developed and successfully employed by zoologists (Douglas-Hamilton 1972, Groze 1972) had to be rejected as they could not guarantee the required accuracies.

It would seem, therefore, that there is a need to bridge the gap between the traditional photogrammetric approach and the ad hoc methods by developing a method for situations in which environmental and other restrictions prohibit the theoretically desirable method whilst the alternative ad hoc technique is not sufficiently accurate.

This need gave rise to the concept investigated in this study, namely, to replace, where necessary, the three-dimensional control network by control distances measured between natural feature points and to develop a simple mathematical model for the effective incorporation of such distances into the photogrammetric restitution of an object.

1.2 METHODS AND PRINCIPLES OF THE INVESTIGATION

To achieve the objective of replacing the conventional three-dimensional control network in the photogrammetric restitution of objects with individual measured distances the following fundamental problems must be considered:

i) an interior orientation method needs to be determined for the calibration of metric and non-metric close-range cameras (Chapter 7.1),

ii) a suitable relative orientation method must be chosen and working formulae for the least squares adjustment and the error analysis must be derived (Chapters 7.2 to 7.9),

iii) model deformation characteristics arising in the relative orientation in close-range application need to be analysed (Chapter 8),

iv) simple mathematical models relying on control distances for the reduction of model deformations caused by errors in elements of interior and relative orientation, must be derived (Chapter 7.10 and 7.11).

Two concepts for the reduction of model deformations emerge from preliminary investigations. Firstly we can postulate the hypothesis that a convergency error (that is an equal and unlike error in φ) plays a major roll in model deformations encountered in close-range photogrammetry (Adams 1978, Granshaw 1979). In this case a convergency correction model must be derived preferably as a restraining condition in the relative orientation (Chapter 7.10). As an alternative one can attempt to reduce model deformations by closely following the concept of the absolute orientation in which the model is scaled to fit some known object dimensions. This scaling can either be uniform for the entire model or affine with different scale factors in the three axis directions of the orthogonal model co-ordinate system (Chapter 7.11).

In a combination of scaling and convergency correction the model can first be scaled using some of the control distances in X and Y model co-ordinate direction and subsequently convergency correction can be applied on the basis of a control distance in Z direction.

v) The suggested model control methods must then be tested in order to judge their efficiency and to obtain an estimate for the accuracies which can be expected when only limited control in form of distances is available. The limitations of the methods must be established.

At the outset of the investigation a decision had to be made regarding the principle to be adopted for the mathematical treatment of the problem in hand.

The writer endeavoured to find a middle course combining the theoretical approach of the "least squares purist" with the more pragmatic concepts of many practising photogrammetrists. Whilst the principles of the least squares adjustment theory were adhered to throughout the investigation, concessions to the pragmatist were made wherever possible.

The analytical as opposed to the analogue solution of the close-range problem was adopted. This has the dual advantage of, firstly, eliminating the need for complex analogue equipment and a highly skilled stereo plotter operator, thus making close-range photogrammetry acceptable to the non-photogrammetrist, and, secondly, permitting a systematic numerical assessment of the methods employed.

For the analytical solutions a desk-top or mini computer was chosen in preference to a main frame computer. In non-technical disciplines especially the mini computer has an advantage over the main frame computer as it is generally more easily available and less difficult to master. The obvious disadvantage of this choice is the loss in computation speed and, more important, the critical reduction in memory space. Special memory saving algorithms have therefore been developed in this study in the interest of the application of close-range photogrammetry in non-technical disciplines. (The computer program in Appendix IV was designed in accordance with this concept). Such algorithms are derived in Appendix I for the equation of the standard deviations of model co-ordinates and in Appendix III for the incorporation of additional control-distance-conditions into the relative orientation adjustment. For the same reason the quasi-

parametric adjustment technique (Chapter 7.4) was chosen for the adjustment of the relative orientation.

For the interior orientation and for the testing of model control methods a laboratory test field (Chapter 4.4) was established. Formulae for three dimensional space intersection are derived (Chapter 3.5) in order to guarantee the precise geodectic determination of the three dimensional test field co-ordinates. The model deformation analysis (Chapter 8) is based on synthetic photography (Chapter 3.3) to permit the controlled introduction of errors. Normal distributed random values (Chapter 3.4) are generated to simulate observation errors for the synthetic photography.

2. OUTLINE OF THE STRUCTURE OF THE INVESTIGATION

To summarise, the objectives at the study were realised by structuring the investigation into the following steps:

2.1 Mathematical groundwork is carried out consisting of a review of the concepts of least squares adjustment and rotation matrices. Computer generated "synthetic photography" of a simulated test field and a set of normal distributed random variables to simulate observation errors are created.

2.2 Suitable equipment in the form of metric cameras, stereo comparators and a computer system is selected and, where necessary, calibration methods are suggested.

2.3 A laboratory test field is established and a precise geodetic method of three-dimensional point determination is developed to define the position of the test field points.

2.4 The photogrammetric orientation, consisting of interior, relative and absolute orientation is analysed in its historical and logical development.

2.5 An interior orientation method is developed.

2.6 Relative orientation is identified as one of the fundamental problems of the investigation and the numerous solution methods available for the relative orientation are studied in their historical context.

2.7 The co-planarity formulation of the relative orientation problem is chosen as a suitable method for the determination of model co-ordinates.

2.8 Deformations of the model space encountered in the relative orientation are investigated in detail. The deformation analysis is based on a sequence of test cases in which errors in the various parameters of the orientation process are simulated. This test sequence is then extended to include a number of cases of real test field photography with metric and non-metric cameras.

2.9 The conventional absolute orientation technique cannot be employed as a model control method because of its need for a three-dimensional network of control points. In its place a few distances measured in the field after completion of the photography are introduced as a means of reducing possible model deformations.

2.10 Concepts in which the measured control distance can be utilised for the reduction of model deformations are investigated. Possible methods are:

(i) homogeneous and affine scaling

(ii) convergency correction

(iii) scaling with subsequent convergency correction

A general analytical convergency error correction method is derived and a special algorithm developed whereby the convergency correction can be applied in mini-computer calculations.

2.11 A set of practical recommendations for the application of close-range photogrammetry to situations with limited control is derived as a result of the investigation.

2.12 The conclusions of the study are finally tested in an application to the survey of shoulder heights of African elephants in their natural habitat.

3. MATHEMATICAL METHODS

In the course of this thesis, it becomes necessary to employ a number of mathematical techniques which are well known in principle. In the following chapter these techniques are described, relevant equations are quoted and, when necessary, formulae are derived for specific applications. Discussed are:

3.1 Rotation Matrices

Rotation matrices are required in this context for the interior and relative orientation adjustment and for the three dimensional transformations used for the deformation analysis in Chapter 8.

3.2 Least Squares Adjustment

Throughout this thesis least squares adjustments in various forms are applied wherever redundant observations are available. Working formulae are derived for the standard cases of the combined adjustment, the condition equation case and the parametric case as well as the quasi-parametric case, which is somewhat neglected in the literature.

3.3 The Synthetic Photograph

For the testing of the interior and relative orientation models and for the analysis of model deformations an error free synthetic photograph without image distortions is introduced in the form of computer generated image co-ordinates.

3.4 Computer Generated Normally Distributed Random Numbers

The tests on synthetic photographs were extended to synthetic images with simulated image point observation errors; such errors had to be "manufactured" . A technique is described which makes it possible to generate normally distributed random values on a computer, thus simulating observation errors of a known standard deviation.

3.5 Space Intersection

A synthetic image alone does not suffice to investigate the efficiency of the mathematical model of the relative orientation and, to analyse photogrammetric model deformation, the establishment of a laboratory test field was considered essential. The geodetic survey of point positions was based on a three dimensional space intersection procedure which is described.

3.6 Transformation of Observed Plate Co-ordinates to Image Co-ordinate System

Before plate co-ordinates, which have been observed on a comparator, can be introduced into a relative orientation calculation they have to be reduced to the principal point. Formulae are derived for this transformation to the fiducial mark system, which represents the image co-ordinate system.

3.1 Rotation Matrices

Rotations from one co-ordinate system into another system with a different orientation in space play an important role in the mathematical treatment of photogrammetric problems. Such

rotations can be achieved with the aid of a rotation matrix $\underline{R}$, which transforms a $\bar{x},\bar{y},\bar{z}$ co-ordinate system into a x,y,z system with a different orientation.

The transformation can then be formulated as:

$$\underline{x} = \underline{R}\,\underline{\bar{x}} \qquad (3.1.1)$$

in which $\underline{R}$ is defined as

$$\underline{R} = \begin{bmatrix} r_{11} & r_{12} & r_{13} \\ r_{21} & r_{22} & r_{23} \\ r_{31} & r_{32} & r_{33} \end{bmatrix} \qquad (3.1.2)$$

$\underline{R}$ is an orthogonal matrix and the typical elements r_{ij} of the matrix must therefore satisfy the condition:

$$\sum_{j=1}^{3} r_{ij}\, r_{kj} = \begin{cases} 0 \text{ for } i \neq k \\ 1 \text{ for } i = k \end{cases} \qquad i,k = 1,2,3 \qquad (3.1.3)$$

Rotation matrices are well-known from analytical geometry and the choice of such a matrix for (3.1.1) might at first sight seem a trivial task. An inspection of the relevant photogrammetric literature, however, reveals the complexity of the problem. A wide variety of rotation matrices is suggested for close-range photogrammetry alone (Gruber (1930), Jordan-Eggert-Kneissl (1972), Manual of Photogrammetry (1965), Adamec (1974), Erlandson and Veress (1975)).

Differences in the various rotation matrices originate in the choice of left- or right-handed systems for image and model co-ordinates, in differences in the directions in which orientations are considered as increasing and in the adopted sequence of rotations. A discussion of the concept of rotation matrices and

their application in close-range photogrammetry is therefore appropriate.

In their general form rotation matrices describing rotations about x y and z axes of a right-handed orthogonal co-ordinate system are:

a. rotation α about x-axis

$$\underline{R}_{x,\alpha} = \begin{bmatrix} 1 & 0 & 0 \\ 0 & \cos\alpha & -\sin\alpha \\ 0 & \sin\alpha & \cos\alpha \end{bmatrix} \quad (3.1.4)$$

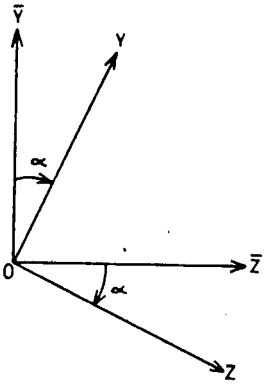

Fig. 3.1-1

b. rotation β about y-axis

$$\underline{R}_{y,\beta} = \begin{bmatrix} \cos\beta & 0 & \sin\beta \\ 0 & 1 & 0 \\ -\sin\beta & 0 & \cos\beta \end{bmatrix} \quad (3.1.5)$$

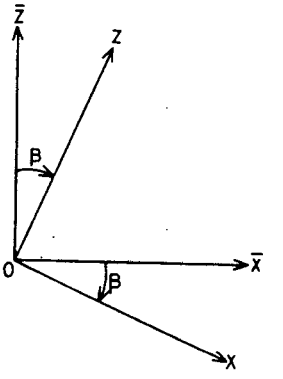

Fig. 3.1-2

c. rotation γ about z-axis

$$\underline{R}_{z,\gamma} = \begin{bmatrix} \cos\gamma & -\sin\gamma & 0 \\ \sin\gamma & \cos\gamma & 0 \\ 0 & 0 & 1 \end{bmatrix} \quad (3.1.6)$$

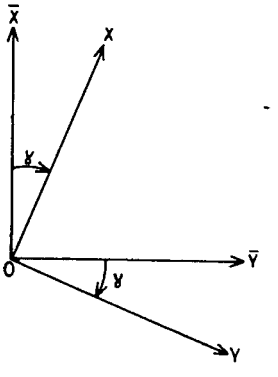

Fig. 3.1-3

The rotations are counted positive in clockwise direction as viewed from the origin of the co-ordinate system in positive axis direction:

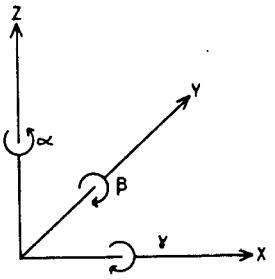

Fig. 3.1-4

In most cases a single rotation about any one axis does not suffice to transform one co-ordinate system into another system and sequential rotations about all three axes are normally necessary. One has to differentiate between a situation in which the co-ordinate axes remain fixed in space with co-ordinated points being rotated about the axes and a situation in which axes are displaced with the co-ordinated points in fixed positions. If, for example, a rotation sequence is chosen in which the primary, secondary and tertiary rotations take place about x, y and z axis respectively we get for matrix $\underline{R}$ in case of rotation about fixed axes:

$$\underline{R} = \underline{R}_z \, \underline{R}_y \, \underline{R}_x \,. \qquad (3.1.7)$$

If the axes are displaced by each rotation the sequence of matrix multiplication is inverted.

$$\underline{R} = \underline{R}_x \, \underline{R}_y \, \underline{R}_z \qquad (3.1.8)$$

In principle the transformation from one co-ordinate system into another system can be achieved by any arbitrary permutation of the rotation sequences (Thompson 1969, p. 138); equation (3.1.1) can

be satisfied by any rotation sequence and merely the magnitude of the three rotation angles will vary with the chosen permutation. For a purely analytical transformation it is therefore not necessary to think in terms of rotation axes.

The situation changes when rotations about actual mechanical axes are to be mathematically described by a rotation matrix $\underline{R}$. In this case the sequence of the rotations must follow the actual rotation order about the mechanical axes. Such a situation arises for example in cases where the results of an analytical relative orientation are to be applied to the settings of a stereo plotter. Here the design of the instrument must be analysed when formulating a rotation matrix for use with the instrument. In a descriptive definition one can say: A rotation about the primary axis changes the orientation in space of secondary and tertiary axes, whilst the primary axis itself remains in position. A rotation about the secondary axis changes only the orientation of the tertiary axis and a rotation about the tertiary axis does not affect any of the three axis orientations. This can best be visualised for a metric camera, which is mounted like a theodolite. Here we have, in terms of the model co-ordinate system using the conventional symbols φ, ω and $\varkappa$ for rotation angles:

Primary axis : y Rotation angle: $\overline{\varphi}$ (equivalent to vertical axis and horizontal angle of the theodolite)

Secondary axis: x Rotation angle: $\overline{\omega}$ (equivalent to trunnion axis and elevation angle)

Tertiary axis : z Rotation angle: $\overline{\varkappa}$ (equivalent to collimation axis and obliquity of cross hair)

When mathematically describing the rotations of a photogrammetric close-range camera with theodolite mounting one has therefore a rotation about fixed axes of the form:

$$\underline{R} = \underline{R}_{y,\bar{\varphi}}\ \underline{R}_{x,\bar{\omega}}\ \underline{R}_{z,\bar{\kappa}} \qquad (3.1.9)$$

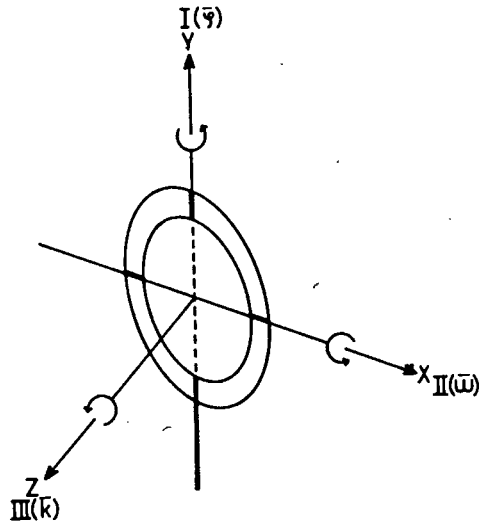

Fig. 3.1-5 Rotation axes of close-range camera in theodolite mounting

The elements of $\underline{R}$ are:

$$\begin{aligned}
r_{11} &= \cos\bar{\varphi}\cos\bar{\kappa} + \sin\bar{\varphi}\sin\bar{\omega}\sin\bar{\kappa} \\
r_{12} &= -\cos\bar{\varphi}\sin\bar{\kappa} + \sin\bar{\varphi}\sin\bar{\omega}\cos\bar{\kappa} \\
r_{13} &= \sin\bar{\varphi}\cos\bar{\omega} \\
r_{21} &= \cos\bar{\omega}\sin\bar{\kappa} \\
r_{22} &= \cos\bar{\omega}\cos\bar{\kappa} \\
r_{23} &= -\sin\bar{\omega} \\
r_{31} &= -\sin\bar{\varphi}\cos\bar{\kappa} + \cos\bar{\varphi}\sin\bar{\omega}\sin\bar{\kappa} \\
r_{32} &= \sin\bar{\varphi}\sin\bar{\kappa} + \cos\bar{\varphi}\sin\bar{\omega}\cos\bar{\kappa} \\
r_{33} &= \cos\bar{\varphi}\cos\bar{\omega}
\end{aligned} \qquad (3.1.10)$$

A possible application of matrix $\underline{R}$ is the space resection in which the true orientation of the camera forms part of the solution. The rotation sequence in a photogrammetric plotting instrument on the other hand varies with the design of the instrument (ZEISS instruments for example are based on a rotation sequence of φ, ω, κ while WILD instruments have a rotation order of ω, φ, κ). A rotation matrix of the corresponding sequence must subsequently be introduced if orientation angles for a specific instrument are to be evaluated.

It is unfortunate that no unique convention exists defining axis system and rotation direction and sequence for close range photogrammetry and it is difficult to find any two publications to agree on the choice of the rotation matrix.

No attempt is made in this thesis to follow any mechanical rotation sequence, since the approach is entirely analytical and orientation angles serve merely as auxiliary values in the determination of model co-ordinates. However, if considered necessary, transformation from one rotation sequence to any other sequence can easily be achieved once a matrix $\underline{R}$ in equation (3.1.1) is known, as will be shown later in this section (equations 3.1.20 to 3.1.25).

The writer has for some time used a rotation matrix, which differs from (3.1.10), and this matrix was employed instead of (3.1.10) for the relative orientation adjustment in this study:

Primary axis : x	Rotation angle: ω	Rotation sense: clockwise
Secondary axis: y	Rotation angle: φ	Rotation sense: clockwise
Tertiary axis: z	Rotation angle: $\varkappa$	Rotation sense: counter-clockwise

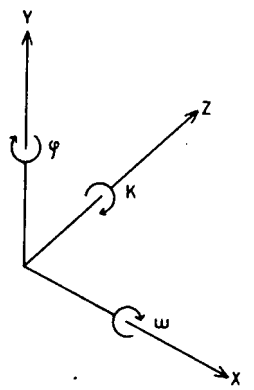

Fig. 3.1-6 Rotation axes and angles adopted for relative orientation

The rotations are based on displaced axes in a left-handed system and hence with (3.1.8)

$$\underline{R} = \underline{R}_{x,\omega}\ \underline{R}_{y,\varphi}\ \underline{R}_{z,\varkappa} \qquad (3.1.11)$$

if we introduce (3.1.11) into (3.1.1)

$$\underline{x} = \underline{R}_{x,\omega}\ \underline{R}_{y,\varphi}\ \underline{R}_{z,\varkappa} \qquad (3.1.12)$$

The elements of $\underline{R}$ are now

$r_{11} = \cos\varphi \cos\varkappa$

$r_{12} = -\cos\varphi \sin\varkappa$

$r_{13} = -\sin\varphi$

$$
\begin{aligned}
r_{21} &= \cos\omega \sin\varkappa + \sin\omega \sin\varphi \cos\varkappa \\
r_{22} &= \cos\omega \cos\varkappa - \sin\omega \sin\varphi \sin\varkappa \\
r_{23} &= \sin\omega \cos\varphi \qquad (3.1.13) \\
r_{31} &= -\sin\omega \sin\varkappa + \cos\omega \sin\varphi \cos\varkappa \\
r_{32} &= -\sin\omega \cos\varkappa - \cos\omega \sin\varphi \sin\varkappa \\
r_{33} &= \cos\omega \cos\varphi
\end{aligned}
$$

A special case arises for the left camera when the "two projector" method of relative orientation is used and $\omega' = 0$. The rotation matrix $\underline{R}$ has then the elements:

$$
\begin{aligned}
a_{11} &= \cos\varphi' \cos\varkappa' \\
a_{12} &= -\cos\varphi' \sin\varkappa' \\
a_{13} &= -\sin\varphi' \qquad (3.1.14) \\
a_{21} &= \sin\varkappa' \\
a_{22} &= \cos\varkappa' \\
a_{23} &= 0 \\
a_{31} &= \sin\varphi' \cos\varkappa' \\
a_{32} &= -\sin\varphi' \sin\varkappa' \\
a_{33} &= \cos\varphi'
\end{aligned}
$$

The least squares adjustment of the relative orientation requires linear expressions for the unknown rotation angles and partial derivatives of the rotation matrix with respect to ω, φ and $\varkappa$ need to be formed.

These are easily verified as being:

$$\frac{\partial \underline{R}}{\partial \omega} = \begin{bmatrix} 0 & 0 & 0 \\ r_{31} & r_{32} & r_{33} \\ -r_{21} & -r_{22} & -r_{23} \end{bmatrix} = \begin{bmatrix} 0 & 0 & 0 \\ 0 & 0 & 1 \\ 0 & -1 & 0 \end{bmatrix} \underline{R}$$

$$\frac{\partial \underline{R}}{\partial \varphi} = \begin{bmatrix} -\cos \varkappa \sin \varphi & \sin \varkappa \sin \varphi & -\cos \varphi \\ \sin \omega \, r_{11} & \sin \omega \, r_{12} & \sin \omega \, r_{13} \\ \cos \omega \, r_{11} & \cos \omega \, r_{12} & \cos \omega \, r_{13} \end{bmatrix} \qquad (3.1.15)$$

$$\frac{\partial \underline{R}}{\partial \varkappa} = \begin{bmatrix} r_{12} & -r_{11} & 0 \\ r_{22} & -r_{21} & 0 \\ r_{32} & -r_{31} & 0 \end{bmatrix} = \underline{R} \begin{bmatrix} 0 & -1 & 0 \\ 1 & 0 & 0 \\ 0 & 0 & 0 \end{bmatrix}$$

for the left camera with $\omega' = 0$ we have

$$\frac{\partial \underline{R}'}{\partial \omega'} = \underline{0}$$

$$\frac{\partial \underline{R}'}{\partial \varphi'} = \begin{bmatrix} -a_{31} & -a_{32} & -a_{33} \\ 0 & 0 & 0 \\ a_{11} & a_{12} & a_{13} \end{bmatrix} = \begin{bmatrix} 0 & 0 & -1 \\ 0 & 0 & 0 \\ 1 & 0 & 0 \end{bmatrix} \underline{R}' \qquad (3.1.16)$$

$$\frac{\partial \underline{R}'}{\partial \varkappa'} = \begin{bmatrix} a_{12} & -a_{11} & 0 \\ a_{22} & -a_{21} & 0 \\ a_{32} & -a_{31} & 0 \end{bmatrix} = \underline{R}' \begin{bmatrix} 0 & -1 & 0 \\ 1 & 0 & 0 \\ 0 & 0 & 0 \end{bmatrix}$$

If all relation angles are small one can approximate

$$\cos \omega = \cos \varphi = \cos \varkappa = 1$$

and

$$\sin \omega = \omega$$

$$\sin \varphi = \varphi$$

$$\sin \varkappa = \varkappa$$

Equations (3.1.13) become then

$$\underline{R} = \begin{bmatrix} 1 & -\varkappa & -\varphi \\ \varkappa & 1 & \omega \\ \varphi & -\omega & 1 \end{bmatrix} \qquad (3.1.17)$$

As previously stated, for analytical photogrammetry it is irrelevant which rotation sequence or direction is chosen when formulating the rotation matrix $\underline{R}$ in equation (3.1.1). In analogue photogrammetry, on the other hand, mechanical rotations about real instrument axes take place and, if analytical methods are involved in the analogue process, rotation matrices must correspond to the actual mechanical rotation sequence. Two situations come to mind in which one might want to express mechanical realities analytically.

a) If the results of an analytical photogrammetric orientation are to be used for the setting up of a stereo pair in a stereo plotter. (Harley, 1971, derives a direct solution to this problem.)

or

b) If the orientation in space of a camera is known and the known orientation angles are to serve as first approximations in a photogrammetric orientation adjustment.

The mathematical approach to these problems would be to introduce, in each case, rotation matrices which correspond to actual rotations. However, from a practical point of view this is not always advisable as it requires major changes (basic formulae, linearisation, error theory) to the adjustment model for application to different instruments.

A more convenient approach can be derived from the following property of rotation matrices:

If a vectorspace $\bar{\underline{x}}$ can be transformed to a vector space $\underline{x}$ by any arbitrary permutation of the three rotations about the coordinate axes, and if therefore

$$\underline{x} = \bar{\underline{R}}\bar{\underline{x}} = \underline{R}\bar{\underline{x}} \text{ for all } \underline{x} \tag{3.1.18}$$

then we also have

$$\bar{\underline{R}} = \underline{R} \tag{3.1.19}$$

Expression (3.1.19) states that the numerical values of all elements of two matrices, which realise the same transformation from $\bar{x}$ to x, are identical.

In the practical application of (3.1.19) we can use any valid rotation matrix $\underline{R}$ in the mathematical formulation of a photogrammetric orientation problem and subsequently determine mechanical rotations of any sequence by forming the trigonometrical expressions for the $\underline{R}$ matrix, which corresponds to the instrument in question. Numerical values for the rotation angles can then be evaluated by comparison of matrices $\underline{R}$ in (3.1.10)with $\underline{R}$ in (3.1.13).

Assuming that numerical values for the elements of $\underline{R}$ in (3.1.13) are known from an adjustment, one can find the mechanical rotation $\bar{\varkappa}$ $\bar{\varphi}$ and $\bar{\omega}$ from:

$$\tan \bar{\varkappa} = \frac{r_{21}}{r_{22}} = \frac{\cos \omega \sin \varkappa + \sin \omega \sin \varphi \cos \varkappa}{\cos \omega \cos \varkappa - \sin \omega \sin \varphi \sin \varkappa} = \frac{\cos \bar{\omega} \sin \bar{\varkappa}}{\cos \bar{\omega} \cos \bar{\varkappa}} \tag{3.1.20}$$

$$\sin \bar{\omega} = -r_{23} = -\sin \omega \cos \varphi \tag{3.1.21}$$

and

$$\tan \bar{\varphi} = \frac{r_{13}}{r_{33}} = \frac{-\sin \varphi}{\cos \omega \cos \varphi} \tag{3.1.22}$$

and similar elements of $\underline{R}$ in (3.1.10) can serve to evaluate the angles in $\underline{R}$ from

$$\tan \varkappa = - \frac{r_{12}}{r_{11}} \qquad (3.1.23)$$

$$\tan \omega = \frac{r_{23}}{r_{33}} \qquad (3.1.24)$$

$$\sin \varphi = - r_{13} \qquad (3.1.25)$$

3.2 LEAST SQUARES ADJUSTMENT

The least squares adjustment technique is adopted in this thesis whenever redundant observations are available. Although this technique is well documented in the relevant literature (Jordan, Eggert, Kneissl, 1961; Wolf, 1968 and 1975; Wells and Krakiwsky, 1971; Hirvonen, 1971, Mikhail, 1976) a brief review of the "general" or "combined" case of adjustment is considered necessary. The condition equation method, the parametric case and the quasi-parametric case are then derived from the general case. Special attention is paid to the quasi-parametric method, as this is seldom mentioned in English survey literature. In the quasi-parametric method, a reduced form of the general case, the extent of matrix manipulation is reduced considerably, making this technique especially suited to desk-top and mini computers with limited memory capacity and relatively low calculation speeds. The quasi-parametric case is repeatedly applied in this thesis. Adjustment methods based on correlated parameters are not discussed here as all observations are assumed to be practicalyy correlation free. Working formulae for the four cases of adjustment mentioned above and for subsequent error analysis are combined in tabular form. (Tab. 3.2-1)

The advantage of the use of least squares adjustment lies in the relative ease with which redundant observations can be accommodated and in the fact that it offers unique measures of accuracy, which are understood throughout the disciplines of science and engineering. It also renders unique solutions for numerical problems provided that the same functional and stochastic model is applied thus making comparative studies simple and rigorous.

The Combined or General Case of the Least Squares Adjustment

The combined case of the least squares adjustment finds application in adjustment situations where condition equations can be formulated as functions of observations and unknown quantities.

In the conventional Gaussian notation a system of such condition equations has the form:

$$\begin{aligned} a_1 v_1 + a_2 v_2 + \ldots + A_a dx + B_a dy + \ldots + w_a &= 0 = F_a \\ b_1 v_1 + b_2 v_2 + \quad + A_b dx + B_b dy + \quad + w_b &= 0 = F_b \\ \vdots \quad \vdots \quad \quad \vdots \quad \vdots \quad \quad \vdots \quad \vdots \quad \vdots & \\ r_1 v_1 + r_2 v_2 + \quad + A_r dx + B_r dy + \quad + w_r &= 0 = F_r \end{aligned} \qquad (3.2.1)$$

Where $a_i \ldots r_i$ are the derivatives of condition equations $F_a \ldots\ldots F_r$ with respect to the observations $\ell_i \ldots \ell_n$:

$$a_i = \frac{\partial F_a}{\partial \ell_i} \qquad b_i = \frac{\partial F_b}{\partial \ell_i} \qquad i = 1 \ldots n \qquad (3.2.2)$$

and A_a, B_a .... are the derivatives of $F_a \ldots F_r$ with respect to the unknowns x, y ...

$$A_a = \frac{\partial F_a}{\partial x} \qquad B_a = \frac{\partial F_b}{\partial y} \qquad \text{etc.} \qquad (3.2.3)$$

In matrix form (3.2.1) can be written as

$$\underline{B}\,\underline{v} + \underline{A}\,\underline{x} + \underline{w} = \underline{0} \qquad (3.2.4)$$

The least squares principle requires that the conditions (3.2.4) are satisfied and that

$$\underline{v}^T \underline{P} \underline{v} = \text{Minimum} \qquad (3.2.5)$$

where p_i are the observation weights and P is the weight matrix with non zero elements on the principal diagonal only. This is realised in the Lagrange equation:

$$\Phi = \underline{v}^T \underline{P}\,\underline{v} - 2\,\underline{k}^T (\underline{B}\underline{v} + \underline{A}\,\underline{x} + \underline{w}) = \text{Minimum} \qquad (3.2.6)$$

We differentiate (3.2.6) with respect to variables $\underline{v}$ and $\underline{x}$

$$\frac{\partial \Phi}{\partial \underline{v}} = 2\,\underline{v}^T \underline{P} - 2\,\underline{k}^T \underline{B} \qquad (3.2.7)$$

and

$$\frac{\partial \Phi}{\partial \underline{x}} = 2\,\underline{k}^T \underline{A} \qquad (3.2.8)$$

To minimise equation (3.2.6) we set (3.2.7) and (3.2.8) equal to zero and obtain with $\underline{P} = \underline{P}^T$

$$\text{from (3.2.7)} \quad \underline{v} = \underline{P}^{-1} \underline{B}^T \underline{k} \qquad (3.2.9)$$

$$\text{and from (3.2.8)} \quad \underline{A}^T \underline{k} = 0 \qquad (3.2.10)$$

Conditions (3.2.4), (3.2.9) and (3.2.10) must be satisfied for a least square solution.

Introducing (3.2.9) into equation (3.2.4) we obtain

$$\underline{B}\underline{P}^{-1}\underline{B}^T \underline{k} + (\underline{A}\underline{x} + \underline{w}) = \underline{0} \qquad (3.2.11)$$

and for the correlates $\underline{k}$ one now has

$$\underline{k} = -(\underline{B}\underline{P}^{-1}\underline{B}^T)^{-1} (\underline{A}\underline{x} + \underline{w}) \qquad (3.2.12)$$

The solution vector $\underline{x}$ is finally found from

$$\underline{x} = -(\underline{A}^T(\underline{B}\underline{P}^{-1}\underline{B}^T)^{-1}\underline{A})^{-1}\underline{A}^T(\underline{B}\underline{P}^{-1}\underline{B}^T)^{-1}\underline{w} \tag{3.2.13}$$

The unknown vector $\underline{x}$ and the correlate vector $\underline{k}$ can also be evaluated in a slightly different form, which is sometimes preferable for mini computer applications. By combining (3.2.10) and (3.2.11) one obtains

$$\begin{bmatrix} \underline{B}\underline{P}^{-1}\underline{B}^T & \underline{A} \\ \underline{A}^T & \underline{0} \end{bmatrix} \cdot \begin{bmatrix} \underline{k} \\ \underline{x} \end{bmatrix} + \begin{bmatrix} \underline{w} \\ \underline{0} \end{bmatrix} = \begin{bmatrix} \underline{0} \\ \underline{0} \end{bmatrix} \tag{3.2.14}$$

Equation system (3.2.14) combines conditions (3.2.4), (3.2.9) and (3.2.10) as required and therefore represents a formulation of the solution for $\underline{k}$ and $\underline{x}$.

Error Theory for the Combined Case of Adjustment

Standard Deviation of Unit Weight (Variance)

$$\sigma_0^2 = \frac{\underline{v}^T\underline{P}\underline{v}}{(r-u)} \tag{3.2.15}$$

where r = number of condition equations and u = number of unknowns.

Standard Deviation of an Observation a priori

$$\sigma_i^2 = \sigma_0^2 \; P_i \tag{3.2.16}$$

Standard Devision of an Unknown

$$\sigma_{x_i}^2 = \sigma_0^2 \; Q_{x_i x_i} \tag{3.2.17}$$

where $Q_{x_i x_i}$ are the elements in the principal diagonal of the variance-covariance matrix $\underline{Q}$

$$\text{with } \underline{Q} = (\underline{A}^T(\underline{B}\underline{P}^{-1}\underline{B}^T)^{-1}\underline{A})^{-1} \tag{3.2.18}$$

Standard Deviation of a Function of the Unknowns and Observations

Given is a function F of observations ℓ_i and unknowns x, y ...)

$$F = F(\ell_1+v_1,\ \ell_2+v_2,\ \ldots,\ x,\ y\ \ldots) \tag{3.2.19}$$

Function F is linearised and expressed in matrix form as

$$F = \underline{f}^T(\underline{\ell}+\underline{v}) + \underline{\bar{f}}^T\underline{x} \tag{3.2.20}$$

$\underline{f}$ and $\underline{\bar{f}}$ are vectors containing the differentials of F with respect to the observations and unknowns respectively

$$\underline{f}^T = \left[\frac{\partial F}{\partial \ell_1}, \frac{\partial F}{\partial \ell_2}, \frac{\partial F}{\partial \ell_3} \ldots\ \right] \tag{3.2.21}$$

$$\underline{\bar{f}}^T = \left[\frac{\partial F}{\partial x}, \frac{\partial F}{\partial y}, \frac{\partial F}{\partial z} \ldots\ \right] \tag{3.2.22}$$

the standard deviation of F is then found from

$$\sigma_F^2 = \sigma_o^2\, Q_{FF} \tag{3.2.23}$$

where

$$\begin{aligned} Q_{FF} = {} & \underline{f}^T(\underline{P}^{-1}\underline{P}^{-1}\underline{B}^T(\underline{B}\underline{P}^{-1}\underline{B}^T)^{-1}\underline{B}\underline{P}^{-1})\underline{f} + \\ & + (\underline{\bar{f}}^T-\underline{f}^T\underline{P}^{-1}\underline{B}^T(\underline{B}\underline{P}^{-1}\underline{B}^T)^{-1}\underline{A})\ (\underline{A}^T(\underline{B}\underline{P}^{-1}\underline{B}^T)^{-1}\underline{A})^{-1}\cdot \\ & \cdot(\underline{\bar{f}}-\underline{A}^T(\underline{B}\underline{P}^{-1}\underline{B}^T)^{-1}\underline{B}\underline{P}^{-1}\underline{f}) \end{aligned} \tag{3.2.24}$$

Formulae for the standard deviation of a function are required when evaluating the standard deviations of model co-ordinates, which are determined in the relative orientation adjustment as

functions of observed plate co-ordinates and unknown orientation angles. The parametric case can be derived from the combined case by setting $\underline{B} = -\underline{I}$ and $\underline{w} = -\underline{\ell}$, the condition equation case is derived by setting $\underline{A} = \underline{0}$ (see Tab. 3.2-1). The combined case is unsuitable for use in mini computers owing to its large matrices in (3.2.13) or (3.2.14), and is best replaced by the quasi-parametric case wherever possible.

Quasi-parametric Case

In cases where each observation occurs in one condition equation only, the combined case can be converted into the quasi-parametric adjustment to save memory space and computation time.

Equation (3.2.1) then takes the form

$$
\begin{array}{llllllll}
a_1 v_1 & + a_2 v_2 & + 0 & + 0 & & + A_a\,dx + B_a\,dy + \ldots + w_a & = 0 \\
0 & + 0 & + b_3 v_3 & + b_4 v_4 & & + A_b\,dx + B_b\,dy + \ldots + w_b & = 0 \\
\vdots & \vdots & \vdots & \vdots & & \vdots & \vdots \\
0 & + 0 & + 0 & + 0 \cdots + r_n v_n & & + A_r\,dx + B_r\,dy + \ldots + w_r & = 0
\end{array}
$$

It is obvious that in this case the matrix $(\underline{B}\underline{P}^{-1}\underline{B}^T)$ takes the form of a principal diagonal matrix, that is, in forming $(\underline{B}\underline{P}^{-1}\underline{B}^T)$ all matrix elements with the exception of those on the principal diagonal are equal to zero.

We can therefore set

$$(\underline{B}\underline{P}^{-1}\underline{B}^T)^{-1} = \underline{P}^* \qquad (3.2.25)$$

where $\underline{P}^*$ is a matrix which resembles the weight matric of the parametric case. For calculation purposes the elements of $\underline{P}^*$ can be interpreted as quasi-weights and $\underline{P}^*$ as a quasi-weight matrix.

Substituting $\underline{P}^*$ into (3.2.13) we obtain

$$\underline{x} = -(\underline{A}^T\underline{P}^*\underline{A})^{-1}\underline{A}^T\underline{P}^*\underline{w} \tag{3.2.26}$$

and with

$$\underline{w} = -\underline{\ell}$$
$$\underline{x} = (\underline{A}^T\underline{P}^*\underline{A})^{-1}\underline{A}^T\underline{P}\underline{\ell} \tag{3.2.27}$$

Equation (3.2.27) resembles the $\underline{x}$ solution equation (Tab. 3.2-1) of the parametric case and the combined case can be solved as a so-called quasi-parametric case. The resulting values for $\underline{x}$ are the true unknowns whilst the corrections

$$\underline{V}^* = \underline{A}\underline{x} - \underline{\ell} = \underline{A}\underline{x} + \underline{w} \tag{3.2.28}$$

are merely calculation values and should be referred to as quasi-corrections.

To convert quasi-corrections $\underline{V}^*$ into corrections $\underline{v}$ we combine (3.2.9) and (3.2.12) and replace $(\underline{B}\underline{P}^{-1}\underline{B}^T)^{-1}$ by $\underline{P}^*$

$$\underline{v} = -\underline{P}^{-1}\underline{B}^T(\underline{B}\underline{P}^{-1}\underline{B}^T)^{-1}\ (\underline{A}\underline{x} + \underline{w}) = -\underline{P}^{-1}\underline{B}^T\underline{P}^*\underline{V}^* \tag{3.2.29}$$

Expressed in conventional notations (3.2.29) becomes

$$v_1 = -\frac{1}{P_a}\ V_a^*\ a_1P_a^*$$
$$v_2 = -\frac{1}{P_{a_2}}\ V_a^*\ a_2P_a^* \tag{3.2.30}$$

Wolf (1975) proves that

$$\underline{v}^T\underline{P}\ \underline{v} = \underline{V}^{*T}\underline{P}^*\underline{V}^* \tag{3.2.31}$$

Formulae for the error theory are listed in Table 3.2-1. σ_0 is evaluated on the basis of (3.2.31).

Table 3.2-1 Formulae for Least Squares Adjustment

	Combined Case	Parametric Case	Condition Equation Case	Quasiparametric Case
Functional model	$\underline{B}\underline{v}+\underline{A}\underline{x}+\underline{w}=\underline{0}$	$\underline{A}\underline{x}-\underline{l}=\underline{v}$ $\quad \underline{B}=-\underline{I}$ $\quad \underline{w}=-\underline{l}$	$\underline{B}\underline{v}+\underline{w}=\underline{0}$ $\quad \underline{A}=\underline{0}$	$\underline{V}^*=\underline{A}\underline{x}-\underline{l}$ with $\underline{P}^*=(\underline{B}\underline{P}^{-1}\underline{B}^T)^{-1}$
Unknowns	$\underline{x}=-(\underline{A}^T\underline{N}^{-1}\underline{A})^{-1}\underline{A}^T\underline{N}^{-1}\underline{w}$ $\quad \underline{N}=\underline{B}\underline{P}^{-1}\underline{B}^T$	$\underline{x}=(\underline{A}^T\underline{P}\underline{A})^{-1}\underline{A}\underline{P}\underline{l}$	———	$\underline{x}=(\underline{A}^T\underline{P}^*\underline{A})^{-1}\underline{A}^T\underline{P}^*\underline{l}$
Correlates	$\underline{k}=-\underline{N}^{-1}(\underline{A}\underline{x}+\underline{w})$	$[\underline{k}=-\underline{P}(\underline{A}\underline{x}-\underline{l})]$	$\underline{k}=-(\underline{B}\underline{P}^{-1}\underline{B}^T)^{-1}\underline{w}$	$\underline{k}=\underline{P}^*\underline{V}^*$
Corrections	$\underline{v}=\underline{P}^{-1}\underline{B}^T\underline{k}$	$\underline{v}=-\underline{P}^{-1}\underline{k}=\underline{A}\underline{x}-\underline{l}$	$\underline{v}=\underline{P}^{-1}\underline{B}^T\underline{k}$	$\underline{V}^*=\underline{A}\underline{x}-\underline{l}$ $\quad \underline{v}=\underline{P}^{-1}\underline{B}^T\underline{P}^*\underline{V}^*$
Variance co-variance matrix	$\underline{Q}=(\underline{A}^T\underline{N}^{-1}\underline{A})^{-1}$	$\underline{Q}=(\underline{A}^T\underline{P}\underline{A})^{-1}$	$\underline{Q}_{kk}=(\underline{B}\underline{P}^{-1}\underline{B}^T)^{-1}$	$\underline{Q}=(\underline{A}^T\underline{P}^*\underline{A})^{-1}$
Variance	$\sigma_o^2=\underline{v}^T\underline{P}\underline{v}/(r-u)$	$\sigma_o^2=\underline{v}^T\underline{P}\underline{v}/(n-u)$	$\sigma_o^2=\underline{v}^T\underline{P}\underline{v}/r$	$\underline{v}^T\underline{P}\underline{v}=\underline{V}^{*T}\underline{P}^*\underline{V}^*$ $\quad \sigma_o^2=\underline{V}^{*T}\underline{P}\underline{V}^*/(r-u)$
Standard deviation of an observation a priori (σ_i)	$\sigma_i^2=\sigma_o^2 p_i$	$\sigma_i^2=\sigma_o^2 p_i$	$\sigma_i^2=\sigma_o^2 p_i$	$\sigma_i^2=\sigma_o^2 p_i$
Standard deviation of an unknown (σ_x)	$\sigma_x^2=\sigma_o^2 Q_{xx}$	$\sigma_x^2=\sigma_o^2 Q_{xx}$	———	$\sigma_x^2=\sigma_o^2 Q_{xx}$
Standard deviation of a function of a) the observations b) the unknowns ab) observations and unknowns	$\sigma_F^2=\sigma_o^2 Q_{FF}$ ab) $Q_{FF}=\underline{f}^T(\underline{P}^{-1}-\underline{P}^{-1}\underline{B}^T\underline{N}^{-1}\underline{B}\underline{P}^{-1})\underline{f}+$ $+(\underline{f}^T-\underline{f}^T\underline{P}^{-1}\underline{B}^T\underline{N}^{-1}\underline{A})(\underline{A}^T\underline{N}^{-1}\underline{A})^{-1}$ $(\underline{f}-\underline{A}^T\underline{N}^{-1}\underline{B}\underline{P}^{-1}\underline{f})$	$\sigma_F^2=\sigma_o^2 Q_{FF}$ a) $\underline{f}=\underline{0}$ $Q_{FF\,obs}=\underline{f}^T\underline{A}(\underline{A}^T\underline{P}\underline{A})^{-1}\underline{A}^T\underline{f}$ b) $\underline{f}=\underline{0}$ $Q_{FFx}=\underline{f}^T(\underline{A}^T\underline{P}\underline{A})^{-1}\underline{f}$	$\sigma_F^2=\sigma_o^2 Q_{FF}$ a) $\underline{f}=\underline{0}$ $Q_{FF\,obs}=\underline{f}^T(\underline{P}^{-1}-\underline{P}^{-1}\underline{B}^T\underline{N}^{-1}\underline{B}\underline{P}^{-1})\underline{f}$ b) ———	$\sigma_F^2=\sigma_o^2 Q_{FF}$ a) $\underline{f}=\underline{0}$ $Q_{FF\,obs}=\underline{f}^T(\underline{P}^{-1}-\underline{P}^{-1}\underline{B}^T\underline{P}^*\underline{B}\underline{P}^{-1})\underline{f}+$ $+\underline{f}^T\underline{P}^{-1}\underline{B}^T\underline{P}^*\underline{A}(\underline{A}^T\underline{P}^*\underline{A})^{-1}\underline{A}^T\underline{P}^*\underline{B}\underline{P}^{-1}\underline{f}$ b) $\underline{f}=\underline{0}$ $Q_{FFx}=\underline{f}^T(\underline{A}^T\underline{P}^*\underline{A})^{-1}\underline{f}$

3.3 THE SYNTHETIC PHOTOGRAPH

> Perspective is nothing more than seeing a place (or object) behind a pane of glass, quite transparent, on the surface of which the objects behind that glass are to be drawn.
>
> Leonardo da Vinci (1452-1519)

A photographic image, which is free of any error or distortion, produced by a camera for which the true values of the interior orientation parameters are known, represents an ideal basis for the testing of mathematical models and the controlled introduction of errors to investigate model deformations.

Such an image obviously cannot be produced by real photography. It can, however, be constructed in a computer simulation in the form of a set of plate co-ordinates for a given principal distance. Object shape, position and attitude of camera and, if required, image distortions and observation errors can then be introduced and modified at will to create different test cases for mono-and stereo photography. Such a computer generated image is referred to here as a 'synthetic' photograph.

The geometrical basis of the synthetic photograph is the central perspective projection as shown in Fig. (3.3-1) for the case of normal oriented photography.

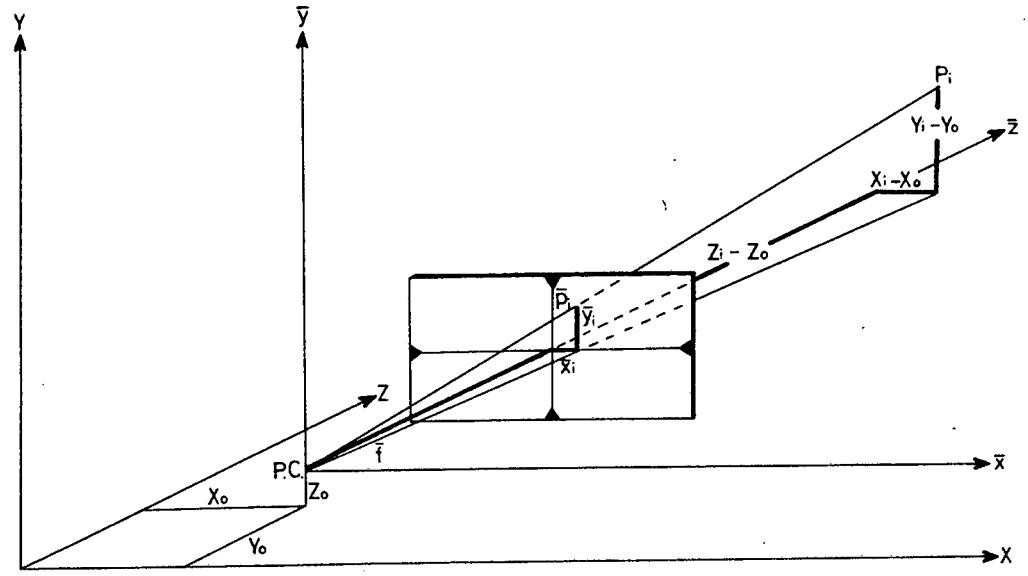

Fig. 3.3-1 Perspective centre (P.C.), positive image and object point Pi in model co-ordinate system

The image co-ordinates $\bar{x}_i$ and $\bar{y}_i$ of model point P_i for a given principal distance f and camera position (X_o, Y_o, Z_o) are easily found with the following calculation steps:

1. Model co-ordinates X_i, Y_i, Z_i are reduced to the camera position X_o, Y_o, Z_o

$$\underline{d} = \begin{bmatrix} X_i - X_o \\ Y_i - Y_o \\ Z_i - Z_o \end{bmatrix} \qquad (3.3.1)$$

2. Rotation angles $\varkappa, \varphi, \omega$ are chosen to suit the required test case, the full rotation matrix $\underline{R}$ as in (3.1.13) is evaluated and the auxiliary vector $\underline{e}$ is formed with

$$\underline{e} = \underline{R}\,\underline{d} \qquad (3.3.2)$$

3. In this form element e_3 in vector $\underline{e}$ (the equivalent of the principal distance) differs from point to point.
A further multiplication by $c = \bar{f}/e_3$ is required to guarantee that the $\bar{z}$ co-ordinate for all points is equal to the required principal distance f of the simulated camera. The image co-ordinates of the synthetic photograph are then

$$\underline{\bar{x}} = c\, \underline{R}\, \underline{d} \qquad (3.3.3)$$

$$\text{with} \quad c = \frac{\bar{f}}{e_3} \qquad (3.3.4)$$

In conventional notation we now have for the image co-ordinates

$$\begin{aligned} \bar{x}_i &= \left[r_{11}\,(X_i-X_o) + r_{12}\,(Y_i-Y_o) + r_{13}\,(Z_i-Z_o)\right] \frac{\bar{f}}{e_3} \\ \bar{y}_i &= \left[r_{21}\,(X_i-X_o) + r_{22}\,(Y_i-Y_o) + r_{23}\,(Z_i-Z_o)\right] \frac{\bar{f}}{e_3} \qquad (3.3.5) \\ \bar{z}_i &= \bar{f} \end{aligned}$$

$$\text{with } e_3 = r_{31}\,(X_i-X_o) + r_{32}\,(Y_i-Y_o) + r_{33}\,(Z_i-Z_o)$$

r_{ij} are the elements of $\underline{R}$ from (3.1.13)

A special case arises for normal oriented photography

where $\underline{R} = \underline{I}$ and $e_3 = Z_i - Z_o$

$$\bar{x}_i = \frac{X_i-X_o}{Z_i-Z_o}\,\bar{f}$$

$$\bar{y}_i = \frac{Y_i-Y_o}{Z_i-Z_o}\,\bar{f}$$

$$\bar{z}_i = \bar{f}$$

These synthetic co-ordinates fully satisfy the mathematical model of the central perspective projection. To create a more realistic simulation random, normally distributed, observation

errors can be added to the error-free image co-ordinates. Image distortion, as caused by lens distortions, emulsion shift and film shrinking, can be incorporated into the image co-ordinates on the basis of one of the various distortion models suggested by, amongst others Hallert (1968[2]), Schenk (1971), Brown (1971), Ziemann (1972), Kraus and Stark (1973) and Thompson (1977).

Examples of simulated photographs of the test field described in Chapter 5 are given in Table 3.3-1 for normal oriented photography and in Table 3.3-2 for a case of general convergent photography.

SIMULATED PLATE CO-ORDINATES FOR NORMAL PHOTOGRAPHY

PRINCIPAL DISTANCE : 100 MM BASE : 3.310 M

(UNITS : MM)

	LEFT IMAGE		RIGHT IMAGE	
	X'	Y'	X''	Y''
1	4.979	23.603	-51.194	23.603
2	4.924	10.846	-51.205	10.846
3	4.781	-1.579	-51.338	-1.579
4	4.809	-14.515	-51.297	-14.515
5	5.411	25.786	-55.639	25.786
6	5.303	11.957	-55.748	11.957
7	5.225	-1.888	-55.826	-1.888
8	5.133	-15.713	-55.900	-15.713
9	6.446	30.896	-66.821	30.896
10	6.386	14.353	-66.901	14.353
11	6.306	-2.288	-66.995	-2.288
12	6.196	-18.919	-67.143	-18.919
13	7.834	38.397	-83.501	38.397
14	7.954	17.846	-83.405	17.846
15	7.998	-2.943	-83.424	-2.943
16	7.934	-23.683	-83.600	-23.683
17	17.821	22.466	-35.875	22.466
18	18.053	10.353	-35.573	10.353
19	18.033	-1.776	-35.596	-1.776
20	17.811	-13.848	-35.871	-13.848
21	20.390	25.759	-40.628	25.759
22	20.330	11.970	-40.699	11.970
23	20.239	-1.862	-40.802	-1.862
24	20.160	-15.710	-40.909	-15.710
25	24.642	30.916	-48.550	30.916
26	24.522	14.334	-48.667	14.334
27	24.482	-2.294	-48.732	-2.294
28	24.378	-18.887	-48.864	-18.887
29	30.623	38.468	-60.908	38.468
30	30.548	17.725	-60.979	17.725
31	30.420	-3.044	-61.090	-3.044
32	30.188	-23.788	-61.300	-23.788
33	30.954	22.364	-22.723	22.364
34	31.091	10.394	-22.520	10.394
35	31.281	-1.768	-22.345	-1.768
36	31.119	-13.805	-22.547	-13.805
37	35.622	25.721	-25.442	25.721
38	35.525	11.917	-25.551	11.917
39	35.456	-1.938	-25.614	-1.938
40	35.431	-15.778	-25.611	-15.778

	LEFT IMAGE		RIGHT IMAGE	
	X'	Y'	X''	Y''
41	42.739	30.874	-30.484	30.874
42	42.649	14.261	-30.569	14.261
43	42.536	-2.296	-30.692	-2.296
44	42.389	-18.923	-30.867	-18.923
45	53.271	38.277	-38.222	38.277
46	53.135	17.544	-38.365	17.544
47	53.115	-3.201	-38.374	-3.201
48	53.154	-23.969	-38.294	-23.969
49	44.860	22.353	-8.802	22.353
50	44.505	10.428	-9.080	10.428
51	44.498	-1.683	-9.089	-1.683
52	44.299	-13.643	-9.358	-13.643
53	50.822	25.843	-10.207	25.843
54	50.738	11.999	-10.297	11.999
55	50.629	-1.869	-10.391	-1.869
56	50.409	-15.658	-10.571	-15.658
57	60.808	30.917	-12.286	30.917
58	60.733	14.304	-12.339	14.304
59	60.537	-2.257	-12.537	-2.257
60	60.462	-18.855	-12.776	-18.855
61	76.042	38.348	-15.420	38.348
62	75.909	17.652	-15.529	17.652
63	75.841	-3.118	-15.632	-3.118
64	75.747	-23.837	-15.812	-23.837
65	58.078	22.363	4.427	22.363
66	57.632	10.543	4.058	10.543
67	57.705	-1.629	4.131	-1.629
68	57.551	-13.563	3.911	-13.563
69	65.873	25.960	4.811	25.960
70	65.796	12.143	4.717	12.143
71	65.701	-1.741	4.606	-1.741
72	65.610	-15.541	4.508	-15.541
73	79.082	30.996	5.863	30.996
74	78.986	14.431	5.762	14.431
75	78.831	-2.183	5.634	-2.183
76	78.667	-18.790	5.474	-18.790
77	98.313	38.569	7.034	38.569
78	98.199	17.893	6.915	17.893
79	98.159	-2.824	6.846	-2.824
80	98.052	-23.544	6.690	-23.544

Table 3.3-1

SIMULATED PLATE CO-ORDINATES FOR CONVERGENT PHOTOGRAPHY

PRINCIPAL DISTANCE : 100 MM BASE : 3.310 M

KAPPA' = 1° PHI' = -20° KAPPA'' = 0° PHI'' = 14° OMEGA'' = 0°

(UNITS : MM)

	LEFT IMAGE		RIGHT IMAGE	
	X'	Y'	X''	Y''
1	-30.424	25.206	-23.289	21.572
2	-30.716	11.877	-23.298	9.912
3	-31.099	-1.109	-23.409	-1.443
4	-31.305	-14.636	-23.374	-13.263
5	-29.913	27.437	-26.966	23.338
6	-30.283	13.013	-27.054	10.819
7	-30.620	-1.437	-27.119	-1.708
8	-30.972	-15.877	-27.179	-14.213
9	-28.699	32.631	-35.906	27.295
10	-29.064	15.437	-35.968	12.678
11	-29.453	-1.867	-36.042	-2.021
12	-29.874	-19.171	-36.157	-16.702
13	-27.073	40.207	-48.476	32.754
14	-27.316	18.936	-48.406	15.226
15	-27.644	-2.561	-48.420	-2.511
16	-28.088	-24.009	-48.548	-20.198
17	-17.050	22.753	-10.044	21.253
18	-17.030	10.637	-9.773	9.801
19	-17.261	-1.472	-9.794	-1.681
20	-17.693	-13.533	-10.040	-13.100
21	-14.454	25.774	-14.251	24.106
22	-14.750	12.120	-14.314	11.200
23	-15.080	-1.583	-14.404	-1.742
24	-15.396	-15.309	-14.497	-14.692
25	-10.259	30.376	-21.067	28.422
26	-10.656	14.193	-21.166	13.175
27	-10.977	-2.050	-21.221	-2.108
28	-11.360	-18.265	-21.332	-17.351
29	-4.551	36.916	-31.232	34.418
30	-4.966	17.065	-31.289	15.857
31	-5.432	-2.822	-31.378	-2.723
32	-5.992	-22.708	-31.546	-21.266
33	-4.518	21.472	2.091	21.813
34	-4.592	10.018	2.284	10.142
35	-4.622	-1.609	2.451	-1.726
36	-4.971	-13.112	2.259	-13.471
37	-0.263	24.239	-0.479	24.928
38	-0.576	11.242	-0.581	11.546
39	-0.865	-1.812	-0.641	-1.877
40	-1.115	-14.855	-0.638	-15.285

	LEFT IMAGE		RIGHT IMAGE	
	X'	Y'	X''	Y''
41	5.984	28.332	-5.159	29.571
42	5.641	13.041	-5.237	13.657
43	5.278	-2.209	-5.350	-2.198
44	4.885	-17.534	-5.510	-18.108
45	14.727	33.866	-12.133	36.016
46	14.297	15.397	-12.259	16.502
47	13.958	-3.099	-12.267	-3.011
48	13.666	-21.614	-12.197	-22.550
49	7.631	20.318	15.784	22.542
50	7.143	9.427	15.502	10.509
51	6.944	-1.663	15.493	-1.696
52	6.586	-12.620	15.220	-13.740
53	12.576	22.992	14.360	25.973
54	12.292	10.566	14.269	12.057
55	11.986	-1.889	14.175	-1.878
56	11.592	-14.284	13.993	-15.723
57	20.454	26.586	12.271	30.917
58	20.145	12.116	12.217	14.302
59	19.744	-2.313	12.020	-2.256
60	19.434	-16.788	11.781	-18.832
61	31.604	31.416	9.161	38.059
62	31.211	14.176	9.053	17.514
63	30.861	-3.139	8.952	-3.092
64	30.494	-20.420	8.775	-23.635
65	18.238	19.330	29.687	23.305
66	17.712	8.966	29.287	10.977
67	17.582	-1.740	29.366	-1.696
68	17.279	-12.237	29.128	-14.116
69	24.161	21.865	30.105	27.079
70	23.897	10.010	30.003	12.663
71	23.619	-1.908	29.882	-1.815
72	23.345	-13.760	29.776	-16.199
73	33.587	25.031	31.253	32.419
74	33.282	11.349	31.142	15.089
75	32.937	-2.380	31.003	-2.282
76	32.585	-16.116	30.828	-19.633
77	46.120	29.427	32.537	40.459
78	45.767	13.231	32.406	18.764
79	45.459	-3.008	32.330	-2.961
80	45.110	-19.256	32.159	-24.677

Table 3.3-2

3.4 COMPUTER GENERATED NORMALLY DISTRIBUTED RANDOM NUMBERS

In order to simulate plate co-ordinate observations for a computer generated synthetic image, it is necessary to incorporate observation errors in the values for the plate co-ordinates. It must be assumed that observations on a comparator are subject to normally or near normally distributed, uncorrelated random errors.

Most mini computers have a random number generator which can produce pseudo random values. These numbers are, however, of uniform distribution and a transformation is required to convert these values into normally distributed quantities.

The mathematically strict transformation from uniform distributed to a normally distributed random numbers would require the evaluation of s_i from the distribution function.

$$r_i = \frac{1}{\sigma\sqrt{2\pi}} \int_{-\infty}^{s_i} e^{-\frac{1}{2}\left(\frac{x-\xi}{\sigma}\right)^2} dx \qquad (3.4.1)$$

r_i = uniform distributed random value in the interval from 0 to 1

s_i = normally distributed random value

σ = standard derivation of distribution

ξ = mean value of distribution

x = integration variable

For standard normal distribution (0,1) one has

$$\xi = 0$$

and $$\sigma = 1$$

The solution of (3.4.1)for s_i is not possible. Heister, Welsch (1972) report on and test an approximation method. They show that (0,1) normally distributed random numbers can be approximated by

$$s_i' = \left(\sum_{j=1}^{k} r_j - \frac{k}{2} \right) \sqrt{\frac{12}{k}} \qquad k \to \infty \tag{3.4.2}$$

This approximation can be improved (Bolsher 1959) by

$$s_i = s_i' - \frac{1}{20k}(3s_i' - s_i'^3) \tag{3.4.3}$$

If (3.4.2) and (3.4.3) are applied in combination one obtains for a k value as small as 5 random numbers s_i which do not differ by more than 0,00037 (Heister,Welsch 1972) from equation (3.4.1). If mean values ξ and standard deviation σ other than 0 and 1 respectively are required, s_i can be easily transformed to a (ξ, σ) normally distributed random number by

$$\bar{s}_i = \sigma s_i + \xi \tag{3.4.4}$$

This approximation technique was used to generate 320 normal distributed random numbers on the random generator of a Tektronix 4051 mini computer. For the seed of the uniform random numbers π was chosen and a value of k = 6 was used in (3.4.2) and (3.4.3). To simulate the observation accuracy of the ZEISS STEKO comparator a standard deviation of σ = 10 µm was stipulated in (3.4.4) while $\xi = 0$.

The generated values are added to the 320 plate co-ordinates of the synthetic stereo pair simulating photography of the 80 point test field. (Because of k = 6 in (3.4.2) 6•320 random values r_i are involved in this process).

When calculating the actual mean value x of the 320 sample values one obtains

$$\bar{x} = 0{,}13 \ \mu m$$

and the standard deviation is

$$\sigma = 9{,}9 \ \mu m$$

The appropriate statistical tests show that at 99% probability level we cannot reject the hypothesis, that $\bar{x}$ does not differ significantly from ξ.

Similarly, using the χ^2 test, at the same probability level, we can see that the sample variance does not differ significantly from the population variance.

Finally the χ^2 Goodness of Fit test shows that the fit of the generated values to the normal distribution curve is good.

The numerical analysis of the data in the Goodness of Fit test takes the form:

∞ -30	-20	-10	-5	0	+5	+10	+20	+30 + ∞	computer generated values in units of µm.
1	8	33	50	69	64	48	39	8	0	computer generated frequency (o)
0,4	7	43	48	61	61	48	43	7	0,4	expected frequency (e)

COMPUTER GENERATED NORMAL DISTRIBUTED RANDOM OBSERVATION ERRORS

(UNITS: MICRON)

ACTUAL STANDARD DEVIATION 9.9
STIPULATED STANDARD DEVIATION 10.0

ACTUAL DISTRIBUTION MEAN 0.1
STIPULATED DISTRIBUTION MEAN 0.0

	X'	Y'	X''	Y''
1	-3.8	3.3	10.1	-16.2
2	6.7	5.7	-8.4	3.8
3	0.7	1.0	-0.4	2.6
4	1.6	0.1	0.7	0.4
5	2.2	-4.0	15.1	-0.4
6	-8.0	-28.2	-5.0	8.4
7	-9.1	3.9	-10.4	-12.6
8	-14.1	-6.8	8.7	6.7
9	25.6	13.5	15.6	-8.1
10	-2.5	-6.2	11.1	-16.6
11	3.2	-2.7	7.5	3.8
12	-8.9	-11.2	-0.9	-5.8
13	-1.2	-20.4	2.5	9.6
14	6.0	8.1	17.3	-6.3
15	2.2	-13.2	1.4	17.9
16	-12.9	-1.6	-14.7	5.1
17	-3.4	6.7	8.4	-2.4
18	-3.3	4.1	21.8	8.1
19	-1.3	5.8	-2.7	-2.2
20	2.5	8.2	5.3	-4.9
21	-11.4	-1.9	-1.4	8.3
22	-0.5	-2.7	10.7	1.0
23	-3.3	-1.5	10.8	18.3
24	7.1	7.4	13.1	-5.1
25	3.1	-6.1	-1.9	-1.9
26	3.9	-7.2	10.5	-4.1
27	2.1	-8.1	-1.1	-2.2
28	-2.7	9.4	6.0	-3.1
29	-1.9	-10.0	-5.8	0.6
30	-3.5	-1.2	1.0	2.1
31	8.1	-2.4	5.9	3.4
32	-11.7	-13.5	12.9	-2.5
33	17.1	-8.8	4.8	-16.3
34	5.9	-7.6	1.7	-18.9
35	15.7	-6.7	1.0	21.9
36	-1.0	-20.5	-5.4	-1.5
37	15.9	-10.7	-7.4	-13.8
38	-14.6	-7.0	15.1	-2.9
39	-12.4	-4.5	7.6	-16.1
40	-0.2	25.5	10.1	-2.0

	X'	Y'	X''	Y''
41	3.5	-6.6	-14.5	4.9
42	-5.7	4.8	8.6	-10.3
43	-6.7	3.5	23.1	-5.2
44	6.2	-16.5	4.5	-3.4
45	-8.2	-16.2	-10.2	-2.3
46	7.2	-32.3	10.7	-13.7
47	5.9	-6.0	1.7	9.0
48	10.7	-19.0	-0.6	-7.6
49	-8.0	3.0	-4.3	-1.4
50	-3.4	6.1	6.2	-7.3
51	-26.7	-6.5	2.1	7.4
52	17.7	4.2	17.8	-8.4
53	20.0	1.6	-1.7	-1.7
54	-9.7	3.6	0.8	-2.7
55	-4.2	-20.4	10.2	2.6
56	-1.0	2.4	-22.4	-5.9
57	4.4	3.3	2.6	8.6
58	10.8	-7.7	28.3	6.9
59	-7.4	16.8	-3.1	-6.5
60	-0.7	-15.2	-3.9	8.1
61	-12.6	12.6	12.9	17.5
62	-7.9	6.4	-19.0	0.3
63	-4.5	2.8	-4.1	3.7
64	3.2	-1.0	-5.8	-1.4
65	0.8	0.8	-7.2	-29.3
66	8.4	-2.0	5.5	-19.4
67	-1.2	-5.7	-12.6	-0.6
68	-4.8	-6.8	14.8	3.5
69	10.8	0.5	6.3	6.3
70	-6.5	11.3	-0.4	5.4
71	3.2	0.6	17.3	1.1
72	-6.0	9.3	-3.2	17.4
73	4.6	27.6	7.8	-6.0
74	-5.7	3.4	0.4	3.5
75	8.5	2.2	-22.5	-8.1
76	10.2	9.0	0.3	-0.7
77	-13.9	-8.3	-6.1	16.7
78	-0.5	24.1	-0.6	5.7
79	11.8	-10.0	7.1	-7.8
80	-4.2	0.2	10.0	13.5

Table 3.4-1

$$\chi^2 = \sum_{i=1}^{k} \frac{(o_i - e_i)^2}{e_i} = 5,56 \qquad (3.4.5)$$

where

k = number of classes = 10

The degrees of freedom are

f = k-3 = 7

and with

$\chi^2_{99,5/7} = 20,3$ and $\chi^2_{0,5/7} = 0,99$

we have

$$20,3 < 5,56 < 0,99$$

Thus all tests for the sample are satisfactory and it can be assumed that the generated values simulate closely a real observation situation. The generated values are listed in Table 3.4-1.

3.5 SPACE INTERSECTION

The relative position of two points in space can be expressed in polar co-ordinates as well as cartesian rectangular co-ordinates.

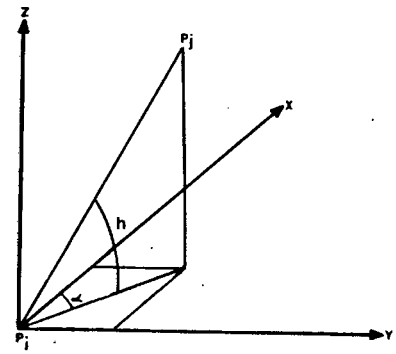

Fig. 3.5-1 Polar and cartesian co-ordinates of space points

The two co-ordinate systems are related by

$$(X_j - X_i) = \ell_{ij} \cos h_{ij} \cos \alpha_{ij} \qquad (3.5.1)$$

$$(Y_j - Y_i) = \ell_{ij} \cos h_{ij} \sin \alpha_{ij} \qquad (3.5.2)$$

$$(Z_j - Z_i) = \ell_{ij} \sin h_{ij} \qquad (3.5.3)$$

with ℓ_{ij} = distance P_i-P_j

α_{ij} = horizontal direction (counted clockwise from positive X-axis)

h_{ij} = elevation angle

If the X,Y,Z system is the usual gravity related co-ordinate system then angle α_{ij} and h_{ij} can be observed with a theodolite set up over point P_i.

The position of a point in space is defined by two oriented horizontal directions α measured at two known points to the new point and by one vertical angle h measured at one of the two points.

Normally more than the minimum number of three angles is observed to fix a point in space and the most probable co-ordinate values can be found in a least squares adjustment.

Condition equations required for the least squares adjustment can be conveniently formulated by combining equations (3.5.1) and (3.5.3):

$$\frac{X_j - X_i}{Z_j - Z_i} = \frac{\Delta X_{ij}}{\Delta Z_{ij}} = \frac{\cos h_{ij} \cos \alpha_{ij}}{\sin h_{ij}} \qquad (3.5.4)$$

and from (3.5.2) and (3.5.3)

$$\frac{Y_j - Y_i}{Z_j - Z_i} = \frac{\Delta Y_{ij}}{\Delta Z_{ij}} = \frac{\cos h_{ij} \sin \alpha_{ij}}{\sin h_{ij}} \qquad (3.5.5)$$

The third ratio which can be formulated by combining equations (3.5.1) and (3.5.2)

$$\frac{X_j - X_i}{Y_j - Y_i} = \frac{\cos \alpha_{ij}}{\sin \alpha_{ij}}$$

is already contained in equations (3.5.4) and (3.5.5) as can be shown by dividing (3.5.4) by (3.5.5).

Each pair of observed horizontal and vertical angles gives rise to a pair of condition equations of type (3.5.4) and (3.5.5). Re-arranging the two condition equations and introducing an orientation unknown δ_i we obtain

$$\Delta X_{ij} \sin h_{ij} - \Delta Z_{ij} \cos h_{ij} \cos (\alpha_{ij} - \delta_i) = 0 \qquad (3.5.4.1)$$

and

$$\Delta Y_{ij} \sin h_{ij} - \Delta Z_{ij} \cos h_{ij} \sin (\alpha_{ij} - \delta_i) = 0 \qquad (3.5.5.1)$$

For a least squares adjustment the condition equations must contain unknowns and observations in a linear form and (3.5.4.1) and (3.5.5.1) need to be differentiated with respect to the observations α and h and to the unknown X_i, Y_i, Z_i, X_j, Y_j and Z_j.

This leads to the general, linearised form of the condition equations (3.5.4) and (3.5.5):

$$a_{ij_1} v_{\alpha_{ij}} + a_{ij_2} v_{h_{ij}} + A_{a_{ij}} dX_j + B_{a_{ij}} dY_j + C_{a_{ij}} dZ_j - A_{a_{ij}} dX_i - B_{a_{ij}} dY_i - C_{a_{ij}} dZ_i - a_{ij} d\delta_i + w_{a_{ij}} = 0 \qquad (3.5.6)$$

$$b_{ij_1} v_{\alpha_{ij}} + b_{ij_2} v_{h_{ij}} + A_{b_{ij}} dX_j + B_{b_{ij}} dY_j + C_{b_{ij}} dZ_j - A_{b_{ij}} dX_i - B_{b_{ij}} dY_i - C_{b_{ij}} dZ_i - b_{ij} d\delta_i + w_{b_{ij}} = 0 \qquad (3.5.7)$$

with

$$a_{ij_1} = \cos h_{ij} \sin (\alpha_{ij} - \delta_i)\Delta Z_{ij}|_o \qquad (3.5.8.1)$$

$$a_{ij_2} = \sin h_{ij} \cos (\alpha_{ij} - \delta_i)\Delta Z_{ij} + \cos h_{ij}\Delta X_{ij}|_o \qquad (3.5.8.2)$$

$$b_{ij_1} = -\cos h_{ij} \cos (\alpha_{ij} - \delta_i)\Delta Z_{ij}|_o \qquad (3.5.8.3)$$

$$b_{ij_2} = \sin h_{ij} \sin (\alpha_{ij} - \delta_i)\Delta Z_{ij} + \cos h_{ij}\Delta Y_{ij}|_o \qquad (3.5.8.4)$$

$$A_{a_{ij}} = \sin h_{ij}|_o \qquad (3.5.8.5)$$

$$B_{a_{ij}} = 0 \qquad (3.5.8.6)$$

$$C_{a_{ij}} = -\cos h_{ij} \cos (\alpha_{ij} - \delta_i)|_o \qquad (3.5.8.7)$$

$$A_{b_{ij}} = 0 \qquad (3.5.8.8)$$

$$B_{b_{ij}} = \sin h_{ij}|_o \qquad (3.5.8.9)$$

$$C_{b_{ij}} = -\cos h_{ij} \sin (\alpha_{ij} - \delta_i)|_o \qquad (3.5.8.10)$$

$$w_{a_{ij}} = \Delta X_{ij} \sin h_{ij} - \Delta Z_{ij} \cos h_{ij} \cos (\alpha_{ij} - \delta_i)|_o \qquad (3.5.8.11)$$

$$w_{b_{ij}} = \Delta Y_{ij} \sin h_{ij} - \Delta Z_{ij} \cos h_{ij} \sin (\alpha_{ij} - \delta_i)|_o \qquad (3.5.8.12)$$

More than one observation is contained in each of the equations (3.5.6) and (3.5.7) in addition to the unknown co-ordinate values. The two condition equations must therefore be adjusted in the "combined case" of the least squares adjustment, where the condition equation has the form (3.2.4)

$$\underline{\underline{B}}\underline{v} + \underline{\underline{A}}\underline{x} + \underline{w} = \underline{0}$$

All relevant formulae for the solution of the space intersection adjustment are listed in Table 3.3-1.

The three dimensional space intersection calculation was adopted for the determination of point positions in space in the case of the testfield survey (Chapter 5) and for the survey of the external pupil position for the interior orientation (Chapter 7.1). The space intersection was given preference over the usual separation of the height determination from the plane position calculation. It was hoped that the inclusion of the vertical angle measurement into the calculation of the plane position might result in a more homogeneous distribution of observation errors over the three space co-ordinates of a point. No comparative investigations were carried out to support this choice of method, but the exceptionally high precision of a few tenths of a millimeter achieved in the testfield and in the external pupil determination is in itself a justification for the choice.

The observing method, which was adopted for the determination of three-dimensional co-ordinates of the close-range test field, makes it possible to simplify considerably the space intersection adjustment described above. All 80 points of the test field were observed from three solid steel tripods. The positions of the tripods were established by means of a free triangulation-trilateration network adjustment based on observations with a single second theodolite, micrometer rods (PAV rods) and forced centering equipment. The adjustment of the three base points resulted in standard deviations of less than 0,1 mm. Fig. 3.5-2 shows the position of

the base points; the two outer points were subsequently used as camera stations for the deformation test described later. Forced centering was maintained for the observations of the test field points and the theodolite at each of the three stations was repeatedly oriented on the other two base points.
Distances from the theodolite to the 80 identical targets varied between 3 and 7 metres thus providing practically equal observation conditions for all points.

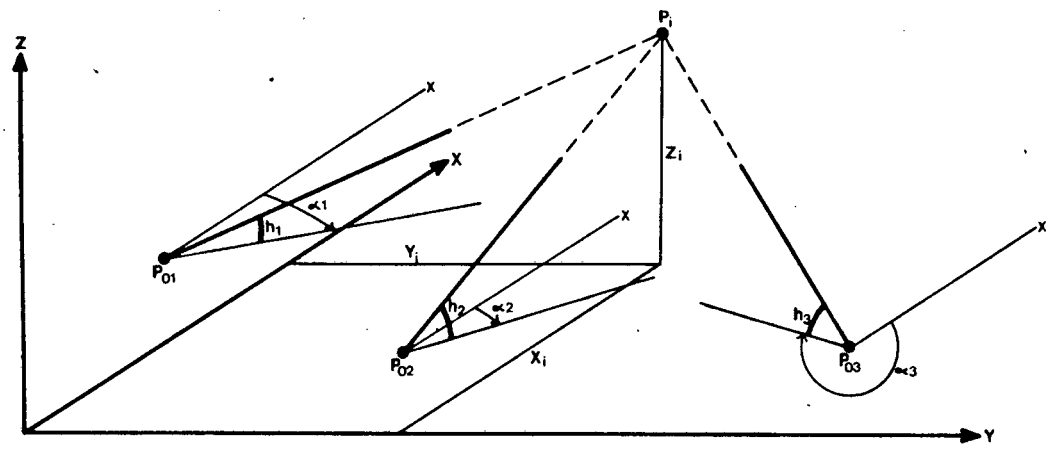

Fig. 3.5-2 Base Points for Space Intersection of Test-field Points

On the basis of this observing design the following three assumptions may be made whereby the computation requirements for the adjustment can be greatly reduced.

I. Base points P_{o1}, P_{o2} and P_{o3} are practically error free and therefore we have $dX_i = dY_i = dZ_i = 0$ in (3.5.6) and (3.5.7).

II. All observations are error free oriented before the adjustment and no orientation unknowns occur in (3.5.6) and (3.5.7) $\delta_i = 0$.

III. All observations have equal weight

On the basis of these assumptions, the condition equation system for the determination of a single new point P_i has the following coefficients in matrices $\underline{B}$ and $\underline{A}$:

$v_{\alpha_{1i}}$	$v_{h_{1i}}$	$v_{\alpha_{2i}}$	$v_{h_{2i}}$	$v_{\alpha_{3i}}$	$v_{h_{3i}}$	dX_i	dY_i	dZ_i	w
a_{1i_1}	a_{1i_2}	0	0	0	0	$\sin h_{1i}$	0	$C_{a_{1i}}$	$w_{a_{1i}}$
b_{1i_1}	b_{1i_2}	0	0	0	0	0	$\sin h_{1i}$	$C_{b_{1i}}$	$w_{b_{1i}}$
0	0	a_{2i_1}	a_{2i_2}	0	0	$\sin h_{2i}$	0	$C_{a_{2i}}$	$w_{a_{2i}}$
0	0	b_{2i_1}	b_{2i_2}	0	0	0	$\sin h_{2i}$	$C_{b_{2i}}$	$w_{b_{2i}}$
0	0	0	0	a_{3i_1}	a_{3i_2}	$\sin h_{3i}$	0	$C_{a_{3i}}$	$w_{a_{3i}}$
0	0	0	0	b_{3i_1}	b_{3i_2}	0	$\sin h_{3i}$	$C_{b_{3i}}$	$w_{b_{3i}}$
$\underline{B}$						$\underline{A}$			$\underline{w}$

The normal equation for the combined case can, with (3.2.14), be written as:

$$\begin{bmatrix} \underline{B}\underline{B}^T & \underline{A} \\ \underline{A}^T & \underline{0} \end{bmatrix} \begin{bmatrix} \underline{K} \\ \underline{x} \end{bmatrix} + \begin{bmatrix} \underline{w} \\ \underline{0} \end{bmatrix} = \begin{bmatrix} \underline{0} \\ \underline{0} \end{bmatrix}$$

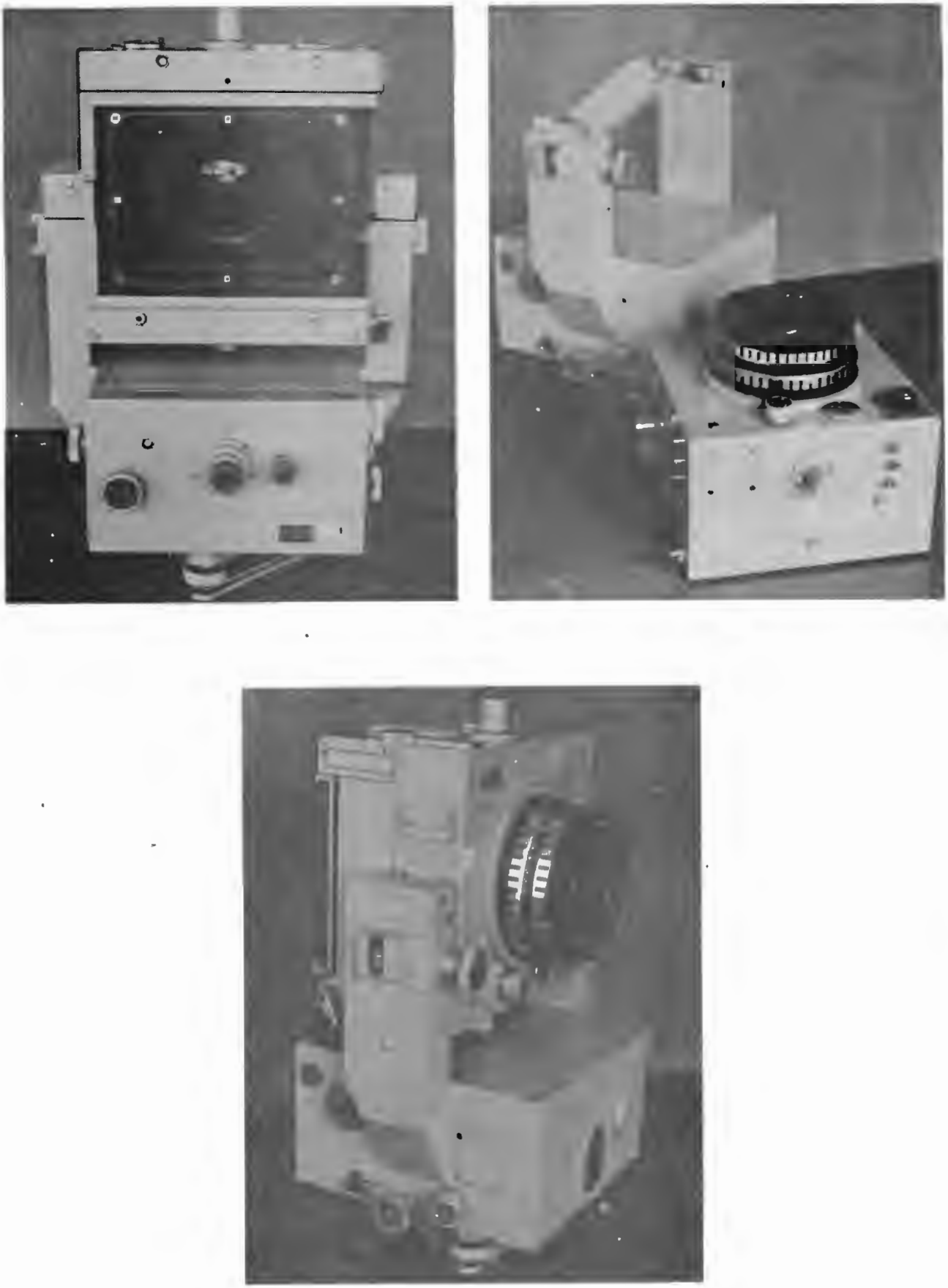

Fig. 4.4-2 Views of a UMK 10/1318 camera showing the camera with its theodolite mounting, the fiducial marks and the axis studs

Fig. 4.2-1 Tektronix 4050 computer system consisting of (from left to right) digitiser tablet and digitiser control unit, central processing unit with VDU, line printer, file manager and plotter

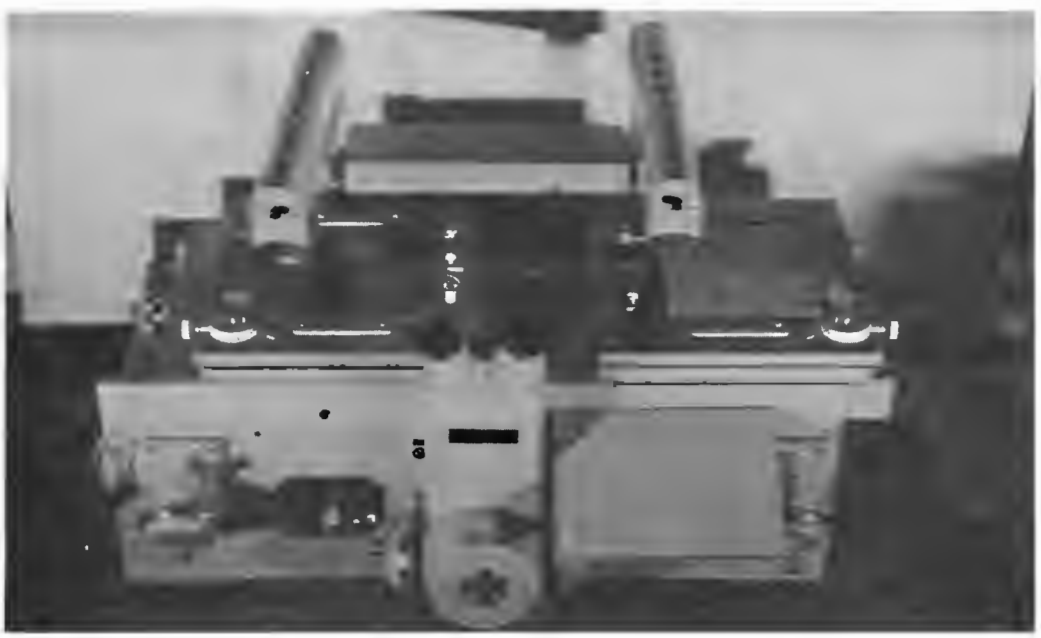

Fig. 4.3-1 STEKO 1818

of correlations reduces the size of adjustment matrices considerably and makes it possible to adjust each test field point individually. This can easily be confirmed when inspecting the example of a normal equation system (3.2.14) and its inverse for a situation with two new points fixed from the same three error free base points:

$$\underbrace{\left[\begin{array}{cc|cc} \underline{C}_I & \underline{0} & \underline{A}_I & \underline{0} \\ \underline{0} & \underline{C}_{II} & \underline{0} & \underline{A}_{II} \\ \hline \underline{A}_I^T & \underline{0} & \multicolumn{2}{c}{\multirow{2}{*}{$\underline{0}$}} \\ \underline{0} & \underline{A}_{II}^T & & \end{array}\right]}_{\underline{D}} \left[\begin{array}{c} \underline{k}_I \\ \underline{k}_{II} \\ \underline{x}_I \\ \underline{x}_{II} \end{array}\right] + \left[\begin{array}{c} \underline{w}_I \\ \underline{w}_{II} \\ \underline{0} \\ \underline{0} \end{array}\right] = \left[\begin{array}{c} \underline{0} \\ \underline{0} \\ \underline{0} \\ \underline{0} \end{array}\right] \qquad (3.5.12)$$

Submatrices in (3.5.12) are of the form given in (3.5.10) and (3.5.11) with indices "I" and "II" referring to new points P_I and P_{II} respectively.

Applying the rules for the inversion of partitioned matrices we obtain for the inverse of $\underline{D}$ in equation (3.5.12)

$$\underline{D}^{-1} = \left[\begin{array}{cc} \underline{E}_{11} & \underline{E}_{12} \\ \underline{E}_{21} & \underline{E}_{22} \end{array}\right] \qquad (3.5.13)$$

with

$$\underline{E}_{11} = \left[\begin{array}{cc} \underline{C}_I^{-1} - \underline{C}_I^{-1}\underline{A}_I (\underline{A}_I^T \underline{C}_I^{-1} \underline{A}_I)^{-1} \underline{A}_I^T \underline{C}_I^{-1} & \underline{0} \\ \underline{0} & \underline{C}_{II}^{-1} - \underline{C}_{II}^{-1}\underline{A}_{II} (\underline{A}_{II}^T \underline{C}_{II}^{-1} \underline{A}_{II})^{-1} \underline{A}_{II}^T \underline{C}_{II}^{-1} \end{array}\right] \qquad (3.5.13.1)$$

$$\underline{E}_{12} = \begin{bmatrix} \underline{C}_I^{-1}\underline{A}_I \ (\underline{A}_I^T \underline{C}_I^{-1}\underline{A}_I)^{-1} & \underline{0} \\ \underline{0} & \underline{C}_{II}^{-1}\underline{A}_{II}(\underline{A}_{II}^T\underline{C}_{II}^{-1}\underline{A}_{II})^{-1} \end{bmatrix} \qquad (3.5.13.2)$$

$$\underline{E}_{21} = \begin{bmatrix} (\underline{A}_I^T \underline{C}_I^{-1}\underline{A}_I)^{-1}\underline{A}_I^T \underline{C}_I^{-1} & \underline{0} \\ \underline{0} & (\underline{A}_{II}^T\underline{C}_{II}^{-1}\underline{A}_{II})^{-1}\underline{A}_{II}^T\underline{C}_{II}^{-1} \end{bmatrix} \qquad (3.5.13.3)$$

where $\underline{E}_{21} = \underline{E}_{12}^T$

$$\underline{E}_{22} = \begin{bmatrix} -(\underline{A}_I^T \underline{C}_I^{-1}\underline{A}_I)^{-1} & \underline{0} \\ \underline{0} & -(\underline{A}_{II}^T\underline{C}_{II}^{-1}\underline{A}_{II})^{-1} \end{bmatrix} \qquad (3.5.13.4)$$

Indicating non-zero submatrices with a bar symbol (-) we get for the inverse of $\underline{D}$:

$$\underline{D}^{-1} = \begin{array}{c} \begin{matrix} \underline{k}_I & \underline{k}_{II} & \underline{x}_I & \underline{x}_{II} \end{matrix} \\ \begin{bmatrix} - & 0 & - & 0 \\ 0 & - & 0 & - \\ - & 0 & - & 0 \\ 0 & - & 0 & - \end{bmatrix} \end{array} \begin{matrix} \underline{k}_I \\ \underline{k}_{II} \\ \underline{x}_I \\ \underline{x}_{II} \end{matrix} \qquad (3.5.14)$$

From (3.5.14) it is obvious that no correlations exist between the two points and that therefore points can be adjusted individually. This proof can obviously be extended to any number of new points. A numerical example of a single point three dimensional intersection adjustment is shown in Table 3.5-1.

ADJUSTMENT OF SPACE INTERSECTION

BASE POINTS

	X	Y	Z	ORIEN. CORR.
PLAR L	10.0010	10.0000	10.0000	331 52 3
PLAR M	9.9990	8.2980	9.9962	331 52 59
PLAR R	10.0030	6.6550	10.0011	331 52 27

	C. LEFT	C. RIGHT	DIFF.	MEAN	ORIENTED
PLAR L	213 8 19	33 8 25	-6	213 8 22	185 0 25
	109 17 13	250 42 33	-14	109 17 20	
PLAR M	188 12 21	8 12 26	-5	188 12 23	160 5 22
	108 14 23	251 45 23	-14	108 14 30	
PLAR R	169 37 10	349 37 11	-1	169 37 10	141 29 37
	105 22 32	254 37 19	-9	105 22 37	

DIRECTIONS

185 0 25 160 5 22 141 29 37

VERT. ANGLES

109 17 20 108 14 30 105 22 37

PROV. CO-ORDINATES OF 31

6.2155 9.6684 8.6701

CORR. 1. ITERATION

0.0000 0.0000 -0.0001

6.2156 9.6684 8.6700

CORR. 2. ITERATION

0.0000 0.0000 0.0000

6.2156 9.6684 8.6700

ADJUSTED CO-ORDINATES OF 31	6.2156	9.6684	8.6700
STANDARD DEVIATION	0.0001	0.0001	0.0001

CORRECTIONS

	DIRECTIONS	VERTICAL ANGLES
PLAR L	0.1	-3.8
PLAR M	0.6	5.3
PLAR R	-0.3	-1.5

FINAL CHECK

185 0 25	185 0 25	0.00	109 17 24	109 17 24	0.00
160 5 23	160 5 23	0.00	108 14 25	108 14 25	0.00
141 29 37	141 29 37	0.00	105 22 38	105 22 38	0.00

Table 3.5-1

3.6 TRANSFORMATION OF OBSERVED PLATE CO-ORDINATES TO IMAGE CO-ORDINATE SYSTEM

Plate co-ordinates observed on a comparator are generally not reduced to the principal point of the image plane as required in the relative orientation calculation. Observed plate co-ordinates must therefore be transformed into the image co-ordinate system (Fig. 3.6-1) before they can be introduced into a relative orientation adjustment.

The origin of the image system, the principal point, is physically defined by the intersection of the lines joining opposite fiducial marks, which must be observed in the same system as the image points. The line defined by the left and right fiducial mark is the $\bar{x}$ axis of the image co-ordinate system. It cannot be assumed that the fiducial mark system is perfectly rectangular and the top-to-bottom line cannot in general serve as the $\bar{y}$-axis. Also one cannot surmise that the plate is mounted exactly parallel to the comparator axes and a possible deviation from parallelism must be allowed for in the transformation.

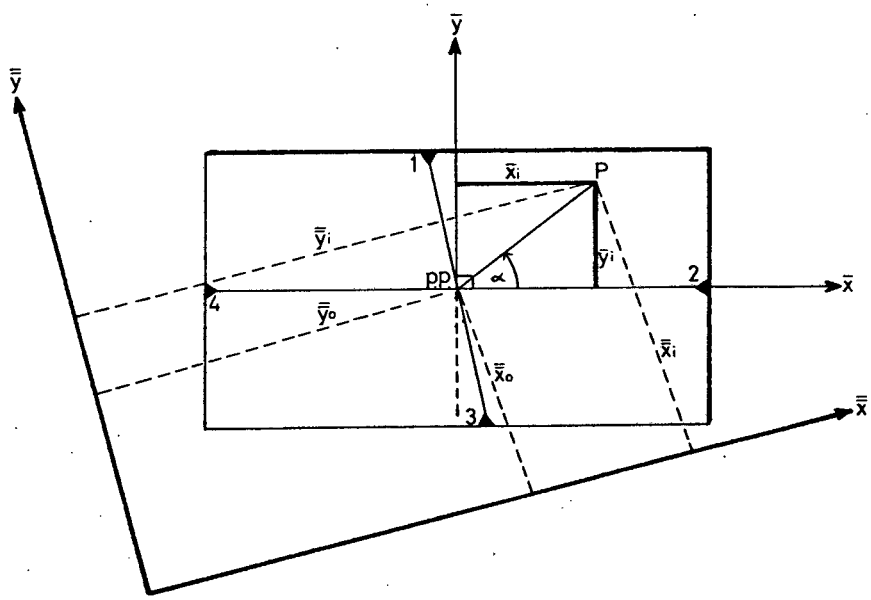

Fig. 3.6-1 Image Co-ordinate System in Relation to Comparator System

$\bar{\bar{x}}_i$, $\bar{\bar{y}}_i$ co-ordinates in the comparator system

$\bar{x}_i$, $\bar{y}_i$ co-ordinates in the image system

$\bar{x}_o$, $\bar{y}_o$ and $\bar{\bar{x}}_o$, $\bar{\bar{y}}_o$ co-ordinates of the principal point in image and comparator system respectively. $\bar{x}_o$ and $\bar{y}_o$ are equal to zero.

First the principal point position must be evaluated. The line connecting the top fiducial mark ($\bar{\bar{x}}_1$, $\bar{\bar{y}}_1$) with the bottom mark ($\bar{\bar{x}}_3$, $\bar{\bar{y}}_3$) is given by the expression

$$\bar{\bar{y}} = \bar{\bar{y}}_1 + \frac{\bar{\bar{y}}_3 - \bar{\bar{y}}_1}{\bar{\bar{x}}_3 - \bar{\bar{x}}_1} \bar{\bar{x}} - \frac{\bar{\bar{y}}_3 - \bar{\bar{y}}_1}{\bar{\bar{x}}_3 - \bar{\bar{x}}_1} \bar{\bar{x}}_1 \qquad (3.6.1)$$

and analogously the line between left and right fiducial mark

$$\bar{\bar{y}} = \bar{\bar{y}}_2 + \frac{\bar{\bar{y}}_4 - \bar{\bar{y}}_2}{\bar{\bar{x}}_4 - \bar{\bar{x}}_2} \bar{\bar{x}} - \frac{\bar{\bar{y}}_4 - \bar{\bar{y}}_2}{\bar{\bar{x}}_4 - \bar{\bar{x}}_2} \bar{\bar{x}}_2 \qquad (3.6.2)$$

If equations (3.6.1) and (3.6.2) are rearranged to take the general form

$$A\bar{\bar{x}} + B\bar{\bar{y}} + C = 0 \qquad (3.6.3)$$

then the intersection ($\bar{\bar{x}}_o$, $\bar{\bar{y}}_o$) is easily obtained from

$$\bar{\bar{x}}_o = \frac{\begin{bmatrix} B_1 & C_1 \\ B_2 & C_2 \end{bmatrix}}{\begin{bmatrix} A_1 & B_1 \\ A_2 & B_2 \end{bmatrix}} \quad \text{and} \quad \bar{\bar{y}}_o = \frac{\begin{bmatrix} A_1 & C_1 \\ A_2 & C_2 \end{bmatrix}}{\begin{bmatrix} A_1 & B_1 \\ A_2 & B_2 \end{bmatrix}} \qquad (3.6.4)$$

$$\text{or} \qquad \bar{\bar{y}}_o = \bar{\bar{y}}_1 + \frac{\bar{\bar{y}}_3 - \bar{\bar{y}}_i}{\bar{\bar{x}}_3 - \bar{\bar{x}}_i} (\bar{\bar{x}}_o - \bar{\bar{x}}_3) \qquad (3.6.5)$$

$$\text{with } A_1 = \frac{\bar{\bar{y}}_3 - \bar{\bar{y}}_1}{\bar{\bar{x}}_3 - \bar{\bar{x}}_1} \qquad A_2 = \frac{\bar{\bar{y}}_4 - \bar{\bar{y}}_2}{\bar{\bar{x}}_4 \quad \bar{\bar{x}}_2} \tag{3.6.6}$$

$$B_1 = -1 \qquad B_2 = -1 \tag{3.6.7}$$

$$C_1 = -\frac{\bar{\bar{y}}_3 - \bar{\bar{y}}_1}{\bar{\bar{x}}_3 - \bar{\bar{x}}_1}\bar{\bar{x}}_1 + \bar{\bar{y}}_1 \qquad C_2 = -\frac{\bar{\bar{y}}_4 - \bar{\bar{y}}_2}{\bar{\bar{x}}_4 - \bar{\bar{x}}_2}\bar{\bar{x}}_2 + \bar{\bar{y}}_2 \tag{3.6.8}$$

For the transformation of individual points from the comparator system to the image system one now has for a point P_i:

$$\begin{aligned} \bar{x}_i &= d_{oi} \cos \alpha_i \\ \bar{y}_i &= d_{oi} \sin \alpha_i \end{aligned} \tag{3.6.9}$$

where $\alpha = t_o^i - t_4^2$

t_o^i = direction from principal point to P_i:

$$t_o^i = \tan^{-1} \frac{\bar{\bar{y}}_i - \bar{\bar{y}}_o}{\bar{\bar{x}}_1 - \bar{\bar{x}}_o} \tag{3.6.10}$$

t_4^2 = direction of left-to-right fiducial mark line

$$t_4^2 = \tan^{-1} \frac{\bar{\bar{y}}_4 - \bar{\bar{y}}_2}{\bar{\bar{x}}_4 - \bar{\bar{x}}_2} \tag{3.6.11}$$

and d_{oi} = distance between principal point and P_i:

$$d_{oi} = \left((\bar{\bar{y}}_i - \bar{\bar{y}}_o)^2 + (\bar{\bar{x}}_i - \bar{\bar{x}}_o)^2 \right)^{\frac{1}{2}} \tag{3.6.12}$$

The "horizontal" fiducial mark line is not necessarily truly horizontal - even if the camera is perfectly level - owing to possible inaccurate positioning of the fiducial marks in the camera or to observation errors in the comparator co-ordinates of the fiducial marks.

Any such error has no ill-effect on the final model co-ordinates as it will only introduce a "false" additional κ to the rotation about the $\bar{z}$ axis.

Non-metric cameras have no fiducial marks, except where these are especially added by their users for photogrammetric application. The writer obtained satisfactory results (Tab.8-3) by simply observing points approximately in the centre of the four image edges and by accepting the mean of the $\bar{\bar{x}}$-values of the left and right edge for $\bar{\bar{x}}_o$ and the $\bar{\bar{y}}$- values of top and bottom edge for $\bar{\bar{y}}_o$.

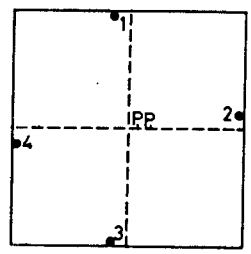

Fig. 3.6-2 Principal Point Definition for Non-metric Camera Image

$$\bar{\bar{x}}_o = \frac{\bar{\bar{x}}_2 + \bar{\bar{x}}_4}{2} \qquad \bar{\bar{y}}_o = \frac{\bar{\bar{y}}_1 + \bar{\bar{y}}_3}{2} \tag{3.6.13}$$

4. EQUIPMENT

Of the equipment used in the course of this investigation, only the cameras, the computer system and the stereo comparator will be described briefly.

4.1 Tektronix 4050 Mini computer System

All algorithms described in this thesis can be realised in mini computers with memory capacities of more than say 10k bytes. The computations for this thesis were executed on a Tektronix 4050 system consisting of (Fig. 4.2-1):

i) Central Processing Unit Tektronix 4051 Graphic System

With a 32k bytes memory and a memory allocation of 8 bytes for each array variable. The C.P.U. is equipped with a high resolution graphics screen and understands the 4051 Graphic System BASIC language. The numeric accuracy of the unit is 14 digits.

ii) Tally Line-Printer

iii) Tektronix 4662 Interactive Digital Plotter

The active plotting area of the plotter is 25,4 cm by 38,1 cm with a claimed resolution of 0,06 mm. The deformation plots and deformation stereograms were produced with the aid of the plotter.

iv) Tektronix 4907 Filemanager

This flexible disk storage system is designed for flexible disks with a storage capacity of 600k bytes.

v) Summagraphics Digitiser with I.D. Data Tablet

The accuracy of digitising is given as 0,1 mm.

Fig. 4.2-1 Tektronix 4050 computer system consisting of (from left to right) digitiser tablet and digitiser control unit, central processing unit with VDU, line printer, file manager and plotter

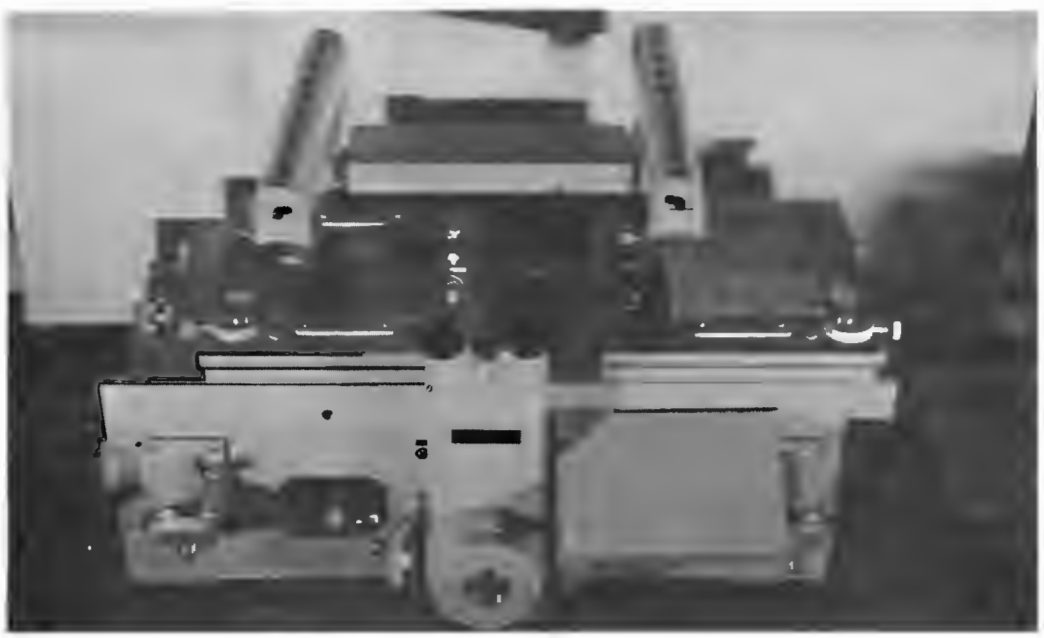

Fig. 4.3-1 STEKO 1818

4.2 TOPOCART STEREO PLOTTER CARL ZEISS JENA

In the initial stages of the study no stereo comparator was directly available to the writer and only occasional short time access was given to a ZEISS PSK stereo comparator with an accuracy of 1 to 2 μm. As a considerable amount of data acquisition from photographic images was envisaged, a different method had to be found to measure image co-ordinates. The solution was provided by a Topocart stereo plotter. After setting all rotations to their nominal zero positions image co-ordinates of single plates were observed on the stereo plotter. As it could not be assumed that all rotation had been fully removed a high precision gridplate was observed each time the plotter was used as a comparator. The observed co-ordinates $\bar{\bar{x}}$, $\bar{\bar{y}}$ of 9 gridpoints were then transformed into the known values of these grid intersections by means of a projective transformation.

$$x = \frac{a_1\bar{\bar{x}}+b_1\bar{\bar{y}}+c_1}{a_3\bar{\bar{x}}+b_3\bar{\bar{y}}+1} \qquad (4.2.1.1)$$

and

$$y = \frac{a_2\bar{\bar{x}}+b_2\bar{\bar{y}}+c_2}{a_3\bar{\bar{x}}+b_3\bar{\bar{y}}+1} \qquad (4.2.1.2)$$

The a, b and c parameters derived in this transformation could then serve to transform the subsequently observed image co-ordinates of photographs into the distortion free grid system, provided, of course, that none of the instrument settings were changed between the observations of the grid plate and the photographs.

Equations (4.2.1.1) and (4.2.1.2) can be rearranged to obtain x and y in an explicit form as required for a least squares adjustment.

$$\bar{\bar{y}} = \frac{(y-c_2)(a_3x-a_1) - (x-c_1)(a_3y-a_2)}{(b_3x-b_1)(a_3y-a_2) - (b_3y-b_2)(a_3x-a_1)} \qquad (4.2.2.1)$$

$$\bar{\bar{x}} = \frac{(x-c_1)(b_3y-b_2) - (y-c_2)(b_3x-b_1)}{(a_3x-a_1)(b_3y-b_2) - (a_3y-a_2)(b_3x-b_1)} \qquad (4.2.2.2)$$

In this form the equations can be linearised with respect to the unknowns a_1, a_2, a_3, b_1, b_2, b_3, c_1, and c_2 and the unknowns as well as the corrections to the observations $\bar{\bar{x}}$ and $\bar{\bar{y}}$ can be determined in a parametric adjustment. To assess the feasibility of the use of the stereoplotter as a comparator, two sets of 100 image co-ordinates were observed five times and transformed to a grid as described above. In the first set, all points were well defined targets (Fig. 5-5), in the second set natural feature points were observed on images obtained in the course of the Wildlife photography described in Chapter 10. The standard deviation was determined from each set of the five observations for each point. The average standard deviation for the 500 observations of the first set was 11,6 µm while the 500 observations of the less well defined natural points yielded an average standard deviation of 13,4 µm. The same image points were also observed on the ZEISS PSK stereo comparator and root mean square errors for the deviations from the stereo plotter readings were 14,6 µm for the first set and 20,1 µm for the second set.

In conclusion one can say that an average reading accuracy of 15 µm can be expected when using the TOPOCART stereo plotter combined with a projective transformation to a precision grid.

4.3 STEREO COMPARATOR STEKO 1818

The modification of the stereo plotter to a comparator became unnecessary when a stereo comparator CARL ZEISS JENA STEKO 1818 (Fig. 4.3-1) was added to the existing close-range photogrammetric equipment. With the addition of the stereocomparator a fully self-contained analogue-analytical close-range system was established, consisting of stereo cameras, stereo plotter, stereo comparator, mini computer and a photographic laboratory.

The STEKO 1818 has a reading accuracy of 10 µm in x and y co-ordinates and 2 µm for px and py readings. A MOTRONIC electronic digital display unit connected to the comparator not only serves to display the results but also interfaces the comparator with a type-writer for permanent recording of the image co-ordinates.

A total of over 200 images of the test field was observed on the comparator. The majority of the photographs were obtained in the course of the shoulder height survey of elephants while approximately 20% of the images consisted of testfield photography.

The standard deviation a priori of observed image co-ordinates evaluated in the relative orientation adjustments of the more than 100 stereo pairs varied with impressive consistency between 11 µm and 14 µm for the elephant photography and between 6 µm and 8 µm for the test field images with their superior target definition.

These results show, as expected, that the stereo comparator's observation accuracy is superior to that of the stereo plotter. Nevertheless it can be sensibly suggested that a stereo plotter, when used as described above, may well serve to substitute for a comparator in cases where a minor accuracy loss is acceptable.

4.4 UNIVERSAL MEASURING CAMERAS UMK10/1318

A pair of ZEISS UMK10/1318 metric cameras was used for the majority of the investigations described in this study. The camera (Fig. 4.4-2) is mounted on a single second theodolite alidade and equipped with a near distortion free LAMEGON 8/100 lens system. The principal distance of the camera can be changed to allow focusing for distances from 3,6 m to infinity.

Some of the camera's specifications are:

Focal distance for infinity setting:	99 mm (approximately)
Distortion (focusing to infinity)	max. 5 µm
Average resolution:	55 lines/mm
Shutter speed:	1 sec. to 1/400 sec.
Stop setting:	8 to 32
Focus setting for distances:	∞; 25 m; 12 m; 8 m; 6 m; 5 m; 4,2 m; and 3,6 m.
Image size:	120 mm x 166 mm.

Field of view (Fig. 4.4-1) Long format (horizontal): 78°

Short format (vertical) : 58°

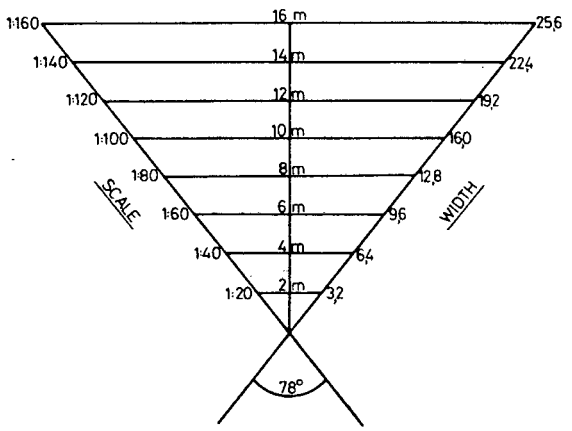

Horizontal field of view of Zeiss UMK 10/1318 Camera

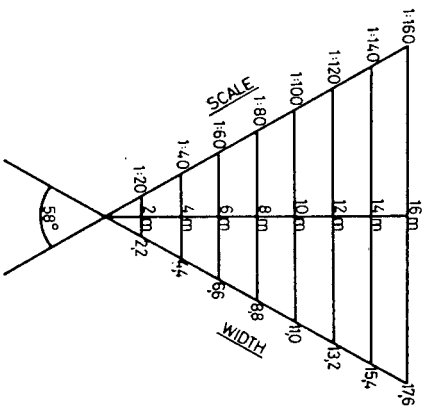

Vertical field of view of Zeiss UMK 10/1318 Camera

Fig. 4.4-1

A switchbox makes it possible to operate the shutters of two cameras simultaneously.

The calibration values for the principal distance of the two cameras are given by the manufacturer as:

Distance setting	P.D. (Camera 74)	P.D. (Camera 49)
	98,84 mm	99,09 mm
25 m	99,26 mm	99,52 mm
12 m	99,68 mm	99,95 mm
8 m	100,10 mm	100,37 mm
6 m	100,52 mm	100,80 mm
5 m	100,94 mm	101,23 mm
4,2 m	101,36 mm	101,66 mm
3,6 m	101,78 mm	102,08 mm

Tab. 4.4-1 Calibration Values for the Principal Distance of the UMK 10/1318 Cameras 74 and 49.

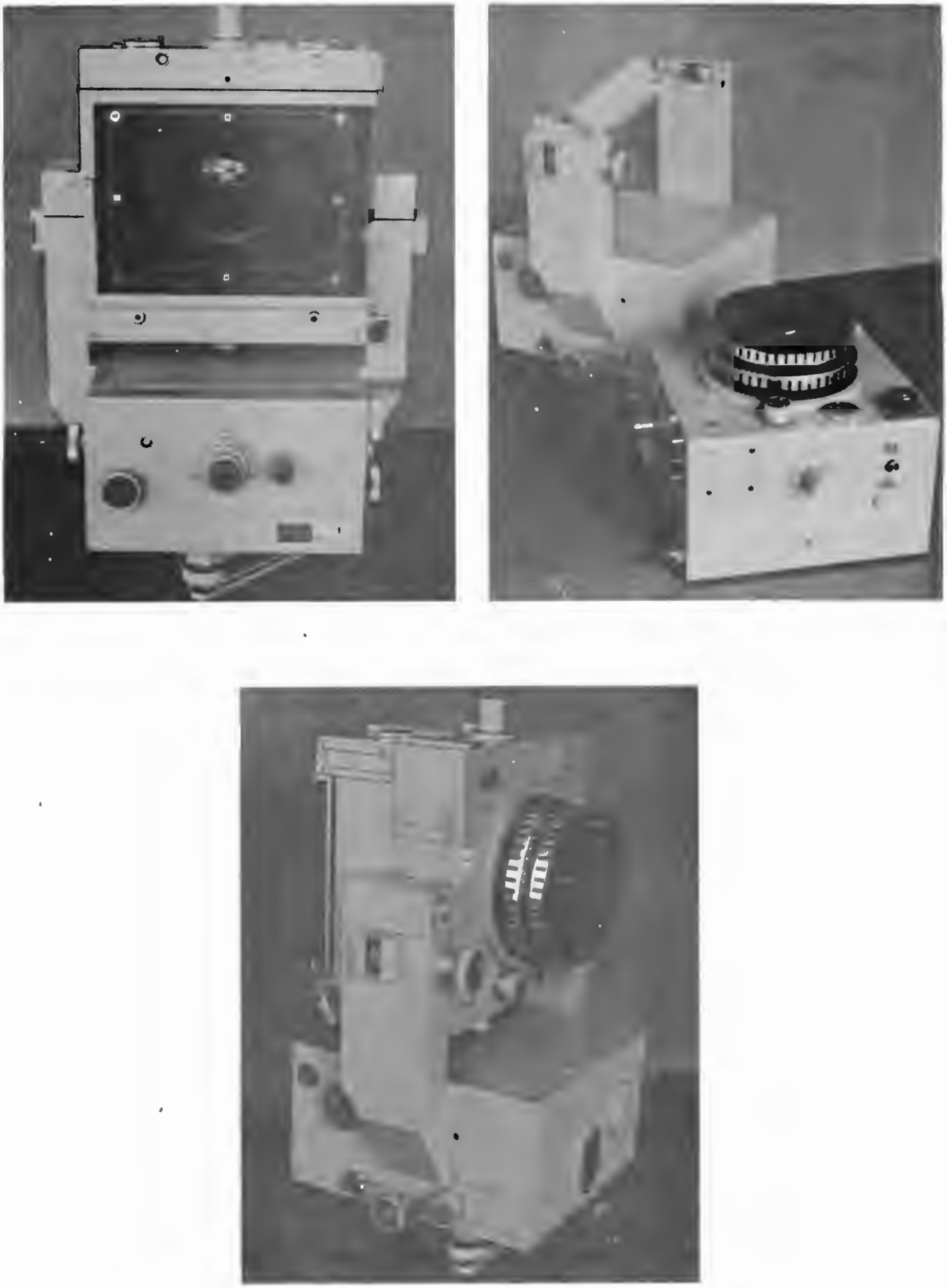

Fig. 4.4-2 Views of a UMK 10/1318 camera showing the camera with its theodolite mounting, the fiducial marks and the axis studs

Both cameras were re-calibrated for expected working distances of 12 m, 5 m and 3,6 m and their inner orientation elements were found to agree within 0,05 mm with the above listed calibration values. The principal distances as given by the manufacturers were therefore accepted for all calculations. The procedure employed to test the calibration values is discussed in a separate chapter.

Shutter speeds of the cameras were tested electronically and found to be:

Nominal shutter speed		Recorded shutter speed			
		Camera 74		Camera 49	
Sec	milli sec	milli sec	deviation	milli sec	deviation
1/15	67	54-67	-	defect	-
1/30	33	28-37	-	23-28,5	-
1/60	16,7	15,5	7%	23	38%
1/125	8	9	13%	10,5	31%
1/250	4	4,5	13%	6,5	63%
1/400	2,5	3,5	40%	4	60%

To ensure correct exposures the deviations from the normal shutter speed had to be taken into consideration when setting aperature and shutter speed.

Emulsion Carrier and Emulsion

The camera is designed to operate with glass plates as emulsion carriers. Although there can be no doubt that glass plates provide the best stability, it was shown that cut sheet film glued (with a UHU glue stick) to used glass plates provided the same accuracy for the final result in the form of model co-ordinates.

This was not true for cut roll film, where an accuracy loss was experienced due to imperfections in the flatness of the film glued to a glass plate. The flatness of glass plate was measured by means of a Tallysurf instrument and found to be better than 5 µm while deviations from flatness in the case of roll film can be larger than 0,1 mm.

The emulsions used were a black and white emulsion with an ASA rating of 400 in the case of the glass plates while the sheet film was black and white Kodak Tri X ortho film with an estimated ASA 320 rating.

5. CLOSE-RANGE PRECISION TEST FIELD

Test Field Description

A test field comprising of a number of well defined and symmetrically distributed points can be useful for the testing of mathematical models for close-range photogrammetry as well as for the calibration of metric and non-metric cameras.

Such a test field was established in a laboratory of the Department of Surveying at the University of Cape Town. The point configuration of the test field was designed to resemble a typical object space as found in close-range photogrammetry.

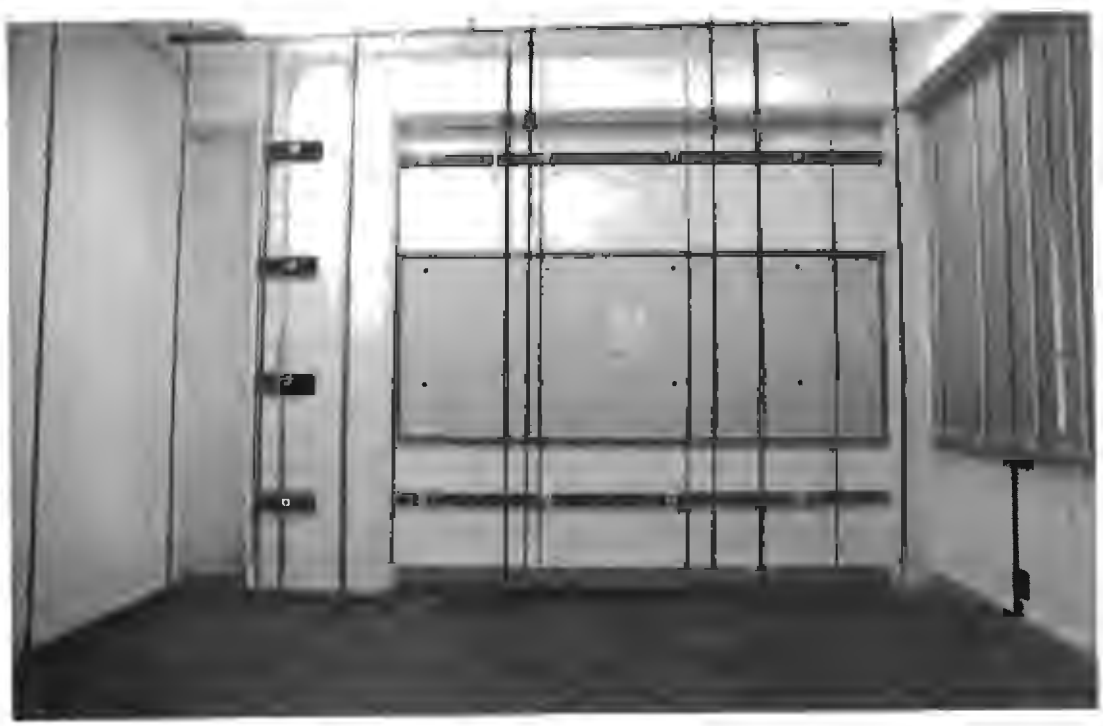

Fig. 5-1 Test Field

The test field dimensions are shown in Fig. 5-2. Overall views of the 80 point test field serve to illustrate further the design of

the field. A protruding section of the wall in the far left corner of the field (Points 1 to 4) disturbs the symmetry of the point distribution without reducing the efficiency of the test field for tests and calibration.

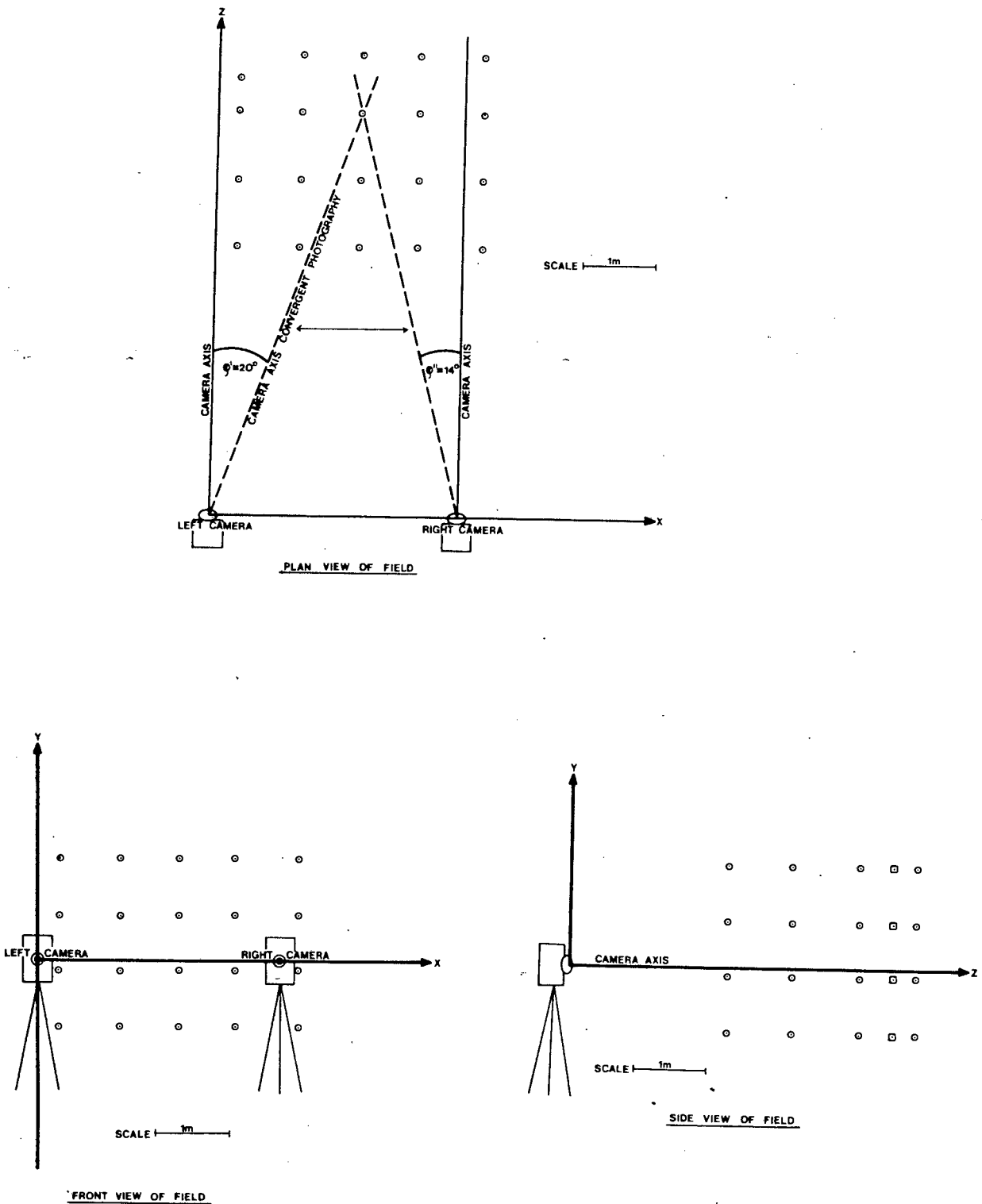

Fig. 5-2 Configuration of the Points of the Test Field

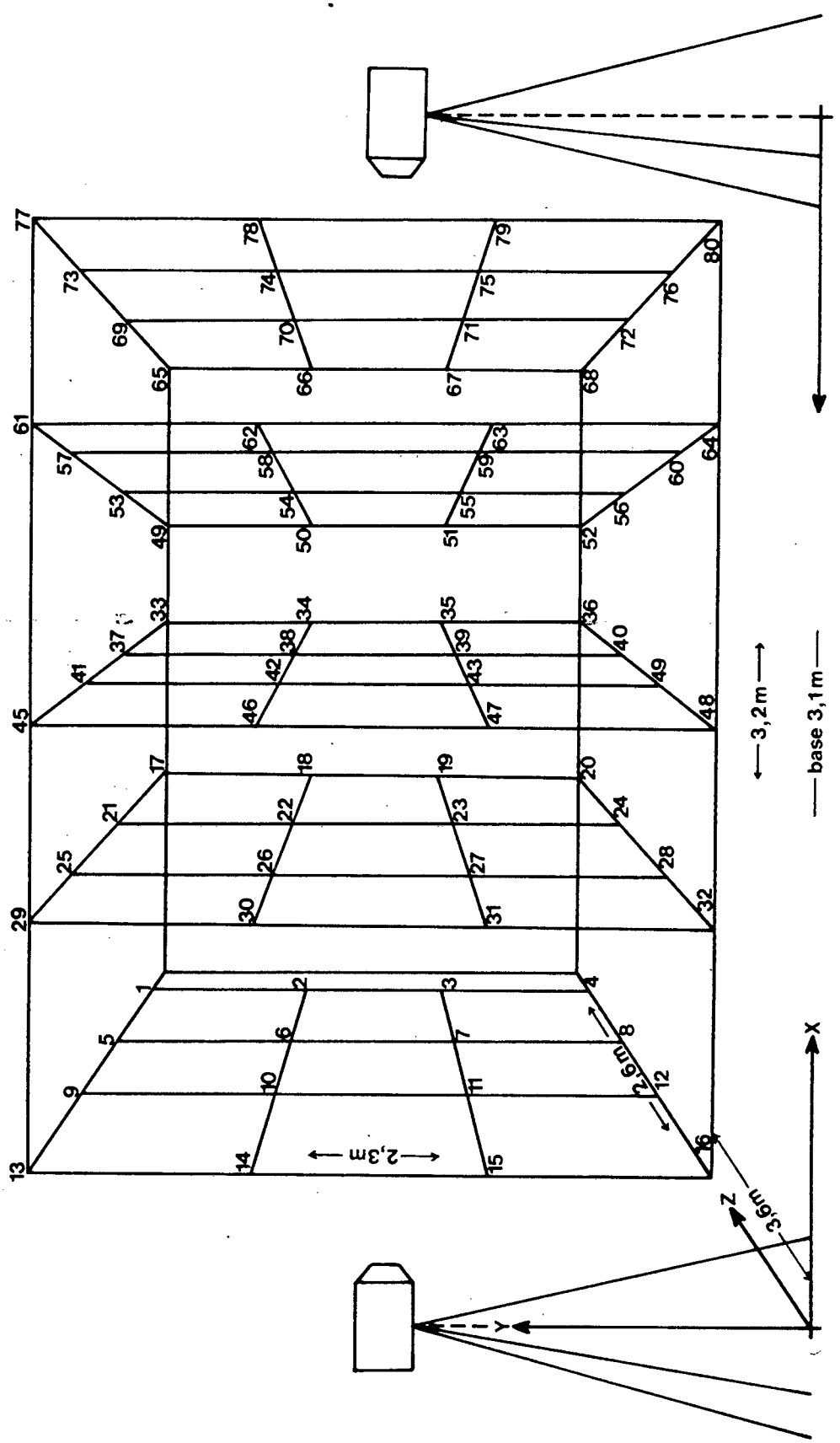

Fig. 5-3 Perspective View of the Test Field

A number of different target designs (Fig. 5-4) was tested to find a target, which images well on photographs of different scales, and which can be observed accurately in a comparator. Three photographs of the target designs were taken with the metric U M K 10/1318 cameras at different distances and each target was observed 60 times on a ZEISS STEKO comparator.

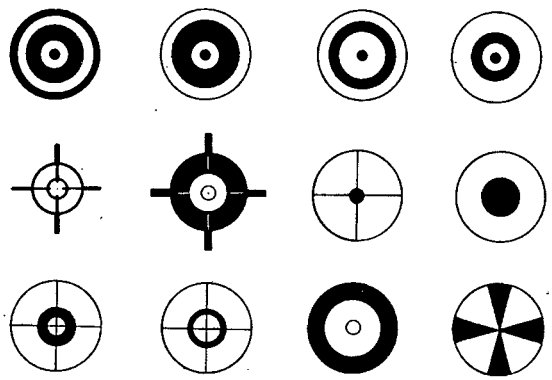

Fig. 5-4 Target Design Test

Observation accuracies for the various designs differed only marginally with standard deviations ranging from 3 µm to 4,5 µm. (This was quite contrary to the expectation of the writer, who anticipated the concentric ring design to fare best in the comparison). The observation "accuracy" of less than 5 µm represents repeatability rather than position accuracy of observed plate co-ordinates, the latter being in the range of 10 to 15 µm.

In the event the concentric black and white ring design (Fig. 5-5) was selected.

Fig. 5-5 Test Field Target

The target consists of brass discs with a diameter of 25 mm. With the exception of 16 wall markers in the far vertical plane all targets are attached to steel rods with a diameter of 12 mm. The rods are suspended from the ceiling and four target discs are attached to each. The maximum separation of two markers on a rod is 2,2 m; over this distance a temperature change of 1° Celsius results in a relative position change of 0,025 mm. Temperature expansion of the field can be catered for if required for high precision tests. In principle the test field must be seen as dynamic and point positions should be determined prior to test photography sequences.

The space positions of the test field points are best determined using high accuracy engineering survey techniques. Precise levelling had to be excluded as it is impossible to hold a levelling staff accurately against a target on a freely suspended rod. The points were, therefore, determined with vertical and horizontal angle measurements from three base points as described in 3.5. A scale for the three dimensional network was obtained by means of a highly precise

set of micrometer rods, which permit the measurements of distances up to 3,5 m with an accuracy of $\pm$ 0,01 mm. The point co-ordinates were found in a space intersection adjustment:
Standard deviations of 0,1 to 0,6 mm were evaluated for the X, Y, and Z co-ordinates of the points. No systematic pattern could be detected in the distribution of the errors through the test field and one can assume that all test field points are of a homogeneous accuracy within the above stated range of $\pm$ 0,6 mm.

The geodetic co-ordinates were determined in a right handed co-ordinate system. This was transformed into a left handed model co-ordinate system. The model co-ordinate system was defined as a left handed system to conform with the left handed image co-ordinate system.

TESTFIELD CO-ORDINATES

GEODETIC CO-ORDINATE SYSTEM

RIGHT HANDED SYSTEM

	X	Y	Z
1	10.2934	11.3908	4.1075
2	10.2904	10.6396	4.1030
3	10.2820	9.9069	4.1019
4	10.2837	9.1437	4.1004
5	10.2934	11.3981	4.5783
6	10.2875	10.6483	4.5783
7	10.2833	9.8976	4.5783
8	10.2784	9.1479	4.5768
9	10.2912	11.3958	5.4823
10	10.2884	10.6483	5.4835
11	10.2848	9.8967	5.4844
12	10.2796	9.1461	5.4867
13	10.2839	11.3915	6.3760
14	10.2882	10.6466	6.3770
15	10.2896	9.8935	6.3794
16	10.2869	9.1436	6.3839
17	11.0986	11.3849	3.8356
18	11.1143	10.6391	3.8276
19	11.1130	9.8904	3.8280
20	11.0982	9.1462	3.8341
21	11.1061	11.3973	4.5753
22	11.1026	10.6492	4.5764
23	11.0975	9.8990	4.5774
24	11.0927	9.1485	4.5799
25	11.1144	11.3982	5.4776
26	11.1090	10.6483	5.4775
27	11.1068	9.8963	5.4790
28	11.1017	9.1465	5.4807
29	11.1074	11.3911	6.3837
30	11.1048	10.6410	6.3836
31	11.1003	9.8899	6.3829
32	11.0922	9.1393	6.3820
33	11.9088	11.3791	3.8335
34	11.9196	10.6417	3.8260
35	11.9308	9.8909	3.8276
36	11.9194	9.1485	3.8322
37	11.9309	11.3942	4.5795
38	11.9253	10.6459	4.5805
39	11.9217	9.8950	4.5801
40	11.9213	9.1445	4.5776

MODEL CO-ORDINATE SYSTEM

LEFT HANDED SYSTEM

	X	Y	Z
1	0.2934	1.3908	5.8925
2	0.2904	0.6396	5.8971
3	0.2820	-0.0931	5.8981
4	0.2837	-0.8563	5.8996
5	0.2934	1.3981	5.4217
6	0.2875	0.6482	5.4217
7	0.2833	-0.1024	5.4217
8	0.2784	-0.8522	5.4232
9	0.2912	1.3958	4.5177
10	0.2884	0.6483	4.5165
11	0.2848	-0.1033	4.5156
12	0.2796	-0.8539	4.5133
13	0.2839	1.3915	3.6240
14	0.2882	0.6465	3.6230
15	0.2896	-0.1065	3.6206
16	0.2869	-0.8564	3.6162
17	1.0986	1.3849	6.1644
18	1.1143	0.6391	6.1724
19	1.1130	-0.1096	6.1720
20	1.0982	-0.8538	6.1659
21	1.1061	1.3973	5.4247
22	1.1026	0.6492	5.4236
23	1.0975	-0.1010	5.4226
24	1.0927	-0.8515	5.4201
25	1.1144	1.3982	4.5224
26	1.1090	0.6483	4.5225
27	1.1068	-0.1037	4.5210
28	1.1017	-0.8535	4.5193
29	1.1074	1.3911	3.6163
30	1.1048	0.6410	3.6164
31	1.1003	-0.1101	3.6171
32	1.0922	-0.8607	3.6180
33	1.9088	1.3791	6.1665
34	1.9196	0.6417	6.1740
35	1.9308	-0.1091	6.1724
36	1.9194	-0.8515	6.1679
37	1.9309	1.3942	5.4205
38	1.9253	0.6459	5.4195
39	1.9217	-0.1050	5.4199
40	1.9213	-0.8555	5.4224

Table 5-1

GEODETIC CO-ORDINATE SYSTEM

RIGHT HANDED SYSTEM

	X	Y	Z
41	11.9320	11.3956	5.4796
42	11.9281	10.6447	5.4793
43	11.9227	9.8962	5.4798
44	11.9153	9.1450	5.4816
45	11.9272	11.3848	6.3822
46	11.9222	10.6346	6.3825
47	11.9217	9.8842	6.3821
48	11.9239	9.1324	6.3805
49	12.7671	11.3788	3.8318
50	12.7491	10.6442	3.8229
51	12.7486	9.8961	3.8231
52	12.7327	9.1584	3.8312
53	12.7564	11.4016	4.5763
54	12.7516	10.6507	4.5769
55	12.7464	9.8986	4.5755
56	12.7362	9.1501	4.5719
57	12.7536	11.4001	5.4716
58	12.7511	10.6479	5.4702
59	12.7421	9.8978	5.4704
60	12.7326	9.1479	5.4805
61	12.7520	11.3878	6.3810
62	12.7479	10.6390	6.3801
63	12.7444	9.8872	6.3814
64	12.7384	9.1383	6.3848
65	13.5831	11.3797	3.8305
66	13.5607	10.6514	3.8217
67	13.5652	9.8994	3.8216
68	13.5513	9.1631	3.8292
69	13.5708	11.4072	4.5792
70	13.5656	10.6580	4.5808
71	13.5595	9.9057	4.5823
72	13.5542	9.1581	4.5828
73	13.5751	11.4012	5.4793
74	13.5705	10.6523	5.4796
75	13.5648	9.9013	5.4780
76	13.5576	9.1503	5.4777
77	13.5651	11.3986	6.3738
78	13.5607	10.6488	6.3740
79	13.5582	9.8976	6.3751
80	13.5524	9.1470	6.3771

MODEL CO-ORDINATE SYSTEM

LEFT HANDED SYSTEM

	X	Y	Z
41	1.9320	1.3956	4.5204
42	1.9281	0.6447	4.5207
43	1.9227	-0.1038	4.5202
44	1.9153	-0.8550	4.5184
45	1.9272	1.3848	3.6178
46	1.9222	0.6346	3.6175
47	1.9217	-0.1158	3.6179
48	1.9239	-0.8676	3.6195
49	2.7671	1.3788	6.1682
50	2.7491	0.6441	6.1771
51	2.7486	-0.1040	6.1769
52	2.7327	-0.8416	6.1688
53	2.7564	1.4016	5.4237
54	2.7516	0.6507	5.4231
55	2.7464	-0.1014	5.4245
56	2.7362	-0.8499	5.4281
57	2.7536	1.4001	4.5284
58	2.7511	0.6479	4.5298
59	2.7421	-0.1022	4.5296
60	2.7326	-0.8522	4.5195
61	2.7520	1.3878	3.6190
62	2.7479	0.6390	3.6199
63	2.7444	-0.1128	3.6186
64	2.7384	-0.8617	3.6152
65	3.5831	1.3797	6.1695
66	3.5607	0.6514	6.1784
67	3.5652	-0.1006	6.1784
68	3.5513	-0.8370	6.1708
69	3.5708	1.4072	5.4208
70	3.5656	0.6580	5.4192
71	3.5595	-0.0943	5.4178
72	3.5542	-0.8419	5.4172
73	3.5751	1.4012	4.5207
74	3.5705	0.6523	4.5204
75	3.5648	-0.0987	4.5221
76	3.5576	-0.8497	4.5223
77	3.5651	1.3986	3.6262
78	3.5607	0.6488	3.6260
79	3.5582	-0.1024	3.6249
80	3.5524	-0.8530	3.6229

Table 5-1 (continued)

6 PHOTOGRAMMETRIC ORIENTATION

6.1 The Principle of Photogrammetric Orientation

If we define the restitution of an object in space by means of photographic images as the principal objective of photogrammetry then photogrammetry's main task in achieving this aim is the determination of the spatial orientation of these images. The position and the attitude of the cameras at the instant of photography must be reconstructed in space, in mathematical terms, the perspective centre and the optical axis of each camera must undergo three translations and three rotations. The perspective centre can be shifted in the three axis-directions of a cartesian coordinate system and the optical axis of the camera can be rotated through three angles. Thus a total of twelve degrees of freedom is available to establish the required camera orientation for a stereoscopic pair of photographs.

The position of the perspective centre and the orientation of the optical axis alone, however, do not suffice to reconstruct the object in space. A photograph can be interpreted as the representation of a bundle of rays with its apex in the perspective centre of the camera and the reconstruction of this bundle of rays will make the restitution of the object in space possible.

Individual rays of the bundle are defined by the perspective centre of the camera and by image points on the photographic plate. The knowledge of the relative position of the perspective centre with respect to the image plane is therefore essential for the analytical interpretation of a photographic plate. The elements which define this relation are traditionally referred to as the inner or interior orientation of a camera. Three parameters describe the

relation between the perspective centre and the photographic plate, namely the x y co-ordinates of the so-called principal point and the principal distance. The mathematical definition of these three parameters is more complex than one might at first assume and they will receive more attention in a later chapter of this thesis. In addition to the six parameters of the spatial or outer orientation the three parameters of the inner orientation are thus required to establish the complete orientation of a camera in a stereoscopic pair. If both photographic plates of a stereoscopic pair are produced with the same camera, the elements of inner orientation are identical for both camera positions and a total number of fifteen (2·6+3) degrees of freedom need to be determined. If the two photographs are taken with different cameras - as necessary for the stereo photography of moving objects - a further three elements of inner orientation for the second camera increase the number of parameters to a total of eighteen (2·(6+3)).

It follows then that the photogrammetric[1] orientation consists of two, not necessarily separate, parts:

I Inner Orientation

The reconstruction of the relation between perspective centre and image plate.

II Outer Orientation

The reconstruction of the attitude and position of the photographic plate in space.

---

(1) To distinguish between the complete orientation procedure and parts thereof, such as inner orientation, the full orientation will be referred to here as photogrammetric orientation.

The outer orientation can in turn be seen as being subdivided into two sections.

II.1 Relative Orientation

The orientation of the two photographic plates of the stereoscopic pair relative to each other.

II.2 Absolute Orientation

The orientation of the stereoscopic pair in space.

A wide variety of mathematical models can be formulated to solve the problem of photogrammetric orientation analytically. Although it is appreciated that there is nothing original in the following, the writer considers it necessary to formulate a generally valid condition for photogrammetric orientation, a condition which forms the common basis for all mathematical models.
If we, for the moment, assume that a photographic image is a true perspective projection, then we can define the photogrammetric orientation condition as:
"A stereoscopic pair of photographic images is in correct photogrammetric orientation when its perspective centres and its image planes are positioned in space in such a way that all homologue rays formed by image points on both photographic plates intersect in their object homologues (their corresponding object points)."
In a true perspective projection perspective centre, image point and object point are collinear. The position of the image point on the photographic plate is, however, affected by imperfections in the lens system of the camera, the emulsion, the emulsion carrier and by atmospheric refraction. Image points suffer further

displacement owing to observation - and instrument errors, when their plate co-ordinates are measured on a comparator. All these factors contribute to a deviation from the collinearity condition and the photographic image can therefore no longer be interpreted as a true perspective projection. It is then obviously impossible for all image-rays to intersect precisely in space and the intersection-condition can never be fully satisfied. A "best-fitting" intersection of the two bundles of rays has to be aimed at rather than the ideal precise intersection of all rays. The orientation condition formulated above has therefore to be modified as follows:

"A stereoscopic pair of photographic images is in photogrammetric orientation when its perspective centres and its image planes are positioned in space in such a way that all homologue rays formed by image points on both photographic plates intersect in a "best fit" in their object homologues."

6.2 CLASSIFICATION OF MATHEMATICAL MODELS FOR ANALYTICAL PHOTOGRAMMETRIC ORIENTATION

A number of solutions for photogrammetric orientation has been suggested during the historical development of photogrammetry. To permit the selection of a method best suited to the problems encountered in the application of photogrammetry to measurements of objects at close range, a classification of the various mathematical models is appropriate.

The data available for the restitution of an object in space by means of photogrammetric orientation are the two-dimensional co-ordinates of image points on a photographic plate and, in cases

where control points can be established, the space co-ordinates of such points. A diagrammatic outline of various mathematical concepts relating these data in photogrammetric orientation models is given in Tab. 6-1. Photogrammetric orientation models can be categorised in four major groups:

1. The "Grand" Solution and Reduced Grand Solution
2. Projective Transformation
3. Double Point Space Resection
4. Sequential Solution

6.2.1 The "Grand" Solution and Reduced Grand Solution

The mathematically most elegant solution of the orientation problem is the simultaneous determination of all 18 (15) parameters of the orientation in one homogenous model. The image co-ordinates are in this solution directly related to the co-ordinates of a number of corresponding object control points. Inner, relative and absolute orientation are solved simultaneously. Schmid (1956-57, 1955) has presented such a solution. Originally it was designed for simultaneous multi-station photography with ballistic cameras, but then adapted for the sequential orientation of aerial-triangulation. The formulae of Schmid's model were designed to accommodate redundant observations in a least squares adjustment; Schmid obviously realised that the simultaneous determination of a large number of unknowns required stabilisation through redundant observations. Because of its complexity and universality the term "Grand solution"

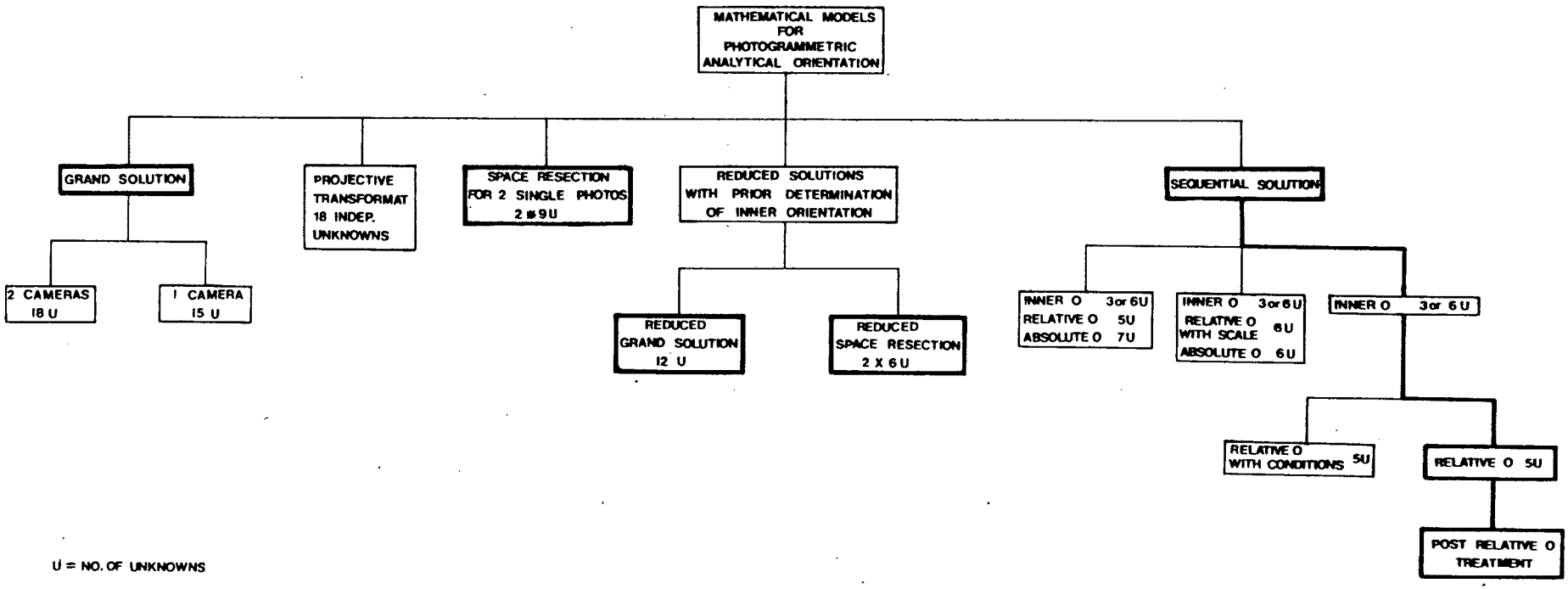
MATHEMATICAL MODELS FOR PHOTOGRAMMETRIC ANALYTICAL ORIENTATION
GRAND SOLUTION
2 CAMERAS 18 U
1 CAMERA 15 U
PROJECTIVE TRANSFORMAT 18 INDEP. UNKNOWNS
SPACE RESECTION FOR 2 SINGLE PHOTOS 2 x 9 U
REDUCED SOLUTIONS WITH PRIOR DETERMINATION OF INNER ORIENTATION
REDUCED GRAND SOLUTION 12 U
REDUCED SPACE RESECTION 2 X 6 U
SEQUENTIAL SOLUTION
INNER O 3 or 6 U
RELATIVE O 5 U
ABSOLUTE O 7 U
INNER O 3 or 6 U
RELATIVE O WITH SCALE 6 U
ABSOLUTE O 6 U
INNER O 3 or 6 U
RELATIVE O WITH CONDITIONS 5 U
RELATIVE O 5 U
POST RELATIVE O TREATMENT
U = NO. OF UNKNOWNS

Table 6-1

is an appropriate designation for this method. The Grand solution does not recommend itself for general application to the practical problems under consideration in this thesis since it requires a knowledge of the space co-ordinates of some of the object points. In close-range photogrammetry situations may arise in which it is impractical or, as in the case of the Wildlife photogrammetry, discussed later, not possible to determine control point positions. Schmid's method and the Grand solution in general are therefore considered unsuitable for the problems in hand.

The writer cannot refrain from expressing some doubt as to the general validity of a solution, which combines the determination of inner and outer orientation. As is well-known, the solution becomes undefined, when all object points fall into one plane, a phenomenon, which is reflected in the strong correlations between the parameters of the inner orientation and those of the outer orientation. We can argue that co-planarity of object points is easily avoided in non-topographical photogrammetry, but the writer noticed, in his own attempts to solve for inner orientation and relative orientation simultaneously, that strong correlations between the elements weaken the solution even if the configuration of the object points deviates from a plane. It must also be noted that principal distances evaluated with this method differ from stereoscopic pair to stereoscopic pair, even though the same camera is used throughout a photographic exercise. Williams (1974) points out that neither Schmid himself nor the United States Coast and Geodetic survey

do apply in practice the method in which the elements of inner orientation are treated as unknowns at each exposure station; instead the inner orientation elements are presumed known from laboratory camera calibrations. This leads to a "reduced grand" solution, in which only the twelve elements of the outer orientation are solved simultaneously.
Traditionally grand solution type models found little favour with photogrammetrists owing to the computational effort associated with the solution of large equation-systems.

6.2.2 Projective Transformation

The projective transformation is a mathematical formulation of the central perspective interpretation of the photographic image.

Although known to mathematicians for some time the projective transformation entered the field of photogrammetry relatively late with publications by, among others, Thompson (1971), Abdel-Azis, Karara (1971) and Bopp and Kraus (1978). The technique has recently experienced a renaissance in a wide range of non-topographic applications (Adams 1978, 1979, 1980 and 1981), where it proved itself as a very efficient and accurate method.
The projective transformation relies on a minimum of six (or more correctly, 5½) known control points in the determination of eleven unknown transformation parameters per image. The control point co-ordinates (X, Y, Z) are related to the observed plate co-ordinates ($\bar{x}$, $\bar{y}$) in the following

transformation equations:

$$x = \frac{b_{11}X + b_{12}Y + b_{13}Z + b_{14}}{b_{31}X + b_{32}Y + b_{33}Z + 1}$$
$$y = \frac{b_{21}X + b_{22}Y + b_{23}Z + b_{24}}{b_{31}X + b_{32}Y + b_{33}Z + 1} \qquad (6.2.2.1)$$

Each observed image point gives rise to a pair of equations of the above type.

As a solution method the projective transformation can be classified with the Grand Solutions, as it solves the entire photogrammetric orientation problem in one step, without requiring any knowledge of the elements of inner orientation. Elements of inner, relative and absolute orientation are, although not apparent, contained in the typical transformation parameters b_{ij}.

There seems to be a contradiction in the number of unknowns when comparing the projective transformation with the Grand Solution; the projective transformation in the form (6.2.2.1) requires the solution of 11 parameters, whereas the photogrammetric orientation problem contains only 9 unknown parameters per image. This implies an interdependence of the parameters of the projective transformation. Such a dependency can be included in a mathematical formulation of the transformation in the form of condition equations. However, Adams (1982) has proved that the interdependence can be neglected without any loss in the accuracy of either point position or inner orientation parameters.

The projective transformation does not have a solution if all control points lie in one plane and is must therefore be expected, that, like the Grand Solution, the projective transformation will lead to poor accuracies when all control points are nearly coplanar. This probably accounts at least partly for the limited interest the projective transformation has received until recently in photogrammetric studies, which were for a long time dominated by aerial applications with their typical near coplanar control point configuration.

In close-range photogrammetry three-dimensional control point fields can generally be judicably established and the projective transformation can be applied without fear of mathematically ill-conditioned situation.

Like the Grand Solution the projective transformation can not be used in cases where no control exists or where insufficient control is available.

6.2.3 DOUBLE POINT SPACE RESECTION

The space resection of the perspective centre of a single photograph was one of the first problems solved in the field of analytical photogrammetry. (G. Schreiber 1829; Finsterwalder 1900, 1903). After some early solutions this intriguing mathematical problem became less prominent in the photogrammetric literature, possibly to some extent as a

result of von Gruber's (1930) much quoted dogmatic remark: "The calculation of resection in space, by either the direct or the differential method is merely a waste of time and is of minor importance". This comment by such an eminent photogrammetrist as von Gruber can only be understood against the background of a time in which highspeed electronic computers could not be anticipated. The publication of Church's method in 1945 seems to have kindled new interest in space resection and in 1958 Szczepanski could list more than 60 analytical and graphical methods in a dissertation on space resection. Only a few of the more well-known methods will be mentioned here. Iterative solutions were derived by Church (1945), Fligor (1968), Schmid (1955) and Hallert (1968[1]); direct solutions were developed by Merrit (1949), Church (1950), Lehmann (1963), Smith (1965), Morse (1966) and Thompson (1971). The distinction between iteration and direct solution is not always clear: Lehmann's technique for example, although generally rated as a direct method, involves an iteration procedure for the solution of a pseudo-quadratic equation.

The space resection consists of the determination of the three space co-ordinates of the exposure station and, in a more extended version, the three orientation elements of the optical axis of the camera. This is generally accomplished by locating a position for the perspective centre for which three ground points subtend the same apex angles as the corresponding plate images of these points subtend at the perspective centre of the camera. In addition to these six

parameters some solutions include the elements of inner orientation as further unknown quantities.

Possible solutions fall into two main groups: the direct or explicit solutions and the iterative or differential solutions. In both groups inner orientation elements can either be assumed as known or they can form part of the solution.

It was generally accepted that "a picture can be resected in space if the interior orientation of the camera and the space co-ordinates of three ground-points (having images) are known". (Thompson, 1975). This statement requires qualification, as it tacitly assumes knowledge of the approximate position or orientation of the camera.(1) The space resection solution based on three points only is in fact not unique and a definite position for the exposure station can only be found with the aid of some approximate values for the unknown quantities. For any set of three control-points as many as eight exposure stations in space can be found which will produce identical image point configurations on a photographic plate; in mathematical terms this means that eight solutions exist for a set of three image points. Only an additional control point, not co-planar with the three original points, will guarantee a unique solution. In most cases this difficulty can be overcome and a solution can be found from three points only, if approximate values for three of the

---

(1) Smith (1965) goes so far as to claim that the need to know the approximate camera position "does not seem to be widely recognised."

six unknown parameters are available. If some of the possible eight solutions, however, lie close together in space, then even known approximate values will not necessarily lead to a unique solution. If the iterative approach is chosen, the iteration process might converge to the incorrect camera position or oscillate without convergence between two solutions. If a direct solution method is applied to the problem, and all eight possible solutions are generated, an indisputable decision cannot be made.

If space resections, with unique solutions, are carried out for both cameras of a stereoscopic pair, then the relative orientation, the scale, the absolute orientation and the inner orientation of the model are known and a full photogrammetric orientation is achieved.

Further object points can then be evaluated, as required, by means of space intersection calculations. The space intersection applied to two cameras is known as the "Double Point Space Intersection". As in the case of the Grand Solution the double point space resection methods can be grouped into full solutions and reduced solutions with known and unknown inner orientation elements respectively. Correlations between the inner orientation elements should theoretically be introduced into a possible adjustment of the reduced solution types; in practice, however, they will have little effect on the numerical values of the orientation parameters. Within the limits of accuracy normally required in photogrammetry all methods described above - Grand Solution, reduced Grand solution, projective transformation and double

point space resection - can be expected to lead to the same results, provided the control points are chosen to guarantee a well-conditioned configuration.

Inspired by Hansen's "Doppelpunkteinschaltung" (Double point fix) von Gruber (1924) derived an interesting variation to the separate treatment of the two camera stations. Von Gruber determines position and orientation of both cameras in a simultaneous space resection for both exposure stations. He refers to the method as "Doppelpunkteinschaltung in Raum", (Double point fix in space").

Owing to the difficulty in finding a unique solution and to the requirement of known control points the writer did not consider the Double Point Space resection as a suitable method for the practical problems in hand.

6.2.4 SEQUENTIAL SOLUTION

The mathematical model most often adopted for the photogrammetric orientation problem especially in the fields of non-topographical and terrestrial photogrammetry is that of the sequential solution. The orientation procedure is carried out in three separate steps in the logical sequence of inner orientation, relative orientation and absolute orientation. Schut (1957) distinguishes between two main groups: in the first the relative orientation is determined without consideration of the scale of the model, the scale being found as part of the absolute orientation. In the second group the scale determination forms part of the relative orientation and the

scale is not allowed to vary in the subsequent absolute orientation. This classification can be extended by adding two categories of orientation models which differ conceptually from Schut's two groups: the relative orientation with restraining conditions and post-relative orientation treatment (other than the traditional absolute orientation).

A variety of restraints can be envisaged for the former group, such as an enforced relative position of two or more points, parallelity of object surfaces or rectangularity of specific object lines. For the problem in hand a restraining condition in the form of one or more control distances was introduced to reduce the effect of possible convergency errors.

The introduction of homogeneous and affine scales subsequent to a relative orientation as an alternative model control method represents an example of post-relative orientation treatment.

Whether to classify the post-relative orientation treatment as an extension to the relative orientation or as a substitute for the absolute orientation is a purely academic question. For the classification in Tab. 6-1 post-relative orientation treatment is listed as an independent step in place of the absolute orientation.

The sequential solution without the absolute orientation is

adopted as the orientation model for this study. The individual steps of the solution sequence, namely: inner orientation and relative orientation plus a case of an additional condition and post-relative orientation treatment are discussed in detail.

A detailed discussion of the historical development of relative orientation methods is included, since the relative orientation forms the nucleus of the mathematical treatment of the orientation problem in this thesis.

7. INNER ORIENTATION AND RELATIVE ORIENTATION

7.1 INNER ORIENTATION
(Camera Calibration, Interior Orientation)

The camera calibration serves to determine the elements of the interior or inner orientation, that is the principal distance and the principal point position and possibly lens distortion characteristics. Interior orientation has attracted the attention of most photogrammetrists and numerous publications on the calibration of close-range cameras with their variable principal distance settings have been presented. To name only a few: Konecny 1965; Torlegård 1976; Hallert 1968[2]; Brown 1971; Kölbl 1972; Kenefick 1972; Thompson 1957 and 1977; Scott 1976 and 1977; Rawiel 1980.

Amongst these, the view of Thompson and Scott are of special interest as they investigate not only calibration methods but also the overall concept of the interior orientation and the role of the lens in photogrammetry, whilst Kölbl's and Kenefick's papers deserve attention as typical examples of self calibration methods without the need of a calibration field. However, it is not the objective of this thesis to assess or compare the various methods and a technique, based directly on the perspective projection, was employed.

In this method, a photograph is taken of a precision calibration field and the image co-ordinates of the field points are related to their corresponding three dimensional field co-ordinates by a three-dimensional transformation in the form:

$$\begin{bmatrix} X \\ Y \\ Z \end{bmatrix} = \begin{bmatrix} X_o \\ Y_o \\ Z_o \end{bmatrix} + \lambda R \begin{bmatrix} \bar{x}+\delta x \\ \bar{y}+\delta y \\ \bar{f} \end{bmatrix} \qquad (7.1.1)$$

Where

X , Y , Z = Field co-ordinates of Point P

X_o, Y_o, Z_o = Field co-ordinates of perspective centre of camera

$\bar{x}$, $\bar{y}$, $\bar{f} \approx \bar{z}$ = Observed image co-ordinates and principal distance

δx, δy = Translations to principal point

λ = Scale factor

$\underline{R}$ = Rotation matrix

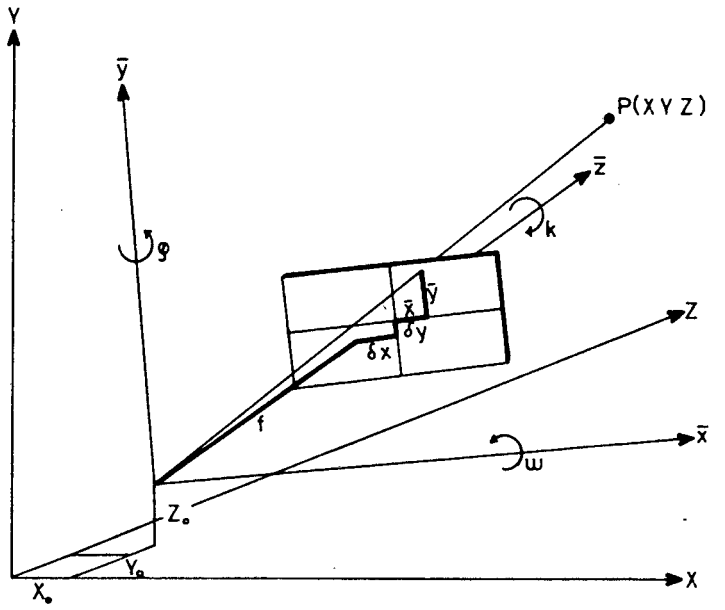

Fig. 7.1-1 Position of Positive Image in Testfield for Camera Calibration

For the calibration process the camera can easily be oriented and levelled to line up with the co-ordinate axes of the test field and it can thus be guaranteed that the rotation angles φ, ω and $\varkappa$ assume small quantities. The rotation matrix can then be written equivalent to (3.1.17) as:

$$\underline{R} = \begin{bmatrix} 1 & -d\varkappa & d\varphi \\ d\varkappa & 1 & -d\omega \\ -d\varphi & d\omega & 1 \end{bmatrix} \qquad (7.1.2)$$

Theoretically the observed plate co-ordinates x and y should not only be corrected for a translation of the principal point but also for possible image distortion. However, it was decided to omit lens distortion from the calibration model because of the high quality of the LAMEGON lens system used for the photography. The manufacturers claim asymmetric distortions of less than 5 µm with average values of 2 µm for the entire image plane at an infinity focal setting. For focal settings other than infinity an additional radial-symmetrical distortion contribution must be expected which only exceeds the 5 µm range for radial distances of more than 60mm, that is for the extreme edges of the long image format. Considering that all images were observed on a comparator with an estimated reading accuracy of not better than 10 µm, the writer felt justified in neglecting such small distortion values and, in fact, no evidence of systematic distortion could be detected in any of the subsequently investigated images.

Neglecting distortions equation system (7.1.1) yields two conditions:

$$\frac{X-X_0}{Z-Z_0} = \frac{\Delta X}{\Delta Z} = \frac{r_{11}(\bar{x}+\delta x)+r_{12}(\bar{y}+\delta y)+r_{13}\bar{f}}{r_{31}(\bar{x}+\delta x)+r_{32}(\bar{y}+\delta y)+r_{33}\bar{f}} \qquad (7.1.3.1)$$

and

$$\frac{Y-Y_0}{Z-Z_0} = \frac{\Delta Y}{\Delta Z} = \frac{r_{21}(\bar{x}+\delta x)+r_{22}(\bar{y}+\delta y)+r_{23}\bar{f}}{r_{31}(\bar{x}+ x)+r_{32}(\bar{y}+ y)+r_{33}\bar{f}} \qquad (7.1.3.2)$$

with (7.1.2) one obtains from (7.3.1) and (7.3.2)

$$\Phi_1 = \Delta X\left[-d\varphi(\bar{x}+\delta x)+d\omega(\bar{y}-\delta y)+\bar{f}\right)-\Delta Z((\bar{x}+\delta x)-d\varkappa(\bar{y}+\delta y)+d\varphi\bar{f})\Big] = 0 \qquad (7.1.4.1)$$

$$\Phi_2 = \Delta Y\left[-d\varphi(\bar{x}+\delta x)+d\omega(\bar{y}+\delta y)+\bar{f}\right)-\Delta Z(d\varkappa(\bar{x}+\delta x)+(\bar{y}+\delta y)-d\omega\bar{f})\Big] = 0 \qquad (7.1.4.2)$$

For a least squares adjustment equations (7.1.4) must be linearised with respect to the unknowns δx, δy, $\bar{f}$, $d\varkappa$, $d\varphi$ and $d\omega$ and the observations x and y.

The determination of the numerical values of the principal point shifts δx and δy and the principal distances f are the final objective of the adjustment.

It is not possible in this approach to also treat the camera position (position of the external perspective centre of the camera X_o, Y_o, Z_o) as unknown. Parameters X_o, Y_o and Z_o are so strongly correlated with δx, δy and f respectively that they cannot be treated as unknowns in the same adjustment. The need to have accurate values for X_o, Y_o, and Z_o represents a weakness of this calibration model which will be discussed later.

Linearisation of (7.4) results in:

$$-(\Delta X d\varphi+\Delta Z)v_{\bar{x}_i}+(\Delta X d\omega+\Delta Z d\varkappa)v_{\bar{y}_i}-(\Delta X d\varphi+\Delta Z)d(\delta x)+$$

$$+(\Delta X d\omega+\Delta Z d\varkappa)d(\delta y)+(\Delta X-\Delta Z d\varphi)d\bar{f}+\Delta Z(\bar{y}+\delta y)d\varkappa- \qquad (7.1.5.1)$$

$$-(\Delta X(\bar{x}+\delta x)+\bar{f}\Delta Z)d\varphi+\Delta X(\bar{y}+\delta y)d\omega+\Phi_1\big|_o = 0$$

$$-(\Delta Y d\varphi+\Delta Z d\varkappa)v_{\bar{x}_i}+(\Delta Y d\omega-\Delta Z)v_{\bar{y}_i}-(\Delta Y d\varphi+\Delta Z d\varkappa)d(\delta x)+$$

$$+(\Delta Y d\omega-\Delta Z)d(\delta y)+(\Delta Y+\Delta Z d\omega)d\bar{f}-\Delta Z(\bar{x}+\delta x)d\varkappa- \qquad (7.1.5.2)$$

$$-\Delta Y(\bar{x}+\delta x)d\varphi+(\Delta Y(\bar{y}+\delta y)+\Delta Z\bar{f})d\omega+\Phi_2\big|_o = 0$$

The condition equations are of the type which require the combined adjustment, but reduction to the more convenient quasi-parametric case is possible, although corrections v_{x_i} and v_{y_i} occur in two equations each. The quasi-parametric case can be applied here as the coefficient of v_{y_i} in the first condition equation Φ_1 and the co-efficient of v_{x_i} in the second equation Φ_2 are near zero, thus effectively removing these co-efficients from the $\underline{B}$ matrix (in 3.2.4) and turning $\underline{B}\underline{B}^T$ into a quasi-weight matrix. Tests comparing the full combined case with the quasi-parametric case yielded identical results provided an iteration procedure was adopted in both cases.

It is necessary to introduce the space co-ordinates of the exterior perspective centre (X_o, Y_o,Z_o) as known quantities into the calibration adjustment owing to the strong correlations between X_o and δx, Y_o and δy, and Z_o and $\bar{f}$. In order to obtain an estimate for the accuracies required for the perspective centre position in a camera calibration adjustment simulated camera calibrations with synthetic test field data were executed. Controlled introduction of errors in X_o, Y_o, and Z_o resulted in errors in the corresponding unknowns δx, δy and $\bar{f}$ of about 1:50 of the introduced error.(1) This implies that, to guarantee accuracies of say 20 µm for interior orientation elements, the co-ordinate value X_o, Y_o and Z_o must be determined with an accuracy of 1 mm. An error of 20 µm

---

(1) The ratio 1:50 is an average value and only valid for the testfield (Fig. 5-3) used for the camera calibration or for calibration fields of similar dimensions.

in the interior orientation elements results in average model errors of 1:4000 to 1:5000 (see Chapter 8 on deformation analysis).

To accurately determine the position of the external perspective centre presented some difficulties, but eventually a technique, inspired by a method suggested by Hallert (1969), provided the required accuracies of better than 1 mm. The external pupil of the camera was observed simultaneously from three theodolite stations using the space intersection method described in 3.5 (Figs. 3.5-2 and 7.1-2).

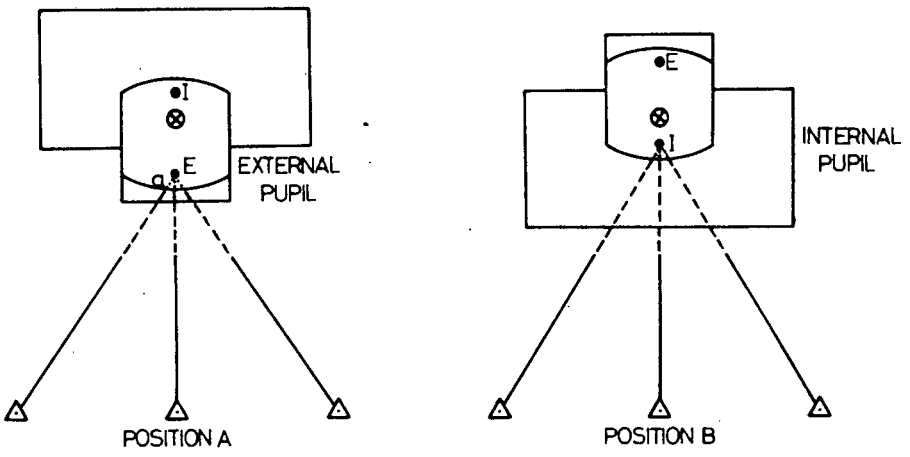

Fig. 7.1-2 Configuration of Theodolite Observations to Determine the Position of the External and Internal Pupils for a Metric Camera on an Alidade Mounting.

Observations were taken to the left and right edge of the external pupil for three focal settings at three different lens apertures. The co-ordinates of the pupil edges were then determined by means of the space intersection adjustment and the pupil centre was evaluated as the midpoint between the aperture edges. The values of the aperture centres agreed to 0,1 mm in all three co-ordinates,

implying that the centre of the external pupil is unaffected (within 0,1) mm by changes in the lens aperture setting and also giving an indication of the repeatability of the position fixes.

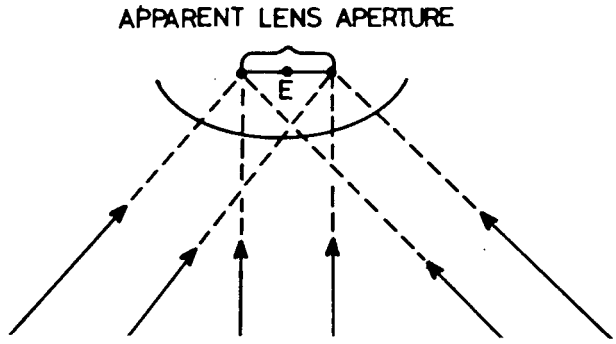

Fig. 7.1-3 Observations to Edges of Aperture to Determine Position of External Pupil (E) or Internal Pupil. (Lens Curvature and Width and Position of Aperture are not to Scale)

The external pupil position was determined for focal setting of 3,6 m, 8 m and infinity. In the same survey, the rotation axis of the camera was fixed by observations to the central axis studs (Fig. 4.4-2) of the camera in camera positions A and B (Fig. 7.1-2). Thus the position of the external pupil relative to the vertical rotation axis of the camera was established for various focal settings.

As a matter of interest the interior pupil and the fiducial marks were also observed in camera position B. The results of the investigation for cameras UMK10/1318-49 and -74 are shown in Fig. 7.1-4.

For the actual calibration of the UMK cameras each camera was mounted on a pillar in a suitable position opposite the calibration field. Theodolites were then set up on three points inside the field and the external pupil of each camera was determined as described above with the camera oriented for calibration photography. The necessary photography of the testfield was executed immediately after the theodolite observations of the lens pupil.

The use of space intersection calculation in the determination of the pupils assumes, as an approximation, that the light rays from the theodolite to the pupil follow straight lines inside the lens.

Scott (1977) comes to the interesting conclusion that the exterior perspective centre of the lens system does coincide with the centre of the external pupil but not with the front node of the lens system whilst the interior perspective centre coincides with the read node at infinity focus but not with the internal pupil. This can be expressed in the form:

Ext. Persp. Centre = External Pupil $\neq$ Front Node

Int. Persp. Centre = Rear Node $\neq$ Internal Pupil

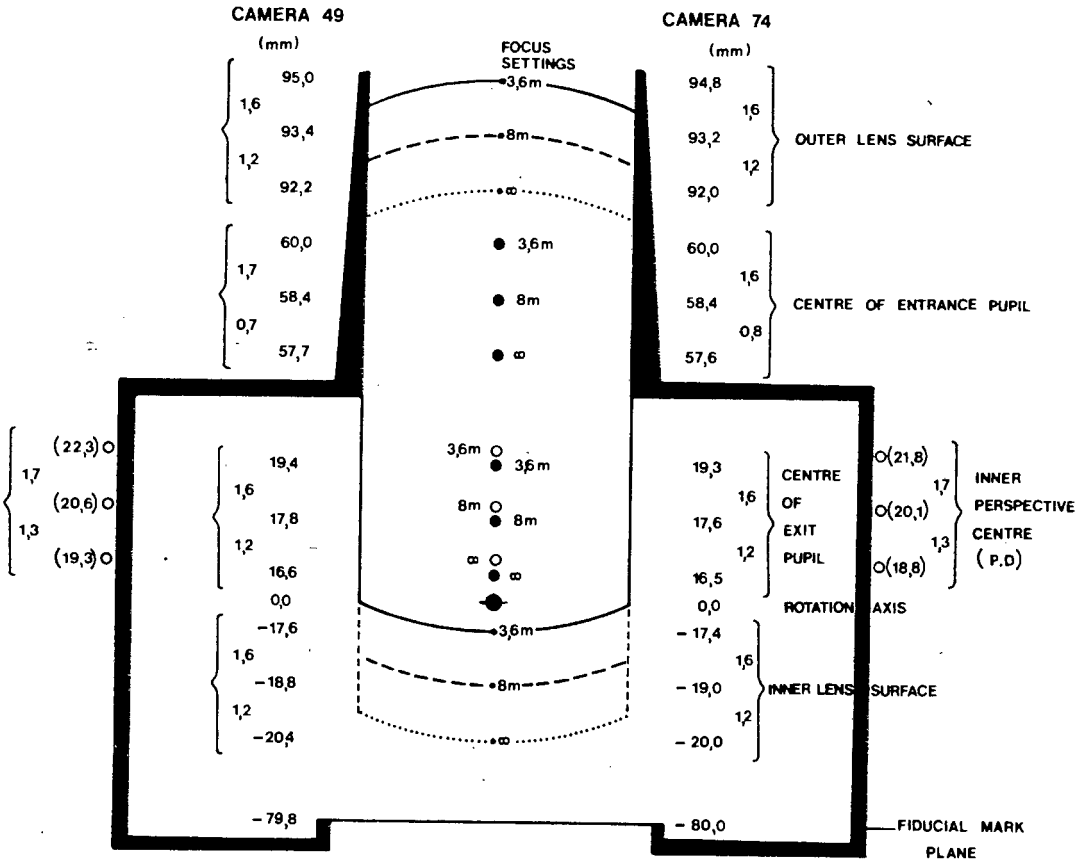

Fig. 7.1-4 Geometry of UMK10/1318 Cameras (-49 and -74) Showing the Position of External (Entrance) and Internal (Exit) Pupil at Three Different Focal Settings, as well as the Position of the Rotation Axis of the Camera and the Focal Plane.

It must be borne in mind here that the front and rear nodes of the lens system have a fixed position relative to the glass body of the lens configuration. This applied to Scott's conclusions implies that the physical shift of the lens system between different focal settings should coincide with the shifts of the internal pupil, as this latter moves with the rear node, while the external pupil should move by different amounts. The change of the principal distance,

on the other hand, should not coincide with either pupils' movement. The result of this lens survey confirms Scott's conclusions in full as inspection of the data listed in Fig. 7.1-4 shows, even to the extent that it confirms that the change of the principal distance differs by 0,2 mm from the corresponding physical shift of the lens system(1), when changing from focus 3,6 m to infinity. The value of 0,2 mm agrees with the amount evaluated using Scott's (1977) formula (1). This, combined with the fact that the external pupil shifts coincide with the amounts given by the manufacturers for corresponding changes in principal distance, seemed adequate evidence to accept the theodolite fix of the external pupil and thus the outer perspective centre co-ordinates as sufficiently accurate.

A final independent confirmation of the external pupil position fixes by space intersection, was obtained by measuring the physical shifts of the lens systems with a dial gauge micrometer and comparing these values to the shifts of the internal pupil as derived from theodolite observations and space intersection calculations. (Tab. 7.1-1).

---

(1) The principal distance changes by 2,99 mm for camera 49 and by 2,94 mm for camera 74; the physical shift of the lens system as determined by theodolite observations is 2.8 mm for both cameras.

Focus	UMK 10/1318 - 49			UMK 10/1318 - 74		
	Dial gauge measure-ment	Space inter-section	P.D. change	Dial gauge measure-ment	Space inter-section	P.D. change
3,6m	2,78mm	2,8mm	2,99mm	2,78mm	2,8mm	2,94mm
4,2	2,37		2,57	2,39		2,52
5	1,97		2,14	1,97		2,10
6	1,57		1,71	1,57		1,68
8	1,17	1,2	1,28	1,17	1,2	1,26
12	0,78		0,86	0,79		0,84
25	0,39		0,43	0,39		0,42
∞	0	0	0	0	0	0

Table 7.1-1 Shifts of Internal Pupil as Derived from Measurements with a Theodolite and with a Dial Gauge Micrometer.

When a camera calibration for the two UMK cameras was executed, based on equations (7.1-5) and using the values given in Fig. 7.1-4 for the position of the exterior perspective centre, the results of the calibration did agree with the calibration values supplied by the manufacturer within 50 µm for all calibrated focal settings. It was therefore decided to accept the calibration values of the calibration certificate. It was in fact not the main object of the calibration investigation to confirm the manufacturers certificate but rather to find a method valid for the calibration of close-range cameras with changing focus setting. It appears that the above discussed technique combining a perspective projection model with a modified version of Hallert's external pupil observation leads to satisfactory results with accuracies of better than 50 µm for all the elements of interior relative orientation. In cases where large distortions are suspected, formula (7.1-5) must be extended by a

term describing the distortion characteristics.

However, the choice of a suitable distortion equation is not as trivial as one is frequently led to believe by publications on camera calibration methods. The often quoted polynomial form of the lens distortion might well describe the phenomenon in a mathematically correct formulation but it is numerically very ill-conditioned in a least squares adjustment, when the polynomial is extended beyond second order terms. This is confirmed in a paper by Schenk (1971) in which the deterioration of the normal equation system for polynomials of higher order is demonstrated.

What a good thing Adam had, - when he said a thing, he knew nobody had said it before. Mark Twain.

7.2 THE HISTORICAL DEVELOPMENT OF RELATIVE ORIENTATION

When studying the historical development of any scientific or technical principle, the question of locating the origin of the principle raises intriguing problems. Reference is continually being made in technical literature to the "father" of a particular principle or idea, and photogrammetry is not free of these references to paternal origins. Laussedat is credited as being the "father of photogrammetry" (Gruber 1930), Pulfrich is named as the "father of stereophotogrammetry" (Schwidefsky 1959) -(English edition) and the development of analytical photogrammetry is ascribed to S. Finsterwalder (Gruber 1930).

These assertions of originality of thought cannot always be upheld if they are critically investigated. Technical progress seldom arises as a result of accidental discovery but rather as a logical sequel to some previous development. Inevitably the advent of

photography had to be followed by its use as a measuring tool and the introduction of airborne platforms led to the development of aerial photogrammetry. As a result of this phenomenon a number of researchers, often simultaneously and generally independently, will become involved in the scientific development of an idea. The real origin of a new concept must therefore generally remain uncertain and its authorship is normally credited to he who first published the new idea.

Interesting examples in the photogrammetric field are those of Fourcade who worked on the concept of stereophotogrammetry at the same time and independently of Pulfrich (Adams 1975[1]) as well as Porro (1853) and Meydenbauer (1858) who published their ideas on photogrammetry only a few years after Laussedat, both were probably unaware of the results of each other's research (Gruber 1930). Similarly the origin of the theory of Relative Orientation is shrouded in a deal of mystery. When tracing the origin of the theory of Relative Orientation it seems that Fourcade emerges as its discoverer with the publication of the theorem of correspondence in 1926. If, however, one considers the problem of relative orientation not in isolation but as part of the more general problem of the restitution of an object in space from two photographs in arbitrary orientation, then some credit must go to Finsterwalder. He produced analytically a digital terrain model[(1)] from a pair of aerial photographs using a balloon as a camera-platform. Finsterwalder describes his analytical solution in

---

(1) Finsterwalder referred to it as "Höhenkarte" (height map).

May 1900 in a report to the Bavarian Academy of Science when he stated categorically the principle of stereophotogrammetry:

Translation:

"If two photographs E' and E" of an object are given and their inner orientation - that is the relative position of their perspective centres - is known, then these are theoretically sufficient to determine (the shape of) the photographed object as well as the position of both perspective centres but not the scale. Knowledge of any distance in the object-space suffices to determine the scale. Up to date no solution for all possible cases has been found".

Finsterwalder then proceeds to present his own "general" solution, which requires the knowledge of the height and positions of four ground points. Space resections provide the positions of the centres of the two photographs. Image co-ordinates are measured and via a projective transformation related to the known ground points. The unknown projection parameters are evaluated and can then be applied to all other image points to determine further heights and ground positions. Finsterwalder claims a mean square error in height of $\pm$ 0,65m; this represents an accuracy of 1:1400 for the balloon's flying height of 900m. Accuracies for point positions are not quoted. It is interesting to note that Finsterwalder suggests in the same report that photographs be enlarged for increased accuracy in point identification. This technique is possible, as any distortion of the photograph resulting from the enlargement procedure is taken up by the projective transformation parameters. Adams applied this method in 1979.

In another interesting development Finsterwalder presented in 1903 a least squares adjustment for a three-dimensional resection. This

solution not only results in the knowledge of the position of the perspective centre of the photograph but also in the three direction cosines of the optical axis of the camera with respect to the nadir direction. The relation to a second perspective centre is not mentioned and the simple (and for today's reader of Finsterwalder's paper so obvious) step to the relative orientation is not made. Although Finsterwalder had theoretically found the answer to the problem of analytical photogrammetry in the projective transformation and later in the space resection, a completely different mathematical principle, the theorem of correspondence was destined to dominate the way of thinking in photogrammetry.

Owing to the absence of suitable highspeed computing facilities at the time, analytical photogrammetry was condemned to remain in the background for nearly half a century. It was restricted to academic dissertations and to the theoretical chapters of textbooks without much application to the reality of the photogrammetric production of maps and plans. Finsterwalder's projective transformation and space resection represented a purely analytical approach and were thus ahead of their time. The solution had to come from the field of analogue photogrammetry.

Fourcade formulated in 1926 a theorem, which was originally oriented to the analogue solution, namely the principle of correspondence. "The correspondence between the pencils of rays joining two centres to any number of points in space is uniquely determined if to five rays in the one there are given the corresponding five rays in the other, provided no three pairs of the rays lie in a plane." (Fourcade May 1926).

This principle also proved extremely suitable for the mathematical formulation of the relative orientation problem and thus forms the basis of the majority of all analytical solutions up to date.

Von Gruber (1930) discussed relative orientation in great detail, deriving formulae from geometrical principles of the projective theory. He formulated the condition for relative orientation based on a principle, which would later (Thompson 1959) be referred to as "the vanishing of y-parallax".

Von Gruber stated:

"The condition for true relative orientation of the two photographs is that for every pair of homologues points on the photographs

$$Y_2 = Y_1$$

when:

"X,Y are the co-ordinates in the common plane of projection, where the X-axis is the line of intersection of the common projection plane and that plane normal to the latter which contains the base-line".

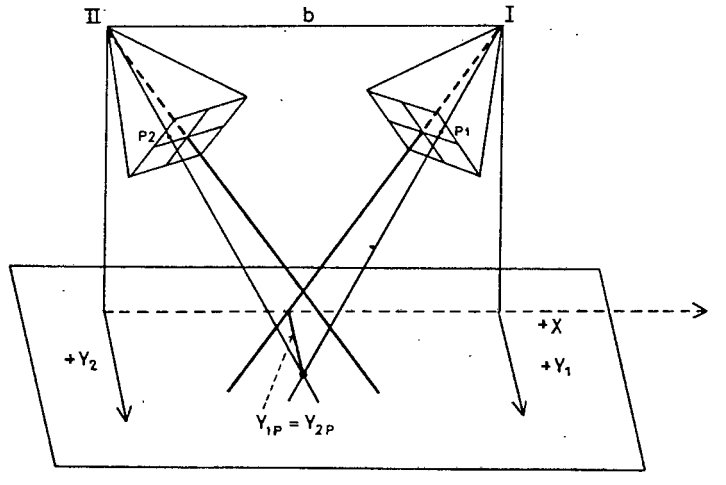

Fig. 7.2-1 "Vanishing of y-parallax" as a Relative Orientation Condition (Von Gruber 1930)

This condition does in fact stipulate that homologous rays must intersect in space. Von Gruber also proved in this context the important principle that relative orientation involves five elements, thus confirming Fourcade's postulate.

He then proceeded to derive expressions for X and Y as functions of the observed plate co-ordinates x,y the principal distance f and the orientation angles ω, α and $\varkappa$. (This is probably the first appearance of the by now classical orientation angles ω and $\varkappa$). For the orientation condition of "vanishing y parallax" only Y is of importance.

$$Y_{ij} = \frac{\{\bar{f}_i \sin\omega_i + (\bar{y}_{ij}\cos\varkappa_i - \bar{x}_{ij}\sin\varkappa_i)\cos\omega_i\}\, h_i}{\{\bar{f}_i \cos\omega_i - (\bar{y}_{ij}\cos\varkappa_i - \bar{x}_{ij}\sin\varkappa_i)\sin\omega_i\}\sin\alpha_i + (\bar{x}_{ij}\cos\varkappa_i + \bar{y}_{ij}\sin\varkappa_i)\cos\alpha_i}$$

i = camera station 1 or 2

j = number of image point

(Subscripts were added by the writer for clarification, they do not appear in the original text.)

h_i - the height of the perspective centre above the common plane of projection - is eliminated in $Y_1 = Y_2$

The elements of Rotation matrix $\underline{R}$ in equation (3.1.10) are identical to Von Gruber's coefficients of x, y and f.

Once again the answer to the problem of analytical relative orientation was within easy reach.

By equating the Y values of five homologous points

$$Y_{1j} = Y_{2j} \qquad j = 1 \ldots 5$$

an equation system of five equations with five unknowns could have been formulated. The disadvantage of the trigonometrical relation-

ships between the unknowns could have been overcome by linearisation and iteration. Von Gruber, however, used the formulae merely in their differential form to obtain information as to the effect of changes in individual orientation elements on the co-ordinates of the projection.

One can only assume that Von Gruber was aware of the potential of his derivations and that only lack of suitable computing facilities and his expressed aversion towards analytical solutions prohibited the so obvious final step to the analytical relative orientation.

The breakthrough to analytical solutions of photogrammetric problems is heralded by Church's work about 1940 (E. Church 1936, 1941, 1945). A fully numerical solution of the photogrammetric orientation, resulting in three-dimensional co-ordinates calculated from measured plate co-ordinates was presented by Church. The orientation was achieved by means of a double point space resection rather than a true relative orientation. In an iterative process the space position for the perspective centres of both cameras was calculated from three known ground points, followed by the determination of the "tilt", "swing" and "azimuth" of the cameras in form of the nine elements of a transformation matrix. The inner orientation of the cameras was assumed to be known.

Church's method was presented in tabular form with detailed instructions and later included with a numerical example in the American "Manual of Photogrammetry" (1965). Both these facts indicate that Church's solution was not merely of academic value, as were many of the previously published analytical methods, but found practical application. Numerous solutions followed, nearly exclusively related

to Fourcade's principle, which by then was obviously so well established in photogrammetry, that it appeared in many forms without any reference to its origin.

The common method was to bring homologous space rays to an intersection in at least five points in space. Some of these techniques stand out in their original mathematical approach to the formulation of the intersection condition. Wassef (1953) for example made use of Eulerian rotation angles and Herget (1954) minimised the space distance between corresponding rays. Herget's method was further developed by Herget and Mahony (1957), McNair, Dodge and Rutledge (1958) and Dodge, Handwerker and Eller (1959).

The principles most frequently referred to, however, were the "vanishing of y-parallax" and the co-planarity condition, while Von Gruber's rotation angles were generally preferred to Eulerian angles. In further developments the co-planarity condition was more and more favoured in analytical solutions, probably as a result of Schut's (1956) method and because of Thompson, who in 1956 expressed his surprise that the vanishing of the y-parallax should be seen as the only[(1)] condition for a correct relative orientation. Thompson recommends the co-planarity condition as a "more convenient criterion". In the nineteen fifties and sixties, solutions became so numerous that a comprehensive discussion becomes impossible in the context of this dissertation. To name some of the more important solutions:

---

(1) The use of "only" must be seen as "an artistic licence" since there were methods in use employing the co-planarity condition before 1956 (e.g. Bartorelli 1955).

Schut 1956, 1957, 1958; Bartorelli 1955; Arthur 1955, 1972; Schmid 1955, 1956; Jerie 1956; Rinner 1957; Gotthard 1959; Thompson 1956, 1959, 1966, 1967; van den Hout 1961; Stefanovic 1973, and van den Hout with Stefanovic 1976. Among these methods those by Arthur, Schut, van den Hout and more especially Thompson, seem to be most frequently referred to in publications and text-books.

A comprehensive comparison of relative orientations techniques in the context of aerial triangulation is given by Schut (1957). Schut stresses "that all methods employ the condition of intersecting rays, that in each group of methods the triangulation result is independent of the choice of the condition of intersection and that the co-planarity condition is the most economical in computation time." In a later comparison of methods by Singh and Mahajan (1972) practicability, efficiency and precision of five relative orientation techniques are investigated. It is again the co-planarity condition which proves superior to other techniques. Mahajan and Singh contradict Schut's statement indirectly by claiming that the co-planarity condition is the "most precise", whereas Schut expects the same results for all methods. However, Mahajan and Singh's assessment must be judged with some reservation. The criterion for their accuracy comparison is the residual y-parallax after three iterations. In all five methods compared the residual parallax is smaller than 1 µm and a comparison of accuracies below one micrometer would appear to be somewhat unrealistic.

7.3 CHOICE OF MATHEMATICAL MODEL FOR RELATIVE ORIENTATION

The survey of the historic development of relative orientation and especially Schut's and Mahajan-Singh's comparison of methods, lead to the conclusion that there is no one method which is superior in accuracy or more suited to application in non-topographical photogrammetry. Economy of formulae and calculations remains therefore as the only criterion for the choice of a technique suited to the problems discussed in this study. This made the co-planarity condition method a natural choice as it distinguishes itself by its mathematical simplicity. Most of the other techniques resort to complicated mathematical formulae. A tendency towards a generally more elaborate mathematical formulation of problems in analytical photogrammetry was noted during the ISP Congress in London, 1960 and, in an attempt to revert to basic methods, the following resolution was formulated:

> In order to facilitate the understanding of theoretical developments of formulae in photogrammetry, it is recommended that the simplest possible mathematical tools and procedures be used
>
> (Resolution No. 5 Commission II)

In conformity with this resolution, the writer attempted to find the mathematical concept which presents the co-planarity condition in its most simple form.

The co-planarity condition is satisfied, when the two exposure stations and two corresponding images points lie in one plane or, in a different formulation, when the base vector $\underline{b}$ and the two homologous image vectors $\underline{p}'$ and $\underline{p}''$ are co-planar.

$$(\underline{b}, \underline{p}', \underline{p}'') = 0 \qquad (7.3.1)$$

The three vectors are co-planar when their determinant vanishes.

$$\begin{vmatrix} b_x & b_y & b_z \\ x' & y' & f' \\ x'' & y'' & f'' \end{vmatrix} = 0 \qquad (7.3.2)$$

in which b_x, b_y and b_z are the baseline components in Model co-ordinates.

$$\begin{aligned} b_x &= X_o'' - X_o' \\ b_y &= Y_o'' - Y_o' \\ b_z &= Z_o'' - Z_o' \end{aligned} \qquad (7.3.3)$$

where X_o, Y_o, Z_o are the co-ordinates of the perspective centres of the two camera stations

and x, y, f are rectified image co-ordinates

As in all other relative orientation solutions there is a choice in the co-planarity method between the "one camera" and the "two camera" solution.

In the "one camera", "one projector", or "one perspective centre" method the left camera is held fixed and intersection of image rays is achieved by translating and rotating the right camera. The five parameters of orientation are b_y, b_z and φ, ω, κ. The parameter b_x is set equal to 1 if the orientation is completed without consideration of scale or it is set equal to the known base length in an approximation, which is later improved in an absolute orientation process or in some other scaling procedure.

For the one camera method, equation (7.3.2) takes the form

$$b_x(y'f''-f'y'') + b_y(f'x''-x'f'') + b_z(x'y''-y'x'') = 0 \quad (7.3.4)$$

The "two camera method" involves the rotation of both cameras; rotation angles are then φ' and $\varkappa'$ for the left camera and φ'', ω'' and $\varkappa''$ for the right camera.

In the two camera method a rectangular model co-ordinate system is defined by the direction of the camera base line as X-axis; the Z-axis is at a right angle to the X-axis in the plane formed by the base line and the optical axis of the left camera and the Y-axis forms right angles with the X- and Z- axis, defining either a righthanded or a lefthanded system. Orientation angles $\varkappa'$, φ', $\varkappa''$ φ'' and ω'' are then a measure of the deviation of the two camera axes from these co-ordinate axes. (Fig. 7.3-1)

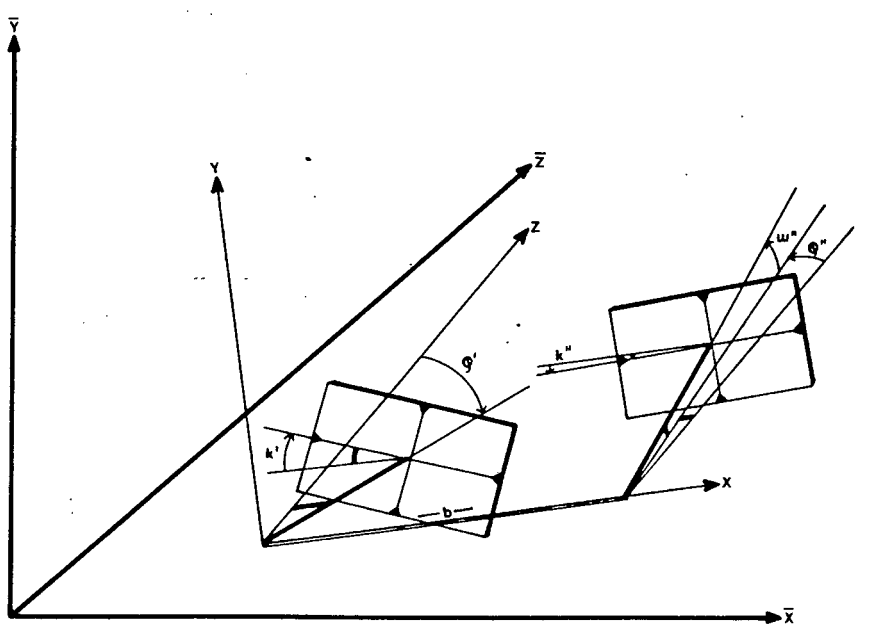

Fig. 7.3-1 Position of Image Plates in Relation to Model Co-ordinate System X, Y and Z and Geodetic System $\bar{X}$, $\bar{Y}$, $\bar{Z}$.

The orientation of the model co-ordinate system is of no practical relevance, if an absolute orientation is executed subsequent to the relative orientation. However, in a situation with limited control, where no transformation into a geodetic co-ordinate system by means of an absolute orientation can be carried out, the model-co-ordinate system serves as the final reference system. It must then be noted, that model co-ordinates are not related to the conventional geodetic (horizon-plumbline) system. Distances evaluated from model co-ordinates are therefore not related to the horizon and the vertical, unless both cameras are set up at the same elevation and the optical axis of the left camera is level.

The one camera method is used in the majority of the relative orientation methods in spite of the fact that formulae for this approach tend to be elaborate. The reason for this preference lies probably in the fact that most relative orientation techniques were developed in the context of aerial triangulation with "Bild Anschluss". Non-topographical photogrammetry deals very rarely with more than two photographs and the two camera method with its simple formulae commends itself.

For the two camera method, equation (7.3.2) becomes with

$$b_y = b_z = 0$$

$$\begin{vmatrix} b_x & 0 & 0 \\ x' & y' & f' \\ x'' & y'' & f'' \end{vmatrix} = 0 \qquad (7.3.5)$$

or

$$b_x (y'' f'' - y'' f') = 0 \qquad (7.3.6)$$

b_x, the baseline, cannot be zero and we therefore have

$$y' f'' - y'' f' = 0 \qquad (7.3.7)$$

or

$$y' - \frac{f'}{f''} y'' = 0 \qquad (7.3.8)$$

We would generally base a relative orientation calculation on more than the minimum number of five pairs of image points. The calculation of the orientation angles, which are hidden in equation (7.3.8) can then be carried out by means of a least squares adjustment. The mathematical model (also known as the functional model) for the least squares adjustment of the relative orientation will be derived in the chapter following.

7.4 THE LEAST SQUARES ADJUSTMENT OF RELATIVE ORIENTATION

The two-camera formulation of the co-planarity condition for the relative orientation adjustment when expressed for a point P_i has with (7.3.8) form:

$$\Phi = y'_i - \frac{f'_i}{f''_i} y''_i = 0 \qquad (7.4.1)$$

In this form the equation contains neither orientation angles nor observed plate co-ordinates in an explicit form. In order to introduce equation (7.4.1) into an adjustment, the rectified values (y'_i, y''_i, f'_i and f''_i) must be expressed in terms of the observed plate co-ordinates $\bar{x}'_i$, $\bar{y}'_i$, $\bar{x}''_i$, $\bar{y}''_i$, the principal distance f' (or, if two different cameras are used for the stereo pair, the principal distances $\bar{f}'$ and $\bar{f}''$) and the unknown orientation angles. The

in the transformations:

$$\underline{x}' = \underline{R}'\underline{\bar{x}}' \quad \text{for the left camera} \tag{7.4.2}$$

$$\text{and} \quad \underline{x}'' = \underline{R}''\underline{\bar{x}}'' \quad \text{for the right camera} \tag{7.4.3}$$

$$\text{with } \underline{\bar{x}}' = \begin{bmatrix} \bar{x}_i' \\ \bar{y}_i' \\ \bar{f}' \end{bmatrix} \quad \text{and} \quad \underline{x}' = \begin{bmatrix} x_i' \\ y_i' \\ f_i' \end{bmatrix} \tag{7.4.2.1}$$

and similar for the right camers.

We define the rotation matrix for the left camera as

$$\underline{R}' = \begin{bmatrix} a_{11} & a_{12} & a_{13} \\ a_{21} & a_{22} & a_{23} \\ a_{31} & a_{32} & a_{33} \end{bmatrix} \tag{7.4.2.2}$$

and for the right camera we have

$$\underline{R}'' = \begin{bmatrix} b_{11} & b_{12} & b_{13} \\ b_{21} & b_{22} & b_{23} \\ b_{31} & b_{32} & b_{33} \end{bmatrix} \tag{7.4.3.2}$$

The elements of the rotation matrices are from (3.1.13 and 3.1.14):

$$a_{11} = \cos \varkappa' \cos \varphi'$$

$$a_{12} = -\sin \varkappa' \cos \varphi'$$

$$a_{13} = -\sin \varphi'$$

$$a_{21} = \sin \varkappa'$$

$$a_{22} = \cos \varkappa' \qquad (7.4.2.3)$$

$$a_{23} = 0$$

$$a_{31} = \cos \varkappa' \sin \varphi'$$

$$a_{32} = -\sin \varkappa' \sin \varphi'$$

$$a_{33} = \cos \varphi'$$

and

$$b_{11} = \cos \varkappa'' \cos \varphi''$$

$$b_{12} = -\sin \varkappa'' \cos \varphi''$$

$$b_{13} = -\sin \varphi''$$

$$b_{21} = \sin \varkappa'' \cos \omega'' + \cos \varkappa'' \sin \varphi'' \sin \omega''$$

$$b_{22} = \cos \varkappa'' \cos \omega'' - \sin \varkappa'' \sin \varphi'' \sin \omega'' \quad (7.4.3.$$

$$b_{23} = \cos \varphi'' \sin \omega''$$

$$b_{31} = -\sin \varkappa'' \sin \omega'' + \cos \varkappa'' \sin \varphi'' \cos \omega''$$

$$b_{32} = -\cos \varkappa'' \sin \omega'' - \sin \varkappa'' \sin \varphi'' \cos \omega''$$

$$b_{33} = \cos \varphi'' \cos \omega''$$

the unknown quantities of the adjustment are the five orientation angles $\varkappa'$, φ', $\varkappa''$, φ'' and ω'', while the principal distances f' and f'' are assumed to be known quantities. (Relative orientation adjustments with principal distances as unknown quantities, so-called "auto" or "self-calibration", were originally attempted in

this study. However, these attempts were abandoned when the resulting normal equation systems proved ill-conditioned, especially for cases with a small Z-range and when satisfactory results were achieved with constant values for the principal distances derived in camera calibrations (7.1)).

The condition equations introduced into the adjustment must be linear and equation (7.4.1) with its non-linear form for unknowns and observations requires linearisation. This is done in the usual manner by means of a Taylor series expansion. The condition equation for a Point P_i is then:

$$\frac{\partial \Phi}{\partial \bar{x}'_i} v_{\bar{x}'_i} + \frac{\partial \Phi}{\partial \bar{y}'_i} v_{\bar{y}'_i} + \frac{\partial \Phi}{\partial \bar{x}''_i} v_{\bar{x}''_i} + \frac{\partial \Phi}{\partial \bar{y}''_i} v_{\bar{y}''_i} + \frac{\partial \Phi}{\partial \varkappa'} d\varkappa' + \frac{\partial \Phi}{\partial \varphi'} d\varphi' +$$

$$\frac{\partial \Phi}{\partial \varkappa''} d\varkappa'' + \frac{\partial \Phi}{\partial \varphi''} d\varphi'' + \frac{\partial \Phi}{\partial \omega''} d\omega'' + \left(y'_i - \frac{f'_i}{f''_i} y''_i\right)\Big|_0 = 0 \qquad (7.4.4)$$

or to simplify the expression

$$a_1 v_{\bar{x}'_i} + a_2 v_{\bar{y}'_i} + a_3 v_{\bar{x}''_i} + a_4 v_{\bar{y}''_i} + A_a d\varkappa' + B_a d\varphi' +$$
$$+ C_a d\varkappa'' + D_a d\varphi'' + E_a d\omega'' + w_a = 0 \qquad (7.4.4.1)$$

$$i = 1, 2, \ldots, m$$

The number of condition equations r is equal to the number of object points m and with n = number of observed plate co-ordinates we can write

$$r = m = \frac{n}{4} \qquad (7.4.5)$$

Each condition equation (7.4.4.1) contains more than one correction simultaneously with a number of unknowns and is therefore of the type requiring a "combined adjustment" (3.2.4).

$$\underline{Bv} + \underline{Ax} + \underline{w} = 0$$

The four corrections which occur in each condition equation are only associated with the specific point for which the equation is formulated and do not occur in any other condition equation. The combined case can thus be reduced to the more convenient quasi-parametric case.

The partial derivatives in (7.4.4) are given by

$$\frac{\partial \Phi}{\partial \alpha} = \frac{\partial y'_i}{\partial \alpha} - \frac{1}{f''^2_i}\left[\left(\frac{\partial f'_i}{\partial \alpha} y''_i + f'_i \frac{\partial y''_i}{\partial \alpha}\right) f''_i - f'_i y''_i \frac{\partial f''_i}{\partial \alpha}\right] \qquad (7.4.6)$$

with

$$\alpha = \bar{x}'_i \;, \bar{y}'_i \;, \bar{x}''_i \;, \bar{y}''_i \;, \varkappa' \;, \varphi' \;, \varkappa'' \;, \varphi'' \;, \omega''$$

The individual partial derivatives in equation (7.4.6) are derived using (3.1.15 and 3.1.16) and listed in Table 7.4-1.

	$\partial y'_i$	$\partial f'_i$	$\partial y''_i$	$\partial f''_i$
$\partial \bar{x}'_i$	a_{21}	a_{31}	0	0
$\partial \bar{y}'_i$	a_{22}	a_{32}	0	0
$\partial \bar{x}''_i$	0	0	b_{21}	b_{31}
$\partial \bar{y}''_i$	0	0	b_{22}	b_{32}
$\partial \varkappa'$	$a_{22}\bar{x}'_i - a_{21}\bar{y}'_i$	$a_{32}\bar{x}'_i - a_{31}\bar{y}'_i$	0	0
$\partial \varphi'$	0	x'_i	0	0
$\partial \varkappa''$	0	0	$b_{22}\bar{x}''_i - b_{21}\bar{y}''_i$	$b_{32}\bar{x}''_i - b_{31}\bar{y}''_i$
$\partial \varphi''$	0	0	$\sin \omega''\ x''_i$	$\cos \omega''\ x''_i$
$\partial \omega''$	0	0	f''_i	$-y''_i$

Table 7.4-1 Partial Differentials for Equation 7.4.6

The coefficent of (7.4.4.1) can now be determined by substituting the individual differentials given in Tab. 7.4-1 into equation (7.4.6) from which we get:

$$a_1 = \frac{\partial \Phi}{\partial \bar{x}'_i} = a_{21} - a_{31}\frac{y''_i}{f''_i}\Big|_0$$

$$a_2 = \frac{\partial \Phi}{\partial \bar{y}'_i} = a_{22} - a_{32}\frac{y''_i}{f''_i}\Big|_0 \qquad (7.4.7.1)$$

$$a_3 = \frac{\partial \Phi}{\partial \bar{x}'_i} = -\left(b_{21} - b_{31}\frac{y''_i}{f''_i}\right)\frac{f'_i}{f''_i}\Big|_0$$

$$a_4 = \frac{\partial \Phi}{\partial \bar{y}'_i} = -\left(b_{22} - b_{32}\frac{y''_i}{f''_i}\right)\frac{f'_i}{f''_i}\Big|_0$$

$$A_a = \frac{\partial \Phi}{\partial \varkappa'} = (a_{22}\bar{x}'_i - a_{21}\bar{y}'_i) - (a_{32}\bar{x}'_i - a_{31}\bar{y}'_i)\frac{y''_i}{f''_i}\Big|_0 \qquad (7.4.7.1)\ \text{contd.}$$

$$B_a = \frac{\partial \Phi}{\partial \varphi'} = -\frac{x'_i y''_i}{f''_i}\Big|_0$$

$$C_a = \frac{\partial \Phi}{\partial \varkappa''} = -\{(b_{22}\bar{x}''_i - b_{21}\bar{y}''_i) - \frac{y''_i}{f''_i}(b_{32}\bar{x}''_i - b_{31}\bar{y}''_i)\}\frac{f'_i}{f''_i}\Big|_0$$

$$D_a = \frac{\partial \Phi}{\partial \varphi''} = -\frac{x''_i f'_i}{f''_i}(\sin\omega'' - \frac{y''_i}{f''_i}\cos\omega'')\Big|_0$$

$$E_a = \frac{\partial \Phi}{\partial \omega''} = -f'_i\{1 + (\frac{y''_i}{f''_i})^2\}\Big|_0$$

The elements of the misclosure vector $\underline{w}$ are given by

$$w_a = y'_i - \frac{f'_i}{f''_i}y''_i\Big|_0 \qquad (7.4.7.2)$$

(The symbol $|_0$ indicates evaluation at provisional values).

Equation (7.4.4) and (7.4.4.1) respectively with the coefficients (7.4.7.1) and the misclosure term (7.4.7.2) represents the condition equation of the relative orientation adjustment.

The partial derivatives are arranged in matrices $\underline{A}$, $\underline{B}$ and $\underline{w}$ of equation (3.2.4)

$$\underset{r,u}{\underline{A}} = \begin{bmatrix} A_a & B_a & C_a & D_a & E_a \\ A_b & B_b & C_b & D_b & E_b \\ & & \vdots & & \\ A_r & B_r & C_r & D_r & E_r \end{bmatrix} \qquad (7.4.8)$$

$$\underset{r,1}{\underline{w}} = \begin{vmatrix} w_a \\ w_b \\ \cdot \\ \cdot \\ w_r \end{vmatrix} \qquad (7.4.9)$$

$$\underset{r,4r}{\underline{B}} = \begin{bmatrix} a_1 & a_2 & a_3 & a_4 & 0 & 0 & 0 & 0 & \cdots & 0 & 0 & 0 & 0 \\ 0 & 0 & 0 & 0 & b_1 & b_2 & b_3 & b_4 & \cdots & 0 & 0 & 0 & 0 \\ & & & \cdot & & & & & & & \cdot & & \\ & & & \cdot & & & & & & & \cdot & & \\ & & & \cdot & & & & & & & \cdot & & \\ 0 & 0 & 0 & 0 & 0 & 0 & 0 & 0 & \cdots & r_1 & r_2 & r_3 & r_4 \end{bmatrix} \qquad (7.4.10)$$

with

u = number of unknowns

and

r = number of condition equations

If individual weights are introduced for each observed plate co-ordinate then the weight matrix $\underline{P}$ is

$$\underset{4r,4r}{\underline{P}} = \begin{bmatrix} P_{\bar{x}_1'} & 0 & 0 & 0 & \cdots & & \\ 0 & P_{\bar{y}_1'} & 0 & 0 & \cdots & & \\ 0 & 0 & P_{\bar{x}_1''} & 0 & \cdots & & \\ 0 & 0 & 0 & P_{\bar{y}_1''} & & & \\ 0 & 0 & 0 & 0 & P_{\bar{x}_2'} & \cdots & \\ & & & & & \cdot & \\ & & & & & \cdot & \\ & & & & & \cdot & P_{\bar{y}_r''} \end{bmatrix} \qquad (7.4.11)$$

The least squares solution is then found by applying the formulae for the quasi-parametric case as given in Table 3.2-1.
The quasi-weight matrix has then the form (3.2.25) and elements on the principal diagonal of $\underline{P}^*$ are

$$P_a^* = \frac{1}{\frac{a_1^2}{P_{\bar{x}'_i}} + \frac{a_2^2}{P_{\bar{y}'_i}} + \frac{a_3^2}{P_{\bar{x}''_i}} + \frac{a_4^2}{P_{\bar{y}''_i}}} = \frac{1}{\left[\frac{a_j^2}{P}\right]_i} \qquad i = 1,2,..r \quad (7.4.12)$$

$$j=1 \text{ to } 4$$

If the same weight is allocated to the four plate co-ordinates of an object point then (7.4.12) becomes

$$P_a^* = \frac{P_a}{\left[a_j^2\right]} \qquad (7.4.13)$$

$$j=1 \text{ to } 4$$

with

$$P_a = P_{\bar{x}'_i} = P_{\bar{y}'_i} = P_{\bar{x}''_i} = P_{\bar{y}''_i}$$

and if all image points are given unit weight we have

$$P_a^* = \frac{1}{\left[a_j^2\right]} \qquad (7.4.14)$$

$$j=1 \text{ to } 4$$

The vector of unknown orientation angles is finally found from (3.2.26):

$$\underline{x} = -(\underline{A}^T \underline{P}^* \underline{A})^{-1} \underline{A}^T \underline{P}^* \underline{w}$$

Equation (3.2.28) generates quasi-corrections

$$\underline{V}^{*} = \underline{A}\,\underline{x} + \underline{w}$$

and the actual corrections are determined with equation (3.2.29)

$$\underline{v} = \underline{P}^{-1}\underline{B}^{T}\underline{P}^{*}\underline{V}^{*} \qquad (7.4.15)$$

or in conventional non-matrix notation we have for individual corrections

$$\begin{aligned} v_{\bar{x}'_i} &= -\frac{1}{P_{a_1}}\, a_1 V^{*} P_a^{*} \\ v_{\bar{y}'_i} &= -\frac{1}{P_{a_2}}\, a_2 V^{*} P_a^{*} \\ v_{\bar{x}''_i} &= -\frac{1}{P_{a_3}}\, a_3 V^{*} P_a^{*} \\ v_{\bar{y}''_i} &= -\frac{1}{P_{a_4}}\, a_4 V^{*} P_a^{*} \end{aligned} \qquad (7.4.16)$$

The adjustment is concluded with a global check. For this check the corrections (7.4.16) are added to the observed plate co-ordinates

$$\begin{aligned} \bar{x}'^{*}_i &= \bar{x}'_i + v_{\bar{x}'_i} \qquad \bar{x}''^{*}_i = \bar{x}''_i + v_{\bar{x}''_i} \\ \bar{y}'^{*}_i &= \bar{y}'_i + v_{\bar{y}'_i} \qquad \bar{y}''^{*}_i = \bar{y}''_i + v_{\bar{y}''_i} \end{aligned} \qquad (7.4.17)$$

and final, "most probable" values for the unknowns are evaluated by adding the $\underline{x}$ vector ($d\varkappa'$, $d\varphi'$, $d\varkappa''$, $d\varphi''$, and $d\omega''$) to the provisonal values $\varkappa'_o$, φ'_o, $\varkappa''_o$, φ''_o, and ω''_o.

Rectified plate co-ordinates are then found by introducing the adjusted plate co-ordinates (7.4.17) together with the most probable values for the orientation angles into equations (7.4.2) and (7.4.3). These adjusted rectified co-ordinates must then satisfy equation (7.4.1)

$$y'_i - \frac{f'_i}{f''_i} y''_i = 0$$

within the calculation accuracy of the computer employed for the adjustment.

7.5 THE WEIGHT MODEL FOR THE RELATIVE ORIENTATION ADJUSTMENT

The functional model of the least squares adjustment is mathematically rigid and does not permit subjective manipulation of observations. This does not hold for the weight model where individual bias and subjective interpretation are unavoidable. Observation weights can be allocated on the basis of previous experience with the instruments used for the observations, as a result of test observations or by assessing the observation procedure on an error theoretical basis.

In order to introduce a suitable weight model for the close-range relative orientation adjustment, four weight concepts were tested in one case of test field photography and for a typical stereographic image pair selected from the Wildlife photography (Chapter 10).

The tested weight models are:

a) Uniform weight

b) Weights based on image definitions

c) Distance related weights

d) Ad hoc weights

a) Uniform Weight

The three "instruments" involved in the data gathering process are the photographic lens, the photographic emulsion and the stereo comparator.

In this weight model it is assumed that the effect of random errors in these three components does not vary over the range of the image plane and unit weight is given to all $\bar{x}$ and $\bar{y}$ image co-ordinates.

Uniform weighting of image points assumes consistent image quality for all observed points; this must be borne in mind when selecting image points for the relative orientation adjustment with this weight model.

b) Weights based on image defintions

Each image point was observed 10 times on the stereo comparator. Standard deviations σ_i were determined and weights were allocated in the usual way as

$$P_i = \frac{\sigma_0^2}{\sigma_i^2} \qquad (7.5.1)$$

In spite of seemingly varying image quality between points, the standard deviations did not vary by more than 5 µm for both tested stereo pairs (Chapter 4.3). Weights for the two image plates of a stereo pair were determined independently.

c) Distance related weights

Weights were allocated inversely proportional to the distance d of the object point from the camera station, assuming that image quality does decrease with this distance

$$P_i = \frac{\text{const}}{d_i} \qquad (7.5.2)$$

This weight model was realised by executing a first adjustment with uniform weights followed by a second adjustment with "distance" weights derived from model co-ordinates of the first adjustment. As in case b) the same object point will generally have image points of different weight on the two images of the stereo pair.

d) Ad hoc weights

In this weight model, the weights were allocated by simply judging the image quality while carrying out the comparator readings and then by allocating weights on a scale ranging from 10 for the best to 1 for the poorest image quality.
The relative orientation adjustment of the test field photography was carried out with all four weight models. The resulting model co-ordinates were compared against the known test field co-ordinates and average displacements were determined.

Root mean square errors evaluated from these differences do not differ significantly when comparing the four weight models, but the corrections v and subsequently the [pvv] values are larger for models b) to d) than for model a).
It appears that either the adjustment is not very sensitive to a change in the weight model or that none of the suggested and investigated weight concepts, that is b) to d), describe the error configuration of the image phase more realistically than the uniform weight model a). Unit weights were therefore adopted for all plate co-ordinates.

7.6 OPTIMUM NUMBER OF IMAGE POINTS FOR A RELATIVE ORIENTATION ADJUSTMENT

In order to reduce computation time and memory space, it is advisable to minimise the number of image points involved in the adjustment of the relative orientation. This is especially relevant if mini computers are used for the adjustment. An investigation of an optimum point number for the relative orientation adjustment must be based on the assumption that an increased point number is accompanied

by increased accuracies for the orientation angles and ultimately the model co-ordinates. One must further assume that the accuracy improvement with increasing point numbers will become less relevant as the point numbers become larger and that eventually a situation will be reached where the addition of further points to the adjustment does not improve the results significantly. To establish such an optimum number of points for the test field configuration or any close range object of similar dimensions, a sequence of relative orientation adjustments with increasing point numbers was executed. Six points in the test field (Fig. 5-3) were chosen for a first adjustment and this point number was increased by one point at a time until 15 points were involved in the adjustment (Fig. 7.6-1).

A final adjustment was carried out using 30 points.

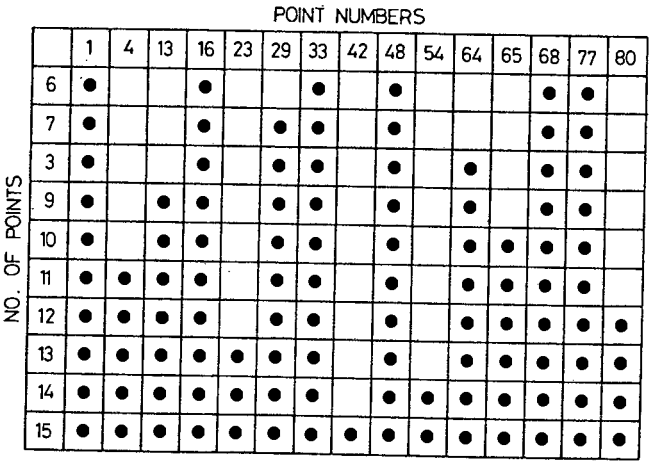

Fig. 7.6-1 Configuration of Points Used in the Relative Orientation Adjustment in Order to Optimise the Number of Points for the Adjustment. (Point Numbers Refer to Fig. 5-3)

Point positions in the test field were selected so as to avoid a bias caused by possibly more favourable point configurations for the cases with larger point numbers. The adjustment results of each of the ten test cases were compared against the 30 point adjustment. It was not possible to predict which of the parameters of the adjustment would be most sensitive to a change in the number of points in the adjustment. Therefore, the reaction of variance factor (σ_0) adjustment unknowns ($\varkappa'$, φ', $\varkappa''$, φ'', ω'') and model co-ordinates (X, Y, Z) to changes in the point number was investigated. Differences between the results of each case and the results of the 30 point adjustment were evaluated and graphically represented in Fig. 7.6-2. For the diagrams of the changes in the model co-ordinates all points involved in the adjustment were compared against their equivalent points in the 30 point reference adjustment and the average deviation was plotted for each case.

The diagrams that follow show that all the tested parameters converge to their final values for point numbers of less than 15. Some of the parameters ($\varkappa'$, φ'' and especially Z) require more points than others to settle for their final values, but all can be considered as stable for a point number of 13.
If lower accuracies for the model co-ordinates are acceptable then as few as 10 points are sufficient for the adjustment.
Generalising, one can say that a minimum of 10 points should be used in a close-range relative orientation adjustment, that a number of say 15 points seems optimal, and that no significant changes in the result can be expected when increasing point numbers beyond 15.

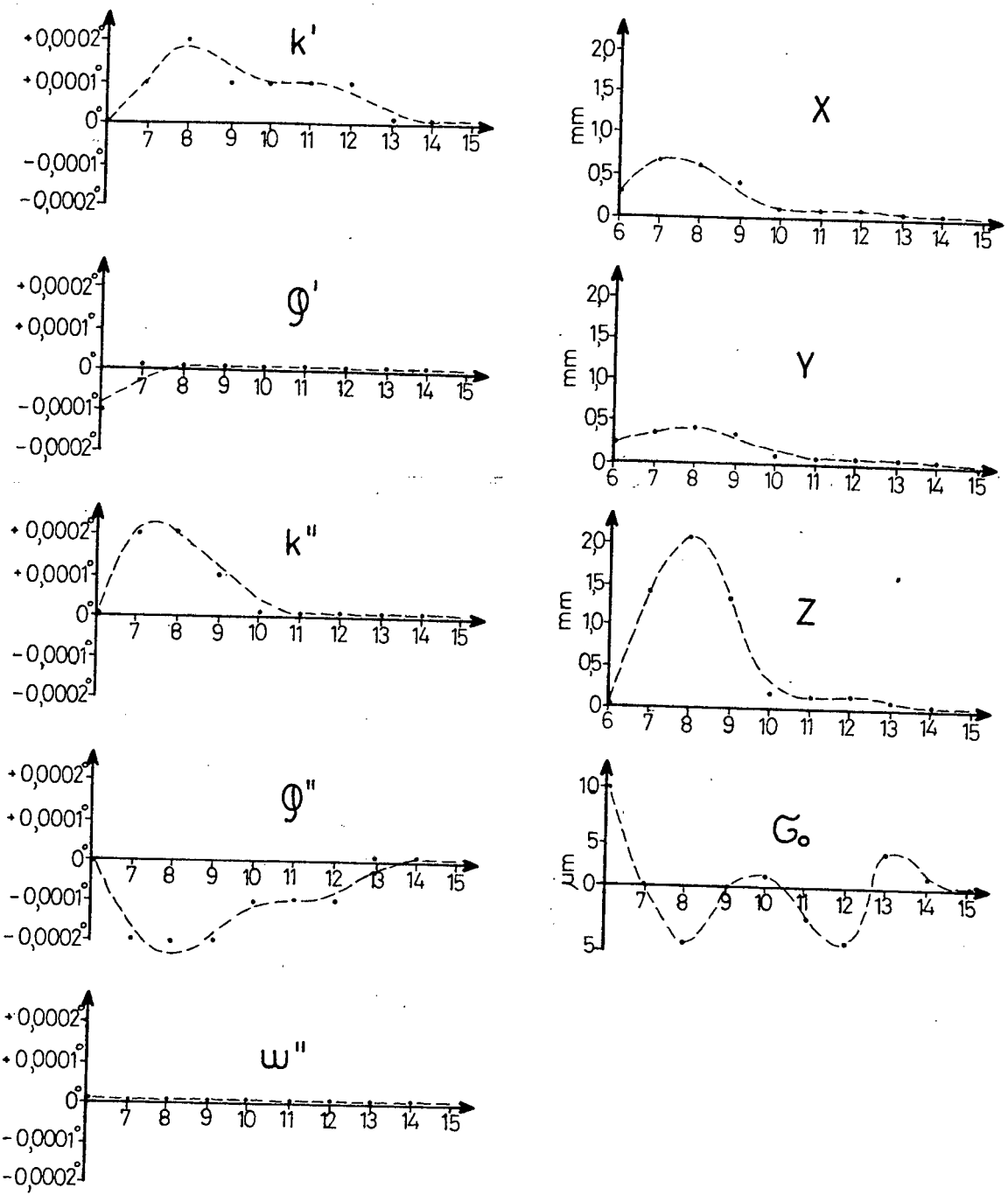

Fig. 7.6-2 Investigation to Establish Optimum Point Numbers for the Relative Orientation Adjustment. The Diagrams Show the Deviation (Vertical Axis) of Adjustment Parameters from their Final Values for Increasing Numbers of Points (Horizontal Axis) Involved in the Adjustment.

7.7 COMPARISON OF COMBINED CASE AND QUASI-PARAMETRIC CASE IN THE RELATIVE ORIENTATION ADJUSTMENT

Before discussing the use of control distances in the relative orientation it seems appropriate to briefly justify the choice of the quasi-parametric case in preference to the combined adjustment.

The advantage of the quasi-parametric adjustment over the combined case lies in the considerably reduced number of matrices used in the calculation. The quasi-parametric adjustment was introduced at a time when adjustments were calculated by hand or on manual calculators and in this event any method reducing the number of calculation steps required was favoured. The introduction of mainframe computers meant that there was less emphasis on methods reducing computation time and saving memory space, but with the advent of the mini computer such methods have regained some of their importance (again only temporarily, until new developments extend the mini computer memory to the size of a mainframe computer).

The superiority of the memory economics of the quasi-parametric case over other adjustment techniques is most convincingly shown in an example. In the following the memory space required for the formation of the matrix of normal equation coefficients is compared for different adjustment algorithms:

If for example we consider a relative orientation based on 15 object points, we have

$n = 15 \cdot 4$ observed plate co-ordinates

$u = 5$ unknowns

and $r = 15$ condition equations

For the combined case the matrix of normal equation coefficents is (Tab. 3.2-1)

$$\underline{Q}^{-1} = \underline{A}^T(\underline{B}\ \underline{P}^{-1}\underline{B}^T)^{-1}\underline{A}$$

The equivalent equation for the quasi-parametric case is

$$\underline{Q}^{-1} = \underline{A}^T\underline{P}^*\underline{A}$$

Matrices $\underline{B}\ \underline{P}^{-1}\ \underline{B}^T$ and $\underline{A}^T\ \underline{P}^*\ \underline{A}$ do not need to be formed in the conventional way by matrix multiplication, instead, the coefficients of each condition equation can be formed in turn and their contribution to the $\underline{Q}^{-1}$ matrix can then be added step by step into the $\underline{Q}^{-1}$ matrix,(Rüther 1982). This "short" method avoids the necessity to formulate the generally large $\underline{B}$ and $\underline{A}$ matrices in the combined and quasi-parametric case respectively. In each case only a vector for one equation at a time is required.

A comparison of the memory requirements for the formulation of the $\underline{Q}^{-1}$ matrix in the conventionally treated combined case (I), the "short" method treatment of the combined case (II), the quasi-parametric case (III) and the short method for the quasi-parametric case (IV) is given in Table 7.7-1. Matrix inversion is assumed to be executed in situ. Matrices such as $\underline{B}\ \underline{P}^{-1}$ and $\underline{A}^T\ \underline{N}^{-1}$ have to be dimensioned as intermediate calculation matrices. For the purpose of this comparison matrix space is maintained in memory and no redimensioning of obsolete matrix space is assumed.
In cases III and IV elements of $\underline{P}^*$ can be formed directly and do not require the more memory space-consuming matrix multiplication.

Matrix	Dimension	Case I	Case II	Case III	Case IV
$\underline{B}$	r•n	900	60	-	-
$\underline{B}^T$	n•r	900	-	-	-
$\underline{P}$	n•n	3600	60	-	-
$\underline{B}\underline{P}^{-1}$	r•n	900	-	-	-
$\underline{B}\underline{P}^{-1}\underline{B}^T=\underline{N}$	r.r	225	225	$225(\underline{P}^*)$	15
$\underline{A}$	r.u	75	75	75	5
$\underline{A}^T$	u.r	75	75	75	-
$\underline{A}^T\underline{N}^{-1}$	u.r	75	75	75	-
$\underline{A}^T\underline{N}^{-1}\underline{A}$	u.u	25	25	$25(\underline{A}^T\underline{P}^*\underline{A})$	25
TOTAL		6775	595	475	45

Tab. 7.7-1 Comparison of Memory Space Requirements for the Formulation of the Q^{-1} Matrix for the Combined Case and the Quasi-parametric Case.

Memory space requirements listed in Table 7.7-1 indicate clearly that the quasi-parametric case should be preferred when mini computers are employed for relative orientation adjustment.

7.8 MODEL CO-ORDINATES

Once the orientation parameters $\varkappa'$, φ', $\varkappa''$, φ'' and ω'' of a stereo pair have been established in a relative orientation adjustment, model co-ordinates can be evaluated for object points. Model co-ordinates X, Y, Z are a function of the adjusted and rectified plate co-ordinates (x', y', f' and x", y",f") as well as the base b.

$$X, Y, Z = f(x', y', f', x'', y'', f'', b). \qquad (7.8.1)$$

Analytically an object point is defined by the intersection of the two mathematically re-established projection rays from the perspective centres of the camera to the object point. Owing to errors in the plate co-ordinates and in the elements of inner orientation of the cameras these space rays generally do not intersect after the most probable relative orientation values for the stereo pair have been established. Only after small corrections ($v_{\bar{x}'}$, $v_{\bar{y}'}$, $v_{\bar{x}''}$, $v_{\bar{y}''}$) have been added to the observed plate co-ordinates in the process of the relative orientation adjustment do all corresponding rays intersect in space, thus forming the object points. In this case any one of a number of possible mathematical solutions to the intersection of space rays will serve to find the unique position of an object point. A problem, however, does arise if additional points are calculated from plate co-ordinates which were not incorporated in the relative orientation adjustment. This situation may well occur if mini computers are employed to determine large numbers of object points. Here it would be impractical, if not impossible, to include all observed plate co-ordinates into the adjustment in which the relative orientation parameters are determined and a minimum number of points (7.6) should be used to reduce computation time and computer memory requirements.

The space co-ordinates of any additional object points must then be calculated in a separate procedure in which the plate co-ordinates are rectified on the basis of the adjusted orientation parameters. Since in this case intersection of corresponding projection rays cannot be expected, some thought must be given to the choice of a mathematical model which can provide the most probable object point positions.

The writer has compared two approaches to the problem of the evaluation of object points from non-intersecting projection rays. The more conventional (Schwidefsky 1959) approach represents the mathematical formulation of the photogrammetric plotting instrument procedure, the other, suggested in principle by Rinner (1957), reflects a more mathematical concept.

In the first method (A) the intersections of the two space rays with a specific Z plane is evaluated and their mean is adopted as a final value. In the second method (B) the points of shortest distance between both rays are found and a point midway along the line of closest approach is accepted as the position of the object point. The writer has derived a simple set of formulae based on Rinner's concept for Method B.

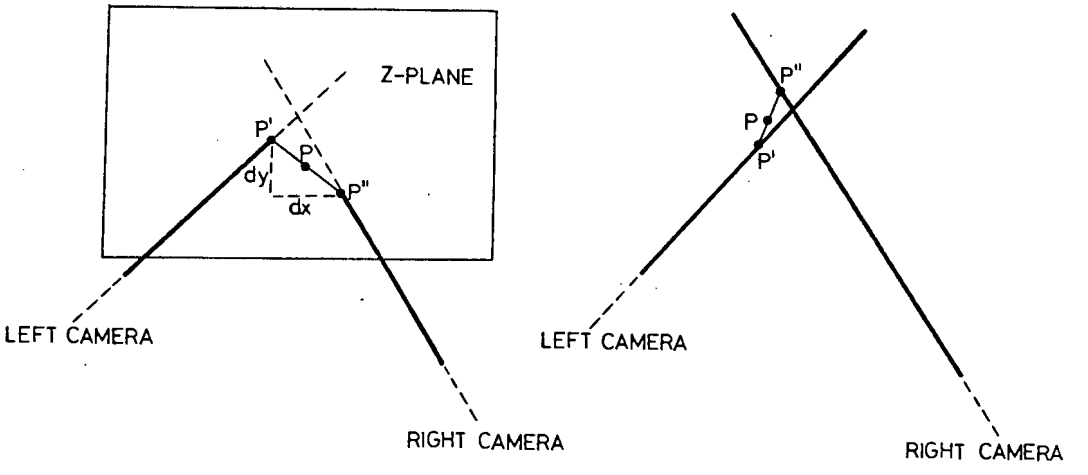

Method A Method B

Fig. 7.8-1 Two Methods of Determination of Model Co-ordinates

7.8.1 Method A

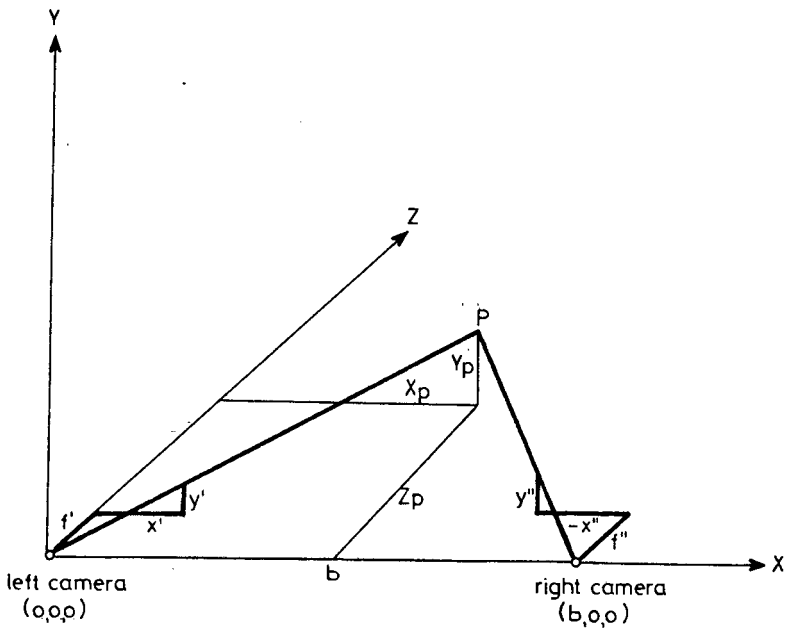

Fig. 7.8.1-1 Derivation of model co-ordinates (A)

From Fig. 7.8.1-1 we have:

$$\frac{X_p}{Z_p} = \frac{x'}{f'} \quad \text{and} \quad \frac{b-X_p}{Z_p} = -\frac{x''}{f''} \tag{7.8.1.1}$$

or

$$Z_p \frac{x'}{f'} = Z_p \frac{x''}{f''} + b \tag{7.8.1.2}$$

hence for the model co-ordinates

$$Z_p = \frac{b}{(\frac{x'}{f'} - \frac{x''}{f''})} \tag{7.8.1.3}$$

$$X_p = Z_p \frac{x'}{f'} \quad \text{or} \quad X_p = Z_p \frac{x''}{f''} + b \tag{7.8.1.4}$$

and

$$Y_p = Z_p \frac{y'}{f'} \quad \text{or} \quad Y_p = Z_p \frac{y''}{f''} \tag{7.8.1.5}$$

If the space rays do not intersect two values each are found for X_p and Y_p while Z_p defines the Z plane of intersection. Final values for X_p and Y_p are then

$$X_p = \frac{X'_p + X''_p}{2} \qquad (7.8.1.6)$$

$$Y_p = \frac{X'_p + Y''_p}{2} \qquad (7.8.1.7)$$

7.8.2 Method B

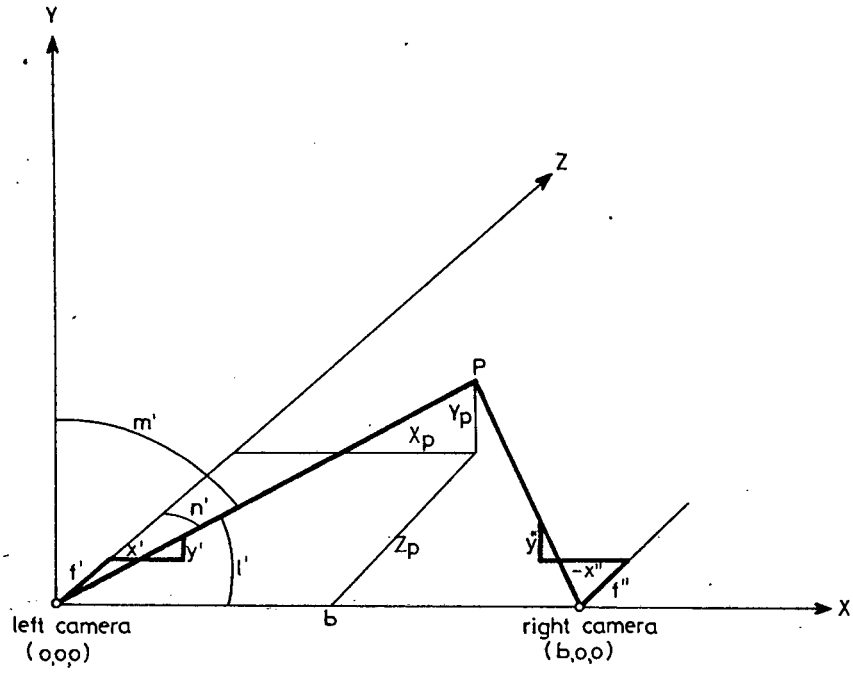

Fig. 7.8.2-1 Derivation of Model Co-ordinates (B)

The direction cosines for the left and right projection rays are

$$\ell' = \frac{x'}{t'} \qquad \ell'' = \frac{x''}{t''}$$

$$m' = \frac{y'}{t'} \qquad m'' = \frac{y''}{t''} \qquad (7.8.2.1)$$

$$n' = \frac{f'}{t'} \qquad n'' = \frac{f''}{t''}$$

with

$$t'^2 = x'^2 + y'^2 + f'^2 \quad \text{and} \quad t''^2 = x''^2 + y''^2 + f''^2 \qquad (7.8.2.2)$$

Co-ordinates of points on the left and right ray are given by

$$\begin{bmatrix} x' \\ y' \\ z' \end{bmatrix} = \lambda' \begin{bmatrix} \ell' \\ m' \\ n' \end{bmatrix} \quad \text{and} \quad \begin{bmatrix} x'' \\ y'' \\ z'' \end{bmatrix} = \lambda'' \begin{bmatrix} \ell'' \\ m'' \\ n'' \end{bmatrix} + \begin{bmatrix} b \\ 0 \\ 0 \end{bmatrix} \qquad (7.8.2.3)$$

Where λ' and λ'' are the vector lengths from the projective centres to the respective points on both rays.

A distance between points P' and P" on corresponding rays is then

$$d = \left(\left[(\lambda'\ell' - (b+\lambda''\ell'') \right]^2 + \left[\lambda'm' - \lambda''m'' \right]^2 + \left[\lambda'n' - \lambda''n'' \right]^2 \right)^{\frac{1}{2}} \qquad (7.8.2.4)$$

The two rays have their point of closest approach where equation (7.8.2.4) reaches its minimum or when equations

$$\frac{\partial d}{\partial \lambda'} = 0 \quad \text{and} \quad \frac{\partial d}{\partial \lambda''} = 0 \qquad (7.8.2.5)$$

are both satisfied.

Differentiation of (7.8.2.4) and some rearranging leads to

$$\lambda'_{min} = -b \frac{C\,\ell''-\ell'}{1-C^2}$$
$$\lambda''_{min} = -b \frac{C\,\ell'-\ell''}{1-C^2} \qquad (7.8.2.6)$$

with $C = \ell'\ell'' + m'm'' + n'n''$

where λ'_{min} and λ''_{min} are the distances from the perspective centres of the cameras to the point P' and P" at minimum distance between the two rays. Final values for the model co-ordinates are then

$$X_p = \frac{\lambda'\ell' + \lambda''\ell'' + b}{2}$$

$$Y_p = \frac{\lambda'm' + \lambda''m''}{2} \qquad (7.8.2.7)$$

$$Z_p = \frac{\lambda'n' + \lambda''n''}{2}$$

Method B is mathematically more appealing as it reflects the principle of the least squares adjustment in its minimum distance solution.

The two methods were compared in over 60 test cases. In each case model co-ordinates of 80 points were calculated by both methods and their mean deviations from the true value of the object poins was determined. Table 7.8.2-1 shows the results of the comparison and it becomes obvious that there are only small differences betwen both methods. There is, however, a tendency in some cases, for the Y co-ordinates to be slightly closer to the true values, when evaluated by method B. Ten of the 80 points have in each case been evaluated as part of the relative orientation adjustment and inspection of these individual points shows that, as expected, Method B results generally in values which are closer to the least squares solution.

It would seem sensible therefore to give preference to Method B in spite of its slightly more elaborate formulae.

If model co-ordinates are evaluated in the process of the least squares solution, Method A must be recommended. In this case ray intersection is guaranteed and both methods lead to the same unique solution, obviously the shorter formulae with shorter computation time must then be favoured.

COMPARISON OF MODEL CO-ORDINATE DETERMINATION METHODS

(UNITS : MM)

	METHOD A			METHOD B			DIFFERENCE A-B		
	DX	DY	DZ	DX	DY	DZ	DDX	DDY	DDZ
SYNRANDOMN	0.6	0.6	1.2	0.6	0.5	1.2	0.0	0.0	0.0
SYNPD1N	4.7	0.4	4.9	4.7	0.3	4.9	0.0	0.1	0.0
SYNPD2N	9.4	0.9	9.7	9.4	0.6	9.7	0.0	0.3	0.0
SYNPD2NS	9.4	1.5	9.3	9.4	0.9	9.4	0.0	0.6	0.0
SYNPD2NB	9.3	3.3	8.6	9.3	2.7	8.7	0.0	0.7	-0.1
SYNPD2NP	9.2	2.5	8.7	9.2	1.8	8.8	0.0	0.6	-0.1
SYNPD3N	0.0	0.0	4.2	0.0	0.0	4.2	0.0	0.0	0.0
SYNPD3NS	0.1	0.0	4.2	0.1	0.0	4.2	0.0	0.0	0.0
SYNPD3NB	2.0	1.6	0.9	2.0	1.6	0.9	0.0	0.0	0.0
SYNPD3NP	2.0	1.6	0.9	2.0	1.6	0.9	0.0	0.0	0.0
SYNPD3ND	4.9	3.7	0.0	4.9	3.7	0.0	0.0	0.0	0.0
SYNPD3NAF	0.0	0.0	0.0	0.0	0.0	0.0	0.0	0.0	0.0
SYNPD4N	9.4	0.9	8.6	9.4	0.6	8.6	0.0	0.3	-0.1
SYNPP1N	15.5	11.3	25.7	15.5	11.3	25.7	0.0	0.0	0.0
SYNPP2N	2.0	8.6	4.6	2.0	8.6	4.6	0.0	0.0	0.0
SYNPP2NS	2.1	8.6	4.6	2.1	8.6	4.6	0.0	0.0	0.0
SYNPP2NB	2.0	8.6	4.6	2.0	8.6	4.6	0.0	0.0	0.0
SYNPP2NP	2.0	8.6	4.6	2.0	8.6	4.6	0.0	0.0	0.0
SYNPP3N	16.0	13.0	25.8	16.0	13.1	25.8	0.0	0.0	0.0
SYNPP4N	8.5	8.5	0.0	8.5	8.5	0.0	0.0	0.0	0.0
SYNPP4NS	8.5	8.5	0.7	8.5	8.5	0.7	0.0	0.0	0.0
SYNPP4NB	8.5	8.5	0.1	8.5	8.5	0.1	0.0	0.0	0.0
SYNPP4NP	8.5	8.5	0.0	8.5	8.5	0.0	0.0	0.0	0.0
SYNPP4NAF	8.5	8.5	0.0	8.5	8.5	0.0	0.0	0.0	0.0
SYNPP5N	31.3	23.2	52.9	31.3	23.4	52.9	0.0	-0.2	0.0
SYNPDPPN	18.7	11.2	27.4	18.7	11.8	27.4	0.0	-0.7	0.0
SYNPDPPNS	12.3	5.9	15.0	12.3	5.8	15.0	0.0	0.1	0.0
SYNPDPPNB	13.3	8.1	12.1	13.3	7.8	12.1	0.0	0.4	0.0
SYNPDPPNP	10.7	4.5	13.0	10.7	4.5	13.0	0.0	0.0	0.0
SYNPDPPNAF	12.4	5.2	11.9	12.5	5.2	11.9	0.0	0.0	0.0
SYNPDPPNO	8.5	8.5	4.2	8.5	8.5	4.2	0.0	0.0	0.0
SYNPDPPNSO	8.5	8.5	4.9	8.5	8.5	4.9	0.0	0.0	0.0
SYNPDPPNBO	8.7	8.6	1.0	8.7	8.6	1.0	0.0	0.0	0.0
SYNPDPPNPO	8.6	8.6	0.9	8.6	8.6	0.8	0.0	0.0	0.0
SYNPDPPNDO	9.2	8.7	0.0	9.2	8.7	0.0	0.0	0.0	0.0
SYNPDPPNFO	8.5	8.5	0.0	8.5	8.5	0.0	0.0	0.0	0.0
SYNPDPPN1	4.2	4.2	1.7	4.2	4.2	1.7	0.0	0.0	0.0
SYNPDPPNS1	4.2	4.2	2.0	4.2	4.2	2.0	0.0	0.0	0.0
SYNPDPPNB1	4.3	4.3	0.7	4.3	4.3	0.7	0.0	0.0	0.0
SYNPDPPNP1	4.3	4.3	0.4	4.3	4.3	0.4	0.0	0.0	0.0
SYNRANDOM	0.8	0.7	1.7	0.8	0.7	1.7	0.0	0.0	0.0
SYNPD1	6.6	4.1	7.2	6.6	3.8	7.3	0.0	0.3	0.0
SYNPD2	13.1	8.1	14.4	13.1	7.6	14.5	0.0	0.5	0.0
SYNPD3	8.2	6.5	10.4	8.2	6.5	10.4	0.0	0.0	0.0
SYNPD3S	2.1	1.4	1.8	2.1	1.4	1.8	0.0	0.0	0.0
SYNPD3B	2.8	1.9	1.0	2.8	1.9	1.0	0.0	0.0	0.0
SYNPD3P	3.3	2.5	2.0	3.3	2.5	2.0	0.0	0.0	0.0
SYNPD3AF	2.3	1.3	1.2	2.3	1.3	1.2	0.0	0.0	0.0
SYNPD4	10.9	1.7	9.6	10.9	1.1	9.7	0.0	0.6	-0.1

Table 7.8.2-1 Comparison of Results of Model Co-ordinate Determination using Method A and Method B

7.9 ERROR THEORY OF THE RELATIVE ORIENTATION ADJUSTMENT

The validity of the numerical results of an adjustment calculation remains in some doubt if the results are not subjected to an error-theoretical scrutiny based on the variance-covariance matrix of the adjustment. From this the accuracy of the observations, the quality of the chosen weight model, the geometry and the mathematical model, as well as the reliability of the estimated parameters and any other derived quantities can be judged. For the relative orientation adjustment the following accuracy measures are the most relevant.

7.9.1 Standard Deviation of Unit Weight

The variance factor or standard deviation of an adjustment, σ_0, that is the standard deviation of an unadjusted observation of weight one, is introduced as a known constant into the adjustment.
Good knowledge of the a priori value of σ_0 is important for the evaluation of a reliable weight model and subsequently for the correct determination of the absolute values of all other error measures of the adjustment. The adjustment yields an estimator for the variance σ_0 a posteriori in the well known form (3.2.15) or for the quasi-parametric case (3.2.31)

$$\sigma_0^2 = \frac{\underline{v}^T \underline{P} \underline{v}}{r-u} \text{ or } = \frac{\underline{V}^{*T} \underline{P}^* \underline{V}^*}{r-u} \tag{7.9}$$

The values for σ_0 a priori and σ_0 a posteriori should not differ significantly. A χ^2 test is generally employed to statistically test if the two values differ significantly at a stipulated probability level (e.g. Mikhail, Ackermann 1976).

If the test is not satisfied an error or errors must be suspected in

a) the value for σ_0 a priori

b) the weight model

c) the geometry of the points used for the orientation

or d) the mathematical model.

The numerical value of σ_0 a posteriori is unreliable if an insufficient number of redundancies is available, and uncritical use of σ_0 here can lead to over-optimistic accuracy estimates. (Chrzanowski (1977) stipulates as many as 30 redundancies or 50% redundancies, whichever is higher, as the minimum for a reliable statistic).

7.9.2 Standard Deviation a priori of an Observation

To determine the accuracy of an observed image co-ordinate before adjustment we evaluate (3.2.16)

$$\sigma_i^2 = \sigma_0^2 P_{a_i}$$

where P_{a_i} (i = 1 to 4) are the weights of the plate co-ordinates of a point pair (for $P_{a_i} = 1$ we have $\sigma_i = \sigma_0$).

7.9.3 Standard Deviation of an Unknown

The standard deviations of the estimated parameters ($\varkappa'$, φ', $\varkappa''$, φ'', ω'') are found from (3.2.17)

$$\sigma_x^2 = \sigma_0^2 Q_{xx}$$

where Q_{xx} are the elements of the principal diagonal of the variance-co-variance matrix from (3.2.27):

$$\underline{Q} = (\underline{A}^T \underline{P}^* \underline{A})^{-1}$$

7.9.4 Standard Deviation of Model Co-ordinates

The ultimate object of the relative orientation is the determination of model co-ordinates. The evaluation of the accuracies of the individual model point determination is therefore of major importance. These errors fall under the group of "errors of a function of the unknowns and observations", and they require elaborate mathematical derivations and time-consuming calculations.

The functions of the co-ordinates of a model point are (7.8.1.3 to 7.8.1.5):

$$Z_p = \frac{b}{(\frac{x'}{\bar{f}'} - \frac{x''}{\bar{f}''})}$$

$$X_p = Z_p \frac{x'}{\bar{f}'}$$

$$Y_p = Z_p \frac{y'}{\bar{f}'}$$

They are functions of the orientation angles, the principal distances and the observed plate co-ordinates:

$$X_i, Y_i, Z_i = f(\varkappa', \varphi', \varkappa'', \varphi'', \omega'', \bar{f}_i, \bar{f}''_i \bar{x}'_i \bar{y}'_i \bar{x}''_i \bar{y}''_i)$$

Following Wolf's (1968) concept of the standard deviation of a function, the expressions for X_i, Y_i and Z_i are linearised and the differentials are combined in two vectors (3.2.20)

$$F = \underline{f}^T(\underline{\ell}+\underline{v}) + \underline{\bar{f}}^T\underline{x} \qquad (7.9.1)$$

with

$$\underline{f}^T = \left[\frac{\partial F}{\partial \bar{x}'_i} \quad \frac{\partial F}{\partial \bar{y}'_i} \quad \frac{\partial F}{\partial \bar{x}''_i} \quad \frac{\partial F}{\partial \bar{y}''_i} \quad 0 \quad 0 \quad \dots \quad 0\right] \qquad (7.9.1.1)$$

and $$\bar{f}^T = \left[\frac{\partial F}{\partial \varkappa'} \quad \frac{\partial F}{\partial \varphi'} \quad \frac{\partial F}{\partial \varkappa''} \quad \frac{\partial F}{\partial \varphi''} \quad \frac{\partial F}{\partial \omega''}\right] \qquad (7.9.1.2)$$

The positions of the four non-zero elements in $\underline{f}$ change from object-point to object-point.

The standard deviation of the model co-ordinates of the object-points are then with 3.2.23.

$$\sigma_m^2 = \sigma_o^2 \; Q_{FF} \qquad m = x, y, z$$

with Q_{FF} from (3.2.24).

Equation (3.2.24) is unsuitable for use in mini computers owing to the large number of matrices and matrix manipulations involved.

An equation for Q_{FF} which is more suitable for mini computers is derived in Appendix I.

Q_{FF} can then be expressed as:

$$Q_{FF} = \sum_{i=1}^{4} \frac{f_i^2}{P_i} - P^* \sum_{i=1}^{4} \left(\frac{a_i}{P_i} f_i\right)^2 + \sum_{i=1}^{5} \sum_{j=1}^{5} \bar{f}_i \bar{f}_j Q_{ij} -$$

$$-2 P^* \sum_{i=1}^{5} (\bar{f}_i Q_i) \sum_{j=1}^{4} \left(\frac{a_j}{P_j} f_j\right) + P^{*2} \bar{Q} \sum_{i=1}^{4} \sum_{j=1}^{4} f_i f_j \frac{a_i a_j}{P_i P_j}$$

with $Q_i = AQ_{i_1} + BQ_{i_2} + CQ_{i_3} + DQ_{i_4} + EQ_{i_5}$ $\qquad i = 1$ to 5 $\qquad (7.9.2.1)$

and $\bar{Q} = AQ_1 + BQ_2 + CQ_3 + DQ_4 + EQ_5 \qquad (7.9.2.2)$

The elements of the function vectors represent a total of 27 partial differentials. These are derived and listed in Appendix I.

7.9.5 Standard Deviation of a Distance in Model Space

If distances between object points are evaluated and their errors are required, a more complex form of the case of standard deviation

of a function of unknowns and observations arises.

The relative differentials are derived in the context of the convergency correction (Chapter 7.10 and Appendix II). However, the inclusion of these formulae in the program for relative orientation is not considered necessary and a more convenient approximation of the distance error is seen as quite sufficient. If we neglect correlations between unknowns and observations the error can be approximated by error propagation of uncorrelated parameters,

from $$d_{ij}^2 = (X_i-X_j)^2 + (Y_i-Y_j)^2 + (Z_i-Z_j)^2 \qquad (7.9.9)$$

follows

$$\sigma_d^2 = \frac{1}{d}\left[(\sigma_{x_i}^2+\sigma_{x_j}^2)(X_i-X_j)+(\sigma_{y_i}^2+\sigma_{y_j}^2)(Y_i-Y_j)+(\sigma_{z_i}^2+\sigma_{z_j}^2)(Z_i-Z_j)\right] \qquad (7.9.10)$$

where σ_{x_i}, σ_{y_i} ... are the standard deviations of model co-ordinates as derived in (7.9.2).

By neglecting correlation in the formulation of the variance of a distance between model points we will evaluate too optimistic quantities for the error values.

7.10 CONVERGENCY CORRECTION

The convergency error is a well known phenomenon in aerial photogrammetry (Thompson 1975[2]). In the relative orientation procedure errors $\Delta\varphi'$ and $\Delta\varphi''$ occur in rotation angles φ' and φ'' about the Y-axes of the two camera stations (Fig. 7.10-1).

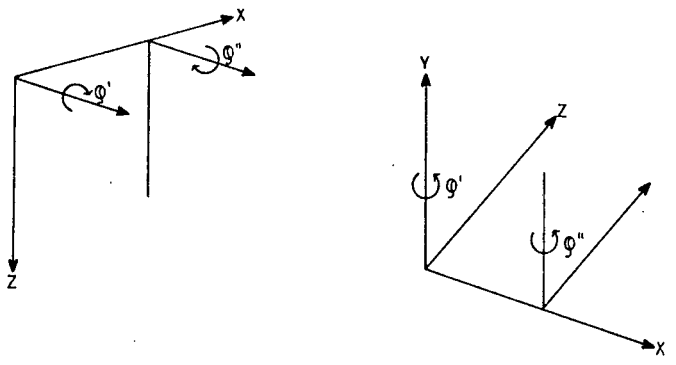

Fig. 7.10-1 φ - Rotation in Aerial and Close-range Photogrammetry.

These errors can be interpreted as consisting of an equal and like part ($\Delta\varphi_1'$ and $\Delta\varphi_1''$) and an equal and unlike part ($\Delta\varphi_2'$ and $\Delta\varphi_2''$) (Fig. 7.10-2).

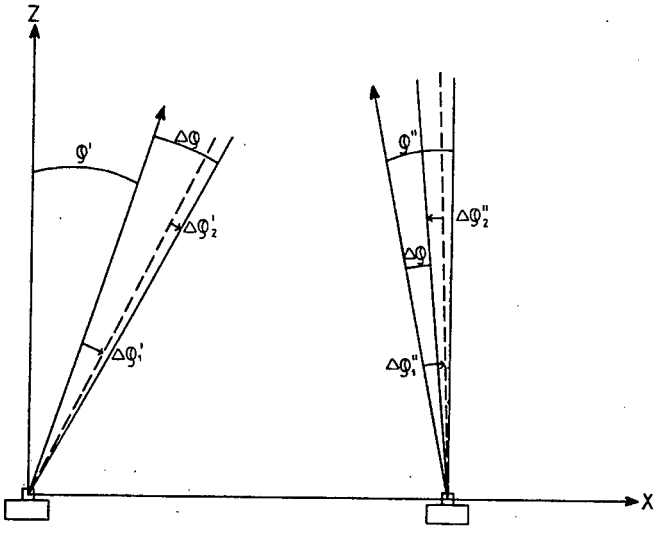

Fig. 7.10-2 "Equal and Like" and "Equal and Unlike" Error in φ

This can be expressed as

$$\Delta\varphi' = \Delta\varphi_1' + \Delta\varphi_2'$$

$$\Delta\varphi'' = \Delta\varphi_1'' - \Delta\varphi_2'' \qquad (7.10.1)$$

with $\Delta\varphi_1' = \Delta\varphi_1''$

and $\Delta\varphi_2' = -\Delta\varphi_2''$

The convergency error is then defined as

$$\gamma = \Delta\varphi' - \Delta\varphi'' = 2\Delta\varphi_2' \qquad (7.10.2)$$

Thompson (1975) shows that such a convergency error causes differential horizontal and vertical scale errors in the model space. The presence of a "vertical" scale error (scale error in Z-direction) as a result of the convergency error deserves special consideration in close-range photogrammetry.

One of the principal differences between close-range and aerial photogrammetry lies in the ratio between object distance from the camera base ("flying height") and object depth ("Z-range"). While in aerial photography the flying height is generally large compared to the depth of the object this is not the case for close-range applications. A typical flying height/object depth ratio in the aerial case is 10/1 whereas the equivalent value for close-range photogrammetry can be as small as 1/5. Adams, 1978, has described the ill-effect of the characteristically large Z-range of a close-range object on the analogue relative orientation procedure. He reports that, in spite of a seemingly perfect visual relative orientation based on the usual six point technique, large errors can occur in the Z co-ordinates of the object (the equivalent to Thompson's vertical scale error), which Adams attributes to a convergency error. As a counter measure, he introduced a "height pole", that is a known distance in Z direction, preferably extending over the entire Z range of the object. Adams then suggests an iterative correction procedure

in which equal and unlike corrections to φ and corrections to the base length are applied alternatively until the height pole reaches its correct length in plotter model co-ordinates. Considerable improvement of the model accuracy was achieved by this method.

The equivalent of the height pole in an analytical solution is a restraint condition in the relative orientation adjustment by which the orientation angles are forced to adopt values which not only guarantee a best fit intersection of image rays but also model co-ordinates which result in the correct length for the known control distance. In principle, this is easily done by introducing a condition equation of the form:

$$\Phi = \left[(X_j-X_i)^2 + (Y_j-Y_i)^2 + (Z_j-Z_i)^2\right]^{\frac{1}{2}} - d = 0 \qquad (7.10.3)$$

This condition equation requires linearisation before it can be added as an additional equation to the normal equation system (3.2.4):

$$\underline{\underline{B}}\underline{v}+\underline{\underline{A}}\underline{x}+\underline{w} = \underline{0}$$

Equation (7.10.3) is a function of the model co-ordinates of the two end points of the control distance. These are functions of rectified plate co-ordinates which in turn are functions of observed plate co-ordinates and the unknown orientation angles. This makes the linearisation of equation (7.10.3) algebraically intricate, (the linearised condition equation is therefore derived separately in Appendix II).

One could argue that the control distance can always be located in direction of the Z-axis and that equation (7.10.3) can therefore be

shortened to

$$(Z_j - Z_i) - d = 0$$

because of $X_j = X_i$ (7.10.4)

and $Y_j = Y_i$

However, this must be rejected after considering the practical implications of the "control distance" or "height pole" method. In practice, such a control distance must be measured between two natural feature points. It would be unrealistic to assume that it is always possible to find two points which are positioned exactly in Z-direction. Equation (7.10.4) would therefore only be applicable if especially pre-marked points are established for the purpose of convergency correction. It seems more sensible to accept any two existing object points in approximately the direction of the Z-axis and to formulate the full equation (7.10.3) rather than the limiting short form (7.10.4). (This argument becomes especially relevant for Wildlife photogrammetry, Chapter 10.)

The final linearisation of equation (7.9.3) has the form:

$$\frac{\partial\Phi}{\partial\kappa'}\,d\kappa' + \frac{\partial\Phi}{\partial\varphi'}\,d\varphi' + \frac{\partial\Phi}{\partial\kappa''}\,d\kappa'' + \frac{\partial\Phi}{\partial\varphi''}\,d\varphi'' + \frac{\partial\Phi}{\partial\omega''}\,d\omega'' +$$

$$+ \frac{\partial\Phi}{\partial\bar{x}'_i}\,d\bar{x}'_i + \frac{\partial\Phi}{\partial\bar{y}'_i}\,d\bar{y}'_i + \frac{\partial\Phi}{\partial\bar{x}''_i}\,d\bar{x}''_i + \frac{\partial\Phi}{\partial\bar{y}''_i}\,d\bar{y}''_i + \frac{\partial\Phi}{\partial\bar{x}'_j}\,d\bar{x}'_j + \qquad (7.10.5)$$

$$+ \frac{\partial\Phi}{\partial\bar{y}'_j}\,d\bar{y}'_j + \frac{\partial\Phi}{\partial\bar{x}''_j}\,d\bar{x}''_j + \frac{\partial\Phi}{\partial\bar{y}''_j}\,d\bar{y}''_j + d_o - d = 0$$

where $\bar{x}'_i$, $\bar{y}'_i$, $\bar{x}''_i$, $\bar{y}''_i$ are the observed plate co-ordinates of the left and right image of Point P_i

and $\bar{x}'_j$, $\bar{y}'_j$, $\bar{x}''_j$ and $\bar{y}''_j$ those for Point P_j.

Points P_i and P_j are the end points of the control distance.

d_o is the value for the control distance as evaluated from provisional values of the orientation angles

d is the field measurement of the control distance.

Equations for the thirteen partial differentials in (7.10.5) are derived and listed in Appendix I . Once one or more distance condition equations are added to the standard relative orientation equation system (7.4.9 and 7.4.10) the quasi-parametric adjustment can no longer be employed for the solution of the unknowns. The $(B^T P^{-1} B)$ matrix contains off diagonal terms and cannot be treated as a quasi-weight matrix. This excludes the use of mini computers for the relative orientation adjustment with restraints unless a special memory space saving algorithm is derived.

Such an algorithm, based on a matrix-bracketing technique, is developed in Appendix III and incorporated into the computer programme described in Appendix V. In the procedure adopted here the relative orientation adjustment is first iterated without restraints until the iteration criterion, that all corrections to the unknown orientation angles be smaller than o,ooo5 radians, is satisfied. The restraining condition equation (7.10.5) is then introduced and treated in the algorithm described in Appendix III. The discrepancy term, $d_o - d$, in (7.10.5) is based on a provisional distance d_o, which is evaluated from provisional model co-ordinates derived in the first adjustment without

restraints. The iteration procedure is then taken up again until the correction to the unknowns once more satisfy the iteration criterion.

A numerical example for a relative orientation adjustment with a restraining control distance is given in Tabs. 7.10-1.1 to 7.10-1.7. The adjustment example is based on 10 points of the test field (Fig. 5-3) obtained from photography with a metric UMK 10/1318 camera. Tab. 7.10-1.1 shows the observed image co-ordinates, the principal distances of the two cameras and the base length. Then the iteration steps for the adjustment without restraints are tabulated (Tab.7.10-1.2), followed by the list of the corrections to the image co-ordinates, the rectified image co-ordinates, the variance factor as well as the intermediate orientation angles and their standard deviations (Tab. 7.10-1.3). Model co-ordinates and some model distances are then given for the first stage of the adjustment (Tab. 7.10-1.4). In Tab. 7.10-1.5 a control distance is introduced and the iteration is re-initiated. Tab. 7.10-1.6 lists the new values for image co-ordinate corrections, rectified image co-ordinates and orientation angles resulting from the introduction of the restraint. In Tab. 7.10-1.7 the final model co-ordinates and a sample of model distances including the control distance are presented.

It should be noted here that the solution does not converge to a minimum value for the discrepancy term w of the distance condition (Tab. 7.10-1.5) as one might expect. It would therefore be incorrect to use the minimisation of the w- term as an iteration criterion. (This was erroneously attempted at first and resulted in discrepancies

in the global check of the adjustment. In the global check, not only the co-planarity condition (7.3.8) must be satisfied for all point pairs, but also the control distance evaluated from model co-ordinates must agree with the stipulated measured control value. However, if the iteration is continued until the corrections to the unknown are sufficiently small all checks are fully satisfied.)

In the numerical example a distance in Z-direction is introduced as control. This distance (between points 8 and 10) is equal to 2,5472 m when evaluted from model co-ordinates obtained in the adjustment without restraints.
The equivalent measured distance is 2,5426 m and the difference of 4,6 mm is eliminated in the convergency correction procedure by a change of the orientation angles of -2" in $\varkappa'$; -46" in φ'; 1" in $\varkappa''$ and 55" in φ''; ω'' remains unaffected. The change in φ is unlike and near equal and by far the largest of the corrections necessary to obtain the correct value for the control distance.

A similar pattern emerged for all adjustments where a convergency correction was applied. In all these cases the introduction of a restraining distance condition resulted in unlike and near equal corrections to φ combined with notably smaller corrections to $\varkappa'$; $\varkappa''$; and ω''. The formulation of the condition equation (7.10.5) is not based on the assumption that the major contribution towards a correct value for the control distance should be a φ-correction, instead, all orientation angles are permitted to change. The fact that in all tested cases equal and unlike changes in φ assume naturally the dominant role in the correction of the control distance implies that,

out of the orientation angles, φ forms the major contribution towards errors in Z-direction. It also confirms that the addition of equation (7.10.5) to the relative orientation adjustment is rightfully termed "convergency correction". Because of this the convergency correction equation will - despite the fact that all angles are free to change - interpret any discrepancy w in a control distance equation as a result of an error of equal and unlike φ, even if such a discrepancy is caused by errors in other parameters such as the principal distances. The effect of such an incorrect use of the convergency correction is shown in the table below.

Distance	Derived in adjustment without restraints	True Value	w	Paral-lel to	Secondary corrections to orientation angles				
					κ'	φ'	κ''	φ''	ω''
68-80	2,5472m	2,5426m	4,6mm	Z-axis	-2"	-46"	1"	55"	0"
1-14	2,2470	2,2430	4,0	Y-axis	-4"	-74"	4"	102"	0"
13-77	3,2810	3,2750	6,0	X-axis	-13"	-151"	8"	163"	0,3"

Here three distances, in X, Y and Z direction of the test field, as derived in the adjustment without restraints (Tabs. 7.10-1.1 to 7.10-1.4) are compared against their true values. The differences w clearly indicate a scale error of approximately 1:550 for the entire model. If convergency corrections are applied using the three distances in turn, equal and unlike corrections to φ result from the adjustments, seemingly justifying the, in fact, incorrect application of the convergency correction.

A convergency correction should therefore only be applied after the model has been corrected for a possible scale factor. This can be done by introducing control distances in X- and possibly also in Y-direction in addition to the Z-control distance. An average scale factor can then be derived from all control distances and applied to the entire model. Any remaining discrepancy between the true (measured) value of the Z-distance and the value derived for this distance from model co-ordinates can then be used for a subsequent convergency correction adjustment.

The efficiency of the convergency correction method in a number of test cases of simulated and real photography, is discussed in Chapter 8.

RELATIVE ORIENTATION AND MODEL CO-ORDINATES

1 TESTFIELD SEP 81

BASE: 3.311 F.D. LEFT: 100.94 F.D. RIGHT: 100.94

OBSERVED PLATE CO-ORDINATES

PT		X'	Y'	Z'	PX	PY	X''	Y''	Z''
1.	1	-32.638	23.916	100.938	0.000	0.000	-22.727	19.991	100.938
2.	4	-33.653	-16.904	100.938	0.000	0.000	-22.582	-15.304	100.938
3.	13	-29.353	38.411	100.938	0.000	0.000	-48.587	30.341	100.938
4.	16	-30.588	-27.779	100.938	0.000	0.000	-48.327	-23.319	100.938
5.	35	-6.233	-3.359	100.938	0.000	0.000	3.513	-3.479	100.938
6.	47	12.728	-5.849	100.938	0.000	0.000	-11.817	-5.934	100.938
7.	65	17.042	17.976	100.938	0.000	0.000	31.143	22.166	100.938
8.	68	16.007	-14.064	100.938	0.000	0.000	30.848	-16.089	100.938
9.	77	45.332	27.426	100.938	0.000	0.000	33.728	38.711	100.938
10.	80	44.252	-21.994	100.938	0.000	0.000	33.822	-28.264	100.938

Table 7.10-1.1 Numerical Example for Relative Orientation Adjustment with Convergency Correction

1 TESTFIELD SEP 81

ITERATION 0

	KAPPA'	PHI'	KAPPA''	PHI''	OMEGA''
PROV. UNKNOWNS	0.0000	0.0000	0.0000	0.0000	0.0000
COR. TO UNKNOWNS	0.0166	-0.3697	-0.0105	0.2733	0.0001

ITERATION 1

	KAPPA'	PHI'	KAPPA''	PHI''	OMEGA''
PROV. UNKNOWNS	0.0166	-0.3697	-0.0105	0.2733	0.0001
COR. TO UNKNOWNS	0.0034	0.0060	0.0031	-0.0136	-0.0006

ITERATION 2

	KAPPA'	PHI'	KAPPA''	PHI''	OMEGA''
PROV. UNKNOWNS	0.0200	-0.3637	-0.0074	0.2597	-0.0005
COR. TO UNKNOWNS	0.0000	-0.0001	0.0000	-0.0002	0.0000

ITERATION 3

	KAPPA'	PHI'	KAPPA''	PHI''	OMEGA''
PROV. UNKNOWNS	0.0200	-0.3638	-0.0074	0.2595	-0.0005
COR. TO UNKNOWNS	0.0000	0.0000	0.0000	0.0000	0.0000

ITERATION 4

	KAPPA'	PHI'	KAPPA''	PHI''	OMEGA''
PROV. UNKNOWNS	0.0200	-0.3638	-0.0074	0.2595	-0.0005
COR. TO UNKNOWNS	0.0000	0.0000	0.0000	0.0000	0.0000

FINAL ROTATION ANGLES IN RADIANS

KAPPA'	PHI'	KAPPA''	PHI''	OMEGA''
0.0200	-0.3638	-0.0074	0.2595	-0.0005

IN DEGREES

KAPPA'	PHI'	KAPPA''	PHI''	OMEGA''
1.1458	-20.8447	-0.4248	14.8692	-0.0279

Table 7.10-1.2

1 TESTFIELD SEP 81

ADJUSTED OBSERVATIONS

	XO	VX	X	YO	VY	Y		PX	PY
1.	-32.638	-0.0001	-32.638	23.916	-0.0006	23.915	L	1.00	1.00
	-22.727	0.0000	-22.727	19.991	0.0007	19.992	R	1.00	1.00
2.	-33.653	0.0000	-33.653	-16.904	0.0001	-16.904	L	1.00	1.00
	-22.582	0.0000	-22.582	-15.304	-0.0001	-15.304	R	1.00	1.00
3.	-29.353	0.0001	-29.353	38.411	0.0005	38.411	L	1.00	1.00
	-48.587	0.0001	-48.587	30.341	-0.0006	30.340	R	1.00	1.00
4.	-30.588	0.0000	-30.588	-27.779	0.0005	-27.779	L	1.00	1.00
	-48.327	0.0000	-48.327	-23.319	-0.0006	-23.320	R	1.00	1.00
5.	-6.233	0.0000	-6.233	-3.359	-0.0001	-3.359	L	1.00	1.00
	3.513	0.0000	3.513	-3.479	0.0001	-3.479	R	1.00	1.00
6.	12.728	0.0000	12.728	-5.849	-0.0014	-5.851	L	1.00	1.00
	-11.817	0.0000	-11.817	-5.934	0.0013	-5.933	R	1.00	1.00
7.	17.042	0.0003	17.042	17.976	0.0027	17.978	L	1.00	1.00
	31.143	0.0001	31.143	22.166	-0.0022	22.164	R	1.00	1.00
8.	16.007	0.0001	16.007	-14.064	-0.0023	-14.067	L	1.00	1.00
	30.848	0.0001	30.848	-16.089	0.0019	-16.087	R	1.00	1.00
9.	45.332	-0.0001	45.332	27.426	-0.0008	27.425	L	1.00	1.00
	33.728	-0.0001	33.728	38.711	0.0006	38.711	R	1.00	1.00
10.	44.252	-0.0001	44.252	-21.994	0.0014	-21.993	L	1.00	1.00
	33.822	-0.0001	33.822	-28.264	-0.0010	-28.265	R	1.00	1.00

RECTIFIED CO-ORDINATES

	X'	Y'	Z'	X''	Y''	Z''	CHECK
1.	4.975	23.258	106.113	-47.724	20.115	91.774	0.000
2.	4.789	-17.574	106.184	-47.837	-15.181	91.727	0.000
3.	7.773	37.817	105.048	-72.644	30.658	85.163	0.000
4.	7.856	-28.385	105.016	-72.777	-23.002	85.101	0.000
5.	30.156	-3.483	96.525	-22.532	-3.553	98.451	0.000
6.	47.919	-5.595	89.762	-37.366	-5.891	94.511	0.000
7.	51.505	18.316	88.396	4.356	21.881	105.602	0.000
8.	51.137	-13.744	88.537	3.797	-16.367	105.435	0.000
9.	77.761	28.326	78.399	6.973	38.409	106.305	0.000
10.	77.676	-21.104	78.432	6.584	-28.567	106.169	0.000

PVV: 0.000031 MO: 0.0025 CHECK PVV: 0.000031

FINAL ROTATION ANGLES IN RADIANS

KAPPA'	PHI'	KAPPA''	PHI''	OMEGA''
0.0200	-0.3638	-0.0074	0.2595	-0.0005

IN DEGREES

KAPPA'	PHI'	KAPPA''	PHI''	OMEGA''
1.1458	-20.8447	-0.4248	14.8692	-0.0279

M.S.E. OF UNKNOWNS IN DEGREES

KAPPA'	PHI'	KAPPA''	PHI''	OMEGA''
0.0044	0.0048	0.0043	0.0053	0.0007

Table 7.10-1.3

Table 7.10-1.4

1 TESTFIELD SEP 81

MODEL CO-ORDINATES BASE 3.3110

	X (M)	Y (M)	Z (M)	MX (MM)	MY (MM)	MZ (MM)
1.	0.2738	1.2801	5.8405	0.5	0.3	1.6
2.	0.2636	-0.9671	5.8434	0.5	0.3	1.5
3.	0.2643	1.2858	3.5718	0.3	0.2	0.7
4.	0.2663	-0.9623	3.5603	0.3	0.2	0.7
5.	1.9110	-0.2207	6.1170	0.4	0.1	1.6
6.	1.9022	-0.2221	3.5633	0.3	0.1	0.6
7.	3.5433	1.2671	6.1155	0.6	0.4	1.7
8.	3.5312	-0.9490	6.1138	0.6	0.3	1.7
9.	3.5455	1.2915	3.5746	0.4	0.3	0.8
10.	3.5322	-0.9597	3.5666	0.4	0.2	0.8

DISTANCES AND DIRECTIONS FROM MODEL CO-ORD.

FROM-TO	DX	DY	DZ	HORIZ. DISTANCE	SPACE	HORIZ. ANGLE	VERT.
1- 4	-0.010	-2.247	0.003	0.011	2.247	164.207	-89.728
13- 77	3.281	0.006	0.003	3.281	3.281	0.049	0.099
68- 80	0.001	-0.011	-2.547	2.547	2.547	270.023	-0.238

CONDITION EQUATION FOR DISTANCE 8- 10 MEASURED LENGTH : 2.543

Xi'	Yi'	X2'	Y2'	Xi''	Yi''	X2''	Y2''	KAPPA'	PHI'	KAPPA''	PHI''	OMEGA''	W
-145.250	3.199	102.402	0.757	62.967	-1.453	-34.344	-0.254	-671.01	7442.09	691.64	-7443.31	0.95	4.650

ITERATION 2

	KAPPA'	PHI'	KAPPA''	PHI''	OMEGA''
COR. TO UNKNOWNS	0.0004	-0.0003	-0.0004	0.0003	0.0000
PROV. UNKNOWNS	0.0204	-0.3641	-0.0078	0.2598	-0.0004

Xi'	Yi'	X2'	Y2'	Xi''	Yi''	X2''	Y2''	KAPPA'	PHI'	KAPPA''	PHI''	OMEGA''	W
-144.884	3.248	102.091	0.799	62.859	-1.476	-34.255	-0.268	-668.44	7417.03	689.97	-7418.89	1.14	0.006

ITERATION 3

	KAPPA'	PHI'	KAPPA''	PHI''	OMEGA''
COR. TO UNKNOWNS	-0.0004	0.0001	0.0004	0.0000	0.0000
PROV. UNKNOWNS	0.0200	-0.3640	-0.0074	0.2598	-0.0005

Xi'	Yi'	X2'	Y2'	Xi''	Yi''	X2''	Y2''	KAPPA'	PHI'	KAPPA''	PHI''	OMEGA''	W
-144.979	3.202	102.166	0.755	62.895	-1.457	-34.279	-0.253	-668.93	7422.67	689.63	-7424.60	1.16	0.988

ITERATION 4

	KAPPA'	PHI'	KAPPA''	PHI''	OMEGA''
COR. TO UNKNOWNS	0.0000	0.0000	0.0000	0.0000	0.0000

Table 7.10-1.5

ADJUSTED OBSERVATIONS

	XO	VX	X	YO	VY	Y		PX	PY
1.	-32.638	0.0000	-32.638	23.916	0.0005	23.916	L	1.00	1.00
	-22.727	0.0000	-22.727	19.991	-0.0006	19.990	R	1.00	1.00
2.	-33.653	0.0000	-33.653	-16.904	-0.0011	-16.905	L	1.00	1.00
	-22.582	0.0000	-22.582	-15.304	0.0012	-15.303	R	1.00	1.00
3.	-29.353	0.0005	-29.353	38.411	0.0034	38.414	L	1.00	1.00
	-48.587	0.0004	-48.587	30.341	-0.0042	30.337	R	1.00	1.00
4.	-30.588	0.0002	-30.588	-27.779	-0.0022	-27.782	L	1.00	1.00
	-48.327	0.0002	-48.327	-23.319	0.0027	-23.316	R	1.00	1.00
5.	-6.233	0.0000	-6.233	-3.359	-0.0001	-3.359	L	1.00	1.00
	3.513	0.0000	3.513	-3.479	0.0001	-3.479	R	1.00	1.00
6.	12.728	0.0000	12.728	-5.849	-0.0013	-5.851	L	1.00	1.00
	-11.817	0.0000	-11.817	-5.934	0.0013	-5.933	R	1.00	1.00
7.	17.042	0.0001	17.042	17.976	0.0014	17.977	L	1.00	1.00
	31.143	0.0001	31.143	22.166	-0.0012	22.165	R	1.00	1.00
8.	16.007	0.0038	16.011	-14.064	-0.0010	-14.065	L	1.00	1.00
	30.848	-0.0027	30.845	-16.089	0.0007	-16.088	R	1.00	1.00
9.	45.332	-0.0007	45.331	27.426	-0.0047	27.421	L	1.00	1.00
	33.728	-0.0004	33.727	38.711	0.0035	38.714	R	1.00	1.00
10.	44.252	-0.0020	44.250	-21.994	0.0050	-21.989	L	1.00	1.00
	33.822	0.0007	33.822	-28.264	-0.0037	-28.268	R	1.00	1.00

RECTIFIED CO-ORDINATES

	X'	Y'	Z'	X''	Y''	Z''	CHECK
1.	4.999	23.259	106.112	-47.749	20.113	91.761	0.000
2.	4.813	-17.575	106.183	-47.862	-15.180	91.714	0.000
3.	7.797	37.820	105.046	-72.666	30.654	85.143	0.000
4.	7.880	-28.387	105.014	-72.799	-22.999	85.082	0.000
5.	30.178	-3.483	96.518	-22.558	-3.553	98.445	0.000
6.	47.939	-5.595	89.751	-37.391	-5.891	94.501	0.000
7.	51.525	18.314	88.385	4.327	21.882	105.603	0.000
8.	51.160	-13.742	88.524	3.766	-16.368	105.436	0.000
9.	77.779	28.322	78.382	6.944	38.412	106.307	0.000
10.	77.691	-21.100	78.415	6.556	-28.569	106.171	0.000

PVV: 0.000128 MO: 0.0050 CHECK PVV: 0.000153

FINAL ROTATION ANGLES IN RADIANS

KAPPA'	PHI'	KAPPA''	PHI''	OMEGA''
0.0200	-0.3640	-0.0074	0.2598	-0.0005

IN DEGREES

KAPPA'	PHI'	KAPPA''	PHI''	OMEGA''
1.1453	-20.8575	-0.4244	14.8846	-0.0279

M.S.E. OF UNKNOWNS IN DEGREES

KAPPA'	PHI'	KAPPA''	PHI''	OMEGA''
0.0089	0.0077	0.0086	0.0080	0.0014

Table 7.10-1.6

1 TESTFIELD SEP 81

MODEL CO-ORDINATES BASE 3.3110

	X (M)	Y (M)	Z (M)	MX (MM)	MY (MM)	MZ (MM)
1.	0.2749	1.2789	5.8346	0.8	0.4	1.6
2.	0.2646	-0.9662	5.8376	0.8	0.4	1.6
3.	0.2649	1.2850	3.5691	0.5	0.3	0.8
4.	0.2669	-0.9617	3.5576	0.5	0.3	0.8
5.	1.9107	-0.2205	6.1110	0.9	0.3	1.6
6.	1.9020	-0.2220	3.5610	0.6	0.2	0.6
7.	3.5613	1.2659	6.1090	1.0	0.5	1.8
8.	3.5291	-0.9480	6.1065	1.0	0.4	1.8
9.	3.5443	1.2906	3.5718	0.7	0.4	0.9
10.	3.5311	-0.9590	3.5640	0.6	0.3	0.9

DISTANCES AND DIRECTIONS FROM MODEL CO-ORD.

FROM-TO	DX	DY	DZ	HORIZ. DISTANCE	SPACE	HORIZ. ANGLE	VERT.
1- 4	-0.010	-2.245	0.003	0.011	2.245	163.910	-89.727
13- 77	3.279	0.006	0.003	3.279	3.279	0.047	0.098
68- 80	0.002	-0.011	-2.543	2.543	2.543	270.044	-0.249

Table 7.10-1.7

7.11 HOMOGENEOUS AND AFFINE SCALING

In the conventional photogrammetric restitution of a model, the absolute orientation in form of a three-dimensional transformation serves to reduce model deformations caused by errors in the elements of interior and relative orientation. The transformation consists of translation, rotation and scaling of the model. Neither the translation nor the transformation affect the shape of the model and the only contribution to a reduction of possible model deformation is the scale correction.

In those close-range applications where only relative point positions are required - and this is probably the majority of all cases - it is therefore less critical than one might assume if no three-dimensional control network for an absolute orientation can be established. Here the establishment of a number of well distributed control distances from which an average scale factor can be derived is geometrically equivalent to a three-dimensional control network.

Investigations of model deformations (Chapter 8) reveal that the model generally suffers different scale distortions in X, Y and Z-direction rather than a uniform scale distortion for the entire model.

To summarise, the following methods emerge from the above as possible techniques to reduce model deformations caused by errors in the parameters of interior and relative orientation in close-range photogrammetry:

i) homogeneous scaling based on

   1. one distance
   2. a number of well-distributed distances

ii) affine scaling based on

   1. one distance in each axis direction
   2. one distance in Z-direction and a second distance in either X- or Y-direction. (This model assumes similar scale errors for X and Y co-ordinates
   3. a number of distances in each axis direction

iii) convergency correction based on

   1. one distance in Z-direction
   2. a number of distances in Z-direction

iv) homogeneous scaling with subsequent convergency correction based on

   1. one distance in X- or Y-direction and one distance in Z-direction
   2. a number of distances distributed through the models including at least one distance in Z-direction

Most of the above listed alternatives were tested in cases of real and synthetic photography. The results of the tests are discussed in the chapter following.

8. MODEL DEFORMATIONS

8.1 THE PRINCIPLES OF MODEL DEFORMATIONS AND A METHOD OF DEFORMATION ANALYSIS

Object point positions in form of model co-ordinates or distances between object points are the ultimate objective of close-range photogrammetry. Inaccuracies in the determination of the relative positions of these points result in a distortion of the object dimensions referred to in photogrammetry as model deformation. Model deformations in analytical close-range photogrammetry can be caused by errors in the following parameters:

i) Elements of Interior Orientation

In the analytical treatment of the relative orientation it is necessary to introduce numerical values for the principal distance $\bar{f}'$ of the camera or, when a pair of cameras is used, of both cameras: $\bar{f}'$ and $\bar{f}''$. It is also necessary to reduce all observed plate co-ordinates to the principal point of the image ($\bar{x}_o$ and $\bar{y}_o$).

If two cameras are employed each set of image co-ordinates must be reduced to its corresponding principal point and four principal point co-ordinates must be introduced into the relative orientation adjustment $\bar{x}'_o$, $\bar{y}'_o$, $\bar{x}''_o$ and $\bar{y}''_o$. Any error in these input values causes deformations in the model co-ordinates. These deformations also occur when the interior orientation elements are not introduced as constants but determined as unknowns of the adjustment, as in the case of "self calibration".

ii) Central Perspective Projection

The mathematical model of the photograph is generally accepted to be that of a central perspective projection, which assumes that perspective centre, image point and object point lie on a straight line. Image points deviate from this line, as a result of observation errors in image co-ordinates, emulsion shifts, emulsion carrier deformations and lens distortions. Such deviations from the true perspective result in shifts of model points to incorrect positions.

iii) Base length

Errors in the base length, that is the distance between the two exterior perspective centres of the two camera station lens systems, have the effect of a scale error on the model. In close-range photogrammetry it is not acceptable to assume that the external perspective centre of the camera coincides with the rotation axis of the camera (Fig.8-1). Here the physical measurement of a distance between the mechanically undefined perspective centres can obviously only lead to an approximation of the true base length. The normally adopted method of measuring the base length between the tribach centres of the two camera stations is especially unsuitable in cases of convergent photography.

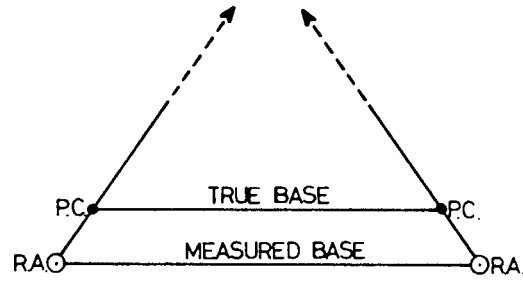

Fig.8.1-1 The deviation of the perspective centre (PC) from the rotation axis (RA) of a metric camera with theodolite mounting and its effect on the base length in convergent photography

In the case of the UMK 10/1318 cameras for example the external perspective centre is displaced 60 mm from the rotation axis of the camera (Fig.7.1-4) when the focus is set to 3,6 m. For convergent photography with $\varphi' = -\varphi'' = 10^{g}$ this displacement would cause an error in the base length of 21 mm, if the base is measured between the rotation axis of the cameras. For a 2 m base this represents the considerable scale error of 1 in 100.

The above listed errors in interior orientation parameters and base length contribute, together with errors in image co-ordinates, to a deformation of the model space.

An understanding of the deformation characteristics in close-range photogrammetry is essential when investigating the introduction of control distances as a form of model control. It was decided to base such an investigation on synthetic photography (3.3) rather than real photography for the following reasons:

i) To investigate the effect of errors in elements of interior

orientation, image co-ordinates and base length on the photogrammetric model, the true values of these errors should be known. Obviously this cannot be achieved in real photography, whilst synthetic photography permits the controlled introduction of errors.

ii) In real photography errors must be expected to be present in all elements of interior orientation, in the base length and in the observed plate co-ordinates. In simulated photography on the other hand errors can be introduced into one parameter at a time.

A purely theoretical determination of the deformations caused by errors in individual parameters as an alternative to simulated and real test photography was considered as less suitable, because the rather complex formulae do not lend themselves to simple interpretation.

The method adopted for the deformation analysis was therefore:

i) to create synthetic photographs simulating normal and general convergent photography of the three dimensional test field described in Chapter 5;

ii) to introduce errors into the individual elements of interior and exterior orientation and into the observed image co-ordinates;

iii) to execute relative orientation adjustment based on the incorrect parameters and evaluate model co-ordinates for the test field points;

iv) to compare the model co-ordinates of each test case with their error free theoretical values (the deviations of the model co-ordinates of a point from their true values represent the deformation of the model space in this point);

v) to obtain real photography of the test field in order to test and confirm the result of the deformation analysis based on simulated

photography.

In the same simulations, error free control distances can be employed to test the various deformation correction models (7.11.i) to 7.11.iv).

8.2 MODEL DEFORMATIONS IN NORMAL ORIENTED ONE-CAMERA PHOTOGRAMMETRY

Before describing the simulated test cases in detail, the mathematically trivial deformations as they occur in the special case of one-camera photography in normal orientation will be derived.

It will later be show that, in normal orientated one-camera photography, errors in interior orientation do not, as in all other cases, distort the orientation angles in the related orientation. If one accepts this submission, then one can derive the deformation for this case as follows:

In the one-camera case, principal point and principal distance are the same for both images and errors in the calibration values of these parameters will affect both images in the same way.

One can argue here that this is not strictly true for the principal point position, as the co-ordinates of the principal point are determined separately for each image plate of a stereo pair from fiducial mark observations. It was shown in a series of test observations, in which the same image plate was observed repeatedly, that the principal point co-ordinates have a standard deviation of less than 10 μm.

The estimate for the accuracy of the principal point position was obtained by observing a set of 15 points eight times and by then transforming seven of the point sets into the eighths set. A comparison

of the principal point positions after transformation yielded standard deviations of 6.8 µm for y and 7.1 µm for x.

As the accuracy for the image points is less than 10 µm we can neglect the differences in the principal point positions of two images obtained with the same camera. We can subsequently assume that the principal point positions of a stereo pair are practically identical for one-camera photography.

Assuming that principal point and principal distance are identical for both images we have for the principal point co-ordinates:

$$\bar{x}'_o = \bar{x}''_o = \bar{x}_o$$

$$\bar{y}'_o = \bar{y}''_o = \bar{y}_o \qquad (8.2.1)$$

and for the principal distance $\bar{f}' = \bar{f}'' = \bar{f}$

and similarly for errors in these parameters

$$d\bar{x}'_o = d\bar{x}''_o = d\bar{x}_o$$

$$d\bar{y}'_o = d\bar{y}''_o = d\bar{y}_o \qquad (8.2.2)$$

$$d\bar{f}' = d\bar{f}'' = d\bar{f}$$

if we set

$$px_i = \bar{x}'_i - (\bar{x}'_o + d\bar{x}'_o) - \left[\bar{x}''_i - (\bar{x}''_o + d\bar{x}''_o)\right] \qquad (8.2.3)$$

we obtain with 8.2.1 and 8.2.2

$$px_i = \bar{x}'_i - \bar{x}''_i \qquad (8.2.3.1)$$

and for the model co-ordinates of a point P_i we have with 7.8.1.3

to 7.8.1.5

$$Z_i = \frac{b\ f}{px_i}$$

$$X_i = \frac{b\ \bar{x}'_i}{px_i} \qquad (8.2.4)$$

and

$$Y_i = \frac{b\ \bar{y}'_i}{px_i}$$

Model deformations in the three axis directions caused by errors in interior orientation elements can be determined by differentiating equations for axis oriented distances with respect to the principal point co-ordinates and the principal distance.

Axis oriented distances between model points P_i and P_j have the equations with 8.2.4

for a distance in X-direction

$$d_x = X_j - X_i = b\left[\frac{\bar{x}_j}{px_j} - \frac{\bar{x}_i}{px_i}\right] \qquad (8.2.5.1)$$

for a distance in Y-direction

$$d_y = Y_j - Y_i = b\left[\frac{\bar{y}_j}{px_j} - \frac{\bar{y}_i}{px_i}\right] \qquad (8.2.5.2)$$

and for a distance in Z-direction

$$d_z = Z_j - Z_i = b\left[\frac{\bar{f}}{px_j} - \frac{\bar{f}}{px_i}\right] \qquad (8.2.5.3)$$

Differentiation of 8.2.5 with respect to $d\bar{f}$ results in equations which reflect the error in distances in the three axis directions - and hence the model deformations in these directions - as a consequence of an error in the principal distance.

$$dd_x = o \tag{8.2.6.1}$$

$$dd_y = o \tag{8.2.6.2}$$

$$dd_z = b \left[\frac{1}{px_j} - \frac{1}{px_i}\right] df = \frac{Z_j - Z_i}{\bar{f}} df = d_z \frac{d\bar{f}}{\bar{f}} \tag{8.2.6.3}$$

Equations 8.2.6 show that only distances in the Z-direction and diagonal distances are affected by an error in the principal distance. Inspection of 8.2.6.3 reveals the deformation in the Z-direction takes the form of a scale error (see also test case 3 in Table 8-1):

$$\bar{d}_z = d_z \left[1 + \frac{d\bar{f}}{\bar{f}}\right] \tag{8.2.7}$$

where $\bar{d}_z$ is the distorted distance.

Similarly an error $d\bar{x}_o$ in the principal point co-ordinates $\bar{x}_o$ results in:

$$dd_x = b \left[\frac{1}{px_j} - \frac{1}{px_i}\right] d\bar{x}_o = \left[\frac{X_j}{\bar{x}'_j} - \frac{X_i}{\bar{x}'_i}\right] d\bar{x}_o \tag{8.2.8.1}$$

$$dd_y = o \tag{8.2.8.2}$$

$$dd_z = o \tag{8.2.8.3}$$

and finally an error $d\bar{y}_o$ in the principal point leads to

$$dd_x = o \tag{8.2.9.1}$$

$$dd_y = \left[\frac{Y_j}{\bar{y}'_j} - \frac{Y_i}{\bar{y}'_i}\right] d\bar{y}_o \tag{8.2.9.2}$$

$$dd_z = o \tag{8.2.9.3}$$

From 8.2.8 it follows that axis oriented distances in Y- and Z-directions are not affected by an error $d\bar{x}_o$ whereas the X-direction is distorted. The X-direction deformation does not have the character of a scale factor as in the case of 8.2.7.

Similarly from 8.2.9 an error $d\bar{y}_o$ does not cause deformations in X- and Z-directions, whilst the Y-direction is affected.

It can easily be seen that an error db in the base length causes an homogeneous scale factor for the entire model.

Table 8.2-1 lists deformations of the model in the three axis directions as a result of errors in interior orientation and in the base length for normal oriented one-camera photography.

Error in	Model deformation X	Y	Z	
b	$\left(1 + \frac{db}{b}\right) d_x$	$\left(1+ \frac{db}{b}\right) d_y$	$\left(1 + \frac{db}{b}\right) d_z$	Homogeneous scale
f	0	0	$\left(1 + \frac{db}{\bar{f}}\right) d_z$	Affine scale in Z
$\bar{x}_o$	$\left(\frac{X_j}{\bar{x}'_j} - \frac{X_i}{\bar{x}'_i}\right) d\bar{x}_o$	0	0	
$\bar{y}_o$		$\left(\frac{Y_j}{\bar{y}'_j} - \frac{Y_i}{\bar{y}'_i}\right) dy_o$	0	

Tab.8.2-1 Model deformation in normal oriented one-camera photography.

8.3 DESIGN OF TEST CASES FOR THE ANALYSIS OF MODEL DEFORMATIONS AND MODEL CONTROL METHODS

The basis for the deformation analysis is a synthetic test field modelled on the laboratory test field discussed in 5. The co-ordinates of the 80 test field points are used to create synthetic photographs, assuming a principal distance of f' = f" = f = 100 mm and a base of 3,310 m. The perspective centre positions are chosen as (0; 0; 0) for the left and (3,310; 0; 0) for the right camera. Synthetic photographs are generated for normal oriented photography ($\varkappa' = \varphi' = \varkappa'' = \varphi'' = \omega'' = 0^o$) and for convergent photography ($\varkappa' = 1^o$, $\varphi' = -20^o$, $\varkappa'' = 0^o$, $\varphi'' = 14^o$ and $\varkappa'' = 0^o$). The odd values for the convergent case are chosen to approximate real photography of

the test field which was taken in roughly this orientation.

Errors are introduced into the parameters of interior orientation and also in the orientation angles to investigate the model deformation resulting from inaccuracies in these parameters. Only 10 of the 80 network points are employed in each case to evaluate the relative orientation and the model co-ordinates of all 80 points are subsequently evaluated by the "shortest-distance-between-project-rays"-method (see 7.8.2).

Test results are listed in Tables 8-1, 8-2, 8-3 and 8-4. These tables contain the analysis of model deformations and also the results of various attempts to reduce deformation by means of control distances.

Table 8-1 combines the results of the computer simulations, Table 8-2 repeats some of the values of Table 8-1 with more significant digits, while Table 8-3 lists the results of real photography tests. The deformations caused by errors in orientation angles are presented in Table 8-4.

An attempt is made to systematically identify and characterise each case by its number (column 1), case name (column 2) and by information contained in columns 3 to 10 in Tables 8-1 and 8-2 and in columns 3 to 7 in Tables 8-3 and 8-4. (A more detailed description of these tables is presented in Chapter 8.4.) The remaining columns give information about the model deformations. The investigation extends to nearly 100 cases and it is necessary to describe which parameters are changed, how the different test cases are created and how the nature of the test cases is reflected in the file name. At this stage only basic principles of the test cases are described, a full case-to-case

description and analysis is presented later.

The following aspects are relevant to the categorisation of the test cases.

I Relative position and orientation of cameras

II Errors in interior orientation parameters

III Number of cameras used to create a stereo pair

IV Accuracy of plate co-ordinates

V Errors in orientation angles

VI Mathematical concept of model control

Test cases are created by different combinations of the various alternatives of the above listed categories.

I Relative position and orientation of cameras

I.1 Normal Case

The optical axes of the cameras are parallel to each other, in the same horizontal[1] plane as the base line and at right angles to the base line. The horizontal fiducial mark connections are in the same horizontal plane as the base line. Orientation angles are $\varkappa' = \varphi' = \varkappa'' = \varphi'' = \omega'' = 0^{g}$. All normal cases are indicated by letter "N" in the file name.

I.2 General Convergent Case

All orientation angles differ from zero. In the simulation the orientation angles are chosen to be approximately equal to a real photography test case as previously discussed. The absence of letter "N" in the file name

---

(1) "horizontal" in terms of model co-ordinates.

indicates convergent photography.

II Errors in the interior orientation parameters

The following parameters are introduced into the relative orientation with incorrect values in order to simulate errors.

II.1 Principal Point

The controlled introduction of errors into the principal point is achieved by simply shifting all plate co-ordinates $\bar{x}$ and/or $\bar{y}$ of one or both images by the same quantity. Columns 5 to 8 of Table 8-1 show which of the principal point co-ordinates ($\bar{x}'_o$, $\bar{y}'_o$, $\bar{x}''_o$, $\bar{y}''_o$) are shifted and by how much they are changed. File names contain the letter combination PP if the principal point position is shifted.

II.2 Principal Distance

An error in the principal distance is simulated by changing the theoretical value of $\bar{f}$ by small negative or positive quantities. Columns 3 and 4 of Table 8-1 show by how much the principal distance has been changed. Letters PD in the file name indicate an incorrect principal distance for the relative orientation.

III Number of cameras used to create a stereo pair

III.1 One-camera Case

One camera only is used to produce the two images of a stereo pair. This simulation is accomplished by changing both principal distances and/or principal points by the same amounts.

$$\bar{f}' = \bar{f}'' \qquad \bar{x}'_o = \bar{x}''_o \qquad \bar{y}'_o = \bar{y}''_o$$

Test cases 0, 3, 8, 11, 12, 23 and 28 are one-camera photography. As mentioned before (8.2), one-camera photography in its practical application does not necessarily guarantee that principal point errors are identical, owing to different observation errors in the fiducial marks of the two images. One can, however, assume that differences in the fiducial mark readings are small compared to calibration errors in the principal point position and errors in the mechanical placing of fiducial marks.

Cases 1, 2, 4, 5, 6, 7, 9, 10, 21, 22, 24, 25, 26, 27 and 29 are two-camera cases.

IV Accuracy of plate co-ordinates

IV.1 Error-free Co-ordinates

Plate co-ordinates are assumed to be error-free so as not to obscure deformation characteristics caused by inaccuracies in parameters under investigation.

IV.2 Plate Co-ordinates with Observation Errors

Here plate co-ordinates are introduced as observed quantities with normal distributed random errors. Such errors with a standard deviation of σ_0 = 10 µm are generated as described in 3.3 and added to the error-free co-ordinates of the synthetic photograph.

Only test cases SYNRANDOMN and SYNRANDOM for normal and convergent photography respectively assume "observed" plate co-ordinates. All other parameters in these two cases are error-free.

V Errors in orientation angles

The introduction of errors into the interior orientation parameters results in the majority of the tested cases in secondary errors in the parameters of the relative orientation, namely the orientation angles (columns 11-15 of Table 8-1). Model deformations in these cases, however, are caused by orientation errors combined with interior orientation errors. Additional simulations are therefore necessary to isolate deformations caused merely by errors in the individual orientation angles.

Deformations caused by the following errors in orientation are investigated for normal and convergent photography.

The results of the simulations are listed in Table 8-4.

V.1 $d\kappa' = 0{,}1^{\circ}$ left camera rotated anticlockwise through 0,1° about Z axis. Cases 13 and 30.

V.2 $d\kappa'' = 0{,}1^{\circ}$ as in V.1 but for right camera. Cases 14 and 31.

V.3 $d\varphi' = 0{,}1^{\circ}$ left camera rotated towards the left in the horizontal plane. Cases 15 and 32.

V.4 $d\varphi'' = 0{,}1^{\circ}$ right camera rotated towards the left in the horizontal plane. Cases 16 and 33.

V.5 $d\varphi' = d\varphi'' = 0{,}1^{\circ}$ equal and like φ, both cameras are rotated towards the left. Cases 17 and 34.

V.6 $d\varphi' = -d\varphi'' = 0{,}1^{\circ}$ equal and unlike φ (the cameras are rotated away from each other. Cases

18 and 35).

V.7 $d\omega'' = 0{,}1^{g}$ the right camera is tilted upwards by $0{,}1^{g}$. Cases 19 and 36.

VI Mathematical concept of model control

To explore the possibility of replacing the conventional absolute orientation technique by simple control parameters, the following concepts of model control are investigated.

VI.1 Homogeneous Scale Factor

A common scale factor is applied to all model points in X, Y and Z. The scale factor is found by comparing a known (measured) distance with its value obtained from model co-ordinates by relative orientation. The common scale is easily applied by either repeating the calculation of model co-ordinates with a new scaled base length or by multiplying all X, Y and Z values by the scale factor. This control method shall in the following be referred to as "homogeneous scaling from X" when the control distance extends in X axis direction and similarly "from Y" or "from Z" for scaling based on distances in the other two axis directions.

In the simulated cases, the true distance between points is known, whilst in the real photography cases control distances can be derived from measured test field co-ordinates. In a field situation a distance measured between any two well-defined points can serve to supply the control.

In the tests only two of the distances are used for homogeneous scaling; distance 4-68 (Fig.5-3) provides control for scaling from X- and distance 35-47 scales the Z-direction.

Case numbers with letter "A" and file names containing letter "S" refer to homogeneous scaling from X, letter "D" in file name and case number to scaling from Z.

VI.2 Affine Scaling (7.11)

In the course of deformation analysis of the test cases there emerged a distinct deformation pattern typical specially of those cases simulating normal photography. The deformation along any one axis was frequently found to be more or less uniform, whereas this deformation generally differed significantly in magnitude from the deformations along either of the other two axes. This yielded a route to an approximate method of reducing model deformations: the applications of a distinct scale factor to each axis. This method shall be referred to as "affine scaling". Not all three scale factors need necessarily differ and a common value for X and Y scaling derived from a control distance in X or Y direction is often satisfactory. In the test cases scale factors are derived from distances (Fig.5-3)

16-80 for scaling in X-direction

1-4 for scaling in Y-direction

35-47 for scaling in Z-direction.

Letter E in the case number and letters AF or F in the file name identify affine scaling.

VI.3 Convergency Correction

Convergency correction as a means of model control is described in detail in Chapter 7.10. For the test sequence known distance 35-47 in the Z-direction is used in a number of cases as control distance in an attempt to reduce model

deformations caused by possible convergency errors. Control distance 35-47, positioned in the centre of the test field, is used in all cases of convergency control with the exception of case 40BB, where the control distance at the side of the field was employed to test Adams' (1978) statement that the position of a convergency control distance within the field is arbitrary, privided it extends in the Z-direction. Convergency correction is applied to unscaled co-ordinates as well as to model co-ordinates, which have first been homogeneously scaled. Scaling cum convergency correction cases are identified by letter "B" in their file name, while an unscaled convergency correction is indicated by letter "P". To compare the deformation reduction by convergency correction as opposed to homogeneous scaling the same Z distance was used for both control techniques in some of the test cases (3D versus 3B and 3P and similarly 11D versus 11B and 11P).

In the following sections of this chapter the presentation of the deformation analysis on the basis of simulated photography is explained and the design of the individual test cases is described. A detailed analysis of the more important test cases is given. The results of the analysis are summarised in Chapter 9.

8.4 PRESENTATION OF TEST RESULTS

The results of the deformation test sequence are presented in a number of different ways to allow a comprehensive interpretation and analysis.

In general it is not important to know the position of the cameras with respect to the test field and only the relative positions of the object points are of interest. Model co-ordinates as obtained from the relative orientation are therefore not directly compared with true point positions. The 80 test field points are first submitted to a block shift into a best fit with the undistorted reference system, before deformations are determined. Scales of both systems, the reference network and the deformed field, as well as rectangularity of both co-ordinate systems are maintained in the transformation in order to guarentee a true representation of the deformation pattern of each case.

Thus displacement or deformation vectors quoted in this analysis are either individual point displacements (IP Tables) of the form

$$dx_i = X_i - \bar{X}_o - \tilde{X}_i \qquad (8.4.1)$$

or average displacement vectors for the 80 points of the test field (Tables 8-1 to 8-4). These are evaluated as:

$$dx = \frac{\sum_{i=1}^{n} [X_i - \bar{X}_o - \tilde{X}_i]}{n} \quad \text{with } n = 80 \qquad (8.4.4.1)$$

and similar for dy_i, dz_i, dy and dz.

Where

X_i, Y_i, Z_i = model co-ordinates as evaluated in relative orientation and, where applicable, corrected by model control.

$\tilde{X}_i, \tilde{Y}_i, \tilde{Z}_i$ = true values of co-ordinates. In cases of real photography the geodetic determinations of the

test field co-ordinates have to serve as "true" values.

$\bar{X}_o, \bar{Y}_o, \bar{Z}_o$ = shifts in axes directions to find best fit

with

$$\bar{X}_o = \frac{1}{n}\sum_{i=1}^{n}(X_i - \tilde{X}_i) \qquad n = 80 \qquad (8.4.2)$$

and similarly for $\bar{Y}_o$ and $\bar{Z}_o$.

The block shifts ($\bar{X}_o$, $\bar{Y}_o$, $\bar{Z}_o$) applied in each case to guarantee a best fit with the reference network are listed in Table 8-5.

In accordance with the least squares principle and in order to detect the presence of outliers and extreme values, in addition to the average absolute deformation vectors, the root mean square errors are found from

$$\sigma_x = \left[\frac{\sum_{i=1}^{n}(X_i - \bar{X}_o - \tilde{X}_i)^2}{n}\right]^{\frac{1}{2}} \qquad n = 80 \qquad (8.4.3)$$

and similarly σ_y and σ_z.

Average point displacement vectors are evaluated from

$$dv = (dx^2 + dy^2 + dz^2)^{\frac{1}{2}} \qquad (8.4.4)$$

and average point root mean square errors from

$$\sigma_v = (\sigma_x^2 + \sigma_y^2 + \sigma_z^2)^{\frac{1}{2}} \qquad (8.4.5)$$

Individual deformation vectors for dx, dy and dz permit a detailed analysis of the deformations, whereas the average values (8.4.1.1 and 8.4.3 to 8.4.5) serve to indicate general trends and relative overall

accuracy improvements or deteriorations after application of different model control techniques.

The numerical results of the analysed deformation test cases are listed in the following tables:

1. TABLE 8-1 Summarised results of cases simulating model deformations caused by errors in elements of interior orientation.

2. TABLE 8-2 Repetition of some of the results listed in Table 8-1 with more significant figures.

3. TABLE 8-3 Summarised results of real photography test cases.

4. TABLE 8-4 Effects of errors in orientation angles on model co-ordinates.

5. IP TABLES Individual point tables.

6. Deformation diagrams
   - 6.1 Vector Plot V
   - 6.2 Vector Plots X, Y and Z

7. Deformation stereograms.

Tables 8-1 to 8-4 as well as the table of the block shifts (Tab.8-5) are given as fold-outs at the end of Chapter 9.

Individual Point Tables (IP Tables)

The most comprehensive information about the deformation in the test cases is contained in the individual point tables (IP Tables) of which two are provided for each of the simulations. (The example of the IP Tables for case SYNPDPPN0 is shown in Tab.8-6, the complete set is found in a separate Appendix.)

VERTICAL PLANE 6.2 M

	- 1 -				- 17 -				- 33 -				- 49 -				- 65 -		
-1.5	0.2	0.9	*	-1.1	1.0	1.4	*	-0.1	-0.3	-0.9	*	-0.5	1.2	1.5	*	-0.1	0.3	1.0	
	- 2 -				- 18 -				- 34 -				- 50 -				- 66 -		
-0.8	0.0	-1.9	*	-0.6	0.9	3.2	*	-0.3	-0.5	0.2	*	0.2	0.7	2.4	*	0.9	0.2	1.6	
	- 3 -				- 19 -				- 35 -				- 51 -				- 67 -		
-1.0	-0.3	-0.2	*	-0.8	-0.1	0.3	*	0.1	0.5	-0.8	*	0.0	0.2	4.7	*	-0.1	0.2	0.7	
	- 4 -				- 20 -				- 36 -				- 52 -				- 68 -		
-0.7	-0.8	0.0	*	-0.3	-0.6	1.0	*	-0.3	-1.0	0.5	*	1.5	-0.4	1.5	*	2.0	-0.5	4.4	

VERTICAL PLANE 5.4 M

	- 5 -				- 21 -				- 37 -				- 53 -				- 69 -		
-1.0	0.3	0.2	*	-1.3	0.8	0.3	*	-0.4	-0.6	-2.3	*	0.0	0.4	-1.6	*	0.7	1.3	0.5	
	- 6 -				- 22 -				- 38 -				- 54 -				- 70 -		
-1.4	-0.6	-0.4	*	-0.5	0.1	0.5	*	-0.2	0.3	2.6	*	0.0	0.7	1.4	*	0.6	1.3	1.7	
	- 7 -				- 23 -				- 39 -				- 55 -				- 71 -		
-1.3	-0.7	-0.7	*	-0.4	0.2	1.0	*	-0.2	-0.7	1.9	*	0.7	-0.4	1.9	*	1.8	0.4	2.5	
	- 8 -				- 24 -				- 40 -				- 56 -				- 72 -		
-1.3	-1.1	1.6	*	0.2	-0.7	0.4	*	0.4	0.1	1.1	*	-0.5	-0.1	-1.2	*	0.9	0.6	1.6	

VERTICAL PLANE 4.5 M

	- 9 -				- 25 -				- 41 -				- 57 -				- 73 -		
0.3	-0.2	-2.4	*	-0.6	-0.1	-1.7	*	-0.7	0.1	-2.1	*	0.1	1.0	-0.5	*	0.9	1.7	0.7	
	- 10 -				- 26 -				- 42 -				- 58 -				- 74 -		
-0.7	-0.7	-0.7	*	-0.2	-0.3	-0.8	*	-0.1	0.2	0.1	*	1.3	0.6	0.8	*	0.8	0.9	0.7	
	- 11 -				- 27 -				- 43 -				- 59 -				- 75 -		
-0.3	-0.5	-1.1	*	-0.2	-0.6	-1.3	*	0.5	-0.2	1.1	*	0.2	0.3	0.1	*	-0.2	0.2	-1.5	
	- 12 -				- 28 -				- 44 -				- 60 -				- 76 -		
-0.7	-1.3	-0.7	*	0.0	-0.6	-0.4	*	0.5	-0.9	-0.7	*	0.4	-0.4	-0.2	*	1.1	0.2	-0.2	

VERTICAL PLANE 3.6 M

	- 13 -				- 29 -				- 45 -				- 61 -				- 77 -		
-0.5	-0.4	-2.1	*	-0.5	-0.3	-2.1	*	-0.5	-0.1	-1.7	*	0.4	1.5	0.0	*	0.4	1.2	-0.3	
	- 14 -				- 30 -				- 46 -				- 62 -				- 78 -		
-0.1	-0.3	-1.8	*	-0.3	-0.2	-1.7	*	0.3	-0.8	-1.3	*	-0.3	0.4	-1.3	*	0.8	1.2	-0.2	
	- 15 -				- 31 -				- 47 -				- 63 -				- 79 -		
-0.1	-0.5	-2.0	*	0.3	-0.4	-1.8	*	0.3	-0.2	-1.5	*	0.4	0.1	-0.8	*	1.3	-0.1	-0.4	
	- 16 -				- 32 -				- 48 -				- 64 -				- 80 -		
-0.4	-0.8	-1.9	*	0.1	-1.2	-0.6	*	0.6	-0.9	-1.7	*	0.6	-0.3	-1.1	*	1.6	-0.1	0.4	

AVERAGE ABSOLUTE X Y Z : 0.6 0.5 1.2 AVERAGE SQUARE ROOTS X Y Z : 0.7 0.7 1.5

Table 8-6 Example for IP Table 1 (case SYNPDPPNO)

Table 8-6 (continued) Example for IP Table 2 (case SYNPDPPNO)

SYMPDPPNO				
DISTANCE	TRUE	SIMULATION	DIFF	SCALE FACTOR
DISTANCES IN X-AXIS DIRECTION				
1 - 65	3.3014	3.3028	-1.4	0.999581
4 - 68	3.2737	3.2820	-3.1	0.999070
5 - 69	3.2774	3.2791	-1.7	0.999483
8 - 72	3.2758	3.2780	-2.2	0.999331
13 - 77	3.2812	3.2820	-0.9	0.999731
16 - 80	3.2655	3.2675	-2.1	0.999364
DISTANCES IN Y-AXIS DIRECTION				
1 - 4	2.2472	2.2481	-1.0	0.999572
33 - 36	2.2306	2.2313	-0.7	0.999678
65 - 68	2.2169	2.2177	-0.8	0.999630
5 - 8	2.2503	2.2517	-1.5	0.999354
37 - 40	2.2498	2.2492	0.6	1.000274
69 - 72	2.2492	2.2499	-0.8	0.999663
13 - 16	2.2480	2.2483	-0.4	0.999827
45 - 48	2.2523	2.2531	-0.7	0.999672
77 - 80	2.2516	2.2529	-1.3	0.999441
DISTANCES IN Z-AXIS DIRECTION				
1 - 13	2.2685	2.2714	-2.9	0.998717
33 - 45	2.5488	2.5496	-0.8	0.999696
65 - 77	2.5434	2.5447	-1.3	0.999484
2 - 14	2.2740	2.2739	0.1	1.000056
34 - 46	2.5566	2.5581	-1.5	0.999395
66 - 78	2.5523	2.5541	-1.8	0.999295
4 - 16	2.2835	2.2854	-1.9	0.999165
36 - 48	2.5484	2.5506	-2.2	0.999147
68 - 80	2.5479	2.5519	-4.0	0.998447

The first of the two tables of each set (IP Table 1) lists the displacement vectors dx, dy, and dz for each of the 80 test field points below the point number arranged in four vertical planes. The planes are parallel to the base line at distances of approximately 3,6 m; 4,5 m; 5,4 m and 6,2 m from the base line. Vectors are quoted in mm units. Points 1 to 4, which are 0,3 m off the 6,2 m plane are for practical reasons included into the 6,2 m plane.

In the second table (IP Table 2) true distances are compared against distances from model-co-ordinates. A set of 27 sample distances is chosen with examples of distances in X-, Y- and Z-directions. Only distances 1-65 and 4-68 are not axis parallel.

Deformation diagrams

The deformation vectors of the more important of the test cases are presented in diagrammetric form. In each of these cases the deformation vectors dx, dy and dz are shown individually on separate plots as well as combined in one plot. In all four plots the test field frame is shown in a quasi perspective view to avoid obscuring the deformation vectors. The deformation vectors are plotted in an isometric perspective for the combined plot (vector plot V), whereas they are shown in a central perspective view for the individual vector plots X, Y and Z.

Vector plot V

In vector plot V deformation vectors dx, dy and dz are plotted for each point at a constant scale throughout the network, exaggerating the vector length considerably against the field dimensions. Deformation vectors have the form shown in Fig.8.4-1.

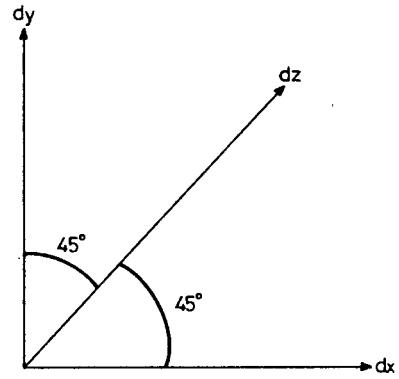

Fig.8.4-1 Isometric presentation of deformation vector in vector-plot V

Vector plots X, Y and Z

A better visual display of the deformation characteristics can be achieved by connecting the end points of the deformation vectors dx, dy and dz in individual plots. It would be confusing to draw the entire network in this matter and only selected planes are displayed in each case. For dx the five vertical planes at right angles to the base are chosen for the presentation.

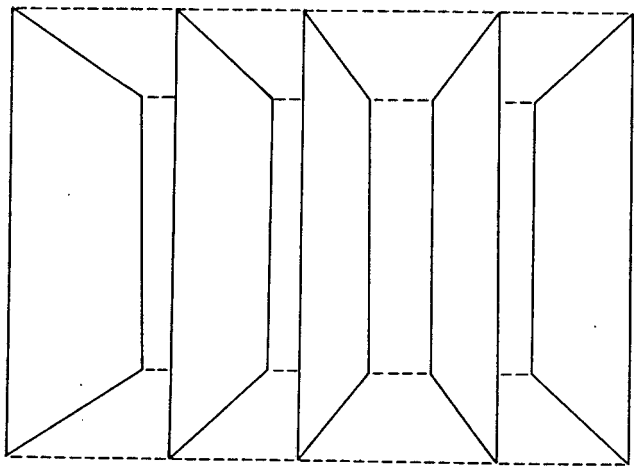

Fig.8.4-2 Planes for vector plot X

for dy the four horizontal planes

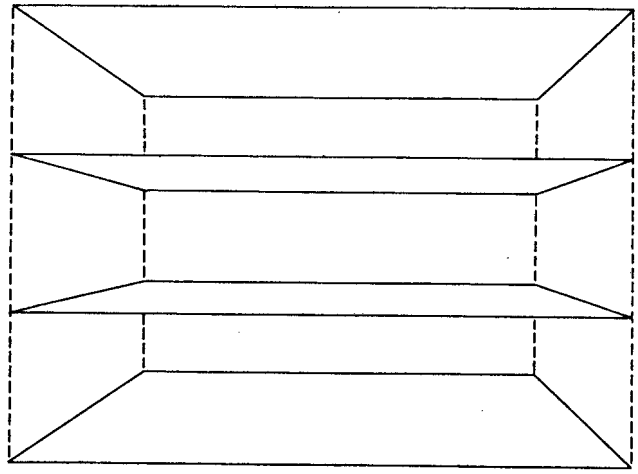

Fig.8.4-3 Planes for vector plot Y

and for dz the four vertical planes parallel to the base

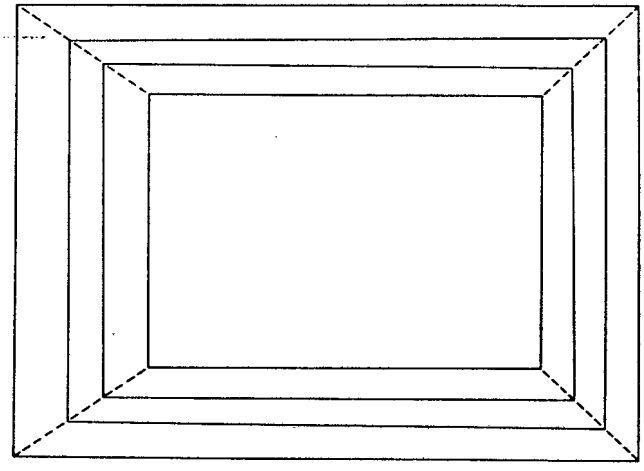

Fig.8.4-4 Planes for vector plot Z

Example of the vector plots are given in Fig.8.4-5 to 8.4-8 for the test case SYNPDPPNO.

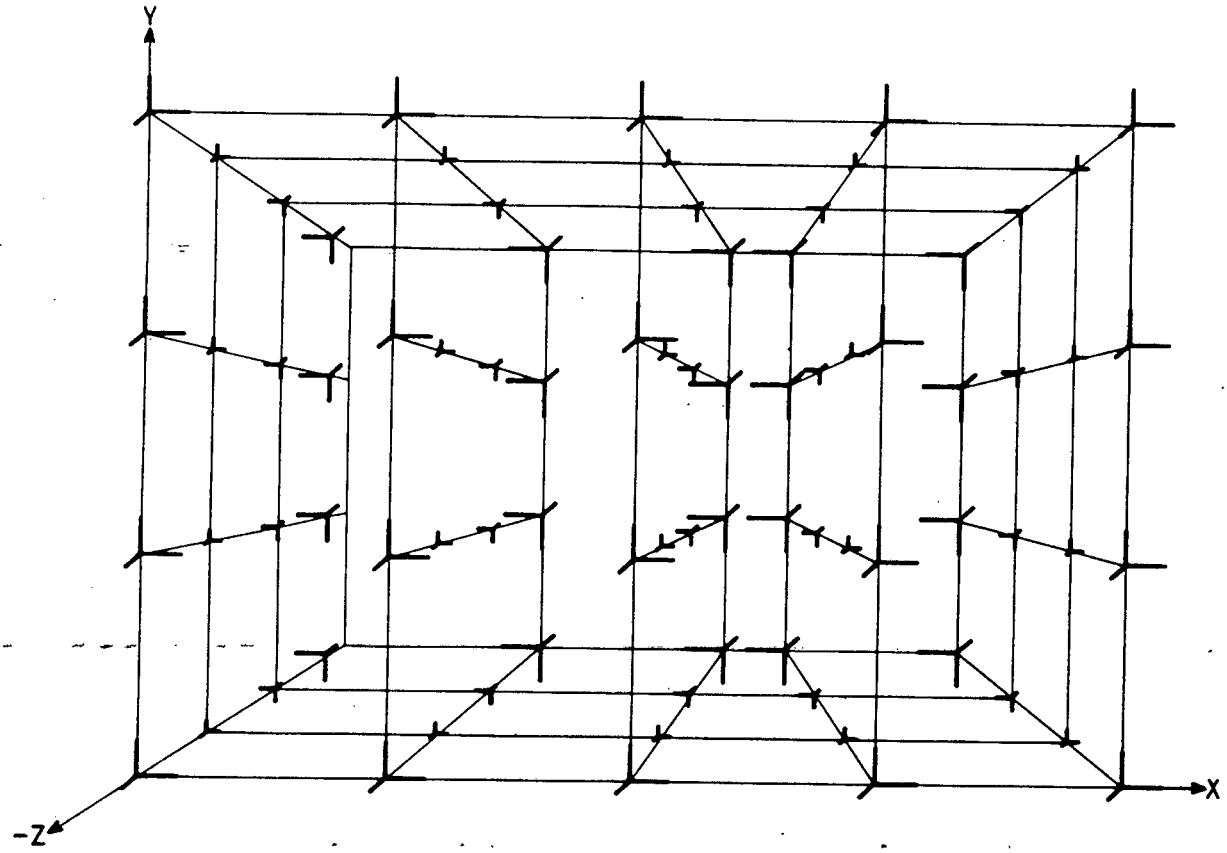

Table 8.4-5 Example for Vector plot V (case SYNPDPPNO)

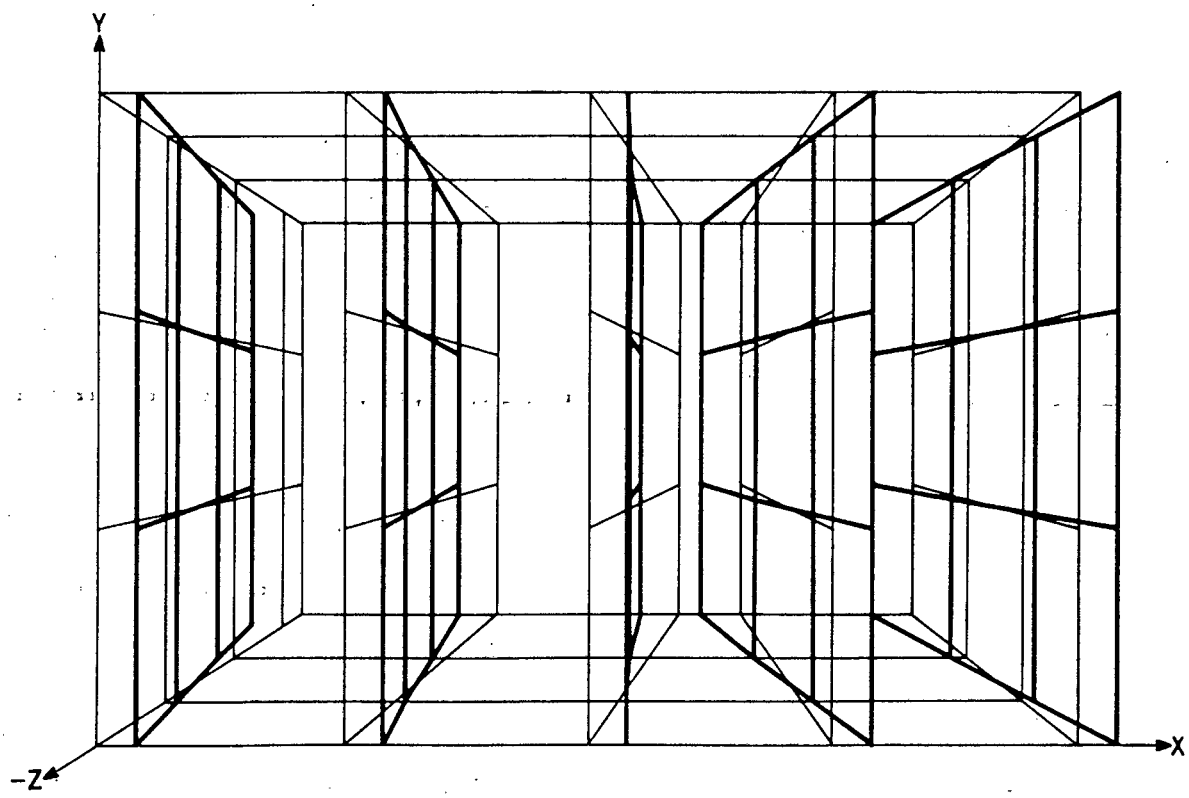

Table 8.4-6 Example for Vector plot X (case SYNPDPPNO)

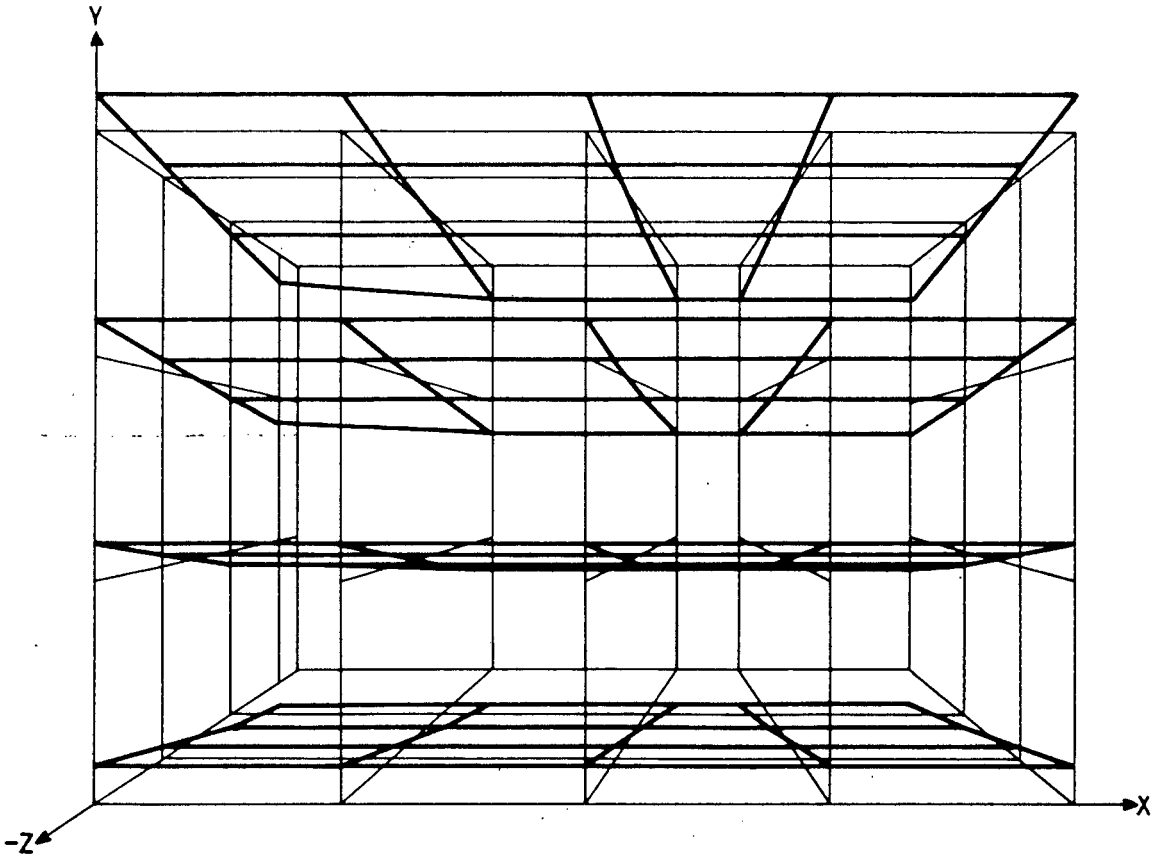

Table 8.4-8 Example for Vector plot Z (case SYNPDPPNO)

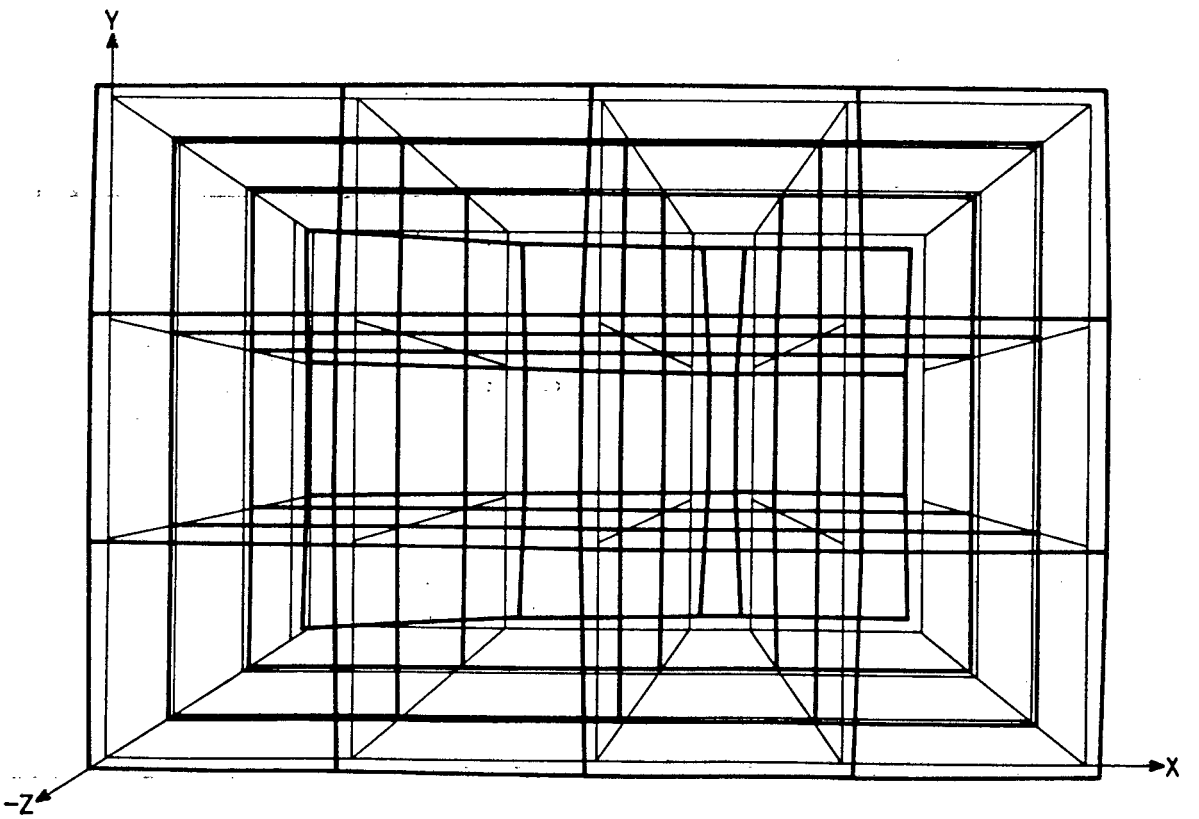

Table 8.4-7 Example for Vector plot Y (case SYNPDPPNO)

Deformation stereograms

Finally, stereograms were created of some typical deformations to allow easier inspection.

All plots must be seen as qualitative conveying the character and shape of the deformation rather than its quantity.

8.5 POINT CONFIGURATIONS FOR DEFORMATION TESTS

Only 10 well distributed of the 80 test field points are taken into consideration for the relative orientation adjustment of each of the simulated photography cases (Fig.8.5-1).

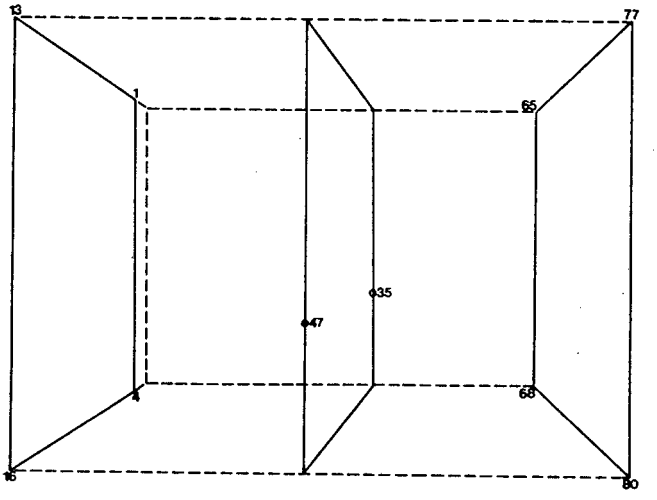

Fig.8.5-1 10-point test field

For the real photography, the point number was varied. While cases 40 and 43 to 48 are based on the 10 original points, case 41 incorporates 30 points (Fig.8.5-2).

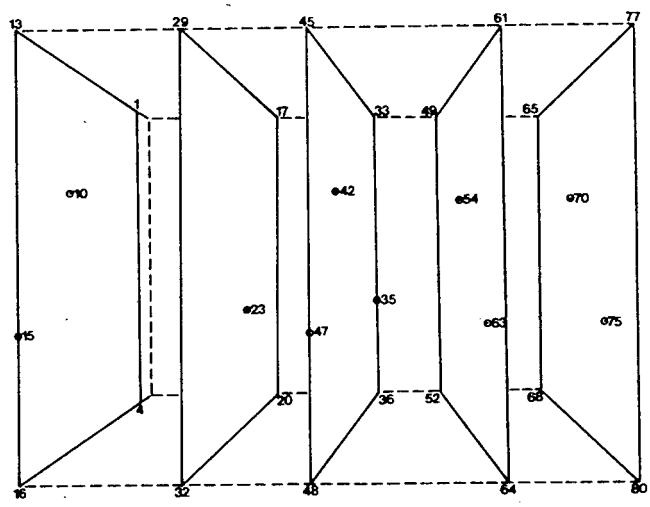

Fig.8.5-2 30-point test field

The first case of test sequences 42 (Table D) combines 12 points in one vertical plane only. A thirteenth point (P 35) off the vertical plane is added in the remaining cases of 42 to provide a control distance in the Z-direction for convergency correction and scaling (Fig.8.5-3)

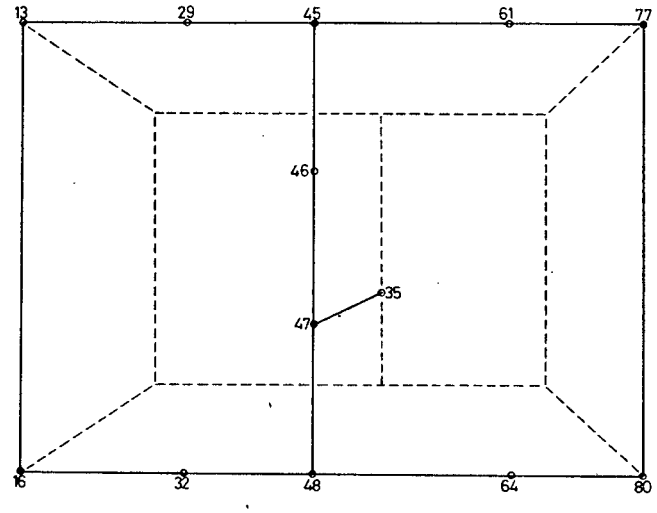

Fig.8.5-3 12-point test field with control distance

8.6 ANALYSIS OF INDIVIDUAL CASES

Case 0 (SYNRANDOMN)

None of the interior orientation parameters are changed but computer generated random errors with a standard deviation of σ_0 = 10 µm are added to the plate or-ordinates to simulate observed values. This case serves to verify the computer program for the relative orientation and the mathematical model of the least squares adjustment. Furthermore, it checks the validity of the random error generation (Chapter 3.4) and it shows how random errors influence the model co-ordinates.

As expected the result indicates that random errors of the order encountered in plate co-ordinate observations on a stereo comparator cause small changes in the orientation angles. The angles are incorrect by 0,5 to 2 minutes of arc without showing any significant difference between the different orientation angle errors. The model co-ordinates suffer average displacement of about 1 mm ranging from 0,5 to 2 mm with a maximum value of 4,4 mm in Z. It becomes obvious that Z co-ordinates, i.e. horizontal distances at right angles from the camera base line, suffer the largest distortions in a relative orientation. This phenomenon is characteristic for close-range photogrammetry and occurs in most test cases.

A value of 14 µm for σ_0 confirms the random error modelling. The deviation of 4 micron from the theoretical value of 10 µm, which was stipulated in the random error model, is explained by the relatively small number of observations involved in the relative orientation. Out of the total number of 320 generated random errors, only 40 values are used in the relative orientation, which is less than the minimum of 60 values required, according to Heister, Welsch (1972), for a

representative sample at a 99% probability level.

Errors in model co-ordinates - that is the difference between the model co-ordinates obtained in the relative orientation adjustment and the true values of the synthetic test field - are small random values, thus confirming the mathematical model of the adjustment.

Cases 1 and 2 (SYNPD1N and SYNPD2N)

The principal distance of the left camera is changed by +0,5 mm (case 1) and +1 mm (case 2). Geometrically seen this means that the bundle of projection rays defined by the plate co-ordinates and the principal distance of the left image is narrowed.

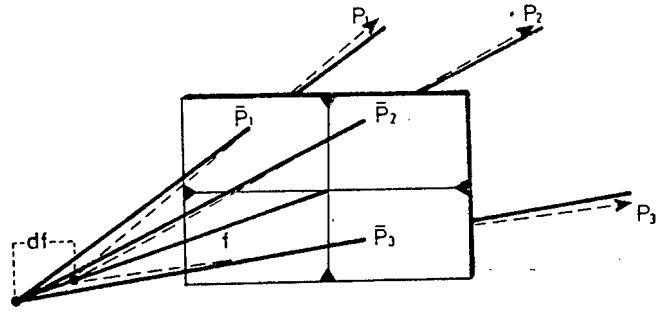

Fig.8.6-1 Effect of error in principal distance on the projection ray bundle

Coplanarity with the unmodified right bundle can no longer be achieved. The least square adjustment can only interpret this lack of coplanarity as inaccuracies in observed plate co-ordinates of both images, as clearly indicated by values of 220 µm (case 1) and 440 µm (case 2) for σ_0 a posteriori in spite of error-free introduced plate co-ordinates. The value for σ_0 is without doubt not representative in this case. An error in the principal distance of one camera leads to an "Equal and

like" change in the two φ values of the relative orientation (Table 8-1, column 11-15). An equal and like φ error in combination with an incorrect principal distance causes a deformation so asymmetrical and irregular that neither homogeneous scaling nor convergency error correction can compensate for the errors. When inspecting errors in distances parallel to axes directions (IP Tables) rather than point positions it becomes obvious, however, that some improvement of the overall distance accuracy is achieved by application of a convergency correction.

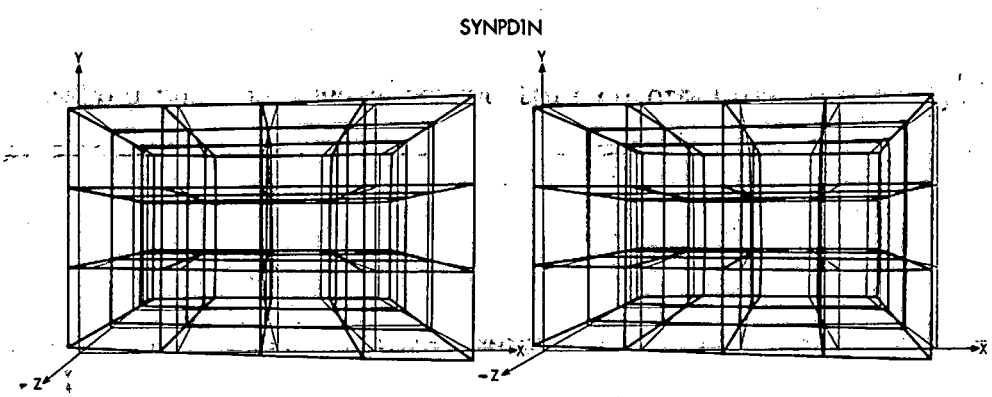

Fig.8.6-2 Model deformations resulting from an error in the left principal distance

Comparison of cases 1 and 2 shows that a near proportional increase of the deformation occurs if the error in the principal distance is increased by small amounts.

Case 3 (SYNDP3N)

Both principal distances are changed by the same amount from 100 mm to 100,5 mm, thus simulating "one-camera" photogrammetry. It can easily

be verified for normal photography (Tab.8.2-1 and Table 8-1) that an equal and like error in both principal distances causes a scale error in Z-axis direction, while X and Y values remain unaffected. Homogeneous scaling (cases 3A and 3D) can, therefore, not serve to remove or reduce deformations if this error occurs. Homogeneous scaling from Z removes errors in this direction and introduces errors into the originally error-free X and Y co-ordinates. Scaling from X or Y, on the other hand, can have no effect as distances in these directions are error-free. Convergency correction, although it does not correctly model the deformation, has some improving influence as it is based on a Z distance. Errors in Z are distributed over all three axis directions reducing errors in Z considerably while introducing small errors in X and Y.

Affine scaling must obviously remove this deformation completely.

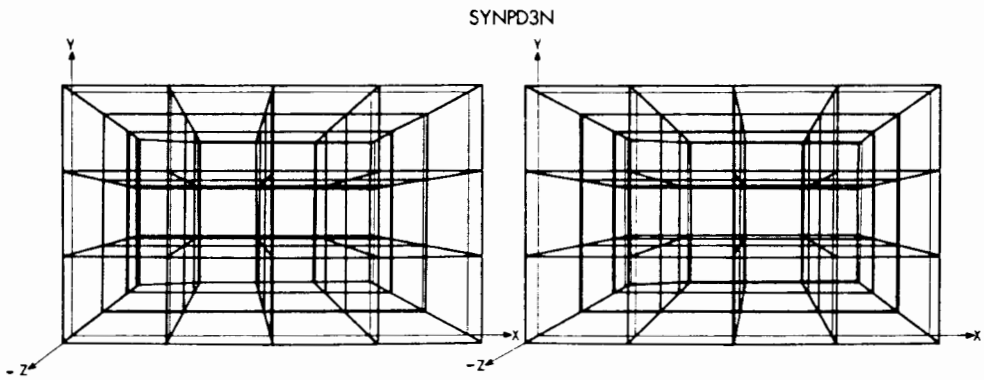

Fig.8.6-3 Model deformation resulting from an equal error in both principal distances

It must be noted here that the equal distortion of both projection ray bundles guarantees perfect coplanarity for corresponding rays.

The standard deviation is, therefore, a true reflection of the accuracy of the observed plate co-ordinates. Inaccuracies in the principal distances are not, and shouldnot be, reflected in the value for σ_0 a posteriori.

Case 4 (SYNPD4N)

Here the principal distances of the two cameras are changed by equal amounts of opposite sign. The effect is similar to that of case 2. The only conclusion which can be drawn here is that the difference in the errors in principal distances is more relevant than the quantity of the individual errors.

Case 5 (SYNPP1N)

The $\bar{x}'_0$ value of the left camera's principal point is changed by 1 mm, causing a sideways distortion of the projection ray bundle.

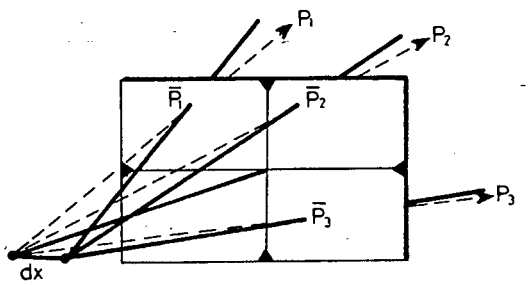

Fig.8.6-4 Effects of error in principal point on the projection ray bundle

Coplanarity is not affected in normal oriented photography as each ray is moved in its original coplanarity plane and, therefore, this error is neither reflected in a change of the orientation angles nor in the σ_0 value (Table 8-1). It has nevertheless a considerable

effect on object point position and distances.

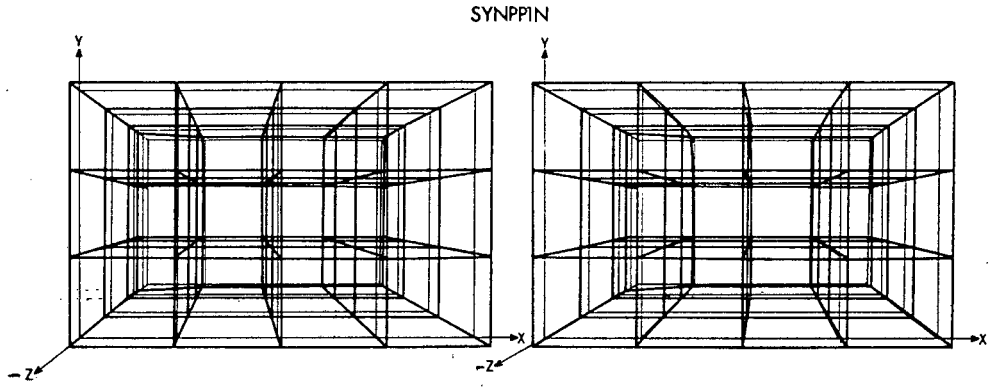

Fig.8.6-5 Deformation caused by error in $\bar{x}_0'$ value of one principal point

It becomes obvious here that in "normal" photography errors in $\bar{x}$-values of image co-ordinates do not contradict the coplanarity condition and no corrections $v_{\bar{x}}$ are allocated to $\bar{x}$ image co-ordinates in an adjustment if the only error present is an error in the $\bar{x}$ co-ordinate of the principal point. This is reflected in the fact that generally corrections to $\bar{x}$ image co-ordinates are considerably smaller than those for the corresponding $\bar{y}$ co-ordinate values.

The IP Table for this case shows that the major part of the deformation can be removed by affine scaling.

The error of 1 mm in a principal point co-ordinate, assumed here, is excessive and better accuracies can be expected for the principal point position even for non-metric cameras. The exaggerated error was, as in all other test cases, introduced to enhance the deformation for analysis purposes.

Case 6 (SYNPP2N)

The $\bar{y}'_o$ value of the left principal point is changed by 1 mm. Although this error changes orientation angle ω" considerably with smaller equal and like changes in φ and κ, model co-ordinates are much less affected than by an error in $\bar{x}'_o$. Especially the distance accuracy is superior to the previous case. Larger errors occur in Y model co-ordinates.

Homogeneous scaling does not improve the model deformations, convergency correction (see IP Table) provides some improvement, while affine scaling can be expected to show the best, though still small, improvement.

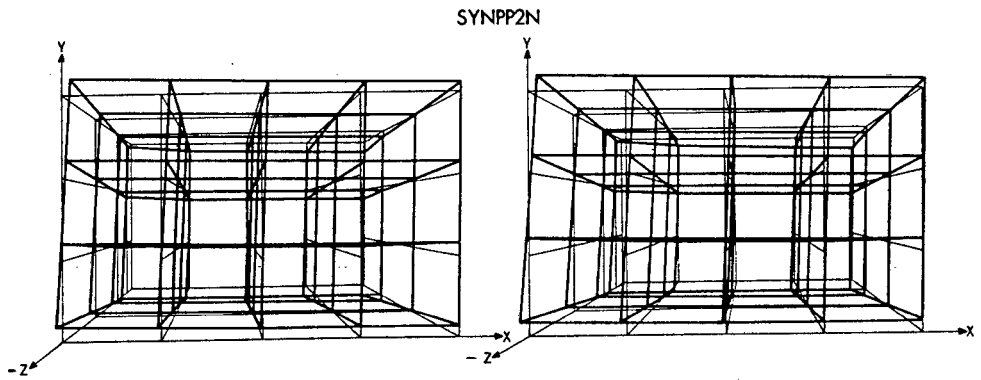

Fig.8.6-6 Deformation due to an error in the $\bar{y}'_o$ value of the principal point

Case 7 (SYNPP3N)

Both principal point co-ordinates of the left image are modified by 1 mm. Large distortions occur in both point position and distances, with the asymmetrical distortion being mainly due to the error in x'_o. The relatively small spread in the scale factors in each axis

direction indicates that once again affine scaling will improve distance accuracy.

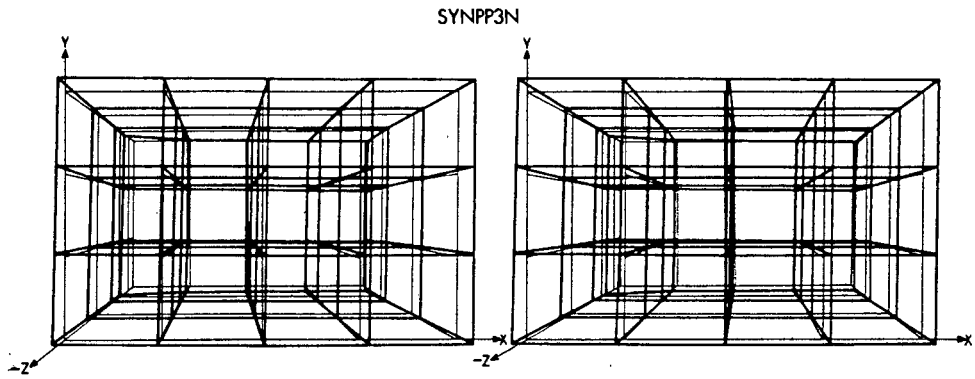

Fig.8.6-7 Deformations due to errors in both principal point co-ordinates of one camera

Case 8 (SYNPP4N)

A one-camera situation is simulated by the controlled introduction of equal errors of 1 mm in both principal point co-ordinates of both images.

As in all other one-camera cases in normal camera orientation incorrect values of interior orientation parameters do not cause distortions in orientation angles and σ_0 reflects true observation accuracy.

Errors of equal sign and quantity in the principal point positions of both images result in distortions of the X and Y co-ordinates of the model only, while Z remains unaffected (Table 8-1).

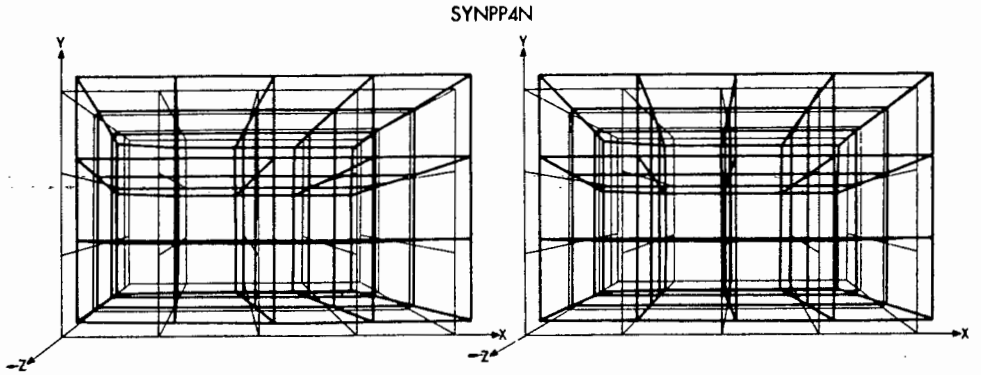

Fig.8.6-8 Deformations caused by equal and like errors in both principal point positions

Distances in the Z-direction are error-free, whereas X and Y distances show only small distortions, owing to a "shearing" effect in the deformation, in which points are shifted by similar quantities within axis parallel planes. In the test case nearly all distances have accuracies better than 1:5000 in spite of large shifts in point positions, with the only exception in distances 1-65 and 4-68 which are not parallel to the co-ordinate system axes.

As distance errors are small scaling cannot be expected to have a significant effect.

Case 9 (SYNPP5N)

Case 9 is in principle similar to case 4 where errors of equal quantity but with opposite signs are applied to the principal distance, case 9 assumes equal and unlike errors for the principal points of both simulated images. The result leads to the same conclusion, namely that differences between the errors in the left and right camera calibration are more relevant than the actual amount of the errors.

Case 10 (SYNPDPPN)

By applying errors of opposite sign to principal distances and principal point positions of the two images of a stereo pair, a realistic two-camera case is simulated, except for the lack of random errors in plate co-ordinates. (The fact that the errors are of equal quantity is coincidental.) This simulation results in an equal and like error in φ, a large error in ω" and a non-zero value for σ_0 in spite of error-free observations.

Large distortions occur in model co-ordinates X and Y and especially in Z co-ordinates with even larger errors in distances, indicating that the two-camera photogrammetry is an inferior method of photogrammetric data acquisition.

An interesting variation of this simulation is created by interchanging the errors in the left and right principal point and principal distance (SYNPDPPNR). In practice this situation would occur if the left and right camera are interchanged after a first stereo pair is taken and a second set of photographs is obtained with the now interchanged cameras. Inspection of the results of this test case shows that a configuration not identical but similar to one-camera photography is achieved by repeated photography with interchanged cameras.

Very good accuracies of axis oriented distances are obtained from the co-ordinate means of the two relative orientation results as shown in the following deformation stereograms and table of distance comparisons.

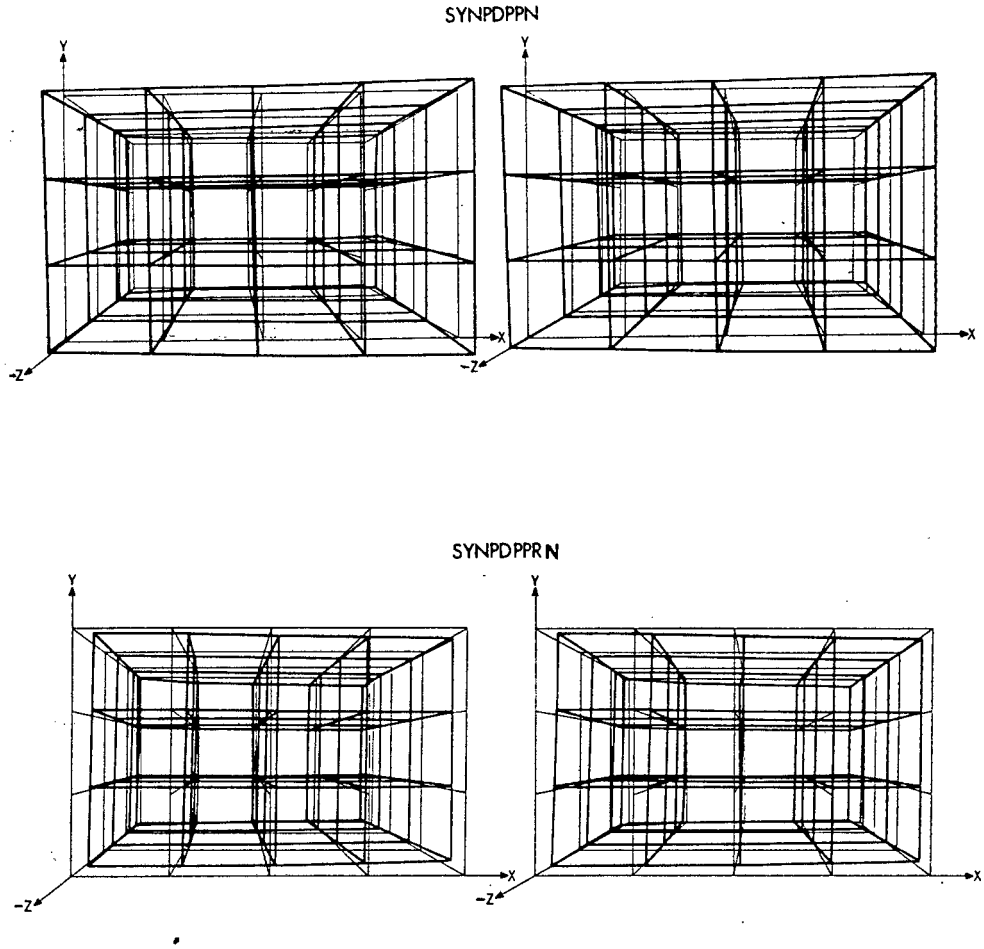

Fig.8.6-9 General two-camera case with different errors in principal point and distance of both cameras. Top: original camera set-up. Bottom: interchanged cameras.

Original Cameras Set-up	Interchanged Cameras	Mean Value
SYNPDPPN	SYNPDPPNR	
Sample distance in X-direction		
- 66,9 mm	64,7 mm	- 1,1 mm
- 62,3	60,7	- 0,8
- 56,5	55,3	- 0,6
- 54,1	53,2	- 0,4
- 36,7	36,7	0
- 33,2	33,2	0
Sample distance in Y-direction		
- 37,4 mm	36,9 mm	- 0,2 mm
- 42,6	41,7	- 0,4
- 46,5	45,1	- 0,7
- 34,6	34,3	- 0,2
- 37,6	37,0	- 0,3
- 40,7	39,8	- 0,4
- 25,4	25,4	0
- 24,4	24,5	0
- 23,5	23,6	0
Sample distance in Z-direction		
- 56,9 mm	55,7 mm	- 0,6 mm
- 78,5	75,8	- 1,4
- 91,5	87,3	- 2,1
- 56,9	55,6	- 0,6
- 79,0	76,3	- 1,4
- 92,2	87,9	- 2,1
- 57,3	55,8	- 0,7
- 78,6	76,0	- 1,3
- 91,5	87,6	- 2,0

Tab.8.6-1 Differences between true distances and distances evaluated from model co-ordinates (see separate Appendix IP Tables 2)

The concept of interchanging cameras to create a near one-camera case can only be applied to photography of moving objects inf the object maintains a similar position in object space (and thus on the image planes) for two consecutive stereo pairs. For the photography of

fixed objects, however, camera interchange is of no advantage, as here the more favourable one-camera photography can be achieved by simply moving one camera from one camera station to the other one.

Case 11 (SYNPDPPNØ)

Case 11 represents a one-camera situation with equal and like errors in principal distance and principal point of both images.

The principal distance is changed by 0,5 mm and the principal point is shifted by 1 mm in both axis directions. Here the point positions are more accurate in Z-than in X- and Y-directions, due to the relatively large error in the principal point which, as shown previously, distorts X and Y co-ordinates.

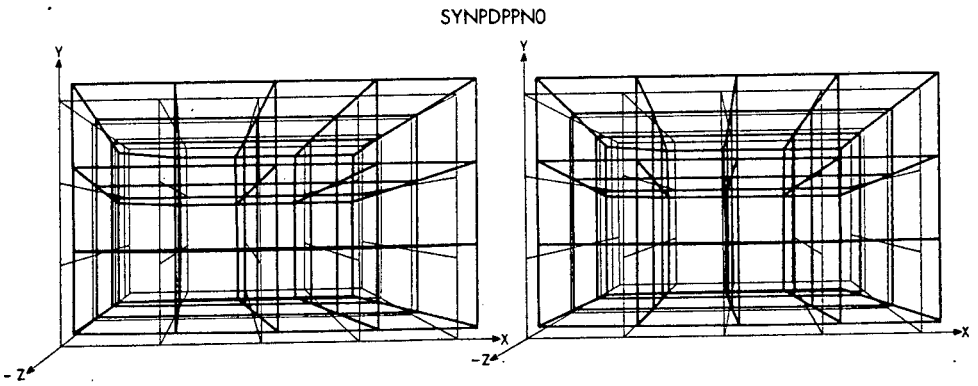

Fig 8.6-10 Stereogram showing deformations caused by equal and like errors in both principal distances and principal points

Deformation diagrams and IP Tables show in X and Y direction the typical shearing effect encountered before, in which distances remain relatively undistorted in spite of large errors in point positions, Z distances are less accurate. Once again it is confirmed that good accuracies can be achieved for distances in axis directions in the

presence of large deformations of model co-ordinates.

As in previous cases, some improvement is achieved by convergency correction while considerably higher distance accuracies are gained from affine scaling, with distance errors smaller and 1 mm.

Case 12 (SYNPDPPN1)

While errors in case 11 are exaggerated to enhance deformations and simplify analysis, case 12 assumes more realistic values in an otherwise identical simulation. The deviations from the true parameters of interior orientation are 0,2 mm for the principal distance and 0,5 mm for the principal point, values which can be achieved for non-metric cameras while they are still somewhat pessimistic for metric cameras. Comparison of case 11 and case 12 shows a virtually linear behaviour of individual deformations within the small range of errors which can be expected to occur in interior orientation parameters.

As a general estimate, allowing for the fact that no ramdom errors in the plate co-ordinates are assumed in the test cases, one can state that position accuracies of 1:500 to 1:1000 and distance accuracies of approximately 1:1000 to 1:2000 in axis direction can be expected from "one-camera" close-range photogrammetry with non-metric cameras and relative orientation adjustment followed by affine scaling. For metric cameras the corresponding accuracy estimates are 1:1000 to 1:2000 for position and 1:2000 to 1:4000 for distances is axis direction.

Similar accuracies can be expected from homogeneous scaling from X with subsequent convergency correction.

GENERAL CONVERGENT PHOTOGRAPHY

General convergent photography for test cases 21 to 29 was simulated in close approximation to some real photography carried out in the laboratory test field.

The synthetic stereo pair was based on the parameters:

$\varkappa' = 1^{\circ}$ $\quad f' = f'' = 100$ mm

$\varphi' = -20^{\circ}$ (positive to the left) $\quad b = 3.310$ m

$\varkappa'' = 0^{\circ}$

$\varphi'' = 14^{\circ}$

$\omega' = 0^{\circ}$

Results of convergent photography tests listed in Table 8-1 reveal clearly that errors in the elements of interior orientation cause much larger deformations in convergent photography than in normal photography. The accuracy, especially in distances, deteriorates by a factor 5 to 20 in the simulated cases.

In normal oriented photography deformation patterns tend to be comparatively regular within planes parallel to the axes. Such regular or near regular deformations can be effectively reduced by affine scaling or similar measures.

In general convergent photography co-ordinate system and camera axis are no longer parallel and deformations lose their regular pattern, thus making deformation correction more difficult.

While in cases of normal photography none of the errors introduced into the simulations results in an equal and unlike error in φ such an error, although comparatively small, can be isolated in most convergent photography simulations as the following table shows (see

8.3 and Tab.8.1 for the meanings of the file names).

Case	φ'	φ''	Equal and like parts		Equal and unlike parts	
SYNPD 1	-23	-18	-20,5+	-20,5	-2,5	+2,5
SYNPD 2	-47	-35	-41	-41	-6	+6
SYNPD 3	- 4	5	0,5	0,5	-4,5	+4,5
SYNPD 4	-42	-41	-41,5	-41,5	-0,5	+0,5
SYNPP 1	-17	-13	-15	-15	-2	+2
SYNPP 2	6	6	6	6	0	0
SYNPP 3	-11	- 7	- 9	- 9	-2	+2
SYNPP 4	-26	-24	-25	-25	-1	+1
SYNPP 5	6	11	8,5	8,5	-2,5	+2,5

Tab.8.6-2 Errors in orientation angles φ for the general convergent case (All units are minutes of arc)

Because of the presence of equal and unlike errors in φ, that is convergency errors, in cases of general convergent photography, it can be expected that the convergency correction control method is more successful here than in the normal photography cases. The results listed in Table 8-1 show that the convergency method does indeed reduce model deformations in all convergent photography cases without, however, removing totally the equal and unlike errors in φ. This can be explained by the fact that the error in the control distance is caused by a combination of errors in orientation angles, image co-ordinates and errors in elements of interior orientation, whereas the convergency correction model assumes that the error is caused exclusively by errors in the orientation angles and image co-ordinates. One-camera photography (case 28) in general convergent camera orientation does not maintain projection ray coplanarity as it does in the

"normal" case; subsequently standard deviations of plate co-ordinates σ_0 will always be too large when convergent photography is used.

In addition to the above observations, little can be learned from the convergent case study which has not already been discussed for the normal photography tests.

A detailed point to point discussion does not therefore seem justified here.

EFFECT OF ERRORS IN ORIENTATION ANGLES ON MODEL CO-ORDINATES

In all previously discussed test cases, deformations are caused by the combined effects of errors in interior orientation elements and a change in the orientation angles resulting from such errors. It is, however, possible that observation errors in plate co-ordinates cause errors in orientation angles in the absence of any significant errors in the interior orientation elements (case 0). The controlled introduction of errors in $\varkappa'$, φ', $\varkappa''$, φ'' and ω'' in cases 13 to 19 for normal photography and cases 30 to 36 for general convergent photography shows the effect of such changes in orientation angles. (The inspection of the deformation diagrams serves best to analyse error effects in these situations.)

Normal Photography

Case 13 (SYNKAPPA1N)

An error of 0,1° is introduced into the rotation $\varkappa'$ about the optical axis of the left camera. Deformations resulting from this error reach their maximum in the Z co-ordinate direction. If we inspect the deformations in terms of the three axis parallel planes of the co-ordinate system (Fig.8.6-11) it emerges that the model space is tilted

about two axes. Deformations in the third plane (X/Y) are less regular and a continuously varying scale factor in this plane becomes obvious. This results in a lower accuracy in distances in this plane as compared to the two other major directions despite the fact that the lowest accuracies occur in the Z-direction.

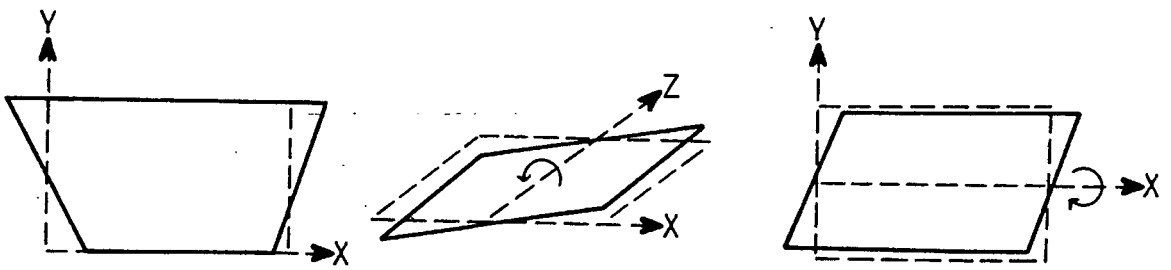

Fig.8.6-11 Model deformation caused by an error in $\varkappa'$

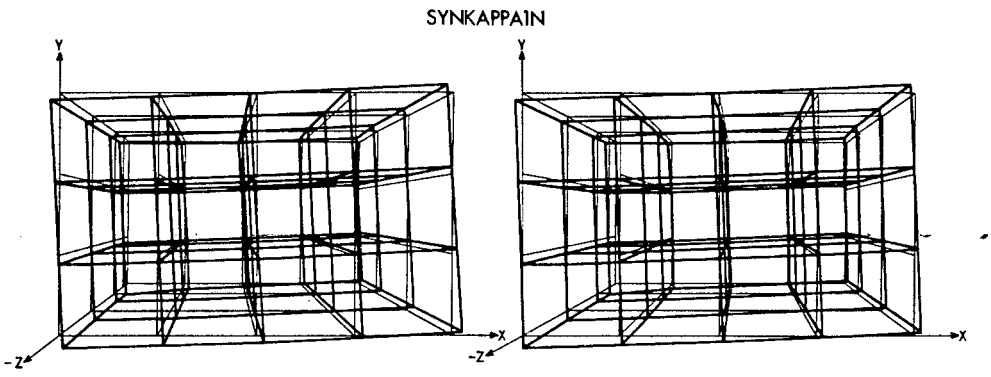

Fig.8.6-12 Stereogram showing model deformations caused by an error in the $\varkappa$ rotation of the left camera ($\varkappa' = +0{,}1^{g}$)

Case 14 (SYNKAPPA2N)

Rotation angles $\varkappa$ of both cameras are changed by the same amount

(0,1°) in the same direction (equal and like error in $\varkappa$).

Here the model is tilted about three orthogonal axes parallel to the co-ordinate system (shearing effect). Comparison with the previous case shows therefore a considerable reduction in distance errors in axis parallel directions in spite of larger errors in X and Y co-ordinates.

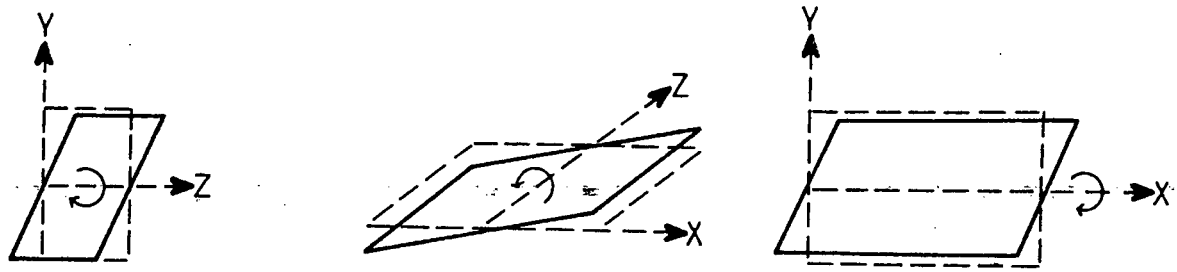

Fig.8.6-13 Model deformations caused by equal and like errors in $\varkappa$

Case 15 (SYNPHI1N)

The left φ value is changed by 0,1°. An error in φ' results in shifts in all co-ordinates; these deformations are larger than those caused by an error of the same quantity in $\varkappa'$. Z co-ordinates once again suffer the largest deformations. The general effect of an error in φ' is that of affine scaling of the model. Subsequently the errors in distances can be reduced if affine scales are applied.

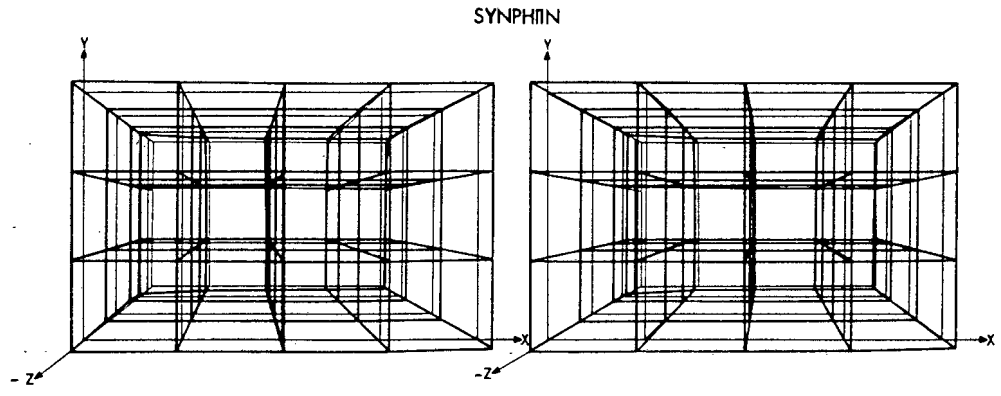

Fig.8.6-14 Stereogram showing model deformation caused by an error in the φ rotation of the left camera

Case 16 (SYNPHI2N)

Here the rotations of the left camera are assumed to be error-free while a φ" error is present in the right camera. The φ" error is introduced in the same direction and with the same quantity as the φ' error in the previous case. In case 15 the two projection ray bundles, which form the model, are brought closer together by the assumed error whereas the bundles in case 16 are separated. The deformations in both simulations are therefore similar, resulting in a reduction of the model size in one case and in an enlargement in the other case. Affine scaling once again reduces the effect of this error.

Case 17 (SYNPHI3N)

In case 17 an equal and like error in φ is introduced. The model suffers a rotation about two axes parallel to the co-ordinate system and a scale factor varying from left to right deforms the model in

the X/Y plane.

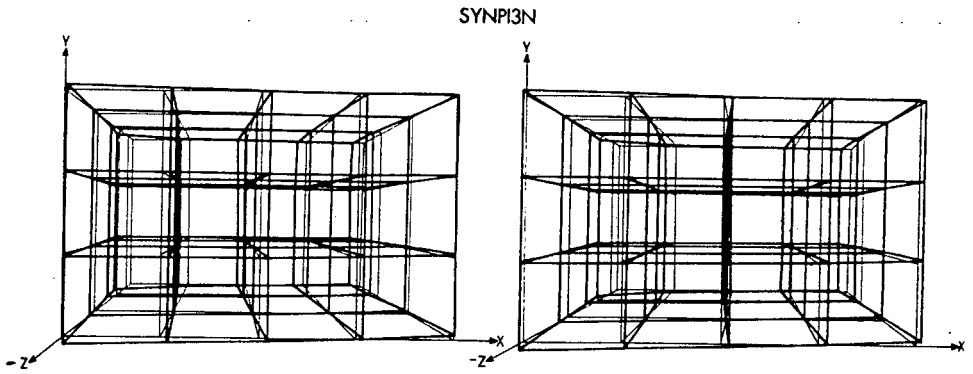

Fig.8.6-14' Model deformations caused by equal and like errors in φ

As in the previous cases there are secondary distoritions present in addition to the above shown major deformations and close inspection of IP Table 2 for this case shows that affine scaling only improves the distance accuracy in the X-direction appreciably.

Case 18 (SYNPHI4N)

An equal and unlike error in φ is simulated.

Model deformations are considerable as both bundles of rays are either tilted inwards or they are separated, thus reducing or enlarging the model space. Differential scale changes in all directions complicate the deformation. The major deformation can nevertheless be identified as affine scaling with the largest scale factor in the Z-direction.

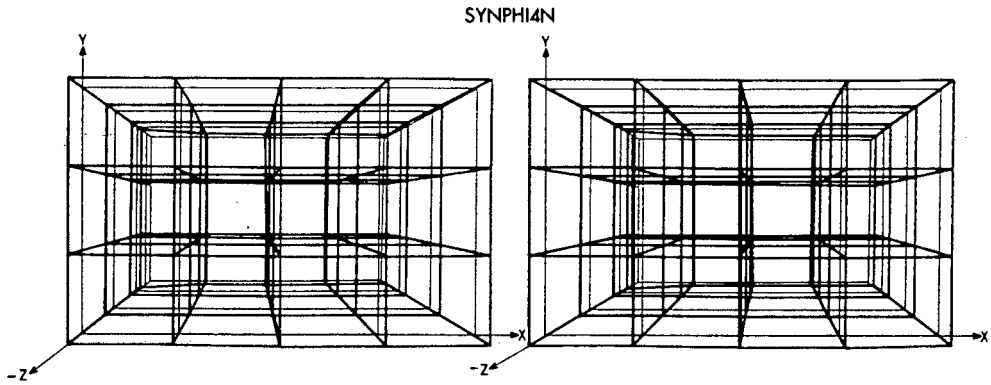

Fig.8.6-15 Stereogram showing model deformation caused by equal and unlike errors in φ (convergency error)

Case 19 (SYNOMEGAN)

An error in rotation angle ω of the right camera does not affect the X co-ordinates at all, while X/Z and X/Y planes are tilted.

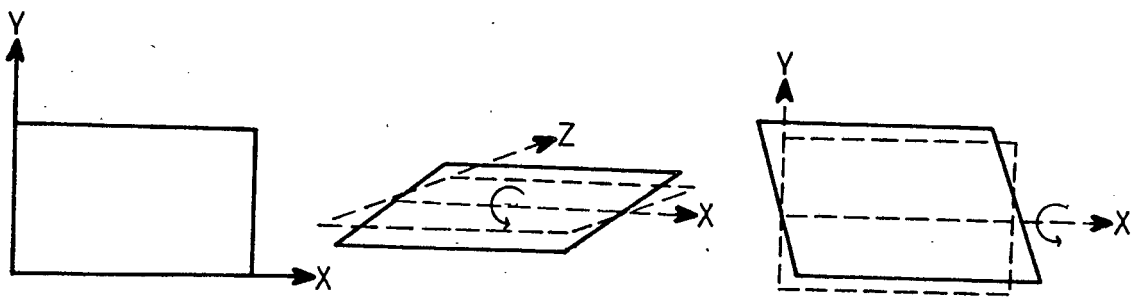

Fig.8.6-16 Model deformations caused by an error in ω"

Distance errors are small in all directions with the largest error occurring in the Z-direction. Position errors are of similar quantity in Y and Z co-ordinates.

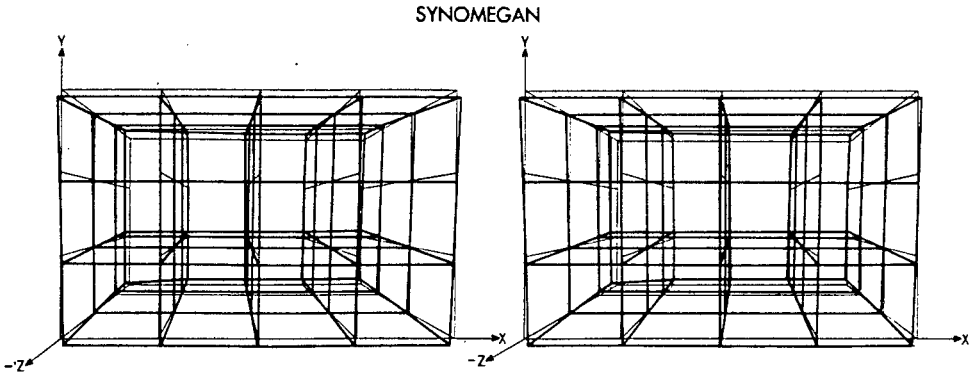

Fig.8.6-17 Stereogram showing model deformations caused by an error in ω"

GENERAL CONVERGENT PHOTOGRAPHY (cases 30-36)

The corresponding test cases for general convergent photography showed no significant differences from the normal photography and no additional conclusions can be drawn.

Results for general convergent photography are recorded in the same manner as the normal photography tests in IP Tables and deformation diagrams.

8.7 AFFINE SCALES IN MODEL DEFORMATION

Tab.8.7-1 shows the average scales of the deformations suffered in the X-, Y- and Z-direction for some cases of normal and convergent photography.

Case	Average			Absolute difference in scales in mm/m		
	X scale	Y scale	Z scale	X-Y	X-Z	Y-Z
3	1	1	0,99502	0	5	5
8	1	1	0,99990	0	0	0
10	0,98641	0,98475	0,97029	1,7	16,1	14,6
11	1	1	0,99493	0	5,1	5,1
23	1,00766	1,00895	1,01226	1,3	4,6	3,3
28	1,00050	1,00075	1,00173	0,3	1,2	1

Tab.8.7-1 Affine scales of the model deformation in X-, Y- and Z-directions

It is obvious that X and Y scales are similar whilst Z scales show a marked difference implying that a combined scale for X and Y can be accepted in circumstances where it is difficult to establish control distances.

A horizontal distance in X-direction will generally be easier to measure than a vertical (Y) distance.

Scales in axis direction, although similar, do show differences in different parts of the model space (IP Table 2) and it is advisable to select control close to the object to be surveyed.

8.8 REAL PHOTOGRAPHY TESTS

The test sequence was concluded with a number of relative orientation calculations based on real photography of the test field. The photography was executed with a metric UMK 10/1318 camera and with a non-metric NIKONOS underwater camera (Tab.8-3).

The cameras were in general convergent orientation with

$$\varkappa' = 1^{o},\ \varphi' = -20^{o},\ \varkappa'' = 0^{o},\ \varphi'' = 14^{o} \text{ and } \omega'' = 0^{o}$$

The co-ordinates obtained from the relative orientations were transformed into a best fit with the co-ordinates determined by space intersection. (The geodetic point fixes have an accuracy of 0,2 to 0,6 mm.) The differences between the two systems are, in an approximation, interpreted as deformations, although they are in fact a combination of deformations and errors in the geodetic position fixes.

An inspection of the deformation pattern confirmed the tendency - noted in the simulations as characteristic for close-range photogrammetry - that Z model co-ordinates are generally the least accurate of the co-ordinates (cases 40, 41, 42, 43, 45 and 46).

Comparison of cases 40 and 41, where 10 and 30 points respectively were used for the relative orientation adjustment, confirmed that no significant accuracy improvement can be achieved by using more than say 10 to 15 points for the adjustment (Chapter 7.6).

In case 42 all points used for the relative orientation are positioned in one horizontal plane parallel to the base line. This coplanarity of all points has no ill-effect on the results.

A consistent pattern emerged for the effect of the introduction of control distances in the relative orientation.

Homogeneous scaling based on one distance in the X-direction (cases 40A, 41A and 42A) reduced the model deformation in all tested cases.

Convergency corrections based on a distance in the Z-direction similarly improved the model accuracy in all cases (compare 40-40C,

41-41C, 42 second case -42C, 43A-43B, 44A-44B, 45A-45B and 46A-46B).

When the distance for the convergency correction was located at the side of the model space (case 40BB) as opposed to the centre of the field (case 40B) the accuracy deteriorated. This does not agree with Adams' (1978) observation that the control distance position in the field is irrelevant. A single test case can obviously not serve to refute Adams' submission; however, case 40BB can serve to confirm that some reduction of the model control is achieved by convergency correction wherever in the object space the control distance is located. As a general rule one should try to place a control distance as close to the object as possible. In all cases when affine scaling was applied to control the model, a common scale factor for X/Y was derived from a distance in the X-direction, in addition to the scale factor derived from a Z distance. Affine scaling reduced deformations in all cases with especially good results for the non-metric cameras (cases 40E, 53E, 44E and 46E).

The elements of interior orientation for the non-metric NIKONOS camera used in cases 43 to 46 had been determined previously by means of projective transformation (Welham 1982). These values were accepted for this study. (Test cases which rely on the projective transformation method of camera calibration are identified in Table 8-3 by the remarks "P.D. calibrated" and "P.P. calibrated".) As an alternative to this technique of calibration, the elements were also determined by a simple approximation. Here the principal point position was derived from the edges of the image as described in Chapter 3.6 (equation 3.6.13); the principal distance was evaluated by relating a vertical distance in the test field d to the corresponding distance on the image $\bar{d}$:

$$\frac{\bar{d}}{d} = \frac{\bar{f}}{D}$$

Where D is the distance between the camera and distance d in the field. (Where this approximation technique is used the remarks "P.D. Approx." and "P.P. derived from frame" appear in Table 8-3.)

When comparing the accuracies of model co-ordinates obtained from the relative orientation based on metric and non-metric photography, the non-metric photography proved considerably less accurate. Accuracies obtained with metric cameras were between two to four times better than those of non-metric cameras. Whilst this had to be expected, it was surprising to find that the approximated values for interior orientation elements led to better results than the values determined by projective transformation. (It is not within the scope of this study to investigate the projective transformation technique, but the comparatively poor accuracy of case 46A, which relies on a projective transformation calibration, cannot pass unnoticed. It would appear that the interior orientation elements as obtained from projective transformation are "calculation values" rather than the physical elements of interior orientation as required for the relative orientation.)

In all cases of non-metric photography the model was first scaled by applying an homogeneous scale factor derived from an X distance. This proved necessary as the cameras were not calibrated in the same way as the UMK10/1318 cameras, where the external pupil position was known owing to the calibration technique (Chapter 7.1). Without knowledge of the external pupil position no reliable measurement of the base length can be made and a model scale can only be obtained by scaling from a field distance.

When a second control distance in the Z-direction was introduced for convergency correction (cases 43B, 44B, 45B and 46B) and affine scaling (43E, 44E and 46E) a significant improvement of the model accuracy could be recorded with an improvement factor of two to four. Affine scaling in all cases resulted in slightly higher accuracies than the convergency correction.

Finally, the relative orientation with one or two control distances was compared with the projective transformation[1] based on 10 control points. Case 47-1 and case 47-2 give the average displacement vectors and root mean square errors for the projective transformation evaluated with the same data as used for the relative orientation in cases 40 and 43. In both cases the discrepancies between geodetic and photogrammetric point fixes show that the projective transformation fits the geodetic co-ordinates better (by a factor of two) than the relative orientation with limited control.

If we treat the average discrepancies between geodetic and photogrammetric point position fixes as a measure of accuracy, we can establish average accuracies for the X, Y and Z co-ordinates over the range of the test field. We can also express these accuracies in terms of Schwidefsky's (1970) measure of accuracy by relating the errors to a mean point distance from the base (this is about 5 m for the test field).

Accuracies are then:

---

(1) Computer programs for the projective transformation were provided by Professor L.P. Adams and L. Welham.

Relative orientations	METRIC CAMERA				NON-METRIC CAMERA			
	X/Y		Z		X/Y		Z	
	mm	1:	mm	1:	mm	1:	mm	1:
Without control distance	2,2	2200	2,5	2000	-	-	-	-
With homogeneous scaling from X	0,3	17000	0,6	8500	3	1700	5	1000
With homogeneous scaling from X and subsequent convergency correction	0,2	25000	0,6	8500	2,5	2000	2	2500
With convergency correction	0,8	6200	0,6	8500	-	-	-	-
With affine scaling	0,2	25000	0,6	8500	1,2	4200	1,8	2800

These accuracy measures - especially those for the non-metric cameras - are better than those predicted on the basis of the simulations. This must be attributed to the quality of the targets and to the fact that the elements of interior orientation were probably determined with a higher accuracy than estimated in the simulations. Further tests with real photography in two other test fields resulted in slightly less accurate results. Some improvement is achieved with all of the above listed control methods. Affine scaling and homogeneous scaling with subsequent convergency correction result in higher accuracies than the other two methods. Convergency correction shows the least improvement.

Combining accuracies of all tests with the predictions derived from the simulations, the writer estimates that the following average accuracies can be achieved for distances of up to about 40 metres.

Relative orientations	METRIC CAMERA		HIGH QUALITY NON-METRIC CAMERA	
	X/Y	Z	X/Y	Z
	1:	1:	1:	1:
Without control distances	2500	2000		
With homogeneous scaling from X	3000	3000	1000	500
With homogeneous sclaing from X and subsequent convergency correction	3000	4000	1000	1000
With convergency correction	3000	3000	1400	1500
With affine scaling	4000	4000	2000	2000

Accuracy estimates for model co-ordinates (the estimates are valid for convergent one-camera photography; small improvements of accuracies can be expected if normal one-camera photography is used whilst accuracy losses must be expected if two cameras are employed).

8.9 SUMMARY OF CONCLUSIONS DERIVED FROM THE ANALYSIS OF MODEL DEFORMATIONS

The following conclusions and recommendations for the application of close-range photogrammetry can be derived from the analysis of model deformations.

i) Errors in Z model co-ordinates

In close-range photogrammetry model co-ordinate errors in the Z axis direction are generally larger than those in the X- and Y- directions.

Adams (1978) and Granshaw (1979), among others, have come to the same conclusion for analogue and analytical close-range orientation respectively.

ii) Affine scale errors and shearing effect

Model deformations in close-range photogrammetry, although irregular and complex in detail, have an overall tendency to occur in the form of affine model scales and "shearing" effects.

The affine scale deformation maintains the orientation of planes parallel to the co-ordinate axes, whilst distances between these planes are reduced or enlarged. The scales generally differ in the three axes directions with small, often negligible, differences between the X and Y scales and larger differences between X/Y and Z scales. Affine deformations are caused mainly by errors in the elements of interior orientation.

In the "shearing" or "tilt" deformation planes parallel to the co-ordinate system tilt without losing their parallelity. Subsequently

distances parallel to the co-ordinate system are undisturbed by this form of deformation while distances in other than axis parallel orientations suffer deformations.

iii) Distances parallel to co-ordinate axes

Because of the shearing effect, distances parallel to the co-ordinate system are generally more accurate than those in any other orientation.

Cameras should be positioned in such a way that important object distances are parallel to the model co-ordinate system.

iv) Convergency error

The original hypothesis, which resulted in the introduction of an analytical convergency correction as a model control method in the relative orientation, postulated that in close-range photogrammetry the major contribution to the large Z errors originates in a significant equal and unlike error in φ (Adams 1978; Granshaw 1979). This hypothesis cannot be upheld for the following reasons:

1. Large errors in the Z co-ordinates do not result mainly from a convergency error but are to the same or to an even larger extent caused by errors in principal distance and principal point position. (This would appear to be contrary to Granshaw's (1979) conclusions.)
2. Convergency errors caused by incorrect elements of interior orientation occur only in cases of two-camera photography and in cases of convergent photography. These convergency errors are generally small and play a minor role in the overall

deformations caused by errors in interior orientation. If the photography is obtained in normal orientated one-camera photography then incorrect interior orientation elements leave the orientation angles undisturbed and subsequently no convergency error caused by errors in elements of interior orientation occurs in this case.

3. Convergency errors are also caused by errors in image co-ordinates as all orientation angles, including φ' and φ'', are affected by incorrect values of the image co-ordinates but again the equal and unlike part of the φ error is not dominant among the contributions towards model deformations. Image point errors affect orientation angles randomly and no systematic pattern emerges.

One can therefore state that a convergency error, although always present (there will always be small differences between the errors in φ' and φ''), is not the major cause for model deformations in analytical close-range relative orientation.

In spite of the above the convergency correction introduced in this study is an effective means of reducing model deformation in the Z-direction. This must be attributed to the character of the Z deformation which is that of an affine scale error.

A convergency correction has an effect similar to that of scaling the model in Z[(1)] and can therefore be expected to reduce affine

---

(1) The convergency error, although its effect is similar to that of a scale error in the Z-direction, is not identical to such a scale error as can easily be confirmed from the expression for the effect of the convergency error on the Z co-ordinate in normal orientated one-camera photography. By combining equations 1.18.2 and 1.18.4 in Appendix I and by then replacing image co-ordinates by model co-ordinates we obtain:

$$dz = \frac{1}{b} (2 Z^2 + 2 X^2 - 2 X b + b^2) d \varphi$$

provide an efficient model control method when only a few measured distances are available to reduce model deformations. This is confirmed by the test sequence in which improved model accuracies were obtained when either of these two methods were applied. No general prediction can be made as to the quantity of the factor by which the accuracy can be improved, as model deformations are a function of errors in image co-ordinates, elements of interior orientation and base length and the quantities of these errors obviously cannot be predicted. (In the cases of real photography investigation average model accuracy was improved by factors varying from 2 to 5.) The choice of the best method for a specific situation is easy if normal orientated one-camera photography is used. Here convergency errors are only caused by errors in image co-ordinates and make only a marginal contribution towards model deformations, even if large errors in principal distance, principal point and base are present. Affine scaling is the method to be employed here.

In all other cases, that is in all convergent and two-camera cases, the choice is more difficult. Here, convergency errors can occur and homogeneous scaling with subsequent convergency correction might be called for. However, such good results were obtained by means of affine scaling in all test cases and in numerous additional tests not reported in the study, that one can state that affine scaling will generally improve accuracies as efficiently as convergency corrections. Convergency correction is considerably more elaborate in its mathematical formulation and should only be employed when large errors in the interior orientation elements are suspected in two-camera and convergent cases.

vii) Relative and absolute point accuracies

The model control methods described above only improve the model shape and not the relative position of the object with respect to the camera stations. Large block shifts (Table 8-5) must therefore be expected. Model points accuracies quoted in Chapter 8.8 refer only to relative and not to absolute point positions.

viii) Deformation tables and diagrams

The deformation tables and diagrams given in the separate Appendix can serve to determine the accuracies to which cameras must be calibrated to achieve specified model co-ordinate accuracies. They also locate areas of minimum model deformation within the model space.

ix) Absolute orientation with affine scaling

If a control point network can be established and an absolute orientation can be executed, then this absolute orientation model should include affine scales rather than an homogeneous scale owing to the affine character of the deformation.
Conventional absolute orientation (translation, rotation, scale) mainly improves the overall position of the object in space; it allows for complex model deformation only in the form of average uniform or affine scales. In situations where only object dimensions and shape are required the absolute orientation is only superior to the two recommended control methods when more distances are involved in the evaluation of the average scale factors for the absolute orientation than for the simple control methods.

The convergency correction method should be superior to absolute orientation if large convergency errors are present.

x) Incorrect variance σ_0^2

Errors in the elements of interior orientation prevent corresponding projection rays of image points from intersecting in space in all cases other than normal orientated one-camera photography and convergent one-camera photography where $\varkappa' = \varkappa'' = \omega'' = 0$ and $\varphi' = -\varphi''$. In all cases of general convergent photography and in all cases of two-camera photography projection rays cannot intersect in space - even if the image co-ordinates were error-free - because of the presence of errors in the elements of interior orientation. (It must be assumed that these errors are always present.)
In a least squares adjustment, such discrepancies will be interpreted as additional errors in image co-ordinates and false corrections (v) must therefore be expected in the abovementioned cases, in which coplanarity cannot be achieved. Subsequently the numerical value for the estimator of the variance factor σ_0^2 will be incorrect, resulting in a scale error in the error analysis. Error estimates will generally be too large. The fact that σ_0^2 is likely to be incorrect must be borne in mind when applying a χ^2 test to the σ_0 a posteriori value.

xi) One- versus two-camera photography

Deformations caused by errors in elements of interior orientation are smaller in all cases of one-camera photography as opposed to two-camera photography. Deformations are also more regular and

symmetrical if only one camera is used and simple model control methods are subsequently more effective. One-camera photography should therefore be used wherever possible. (See also x).

xii) Repeated photography with interchanged cameras

A situation approximating one-camera photography can be created in some cases where two cameras are required for the simultaneous photography of moving objects. If the photography is repeated with interchanged cameras then the deformation pattern is reversed and distances which are too long in the relative orientation based on the first stereo pair are, by a similar amount, too short in the second relative orientation, and vice versa. Average distances derived from two stereo pairs with interchanged cameras are of an accuracy similar to that achieved in one-camera photography. This method can only be employed if the object remains in approximately the same position for both pairs of photographs and if the camera orientations are not changed significantly.

xiii) Normal versus convergent photography

Normal orientated photography is preferable to convergent photography from the same base. Model co-ordinate errors resulting from errors in the elements of interior orientation are larger in the convergent case. If the photography is taken in general convergent orientation then model deformations are irregular and simple model control is inefficient.

Cameras should therefore be placed in normal orientation unless the application of general convergent photography makes a considerable

enlargement of the base length possible. (The base length must be at least doubled to obtain accuracies similar to those of normal orientated photography.)

xiv) Normal orientated one-camera photography

From xii) and xiii) it follows that normal orientated one-camera photography should be employed whenever possible.

xv) Economical point numbers for relative orientation adjustment

The relative orientation parameters do not change significantly if more than 10 to 15 points are used to establish relative orientation.

9. OVERALL SUMMARY AND CONCLUSIONS[1]

At the outset of this study it was assumed that a significant reduction in object point accuracies must be expected in circumstances when no three-dimensional control network had been established and where, subsequently, no absolute orientation could be executed. In the course of the investigation it was established that the availability of only a limited number of control points does not necessarily represent a critical limitation in the photogrammetric determination of object dimensions.

In most cases of close-range photogrammetry object dimensions and object shape rather than the absolute position of the object in a co-ordinate system are required. In these cases accuracies better than 1/1000th (standard deviation at point position/distance from the camera) can be obtained with simple model control methods for photography with metric and high quality non-metric cameras. Schwiedefsky (1970) classifies photogrammetric results of this accuracy as precision photogrammetry.

A large part of the model deformations which are caused by errors in the elements of interior orientation, in image co-ordinates and in the base length can be removed by affine scaling of the model in all cases of close-range photogrammetry. In situations where two cameras are positioned in a general convergent orientation, convergency correction subsequent to homogeneous scaling of the model can be employed as an alternative to affine scaling.

In both methods a number of distances between well defined natural

---

(1) This summary must be read in conjunction with the summary of the deformation analysis in Chapter 8.9.

feature points or between especially marked control points, located close to the object to be surveyed, must be measured either before or after the execution of photography. The distances should be near parallel to the model co-ordinate axes. At least one distance in the X-direction and one distance in the Z-direction must be measured.

When the photographic images are observed in a comparator to obtain plate co-ordinates for the relative orientation adjustment, those image points which represent the end points of the measured control distances must be incorporated into the observations.

If affine scaling is used as a control method, a conventional relative orientation is carried out and model distances are evaluated for the control distances. Comparison of the control distances with the model distances yields two scale factors for X/Y and Z or three scale factors for X, Y and Z co-ordinates. If more than one distance is measured in a direction, an average scale factor is determined from the simple mean.

If a convergency correction is applied, a relative orientation adjustment is carried out and an homogeneous scale factor is derived by comparing measured control distances with their corresponding model distances. This scale factor is applied to the base length and the relative orientation adjustment is repeated with an additional constraint equation for one or more distances in the Z-direction (Chapter 7.10 and Appendix II). This constraint forces the relative orientation angles to assume quantities resulting in model co-ordinates which correspond to the measured length of the control distances. In this approach the sum of the squares of the corrections to observed plate co-ordinates is minimised as in the conventional relative orientation adjustment.

The convergency error does not represent a major source of model errors in all cases of close-range photogrammetry as was originally assumed. It is therefore recommended to apply a convergency correction only in situations where significant convergency errors are suspected; such a case occurs for example if non-metric cameras with unstable interior orientation elements are used in general convergent two-camera photography.

If the convergency correction adjustment is carried out in computers with limited memory space a memory saving technique is required. Such a technique is derived in Appendix III.

A further objective of this study was an investigation of model deformations in close-range photogrammetry. The results of this analysis of model deformations is summarised in Chapter 8 and, as a consequence of the analysis, recommendations for the practical application of close-range photogrammetry are made (8.9).

A set of deformation tables and diagrams is provided in a separate Appendix to this thesis. There the effects of errors in interior orientation on the model co-ordinates as derived from a relative orientation adjustment are shown for cases of normal one- and two-camera photography and for cases of general convergent one- and two-camera photography. These tables and diagrams have mainly theoretical relevance.

In the course of the study a precise method for the geodetic determination of three-dimensional point positions in a photogrammetric test field was employed (Chapters 3.5 and 5) and sub-millimetre accuracies were achieved.

In Chapter 7.1 a method combining perspective projection with

theodolite observations of exterior and interior pupil of the lens system was employed to calibrate the cameras used for the test photography. The method resulted in values for interior orientation elements which differ by less than 50 μm from the calibration values supplied by the manufacturer. The technique of observing the external pupil of a lens system (Hallert 1969) was combined with the three-dimensional space intersection and extended to other lens parameters (Chapter 7.1).

It was shown that the position in space of camera parameters such as exterior and interior pupil for different focal settings, lens surfaces, fiducial marks and the vertical instrument axis, can be determined with accuracies of a few tenths of a millimetre.

DESCRIPTION OF TABLES 8-1 to 8-4

Information about the nature of each tested case is contained in the file name, indicated by letters used to form the name.

SYN	simulated photography based on synthetic photography
UMK	real photography with metric UMK cameras
NIKONOS	real photography with non-metric NIKONOS cameras
N	photography with cameras in normal orientation as opposed to convergent photography
PD	controlled introduction of an error in the principal distance
PP	controlled introduction of an error in one or both principal point co-ordinates
S	the model is controlled by homogeneous scaling from X
D	the model is controlled by homogeneous scaling from Z
AF or F	the model is controlled by affine scaling
P	the model is controlled by convergency correction
KAPPA PHI OMEGA	orientation angles $\varkappa'$, φ', $\varkappa''$, φ'' and ω'' are changed by differential amounts to simulate errors

Table 8-1: SUMMARISED RESULTS OF SIMULATED CASES

Table 8-1 summarises the results of the computer simulations of normal and convergent photography, listing average absolute deformation vectors and average standard deviations for each case in addition to the case characteristics and the effect of the simulated errors in interior orientation parameters on the orientation angles.

Columns of Table 8-1 contain:

Col. 1 case number

2 file name

3-8 errors introduced into the elements of interior orientation in units of mm

9 presence of symbol "x" indicates that affine or homogeneous scaling has been applied

10 symbol "x" indicates convergency error correction has been attempted

11-15 changes in the orientation angles resulting from the introduced errors. The values represent differences between the orientation angles on which the original synthetic photograph was based and the results of the relative orientation executed with modified parameters. Units : minutes of arc

16 σ_o = standard deviation of unit weight. As all image coordinates are assumed to have equal weight (P = 1), σ_o is also the standard deviation of an "observed" image coordinate a priori. Units : micrometres

17 arrows indicate which cases should be compared when investigating possible improvements through the introduction of convergency corrections

18-20 average displacement vectors dx, dy and dz

21 average total displacement vector dv

22-24 root mean square errors σ_x σ_y σ_z

25 average total root mean square error σ_v

1	2	3	4	5	6	7	8	9	10	11	12	13	14	15	16	17	18	19	20	21	22	23	24	25
CASE	FILENAME	dF'	dF''	dX_o'	dY_o'	dX_o''	dY_o''			k'	φ'	k''	φ''	ω''	σ_o		dX	dY	dZ	dV	σ_x	σ_y	σ_z	σ_v
0	SYNRANDOMN									1	1	1	0	1	14		0.6	0.5	1.2	1.4	0.7	0.7	1.5	1.8
1	SYNPD1N	0.5								-1	-20	-1	-20	-1	220		4.7	0.3	4.9	6.8	5.2	0.4	5.9	7.9
2	SYNPD2N	1								-1	-40	-2	-40	-1	440		9.4	0.6	9.7	13.5	10.5	0.8	11.8	15.8
2A	SYNPD2NS	1						X		-1	-40	-2	-40	-1	440		9.4	0.9	9.4	13.3	10.5	1.2	11.4	15.5
2B	SYNPD2NB	1						X	X	-2	-42	-1	-38	-1	430		9.3	2.7	8.7	13.0	10.8	3.1	10.6	15.4
2C	SYNPD2NP	1							X	-2	-42	-1	-37	-1	430		9.2	1.8	8.8	12.9	10.4	2.2	10.6	15.0
3	SYNPD3N	0.5	0.5							0	0	0	0	0	0		0.0	0.0	4.2	4.2	0.0	0.0	4.7	4.7
3A	SYNPD3NS	0.5	0.5					X		0	0	0	0	0	0		0.1	0.0	4.2	4.2	0.1	0.1	4.7	4.7
3B	SYNPD3NB	0.5	0.5					X	X	0	-2	0	-3	0	130		2.0	1.6	0.9	2.7	2.4	1.9	1.0	3.2
3C	SYNPD3NP	0.5	0.5						X	0	-2	0	3	0	130		2.0	1.6	0.9	2.7	2.4	1.8	1.0	3.2
3D	SYNPD3ND	0.5	0.5					X		0	0	0	0	0	0		4.9	3.7	0.0	6.1	5.7	4.1	0.0	7.0
3E	SYNPD3NAF	0.5	0.5					X		0	0	0	0	0	0		0.0	0.0	0.0	0.0	0.0	0.0	0.0	0.0
4	SYNPD4N	0.5	-0.5							-2	-40	-2	-40	-1	440		9.4	0.6	8.6	12.8	10.4	0.8	10.6	14.9
5	SYNPP1N			1						0	0	0	0	0	0		15.5	11.3	25.7	32.1	18.1	12.9	28.4	36.1
6	SYNPP2N				1					-4	6	-4	6	-36	260		2.0	8.6	4.6	10.0	2.5	9.8	5.7	11.6
6A	SYNPP2NS				1			X		-4	6	-4	6	-36	260		2.1	8.6	4.6	10.0	2.6	9.8	5.8	11.7
6B	SYNPP2NB				1			X	X	-4	6	-4	6	-35	240		2.0	8.6	4.6	10.0	2.5	9.7	5.7	11.5
6C	SYNPP2NP				1				X	-4	6	-4	6	-35	240		2.0	8.6	4.6	10.0	2.5	9.8	5.7	11.6
7	SYNPP3N			1	1					-4	6	-4	6	-36	260		16.0	13.1	25.8	33.1	16.8	15.9	29.2	38.2
8	SYNPP4N			1	1	1	1			0	0	0	0	0	0		8.5	8.5	0.0	12.0	9.4	9.4	0.0	13.3
8A	SYNPP4NS			1	1	1	1	X		0	0	0	0	0	0		8.5	8.5	0.7	12.0	9.4	9.4	0.8	13.3
8B	SYNPP4NB			1	1	1	1	X	X	0	0	0	0	0	20		8.5	8.5	0.1	12.0	9.5	9.4	0.2	13.4
8C	SYNPP4NP			1	1	1	1		X	0	0	0	0	0	1		8.5	8.5	0.0	12.0	9.4	9.4	0.0	13.3
8E	SYNPP4NAF			1	1	1	1	X		0	0	0	0	0	0		8.5	8.5	0.0	12.0	9.4	9.4	0.0	13.3
9	SYNPP5N			1	1	-1	-1			-8	13	-8	13	-71	520		31.3	23.4	52.9	65.8	36.6	27.8	59.7	75.3
10	SYNPDPPN	0.5	-0.5	0.5	-0.5	-0.5	0.5			2	-47	3	-47	34	520		18.7	11.8	27.4	35.2	22.7	14.2	32.3	42.0
10A	SYNPDPPNS	0.5	-0.5	0.5	-0.5	-0.5	0.5	X		2	-47	3	-47	34	520		12.3	5.8	15.0	20.2	14.6	7.1	18.1	24.3
10B	SYNPDPPNB	0.5	-0.5	0.5	-0.5	-0.5	0.5	X	X	2	-52	3	-41	34	560		13.3	7.8	12.1	19.6	16.2	9.4	14.8	23.9
10C	SYNPDPPNP	0.5	-0.5	0.5	-0.5	-0.5	0.5		X	1	-59	4	-30	34	940		10.7	4.5	13.0	17.4	12.5	5.4	16.0	21.0
10E	SYNPDPPNAF	0.5	-0.5	0.5	-0.5	-0.5	0.5	X		2	-47	3	-47	34	520		12.5	5.2	11.9	18.0	15.3	6.4	14.5	22.0
10R	SYNPDPPNR	-0.5	0.5	-0.5	0.5	0.5	-0.5			-3	46	-2	46	-35	510		17.9	11.7	26.6	34.1	21.9	13.9	31.4	40.7
11	SYNPDPPN0	0.5	0.5	1	1	1	1			0	0	0	0	0	0		8.5	8.5	4.2	12.7	9.4	9.4	4.7	14.1
11A	SYNPDPPNS0	0.5	0.5	1	1	1	1	X		0	0	0	0	0	0		8.5	8.5	4.9	13.0	9.4	9.4	5.5	14.4
11B	SYNPDPPNB0	0.5	0.5	1	1	1	1	X	X	0	-2	0	3	0	150		8.7	8.6	1.0	12.3	9.8	9.6	1.2	13.8
11C	SYNPDPPNP0	0.5	0.5	1	1	1	1		X	0	-2	0	3	0	130		8.6	8.6	0.8	12.2	9.9	9.7	1.0	13.9
11D	SYNPDPPN00	0.5	0.5	1	1	1	1	X		0	0	0	0	0	0		9.2	8.7	0.0	12.7	11.1	10.3	0.0	15.1
11E	SYNPDPPNR0	0.5	0.5	1	1	1	1	X		0	0	0	0	0	0		8.5	8.5	0.0	12.0	9.4	9.4	0.0	13.3
12	SYNPDPPN1	0.2	0.2	0.5	0.5	0.5	0.5			0	0	0	0	0	0		4.2	4.2	1.7	6.2	4.7	4.7	1.9	6.9
12A	SYNPDPPNS1	0.2	0.2	0.5	0.5	0.5	0.5	X		0	0	0	0	0	0		4.2	4.2	2.0	6.3	4.7	4.7	2.2	7.0
12B	SYNPDPPNB1	0.2	0.2	0.5	0.5	0.5	0.5	X	X	0	-1	0	1	0	60		4.3	4.3	0.7	6.1	4.8	4.8	0.8	6.8
12C	SYNPDPPNP1	0.2	0.2	0.5	0.5	0.5	0.5		X	0	-1	0	1	0	50		4.3	4.3	0.4	6.1	4.9	4.8	0.4	6.9

1	2	3	4	5	6	7	8	9	10	11	12	13	14	15	16	17	18	19	20	21	22	23	24	25
CASE	FILENAME	dF'	dF''	dX_o'	dY_o'	dX_o''	dY_o''			k'	φ'	k''	φ''	ω''	σ_o		dX	dY	dZ	dV	σ_x	σ_y	σ_z	σ_v
20	SYNRANDOM									1	2	1	0	0	14		0.8	0.8	1.7	2.0	1.0	0.9	2.0	2.4
21	SYNPD1	0.5								-1	-23	-1	-18	0	190		6.6	3.8	7.3	10.5	7.9	4.3	8.9	12.7
22	SYNPD2	1								-1	-47	-1	-35	0	370		13.1	7.6	14.5	21.0	15.8	8.6	17.8	25.3
23	SYNPD3	0.5	0.5							0	-4	0	5	0	10		8.2	6.5	10.4	14.8	9.7	7.4	11.5	16.8
23A	SYNPD3S	0.5	0.5					X		0	-4	0	5	0	10		2.1	1.4	1.8	3.1	2.9	1.9	2.3	4.1
23B	SYNPD3B	0.5	0.5					X	X	0	-3	0	4	0	50		2.8	1.9	1.0	3.5	3.7	2.4	1.2	4.6
23C	SYNPD3P	0.5	0.5						X	0	1	0	-1	0	290		3.3	2.5	2.0	4.6	3.9	2.8	2.4	5.4
23F	SYNPD3AF	0.5	0.5					X		0	-4	0	5	0	10		2.3	1.3	1.2	2.9	3.1	1.8	1.2	3.8
24	SYNPD4	0.5	-0.5							-1	-42	-1	-41	0	390		10.9	1.1	9.7	14.6	12.1	1.4	11.4	16.7
25	SYNPP1			1						0	-17	-1	-13	-1	140		12.3	10.1	22.9	27.9	14.4	11.5	25.6	31.5
26	SYNPP2				1					8	6	-4	6	-35	230		1.5	8.8	7.7	11.8	1.9	10.0	9.4	13.9
27	SYNPP3			1	1					8	-11	-5	-7	-36	270		12.6	12.6	23.5	29.5	14.6	15.3	27.6	34.8
28	SYNPP4			1	1	1	1			12	-26	-9	-24	-2	230		2.9	9.3	8.2	12.7	3.6	10.5	10.0	14.9
28A	SYNPP4S			1	1	1	1	X		12	-26	-9	-24	-2	230		3.3	9.4	8.2	12.9	4.1	10.7	10.0	15.2
28B	SYNPP4B			1	1	1	1	X	X	12	-26	-9	-25	-2	210		3.3	9.4	8.2	12.9	4.2	10.7	10.0	15.2
28C	SYNPP4P			1	1	1	1		X	12	-25	-9	-26	-2	220		2.8	9.3	8.2	12.7	3.5	10.5	10.0	14.9
28E	SYNPP4AF			1	1	1	1	X		12	-26	-9	-24	-2	230		3.0	9.6	8.2	13.0	3.7	11.1	10.0	15.4
29	SYNPP5			1	1	-1	-1			4	6	0	11	-70	460		25.5	21.6	48.2	58.7	30.0	25.7	54.8	67.6

Table 8-2: EFFECTS OF ERRORS IN PARAMETERS ON ORIENTATION ANGLES

This table merely repeats some of the information given in Table 8-1 with higher numerical accuracy. In Table 8-1, orientation angle errors are quoted in minutes of arc only to simplify presentation and analysis. This can, however, lead to misinterpretations and results of two cases might be judged identical from Table 8-1 when, in fact, they differ slightly. Table 8-2 lists the orientation angle errors caused by errors in the parameters of interior orientation in decimals of degrees for a more critical analysis.

Col. 1 case number

2 file name

3-10 as in columns 3-10 in Table 8-1

11 as in column 17 in Table 8-1

12-16 as in columns 11-15 in Table 8-1 but with more significant figures

1	2	3	4	5	6	7	8	9	10	11	12	13	14	15	16
CASE	FILENAME	DF'	DF"	DX_o'	DY_o'	$DX_o"$	$DY_o"$				k'	φ'	k"	φ"	ω"
0	SYNRANDOMN										0.0127	0.0224	0.0168	0.0060	0.0104
1	SYNPD1N	0.5°									-0.0125	-0.3350	-0.0126	-0.3360	-0.0091
2	SYNPD2N	1									-0.0249	-0.6702	-0.0252	-0.6718	-0.0194
2A	SYNPD2NS	1						X			-0.0249	-0.6702	-0.0252	-0.6718	-0.0194
2B	SYNPD2NB	1						X	X		-0.0288	-0.7007	-0.0243	-0.6298	-0.0206
2C	SYNPD2NP	1							X		-0.0294	-0.7083	-0.0236	-0.6188	-0.0206
3	SYNPD3N	0.5	0.5								0.0000	0.0000	0.0000	0.0000	0.0000
3A	SYNPD3NS	0.5	0.5					X			0.0000	0.0000	0.0000	0.0000	0.0000
3B	SYNPD3NB	0.5	0.5					X	X		-0.0023	-0.0333	-0.0029	-0.0450	0.0000
3C	SYNPD3NP	0.5	0.5						X		-0.0023	-0.0333	-0.0029	0.0450	0.0000
3D	SYNPD3ND	0.5	0.5					X			0.0000	0.0000	0.0000	0.0000	0.0000
3E	SYNPD3NAF	0.5	0.5					X			0.0000	0.0000	0.0000	0.0000	0.0000
4	SYNPD4N	-0.5	-0.5								-0.0250	-0.6702	-0.0253	-0.6718	-0.0196
5	SYNPP1N			1							0.0000	0.0000	0.0000	0.0000	0.0000
6	SYNPP2N				1						-0.0689	0.1022	-0.0683	0.1009	-0.5930
6A	SYNPP2NS				1			X			-0.0689	0.1022	-0.0683	0.1009	-0.5930
6B	SYNPP2NB				1			X	X		-0.0657	0.1023	-0.0657	0.0961	-0.5910
6C	SYNPP2NP				1				X		-0.0661	0.1028	-0.0653	0.1034	-0.5910
7	SYNPP3N			1	1						-0.0690	0.1033	-0.0683	0.1020	-0.5923
8	SYNPP4N			1	1	1	1				0.0000	0.0000	0.0000	0.0000	0.0000
8A	SYNPP4NS			1	1	1	1	X			0.0000	0.0000	0.0000	0.0000	0.0000
8B	SYNPP4NB			1	1	1	1	X	X		-0.0003	-0.0058	0.0004	0.0075	0.0000
8C	SYNPP4NP			1	1	1	1		X		0.0000	-0.0002	0.0000	-0.0003	0.0000
8E	SYNPP4NAF			1	1	1	1	X			0.0000	0.0000	0.0000	0.0000	0.0000
9	SYNPP5N			1	1	-1	-1				-0.1376	0.2215	-0.1338	0.2216	-1.1830
10	SYNPDPPN	0.5	-0.5	0.5	-0.5	-0.5	0.5				0.0386	-0.7892	0.0463	-0.7872	0.5727
10A	SYNPDPPNS	0.5	-0.5	0.5	-0.5	-0.5	0.5	X			0.0386	-0.7892	0.0463	-0.7872	0.5727
10B	SYNPDPPNB	0.5	-0.5	0.5	-0.5	-0.5	0.5	X	X		0.0292	-0.8646	0.0488	-0.6822	0.5701
10C	SYNPDPPNP	0.5	-0.5	0.5	-0.5	-0.5	0.5		X		0.0215	-0.9839	0.0605	-0.5073	0.5711
10E	SYNPDPPNAF	0.5	-0.5	0.5	-0.5	-0.5	0.5	X			0.0386	-0.7892	0.0463	-0.7872	0.5727
10R	SYNPDPPNR	-0.5	0.5	-0.5	0.5	0.5	-0.5				-0.0465	0.7699	-0.0395	0.7716	-0.5770
11	SYNPDPPNO	0.5	0.5	1	1	1	1				0.0000	0.0000	0.0000	0.0000	0.0000
11A	SYNPDPPNSO	0.5	0.5	1	1	1	1	X			0.0000	0.0000	0.0000	0.0000	0.0000
11B	SYNPDPPNBO	0.5	0.5	1	1	1	1	X	X		-0.0024	-0.0399	0.0027	0.0515	-0.0001
11C	SYNPDPPNPO	0.5	0.5	1	1	1	1		X		-0.0021	-0.0345	0.0023	0.0445	-0.0001
11D	SYNPDPPNDO	0.5	0.5	1	1	1	1	X			0.0000	0.0000	0.0000	0.0000	0.0000
11E	SYNPDPPNFO	0.5	0.5	1	1	1	1	X			0.0000	0.0000	0.0000	0.0000	0.0000
12	SYNPDPPN1	0.2	0.2	0.5	0.5	0.5	0.5				0.0000	0.0000	0.0000	0.0000	0.0000
12A	SYNPDPPNSJ	0.2	0.2	0.5	0.5	0.5	0.5	X			0.0000	0.0000	0.0000	0.0000	0.0000
12B	SYNPDPPNB1	0.2	0.2	0.5	0.5	0.5	0.5	X	X		-0.0010	-0.0161	0.0013	0.0213	0.0000
12C	SYNPDPPNPJ	0.2	0.2	0.5	0.5	0.5	0.5		X		-0.0009	-0.0135	0.0010	0.0178	0.0000

1	2	3	4	5	6	7	8	9	10	11	12	13	14	15	16
CASE	FILENAME	DF	DF	DX_o'	DY_o'	$DX_o"$	$DY_o"$				k'	φ'	k"	φ"	ω"
20	SYNRANDOM										0.0142	0.0345	0.0174	0.0062	0.0014
21	SYNPD1	0.5									-0.0117	-0.3890	-0.0114	-0.2971	-0.0017
22	SYNPD2	1									-0.0233	-0.7752	-0.0226	-0.5917	-0.0034
23	SYNPD3	0.5	0.5								0.0008	-0.0723	0.0008	0.0870	0.0001
23A	SYNPD3S	0.5	0.5					X			0.0008	-0.0723	0.0008	0.0870	0.0001
23B	SYNPD3B	0.5	0.5					X	X		0.0019	-0.0573	-0.0004	0.0686	0.0001
23C	SYNPD3P	0.5	0.5						X		0.0069	0.0154	-0.0064	-0.0214	-0.0002
23E	SYNPD3AF	0.5	0.5					X			0.0008	-0.0723	0.0008	0.0870	0.0001
24	SYNPD4	0.5	-0.5								-0.0244	-0.7080	-0.0236	-0.6830	-0.0036
25	SYNPP1			1							-0.0062	-0.2858	-0.0096	-0.2182	-0.0115
26	SYNPP2				1						0.1400	0.1017	-0.0666	0.0984	-0.5690
27	SYNPP3			1	1						0.1349	-0.1835	-0.0758	-0.1193	-0.6010
28	SYNPP4			1	1	1	1				0.2040	-0.4409	-0.1513	-0.4070	-0.0351
28A	SYNPP4S			1	1	1	1	X			0.2040	-0.4409	-0.1513	-0.4070	-0.0351
28B	SYNPP4B			1	1	1	1	X	X		0.2031	-0.4407	-0.1523	-0.4087	-0.0352
28C	SYNPP4P			1	1	1	1		X		0.2042	-0.4227	-0.1535	-0.4308	-0.0352
28E	SYNPP4AF			1	1	1	1	X			0.2040	-0.4409	-0.1513	-0.4070	-0.0351
29	SYNPP5			1	1	-1	-1				0.0709	0.0917	0.0065	0.1900	-1.1672

Table 8-3: SUMMARISED RESULTS OF REAL PHOTOGRAPHY TESTS

Table 8-3 contains the results of the real photography of the test field. This table resembles Table 8-1 with the exception of the orientation angle directions, which cannot be evaluated as the true value for the orientation angles are unknown.

Col. 1 case number
2 file name
3 number of points used for the relative orientation adjustment
4 number of additional points, not included in the relative orientation adjustment but based on the orientation parameters evaluated in the adjustment
5 number of all points considered in the determination of average displacement vectors and the root mean square errors
6-7 as in columns 9-10 of Table 8-1
8-16 as in columns 17-25 of Table 8-1
17 remarks

In the last five cases of Table 8-3 (47-1 to 48-3), the results of the relative orientation adjustment are compared with the results achieved by means of the projective transformation method. In cases 47-1 and 47-2 the same image co-ordinates which were previously processed in a relative orientation adjustment (see cases 40 to 46) are now introduced into a projective transformation adjustment. The projective transformation results are compared against the geodetically determined test field co-ordinates and average displacement vectors and average root square errors are evaluated as before in order to obtain a compatible measure of accuracy for the projective transformation.

The projective transformation results are then directly compared with the model co-ordinates obtained in the relative orientation adjustment using both convergency corrections and affine scaling. The average displacement vectors between the model co-ordinates obtained from the two methods are given under case numbers 48-1 to 48-3.

1	2	3	4	5	6	7	8	9	10	11	12	13	14	15	16	17
CASE	FILENAME	NO. OF POINTS						DX	DY	DZ	DV	σ_x	σ_y	σ_z	σ_v	REMARKS
40	UMK 1	10		10				2.5	1.8	2.6	4.0	2.7	1.8	2.7	4.2	
40A	UMK 1 S	10		10	X			0.2	0.2	0.5	0.6	0.3	0.3	0.6	0.7	
40B	UMK 1 B	10		10	X	X		0.3	0.2	0.4	0.5	0.3	0.3	0.5	0.7	Z-DISTANCE IN CENTRE OF FIELD
40BB	UMK 1 BB	10		10	X	X		1.3	0.9	0.5	1.7	1.4	1.0	0.7	1.9	Z-DISTANCE LEFT SIDE OF FIELD
40C	UMK 1 P	10		10		X		0.2	0.2	0.6	0.7	0.3	0.3	0.7	0.8	CONVERGENCY CORRECTED
40E	UMK 1 AF	10		10	X			0.2	0.2	0.4	0.5	0.3	0.3	0.5	0.7	AFFINE SCALING
41	UMK 2	30		30				1.8	1.6	2.4	3.4	2.3	1.7	2.5	3.8	
41A	UMK 2 S	30		30	X			0.2	0.2	0.7	0.8	0.2	0.2	0.9	0.9	SCALED FROM DIST. IN X-DIR.
41B	UMK 2 B	30		30	X	X		0.2	0.2	0.6	0.7	0.2	0.3	0.8	0.9	SCALED AND CONVERGENCY CORRECTED
41C	UMK 2 P	30		30		X		1.0	0.9	0.9	1.6	1.1	1.0	1.0	1.8	CONVERGENCY CORRECTED
42	UMK 3	12	12	24	X			0.3	0.3	0.5	0.7	0.3	0.3	0.7	0.8	ONLY POINTS IN FRONT PLANE
42	UMK 3	13	11	24				0.7	1.6	1.8	2.5	1.2	1.6	1.9	2.8	
42A	UMK 3 S	13	11	24	X			0.2	0.3	0.6	0.7	0.3	0.3	0.6	0.7	SCALED FROM DIST. IN X-DIR.
42B	UMK 3 B	13	11	24	X	X		0.2	0.2	0.5	0.6	0.3	0.3	0.6	0.7	SCALED AND CONVERGENCY CORRECTED
42C	UMK 3 P	13	11	24		X		0.6	1.0	0.8	1.4	0.9	1.1	0.9	1.7	CONVERGENCY CORRECTED
42D	UMK 3 D	13	11	24	X			0.2	0.2	0.5	0.6	0.2	0.3	0.6	0.7	SCALED FROM DIST. IN Z-DIR.
43A	NIKONOS 1 S	10		10	X			1.6	1.4	4.2	4.7	2.1	1.6	4.7	5.4	PD: APPR. -PP: DERIVED FROM FRAME
43B	NIKONOS 1 B	10		10	X	X		2.2	1.4	1.6	3.1	2.8	1.6	2.1	3.8	SCALED AND CONVERGENCY CORRECTED
43E	NIKONOS 1 AF	10		10	X			1.6	1.2	2.0	2.8	2.1	1.4	3.5	4.3	AFFINE SCALING
44A	NIKONOS 2 S	10		10	X			3.7	2.4	2.2	4.9	4.3	2.5	2.8	5.7	PD: CAL. -PP: DERIVED FROM FRAME
44B	NIKONOS 2 B	10		10	X	X		3.3	2.1	1.7	4.3	3.9	2.2	2.4	5.1	SCALED AND CONVERGENCY CORRECTED
44E	NIKONOS 2 AF	10		10	X			1.5	0.9	1.7	2.4	1.7	1.0	2.3	3.0	AFFINE SCALING
45A	NIKONOS 3 S	10		10	X			2.7	1.9	2.9	4.4	3.1	2.1	3.3	5.0	PD: APPR. -PP: CALIBRATED
45B	NIKONOS 3 B	10		10	X	X		2.2	1.4	2.1	3.3	2.5	1.6	2.5	3.9	SCALED AND CONVERGENCY CORRECTED
46A	NIKONOS 4 S	10		10	X			6.9	5.0	9.2	12.5	7.6	5.3	9.3	13.1	PD: CAL. -PP: CALIBRATED
46B	NIKONOS 4 B	10		10	X	X		3.4	2.2	2.2	4.6	3.7	2.3	2.8	5.2	SCALED AND CONVERGENCY CORRECTED
46E	NIKONOS 4 AF	10		10	X			1.5	0.9	1.8	2.5	1.8	1.1	2.2	3.0	AFFINE SCALING
47-1	UMK P.T.			10				0.1	0.1	0.2	0.2	0.1	0.1	0.3	0.3	PROJECTIVE TRANSFORMATION
47-2	NIK P.T.			10				0.5	0.5	1.1	1.3	0.6	0.7	1.3	1.6	PROJECTIVE TRANSFORMATION
48-1	UMK			10				0.2	0.2	0.3	0.4	0.2	0.3	0.4	0.5	REL. OR. - PROJ. TRANSF. CASE 40E
48-2	NIKONOS			10				2.1	1.2	1.5	2.8	2.7	1.6	1.8	3.6	REL. OR. - PROJ. TRANSF. CASE 43B
48-3	NIKONOS			10				0.6	0.6	1.1	1.4	0.7	0.7	1.4	1.7	REL. OR. - PROJ. TRANSF. CASE 43E

Table 8-4: EFFECTS OF ERRORS IN ORIENTATION ANGLES ON MODEL CO-ORDINATES

Model deformations caused exclusively by errors in orientation angles without any additional error source are treated in this table in a manner similar to the presentation in Table 8-1.

Col. 1 case number

2 file name

3-7 errors introduced into the orientation angles in units of degrees

8-15 as in columns 18-25 in Table 8-1

EFFECT OF ERRORS IN ORIENTATION ANGLES ON MODEL CO-ORDINATES

AVERAGE ABSOLUTE ERRORS AND ROOT MEAN SQUARE ERRORS

NORMAL PHOTOGRAPHY

1	2	3	4	5	6	7	8	9	10	11	12	13	14	15
Case	File Name	k'	φ'	k"	φ"	ω"	dx	dy	dz	dv	Gx	Gy	Gz	Gv
13	SYNKAPPA1N	0.1					0.7	1.0	2.1	2.4	0.9	1.1	2.5	2.8
14	SYNKAPPA2N			0.1			1.4	1.8	0.3	2.3	1.5	2.1	0.4	2.6
15	SYNPHI1N		0.1				2.7	2.1	4.6	5.7	3.2	2.4	5.5	6.8
16	SYNPHI2N				0.1		2.6	2.0	4.4	5.5	3.1	2.3	5.1	6.4
17	SYNPHI3N		0.1		0.1		1.4	0.3	3.4	3.7	1.6	0.4	4.0	4.3
18	SYNPHI4N		0.1		-0.1		5.1	4.1	8.9	11.0	6.1	4.7	9.9	12.5
19	SYNOMEGAN					0.1	0.0	0.7	0.7	1.0	0.0	0.8	0.7	1.1

CONVERGENT PHOTOGRAPHY

1	2	3	4	5	6	7	8	9	10	11	12	13	14	15
Case	File Name	k'	φ'	k"	φ"	ω"	dx	dy	dz	dv	Gx	Gy	Gz	Gv
30	SYNKAPPA1	0.1					0.6	0.9	2.2	2.5	0.8	1.1	2.5	2.8
31	SYNKAPPA2			0.1			1.3	1.7	0.3	2.2	1.5	2.0	0.3	2.5
32	SYNPHI1		0.1				2.7	2.1	4.6	5.7	3.2	2.4	5.5	6.8
33	SYNPHI2				0.1		2.6	2.0	4.4	5.5	3.1	2.3	5.1	6.4
34	SYNPHI3		0.1		0.1		1.4	0.3	3.4	3.7	1.6	0.4	4.0	4.3
35	SYNPHI4		0.1		-0.1		5.1	4.1	8.9	11.0	6.1	4.7	9.9	12.5
36	SYNOMEGA					0.1	0.0	0.7	0.7	1.0	0.0	0.8	0.7	1.1

BLOCK SHIFTS OF TESTFIELD CAUSED BY DEFORMATIONS

(UNITS : MM)

	X	Y	Z
SYNRANDOMN	-1.2	0.5	2.9
SYNPD1N	28.6	-0.5	11.2
SYNPD2N	57.3	-0.9	21.9
SYNPD2NS	55.0	-1.2	16.1
SYNPD2NB	53.5	-2.1	2.1
SYNPD2NP	55.8	-1.8	7.9
SYNPD3N	0.0	0.0	24.6
SYNPD3NS	-0.1	0.0	24.3
SYNPD3NB	-1.2	-0.7	12.3
SYNPD3NP	-1.1	-0.7	12.5
SYNPD3ND	-9.5	-1.3	0.1
SYNPD3NAF	0.0	0.0	0.1
SYNPD4N	57.0	-0.9	-2.7
SYNPP1N	-20.8	4.1	77.0
SYNPP2N	-8.7	-50.5	2.3
SYNPP2NS	-10.3	-50.7	-1.7
SYNPP2NB	-10.2	-50.5	0.0
SYNPP2NP	-8.9	-50.4	2.0
SYNPP3N	-29.7	-47.1	79.3
SYNPP4N	-49.2	-49.2	0.0
SYNPP4NS	-47.7	-49.0	4.0
SYNPP4NB	-47.8	-49.1	2.0
SYNPP4NP	-49.2	-49.2	-0.1
SYNPP4NAF	-49.2	-49.2	-0.2
SYNPP5N	-11.1	-45.0	161.4
SYNPDPPN	72.2	29.2	71.4
SYNPDPPNS	34.9	23.6	-21.8
SYNPDPPNB	31.9	21.8	-49.7
SYNPDPPNP	63.8	24.6	-2.6
SYNPDPPNAF	52.2	24.3	-78.4
SYNPDPPND	-49.2	-49.2	24.6
SYNPDPPNSO	-47.7	-49.0	28.5
SYNPDPPNBO	-48.8	-49.7	14.3
SYNPDPPNPO	-50.1	-49.8	12.4
SYNPDPPNDO	-58.5	-50.3	0.0
SYNPDPPNFO	-49.1	-49.2	0.0
SYNPDPPNI	-24.6	-24.6	9.8
SYNPDPPNSI	-23.9	-24.5	11.7
SYNPDPPNBI	-24.3	-24.8	6.9
SYNPDPPNPI	-25.0	-24.8	5.0

	X	Y	Z
SYNRANDOM	-1.6	0.2	4.8
SYNPD1	32.0	-1.4	-16.3
SYNPD2	63.5	-2.9	-32.9
SYNPD3	-1.7	-2.3	-21.8
SYNPD3S	18.1	0.4	28.6
SYNPD3B	18.5	0.7	33.8
SYNPD3P	0.7	-0.8	8.3
SYNPD3AF	10.2	0.4	39.0
SYNPD4	65.9	-0.5	-11.3
SYNPP1	1.7	2.7	75.4
SYNPP2	-8.5	-50.8	2.3
SYNPP3	-7.0	-48.9	77.8
SYNPP4	-11.2	-52.4	-3.0
SYNPP4S	-6.3	-51.8	9.5
SYNPP4B	-6.2	-51.8	9.8
SYNPP4P	-10.6	-52.1	3.5
SYNPP4AF	-7.8	-51.5	10.2
SYNPP5	-4.8	-45.4	160.6

Table 8-5

10. THE PHOTOGRAMMETRIC MEASUREMENT OF SHOULDER HEIGHTS OF AFRICAN ELEPHANTS IN THEIR NATURAL HABITAT

10.1 THE SIGNIFICANCE OF SHOULDER HEIGHT MEASUREMENTS IN RESEARCH ON AFRICAN ELEPHANT (LOXODONTA AFRICANA)

Elephant populations are an important factor in the wildlife management of many African national parks and game reserves. The age structure of populations of African elephants is a valuable parameter for environmental impact studies and for research activities necessary to guarantee the survival of this species in its natural habitat. Attempts were made to find correlations between various body dimensions of elephants and their age (Hanks 1972). Among these the shoulder height proved to be strongly correlated to the age of the animal (Hanks 1972, Croze 1972, Laws et al 1970). Elephant shoulder height/age curves were developed by Laws et al (1970) based on mathematical concepts derived by Bertalanffy in 1934 and 1938 (Fig. 10-9).

Shoulder height measurements can also serve to compare growth rates of animals in different environments and for the estimation of body mass (Laws 1966, Hanks 1972, Krumrey and Buss 1968). Body measurements are normally obtained from recumbent dead or immobilised elephants. Low-accuracy aerial-photogrammetric techniques were employed by Croze (1972), Glover (1963) and Laws (1969) and close-range photogrammetry was used by Douglas-Hamilton (1972). Non-metric 35 mm cameras were used in all cases. Douglas-Hamilton attached a beam-splitter to the camera to obtain stereo photography whilst Croze and Laws based their measurements on single photographs. The beam-splitter photography was taken from the ground at close range and shoulder heights were measured, whilst in the aerial technique the distance between the

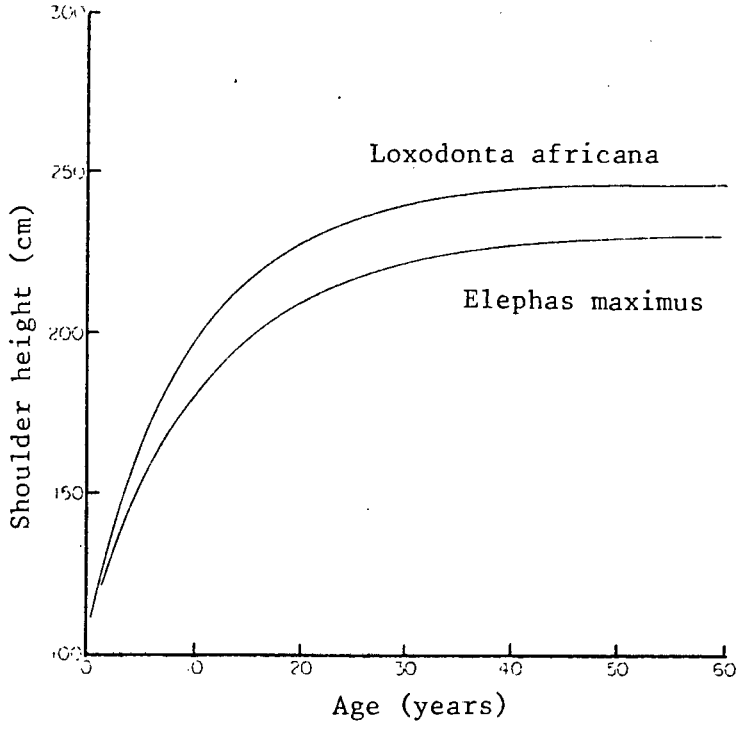

Fig.10-9 Comparison of theoretical von Bertalanffy computer-calculated growth in height curves for female African and Asiatic elephant (Hanks 1972). The curves show that elephants grow relatively slowly "which means that distinctions in size can be made between different-aged animals up to at least middle age (around 30 years)" (Croze 1972).

junction of the ears with the head and the anal flap was determined. Measurements from dead animals cannot provide representative samples and immobilising elephants is a difficult and expensive process, sometimes resulting in the death of the animal. The pragmatic photogrammetric techniques on the other hand are of low accuracy and often unreliable. A more accurate photogrammatric method for the measurements of shoulder heights of live animals therefore needs to be developed.

Inspired by Dr Douglas-Hamilton (Kenya), a study was initiated with the co-operation of Dr Hall-Martin (Addo Elephant National Park R.S.A.) in which an attempt was made to develop such a technique and to apply more rigorous photogrammetric methods to measurements of live elephants.

The objectives of the study were to develop photogrammetric techniques in order to obtain more accurate measurements of body dimensions of elephants (and wildlife in general) and to overcome some of the inherent sources of difficulty in Douglas-Hamilton's method, such as possible errors due to displacements of the mirrors of the beam-splitter attachment, the need for time-consuming calibrations and the small size of the image on 35 mm film.

The elephant population of the Addo Elephant National Park provided an ideal study object, as the ages of some 20 of the approximately one hundred elephants at the reserve were known and animals could be immobilised to verify the results obtained by photogrammetric means.

10.2 EQUIPMENT

In preparation of the field photography a pair of metric UMK 10/1318 cameras was mounted on the back of a four-wheel-drive truck by means of a metal frame structure (Fig. 10-1). This consisted of a base frame bolted to the truck with struts, and attached to this a camera carriage frame fixed to the base frame. The carriage frame had two wooden boxes bolted to either end by means of metal plates riding on springs against which the butterfly nuts holding the camera boxes were tensioned to absorb shock (Fig. 10-2). The inside of the camera box had two vertical grooves into which the camera side trunnions fitted snugly. A hole in the floor of the box accommodated

Fig. 10-1 A pair of UMK 10/1318 cameras set up for simultaneous operation on a base frame secured to the back of a light truck

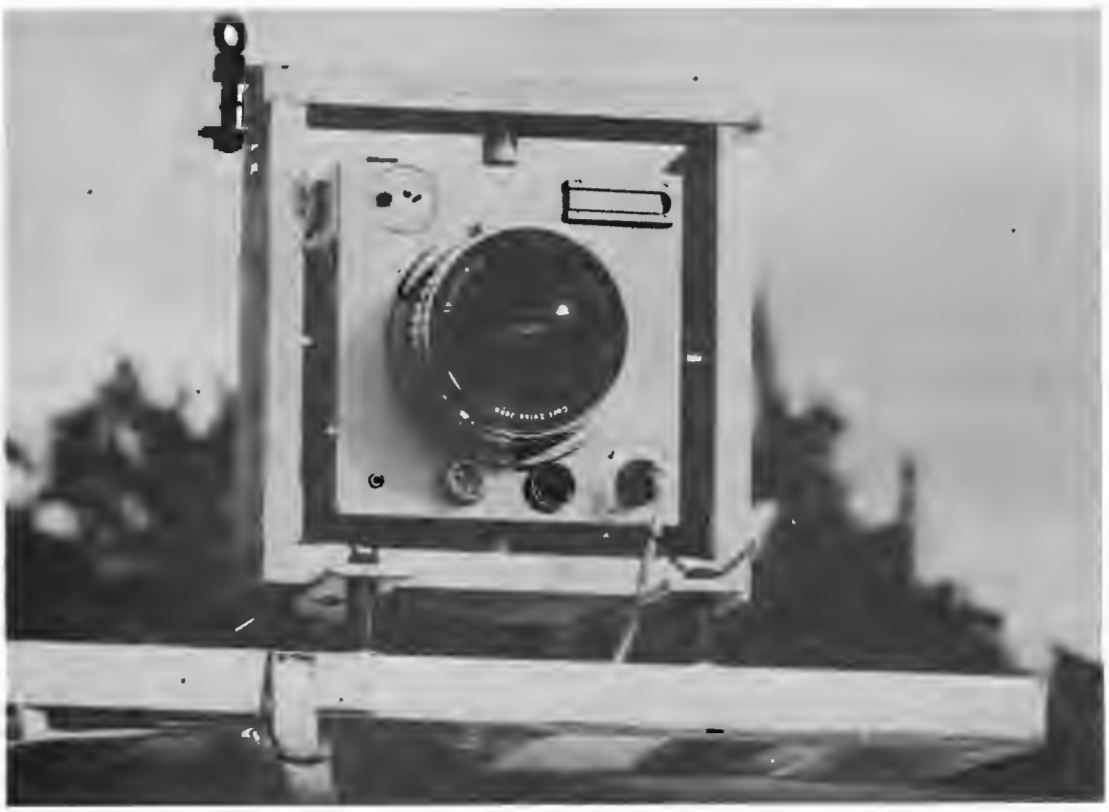

Fig. 10-2 UMK camera mounted in wooden frame

the lower trunnion and the lid of the box was screwed down against the upper trunnion. The floor of the box was padded with high-density rubber. The metal construction was of 16 gauge 40 mm square piping so as to provide a rigid base for the cameras. An electrical shutter trigger mechanism for simultaneous operation of the cameras was fixed to the camera carriage frame. As the sensitivity of the camera mechanism prohibited a permanent mounting of the cameras on the frame, they were removed from their holders when travelling and kept in their well-cushioned cases.

Once the vehicle was in position near an elephant the equipment was set up in less than a minute (Fig. 10-6). This procedure is obviously disadvantageous, especially as it necessitates a relative orientation calculation for each new pair of photographs owing to the fact that an exact repetition of the cameras' attitude in the frame cannot be guaranteed for each new position.

In spite of these drawbacks the procedure had to be maintained in order to protect the metric cameras against the poor conditions of the tracks in the National Park. If non-metric cameras are used one can consider leaving the cameras permanently mounted.

The camera frame was later modified to incorporate a revolving hub (Fig. 10-3) whose axis was fixed to the base frame in order to allow all-round photography. The original fixed mounting proved restrictive in many of the field situations.

10.3 FIELD WORK

At the outset of the elephant project, attempts were made to apply conventional photogrammetric techniques. A control network was

Fig. 10-3 Camera frame with camera mounted in working position after revolving hub was added to the frame to permit all-round photography

Fig. 10-4 African elephant and points used for shoulder height measurement

for relative orientation and shoulder height measurement as well as control

Figs. 10-5 and 10-6 Stereo cameras in operation at close range to elephants in the Addo Elephant National Park

established near a waterhole with the camera set up on the vehicle placed in an optimum position. The previously well frequented area was avoided by elephants after the vehicle was in working position close to the waterhole. It became apparent that it is difficult, if not impossible, and certainly time-consuming to obtain stereographic wildlife photography against a background of premarked control points. Driving slowly through the area in search of elephants was then resorted to and 28 animals were eventually recorded on a total of 80 stereo pairs. In some cases individuals were photographed in different attitudes and locations as many as five times. The elephants displayed little aggression towards the field team and only a few mock charges by young bulls and protective females with calves disrupted the photography. Eventually the majority of the elephants allowed the vehicle with the cameras to approach to within a range of five to 15 metres without paying much attention to the intruders (Figs. 10-5 and 10-6).

Difficulties were presented by the need to photographically capture the highest point on the elephant's shoulder simultaneously with a ground point immediately next to the animal's front foot (Fig. 10-4). Often the animal's ear or grass obscured these points between which the shoulder height was measured. Examples of ideal stereo pairs are given in Figs. 10-7 and 10-8 where either both shoulder and foot are clearly visible or where an entire group of animals can be captured in a single photographic pair.

Once the elephants had moved off, well-defined points such as small stones or a kink in a branch were selected within the overlap area of the stereo pairs and two or three axis parallel control distances were measured with a tape for affine scaling or convergency correction

Figs. 10-7 and 10-8 Stereograms of elephants showing points used distances

subsequent to homogeneous scaling.

10.4 EVALUATION OF PHOTOGRAPHIC IMAGES

A problem arose in the subsequent evaluation of the images in a stereo comparator because it proved difficult to identify exactly the same point on the shoulder of the elephant on both images. Stereoscopic viewing of shoulder height points, as well as points for relative orientation and model control, was often impeded because of considerable differences in the appearance of objects as seen from the two cameras. Repeated photography of the same individual helped to overcome this difficulty.

Experiments with pug marking did not result in an improvement of image co-ordinate accuracies, as the problem in obtaining high quality image co-ordinates was not so much presented by the difficulty encountered in measuring specific points accurately but rather by the above-mentioned lack of an unambiguous stereo image of the object points.

The image co-ordinates of shoulder and foot points as well as points used for the relative orientation and control-distance-end-points were processed in the relative orientation adjustment program described in Appendix IV. Model deformations were removed by affine scaling and in some cases also by convergency corrections. Model co-ordinates were then used to determine shoulder height measurements.

10.5 RESULTS

The accuracy of the results was gauged in two ways: by comparing results of repeated photography of the same individual and by comparing photogrammetric results with manual measurements obtained with a tape

on immobilised elephants. The animals in the Addo population are individually known and it was possible to select for immobilisation six animals that had been repeatedly photographed. To minimise disturbance to the population, only adult and young bulls were immobilised. Shoulder heights of the recumbent animals were measured four to six times with a steel tape. The results of the field measurement are listed in Table 10-1 against the photogrammetric results.

Subject	Field measurements			Photogrammetric measurements		
	cm	σ	n	cm	σ	n
♂ 2	306	0,5	5	307	3,8	4
♂ 3	285	1,9	5	284	2,0	2
♂ 4	299	1,3	5	290	1,7	3
♂ 9	286	1,3	5	285	1,8	2
♂ 12	246	1,6	6	240	1,2	3
♂ 13	303	0,8	4	293	2,1	5

Tab. 10-1 Comparison of field measurements of immobilised African elephants with photogrammetric measurements of the same animals when in a standing posture (Rüther, Hall-Martin 1979).

The differences in corresponding shoulder height values and standard deviations do not do justice to the photogrammetric technique. In the photogrammetric approach the elephant was measured at different times in different positions, whilst the manual measurements were taken as one set with the animal in a specific unchanging (recumbent) position.

The shoulder blade of the elephant is not attached to the skeleton and "floats" supported by shoulder muscles. It therefore can adopt different attitudes depending on the posture of the elephant and subsequently the same animal can have a variation of a few centimetres in its shoulder height. A limitation in the repeatability of results is therefore inherent in all shoulder height measurement techniques executed on elephants in a standing position. It must also be assumed that an immobilised animal would not necessarily adopt the same recumbent position when immobilised repeatedly. Thus the high accuracy of the manual measurements recorded in Table 10-1 reflects repeatability for one specific posture rather than real accuracy. Because of the natural margin in the shoulder height owing to the floating shoulder blades of the elephants, the results of the photogrammetric survey with standard deviations of one to four centimetres can be rated as fully satisfactory. Comparison of affine scaling with homogeneous scaling followed by convergency correction resulted in marginal differences of one to two centimetres for individual stereo pairs, whereas the mean values obtained from each of the two methods differed by less than one centimetre.

A noticeable improvement was achieved by both methods in comparison with the relative orientation without control. Standard deviations improved by 2,5 cm for elephant number 13 and by 2 cm for elephant number 2 (Table 10-1). The approach described above could be made even more acceptable for the biologist if lightweight non-metric cameras can be adapted for the measurements. Test field experiments carried out with such cameras promise accuracies of 3 to 6 cm. for the shoulder height measurements.

In conclusion it can be said that the photogrammetric technique of

relative orientation with a few measured control distances provides satisfactory results for measurements of wildlife or objects the measurement of which poses similar difficulties.

REFERENCES

The following abbreviations have been used:

BuL. for Bildmessung und Luftbildwesen

Phia. for Photogrammetria

Photogram. Eng. for Photogrammetric Engineering

Photogram. Eng. and R.S. for Photogrammetric Engineering and Remote Sensing

Photogram. Rec. for Photogrammetric Record

Abdel-Aziz, Y. and Karara, H.M. 1971 Direct Linear Transformation from Comparator Co-ordinates into Object Space Co-ordinates in Close Range Photogrammetry. Proceedings of the Symposium on Close Range Photogrammetry. Urbana. Illinois.

Abdel-Aziz, Y and Karara, H.M. 1974 Accuracy Aspects of Non-Metric Imageries. Photogram. Eng. 40(9): 1107-1117.

Abdel-Aziz, Y. 1979 An Application of Photogrammetric Techniques to Building Construction. Photogram. Eng. 45(4): 539-544.

Adamec, A. 1974 Let's Not Forget Terrestrial Photogrammetry. The Australian Surveyor 26(3): 172-183.

Adams, L.P. 1975[1] Fourcade. S.A. Journal of Photogram. 7(1): 4-20.

Adams, L.P. 1975[2] H.G. Fourcade. Photogram. Rec. 8 (45): 287-296.

Adams, L.P. 1978 The Use of a Non-Metric Camera for Very Short Range Dental Stereo-Photogrammetry. Photogram. Rec. 9 (51): 405-414.

Adams, L.P. 1979 An Experiment with Analytical Shadow Stereo-Photogrammetry. Photogram. Rec. 9(54): 835-847.

Adams, L.P. 1980[1] The Use of Short Range Photogrammetry in the Study of the Morphology of the Shoebill Bill. Photogram. Rec. 10(55): 73-84.

Adams, L.P. 1980[2] The Use of Non-Metric Cameras in Short Range Photogrammetry. Presented Paper Commission V, 14th Congress of the International Society for Photogrammetry, Hamburg 1980. Published: Phia. 36(1981): 51-60.

Adams, L.P.	1981	X-Ray Stereo-Photogrammetry Locating the Precise Three Dimensional Position of Image Points. Med. & Bio. Eng. & Comput. 19: 569-578.
Adams, L.P.	1982	Personal communication.
Arthur, D.W.G.	1955	A Stereocomparator Technique for Aerial Triangulation. Ordnance Survey Professional Papers, New Series, No 20.
Arthur, D.W.G.	1972	A Generalised Analytical Relative Orientation Procedure and Its Application to Apollo 14 Close Up Photography. Photogram. Rec. 7(40): 442-453.
Atkinson, K.	1976	A Review of Close Range Engineering Photogrammetry. Photogram. Eng. and R.S. 42(1): 57-69.
Atkinson, K.	1980	Developments in Close Range Photogrammetry - 1. Applied Science Publishers, London: 222 pages.
Badekas, J.	1974	Photogrammetric Surveys of Monuments and Sites. Proceedings of the First Symposium on Photogrammetric Surveys of Monuments and Sites, Athens (edited by J. Badekas): 176 pages.
Bartorelli, U.	1955	An Analytical Method of Aerial Triangulation. Phia. 12(4): 319-324.
Beattie, A. and Lozowski, E.	1976	Determining the Kinematics of Falling Hailstones with Imprecisely Aligned Cameras. Photogram. Eng. 42 (10): 781-793.
Bertalanffy, L. von	1934	Untersuchungen uber die Gesetzlichkeit des Wachstums. Archiv. fur Entwicklungs Mech. 131: 613-652.
Bertalanffy, L. von	1938	A Quantitative Theory of Organic Growth. Hum. Biol. 10: 181-213.
Bopp, H. and Krauss, H.	1978	An Orientation and Calibration Method for Non-Topographic Application. Photogram. Eng. 44(9): 1191-1196.
Brown, D.C.	1971	Close Range Camera Calibration. Photogram. Eng. 37(8): 855-866.
Buss, I.O. and Krumrey, W.A.	1968	Age Estimation, Growth and Relationship Between Body Dimensions of Female African Elephants. J. Mammal. 49: 22-31.

Church, E. 1936 Analytical Computations in Aerial Photogrammetry. Ann Arbor, Michigan.

Church, E. 1941 Analytical Computations in Aerial Photogrammetry. Photogram. Eng. 7 (4): 212-252.

Collins, S. and Moon, G. 1979 Stereometric Measurement of Stream Bank Erosion. Photogram. Eng. and R.S. 45(2): 183-190.

Croze, G. 1972 A Modified Photogrammetric Technique for Assessing Age-Structure of Elephant Populations and Its Use in Kideo National Park. E. Afr. Wildlife J. 10(2): 91-116.

Danphin, E. and Torlegård, A.K.I. 1977 Displacement and Deformation Measurements Over Long Periods of Time. Phia. 33(6): 225-239.

Dikkers, K. and Welch, R. 1978 Educational and Research Aspects of Non-Metric Close Range Analogue Photogrammetry. Photogram. Rec. 9 (52): 537-547.

Douglas-Hamilton, I. 1972 On the Ecology and Behaviour of the African Elephant. Ph.D. Dissertation, University of Oxford.

Erlandson, J. and Veress, S. 1975 Monitoring Deformations of Structures. Photogram. Eng. and R.S. 41 (11): 1375-1384.

Faddeev and Faddeeva 1963 Computational Methods of Linear Algebra. Freeman and Company, San Francisco and London: 163-167.

Faig, W. 1971 Shapes of the Soap Membranes. Photogram. Eng. 37(10): 1075-1082.

Finsterwalder, S. 1897 Die Geometrischen Grundlagen der Photogrammetrie. Jahresbericht der Deutschen Mathematiker Vereinigung. VI(2)1897, Leipzig 1899.

Finsterwalder, S. 1900 Ueber die Konstruktion von Höhenkarten aus Ballon Aufnahmen. Bayrische Akademie der Wissenschaften. Math. Nat.

Finsterwalder, S. 1903 Das Rückwärts Einschneiden in Raum. Bay rische Akademie der Wissenschaften. Sitzungsbericht Math. Nat. XXIII(4): 519-614

Fligor, P.D. 1968 Resection Without Camera or Station Parameters. Photogram. Eng.: 91-103.

Fourcade, H.G. 1902 A Stereoscopic Method of Photographic Surveying. Nature (June) 139-141.

Fourcade, H.G.	1926	A New Method of Aerial Surveying. Transactions of the Royal Society of South Africa XIV(1): 93-112.
Garfield, J.	1964	The Photogrammetry of the Tracks of Elementary Particles in Bubble Chambers. Photogram. Eng. 30(5): 824-832.
Glover, J.	1963	The Elephant Problem at Tsavo. E. Afr. Wildlife 1: 30-39.
Gotthard, E.	1959	Erfahrungen mit Analytischer Einpassung Von Luft Bildern. BuL: 109-121.
Granshaw, S.I.	1979	Relative Orientation Problems. Photogram. Rec. 9(53): 669-675.
Gruber, O. von	1924	Einfache und Doppelpunkt Einschaltung im Raum. Jena.
Gruber, O. von	1930	Photogrammetry: Collected Lectures and Essays. London. Compiled from Lectures delivered during the 6th Vacation Course on Photogrammetry, 1929. First German edition: 1930. First English edition: 1932.
Hallert, B.	1968[1]	Fundamental Formula Systems for Analytical Photogrammetry. Third South African Nat. Surv. Conf. Conference Paper 3/1: 1-27.
Hallert, B.	1968[2]	Notes on Calibration and Photographs in Photogrammetry. Phia. 23: 163-178.
Hallert, B.	1969	Perspective Center Determination. Photogram. Eng. 35: 1055-1058.
Hanks, J.	1972	Growth of African Elephant (Loxodonta Africana). E. Afr. Wildlife 10(4): 251-272.
Harley, I.A.	1971	An Exact Procedure for Numerical Orientation of a Plotting Instrument. Photogram. Rec. 7(37): 27-38.
Heister, H. and Welsch, W.	1972	Erzeugung und Test Normalverteilter Zufallszahlen. Z.f.V. 97(10): 446-456.
Herget, P.	1954	The Reduction of Aerial Photographs on Electronic Computers. Photogram. Eng. 20(5): 842-844.
Herron, R.	1972	Stereophotogrammetry in Biology and Medicine. I.S.P. Congress. Ottawa 1972.
Hirvonen, R.A.	1971	Adjustment by Least Squares in Geodesy and Photogrammetry. New York.

Hohler, J.	1971	Reconstruction of the Underwater Object. Photogram. Eng. 37(9): 948-954.
Jerie, H.G.	1956	A Contribution to the Problem of Analytical Aerial Triangulation. Photogram. Eng. 12(1): 40-52.
Jordan, Eggert and Kneissl	1961	Handbuch der Vermessungskunde Band I. J.B. Metzlersche Verlagsbuchhandlung. Stuttgart: 808 pages.
Jordan, Eggert and Kneissl	1972	Handbuch der Vermessungskunde Band IIIa 1/2/3. Photogrammetrie Edits. Rinner/Burkhardt. J.B. Metzlersche Verlagsbuchhandlung. Stuttgart: 2321 pages.
Karara, H.M.	1979	Handbook of Non-Topographical Photogrammetry. American Society of Photogrammetry. Falls Church: 206 pages.
Kenefik, J.F.	1972	Analytical Selfcalibration. Photogram. Eng. 38: 1117-1126.
Kenefik, J.F.	1977	Applications of Photogrammetry in Shipbuilding. Photogram. Eng. and R.S. 43(9): 1169-1175.
Kölbl, O.	1972	Selbst Kalibrierung von Aufnahmekammern. BuL. 40(1): 31-37.
Kölbl, O.	1976	Metric or Non-Metric Cameras. Photogram. Eng. and R.S. 42(1): 103-113.
Konecny, G.	1965	Interior Orientation and Convergent Photography. Photogram. Eng. 31(4): 625-634.
Kratky, V.	1976	Analytical On Line System in Close Range Photogrammetry. Photogram. Eng. 42(1): 81-90.
Kratky, V.	1979	Real-Time Photogrammetric Support of Three Dimensional Control. Photogram. Eng. 45(9): 1231-1242.
Kraus, K. and Stark, E.	1973	Flächenhafte Verzeichnungs Korrektur in der Numerischen Photogrammetrie. BuL. 2: 50-56.
Le Brun, S.	1977	Stereophotographic Survey of Elephants. Unpublished B.Sc. Thesis. University of Cape Town, Department of Surveying.
Lehman, E.H.	1963	Determining Exposure Point, Tilt and Direction of Photograph from Three Known Ground Positions and Focal Length. Photogram. Eng. 29.

Laws, R.M. 1969 The Tsavo Research Project. Journal for Repr. Fert. Supplement 6: 495-531.

Laws, R.M., Parker I.S.C. and Johnstone, R.C.B. 1970 Elephants and Habitats in North Bunyoro, Uganda. E. Afr. Wildlife 8: 163-180.

Mahajan, S.K. and Singh, V. 1972 Comparison of Analytical Relative Orientation Methods. Journal of the Surveying and Mapping Division, SUI: 73-86.

Manual of Photogrammetry 1965 Ed. Thompson, M.M. American Society of Photogrammetry 1,2. Third edition, 1965: 1199 pages.

McNair, A.J. 1957 General Review of Analytical Aerotriangulation. Photogram. Eng. 13 (3): 573-582.

McNeil, G.T. 1969 Underwater Photography. Photogram. Eng. 35(11): 1135-1152.

Merrit, E.L. 1949 Explicit Three Point Resection in Space. Photogram. Eng. 15(4)

Meydenbauer, A. 1894 Ein Deutsches Denkmaler Archiv. (Monumenta Germaniae). Deutsche Bauzeitung: 629-631.

Mikhail, E.M. and Ackermann, F.E. 1976 Observations and Least Squares. New York, I.E.P., 1975: 497 pages.

Morse, M. 1966 Projective Methods. Photogram. Eng. 32.

Munzer, U. 1979 Documenting of Geological Objects in Alpine Areas. BuL. 9: 149-155.

Newton, J. 1974 Dimensional Quality of Large Ship Structures by Photogrammetry. Photogram. Rec. 8(44): 139-153.

Newton, J. 1975 Close Range Photogrammetry as an Aid to Measurements of Marine Structures. Photogram. Eng. 41(12): 1501-1512.

Oshima, T. 1976 Recent Developments of Industrial Photogrammetry in Japan. Photogram. Eng. and R.S. 42(3): 339-342.

Rawiel, R. 1980 A Direct Solution for a Three Dimensional Rotation of a Stereo Model. The South African Journal of Photogrammetry: 19-27.

Renner, W. 1977 A Photogrammetric Technique for Use in Radiation Therapy. Photogram. Eng. and R.S. 42(3): 339-342.

Rinner, K. 1957 Analytisch Photogrammetrisch Triangulation mit Formtreuen Bundeln. DGK Reihe A Heft 25: 40 pages.

Rüther, H. and Hall-Martin, A 1979 Application of Stereo Photogrammetric Techniques for Measuring African Elephants. Koedoe 22: 187-198.

Rüther, H. 1981 Survey Network Adjustment. South African Survey Journal 18(2): 21-30 and 18(3): 13-22.

Rüther, H. 1982 Wildlife Stereo Photogrammetry at Close Range. Presented Paper at International Symposium on Precision and Speed in Close Range Photogrammetry. York.

Schenk, T. 1971 Nochmals: Darstellung von Verzeichnungs Kurven mittels Potenzreihen. BuL. 3.

Schmid, H. 1955 An analytical Treatment of the Orientation of a Photogrammetric Camera. Ballistics Lab. Report 961. (October) 1955.

Schmid, H. 1956 An Analytical Treatment of the Problem of Triangulation by Stereophotogrammetry. Phia. 13(2): 67-77 and 13(3): 91-116.

Schut, G.H. 1956 Analytical Aerial Triangulation. Phia. (1955/1956). 12(4): 311-318.

Schut, G.H. 1957 An Analysis of Methods and Results in Analytical Aerial Triangulation. Phia. (1957/1958). 14(1): 16-33.

Schut, G.H. 1958 Construction of Orthogonal Matrices and Their Application to Analytical Photogrammetry. Phia. (1958/1959). 15/4: 149-162.

Schwidefsky, K. 1959 Grundriss der Photogrammetrie. 1. English edition, London 1959. 6. German edition, Teubner Verlags Gesellschaft, Stuttgart, 1963: 362 pages.

Schwidefsky, K. 1970 Precision Photogrammetry at Close Ranges with Simple Cameras. Photogram. Rec. 6(36): 567-589.

Scogings, D.A. 1978 An Experimental Recording of Petroglyphs and Archaeological Sites. Photogram. Rec. 9(51): 327-341.

Scott, P.J. 1976 Close Range Camera Calibration - A New Method. Photogram. Rec. 8(48): 806-812.

Scott, P.J. 1977 The Pupil in Perspective. Photogram. Rec. 3(49): 83-92.

Scott, P.J. 1978 Structural Deformation Measurement of a Model Box Girder Bridge. Photogram. Rec. 9(51): 361-376.

Shmutter, B. and Perlmutter, A. 1974 Spatial Intersection. Photogram. Rec. 8(43): 94-100.

Shmutter, B. and Ertrag, U. 1971 Calibration of Storage Tanks. Photogram. Eng. 37(31): 261-266.

Smith, A.D.N. 1965 The Explicit Solution of the Single Picture Resection Problem with a Least Squares Adjustment to Redundant Control. Photogram. Rec. 5 (26): 113-121.

Stefanovic, P. 1973 Relative Orientation: A New Approach. I.T.C.Journal 3: 417-448.

Stefanovic, P. and van den Hout, C.M.A. 1976 Efficient Analytical Relative Orientation. I.T.C. Journal 2: 304-323.

Szczepanski, W. 1958 Die Lösungsvorschläge für den Räumlichen Rückwärtseinschnitt. DGK Reihe C 29, München.

Thompson, E.H. 1956 A Method of Relative Orientation in Analytical Aerial Triangulation. Photogram. Rec. 2(8): 145-150.

Thompson, E.H. 1957 The Geometrical Theory of the Camera and its Application in Photogrammetry. Photogram. Rec. 2(10): 241-263.

Thompson, E.H. 1959 A Rational Algebraic Formulation of the Problem of Relative Orientation. Photogram. Rec. 3(14): 152-159.

Thompson, E.H. 1969 An Introduction to the Algebra of Matrices with some Applications. Adam Hilger Limited, London: 229 pages.

Thompson, E.H. 1971 Space Resection Without Interior Orientation. Photogram. Rec. 7(37): 39-45.

Thompson, E.H. 1975[1] Resection in Space. Photogram. Rec. 8(45): 333-334.

Thompson, E.H. 1975[2] Convergence. Photogram. Rec. 8 (45): 330-332.

Thompson, E.H. 1977 A Note on Distortion. Photogram. Rec. 9(49): 93-99.

(Most of the above publications by E.H. Thompson are to be found in "Photogrammetry and Surveying", a selection of papers by E.H. Thompson, 1910-1976, Phot. Soc., London 1977. 359 pages.)

Torlegård, A.K.I. 1967 On the Determination of Interior Orientation of Close Up Cameras under Operational Conditions using Three Dimensional Test Objects. Thesis, Stockholm.

Torlegård, A.K.I. 1976 State-of-the-Art of Close Range Photogrammetry. Photogram. Eng. and R.S. 44(3): 273-283.

Van den Hout, C.M.A. 1961 Analytical Orientation Method. Bulletino di Geodesia e Scienze, Affini Anno 20(3): 418-427.

Wassef, A.M. 1953 Some Recent Developments in Analytical Photogrammetry. The Use of Eulerian Angles and Computational Procedure. Phia. 10(2): 76-82.

Welham, L. 1982 Underwater Stereometrology for Scientists and Engineers using Non-Metric Cameras. M.Sc. Thesis in preparation.

Wells, D.E. and Krakiwsky, E.J. 1971 The Method of Least Squares. Department of Surveying Engineering, University of New Brunswick, Fredericton, N.B.: 180 pages.

Williams, H.S. 1974 A Control Investigation of the Metrical Requirements and Practical Accuracies of Analytical Photogrammetry. Ph.D. Thesis, University of the Witwatersrand.

Wolf, H. 1968 Ausgeichungsrechnung nach der Methode der Kleinsten Quadrate. Ferd. Dummlers Verlag. Bonn: 591 pages.

Wolf, H. 1975 Ausgleichungsrechnung. Ferd. Dummlers Verlag. Bonn. I: 323 pages, II: 353 pages.

Ziemann, H. 1972 Economics of Image Deformation Corrections. Photogram. Eng. 3(2): 155-167.

APPENDIX I

STANDARD DEVIATION OF MODEL CO-ORDINATES

Model co-ordinates are a function of the observed plate co-ordinates and of the unknown orientation angles. The standard deviation of model co-ordinates fall thus into the category of "standard deviations of a function of observations and unknowns" (3.2.23).

$$\sigma_F^2 = \sigma_0^2 \, Q_{FF}$$

with Q_{FF} from (3.2.24) and (3.2.25)

$$Q_{FF} = \underline{f}^T(\underline{P}^{-1} - \underline{P}^{-1}\,\underline{B}^T\underline{P}^*\underline{B}\,\underline{P}^{-1})\underline{f} + (\bar{\underline{f}}^T - \underline{f}^T\underline{P}^{-1}\underline{B}^T\underline{P}^*\underline{A})(\underline{A}^T\underline{P}^*\underline{A})^{-1}(\bar{\underline{f}} - \underline{A}^T\underline{P}^*\underline{B}\,\underline{P}^{-1}\underline{f}) \quad (I.1)$$

In this form equation I.1 is unsuitable for use in mini computers because of its considerable memory requirement. A more suitable formulation of the equation for Q_{FF} can be developed by rearranging I.1 and by replacing matrix algebra with conventional notations.

We set

$$\underline{S}^T = \underline{P}^{-1}\underline{B}^T\underline{P}^*\underline{A} \quad (I.2)$$

$\underline{P}$ and $\underline{P}^*$ are principal diagonal matrices, hence

$$\underline{S} = \underline{A}^T\underline{P}^*\underline{B}\underline{P}^{-1} \quad (I.3)$$

The adjustment is of the quasi-parametric type and we have from (3.2.27) the variance-co-variance matrix

$$\underline{Q} = (\underline{A}^T\underline{P}^*\underline{A})^{-1} \quad (I.4)$$

Substituting I.2, I.3 and I.4 into I.1 one obtains because of:

$$\underline{Q} = \underline{Q}^T \tag{I.5.1}$$

and $$(\underline{f}^T\underline{S}^T\underline{Q}\ \bar{\underline{f}})^T = \underline{f}^T\underline{S}^T\underline{Q}\ \bar{\underline{f}} = \bar{\underline{f}}^T\underline{Q}\ \underline{S}\ \underline{f} \tag{I.5.2}$$

for equation (I.1)

$$Q_{FF} = \underline{f}^T\underline{P}^{-1}\underline{f} - \underline{f}^T\underline{P}^{-1}\underline{B}^T\underline{P}^*\underline{B}\underline{P}^{-1}\underline{f} + \bar{\underline{f}}^T\underline{Q}\ \bar{\underline{f}} - 2\bar{\underline{f}}^T\underline{Q}\ \underline{S}\ \underline{f} + \underline{f}^T\underline{S}^T\underline{Q}\underline{S}\underline{f} \tag{I.6}$$

For further derivation we set

$$Q_{FF} = I - II + III - IV + V \tag{I.6.1}$$

When evaluating standard deviations for the model co-ordinates a Q_{FF} value (I.6) must be determined for each of the three model co-ordinates of each model point.

In equation (I.6) matrices $\underline{Q}$ (I.4 and 7.4.8), $\underline{B}$ (7.4.10) and $\underline{P}$ (7.4.11) are identical for all Q_{FF} values of the adjustment, whereas the vector $\underline{f}$ and $\bar{\underline{f}}$ differ from point to point and also for the X, Y and Z co-ordinates.

Vector $\underline{f}$ for the X co-ordinate of a point P_a is:

$$\underline{f}^T_{x_a} = \left[\frac{\partial F_{x_a}}{\partial \bar{x}'_a}\ \frac{\partial F_{x_a}}{\partial \bar{y}'_a}\ \frac{\partial F_{x_a}}{\partial \bar{x}''_a}\ \frac{\partial F_{x_a}}{\partial \bar{y}''_a}\ 0\ 0\ 0\ 0\ \ldots\right] \tag{I.7}$$

where F_{x_a} is the function for an X model co-ordinate (7.8.1.4).

Equation (I.7) can be written as

$$\underline{f}^T_{x_a} = \left[f_{x_{a_1}}\ f_{x_{a_2}}\ f_{x_{a_3}}\ f_{x_{a_4}}\ 0\ 0\ 0\ 0\ \ldots\right] \tag{I.7.1}$$

and similarly for the Y co-ordinate

$$\underline{f}_{y_a}^T = \left[f_{y_{a_1}} \quad f_{y_{a_2}} \quad f_{y_{a_3}} \quad f_{y_{a_4}} \quad 0 \quad 0 \quad 0 \quad 0 \ldots \right] \tag{I.7.2}$$

and for the Z co-ordinate

$$\underline{f}_{z_a}^T = \left[f_{z_{a_1}} \quad f_{z_{a_2}} \quad f_{z_{a_3}} \quad f_{z_{a_4}} \quad 0 \quad 0 \quad 0 \quad 0 \ldots \right] \tag{I.7.3}$$

Each $\underline{f}$ vector has four non-zero elements, their position within the vector corresponds to the position of the coefficients pertaining to the point in question in matrix $\underline{B}$ (7.4.10).

Vector $\bar{\underline{f}}$ for the X co-ordinate of point P_a has the form

$$\bar{\underline{f}}_{x_a}^T = \left[\frac{\partial F_{x_a}}{\partial \varkappa'} \quad \frac{\partial F_{x_a}}{\partial \varphi'} \quad \frac{\partial F_{x_a}}{\partial \varkappa''} \quad \frac{\partial F_{x_a}}{\partial \varphi''} \quad \frac{\partial F_{x_a}}{\partial \omega''} \right] \tag{I.8}$$

or

$$\bar{\underline{f}}_{x_a}^T = \left[\bar{f}_{x_{a_1}} \quad \bar{f}_{x_{a_2}} \quad \bar{f}_{x_{a_3}} \quad \bar{f}_{x_{a_4}} \quad \bar{f}_{x_{a_5}} \right] \tag{I.8.1}$$

and similarly for $\bar{\underline{f}}_{y_a}^T$ and $\bar{\underline{f}}_{z_a}^T$

In order to derive a general form for a memory-saving expression for (I.6) we introduce

$$f_i = f_{x_{a_i}} \text{ or } = f_{y_{a_i}} \text{ or } = f_{z_{a_i}} \quad \text{for } i = 1 \text{ to } 4 \tag{I.9}$$

and

$$\bar{f}_j = \bar{f}_{x_{a_j}} \text{ or } = \bar{f}_{y_{a_j}} \text{ or } = \bar{f}_{z_{a_j}} \quad \text{for } j = 1 \text{ to } 5 \tag{I.10}$$

For equation (I.6.1) we have then for the individual terms:

Term (I)

$$\underline{f}^T \underline{P}^{-1} \underline{f} = \frac{f_1^2}{P_1} + \frac{f_2^2}{P_2} + \frac{f_3^2}{P_3} + \frac{f_4^2}{P_4} = \sum_{i=1}^{4} \frac{f_i^2}{P_i} \qquad (I.11)$$

Term (II)

Matrix multiplication results in

$$\underline{f}^T \underline{P}^{-1} \underline{B}^T \underline{P}^* \underline{B} \underline{P}^{-1} \underline{f} = P^* \left[\left(\frac{a_1}{P_1} f_1\right)^2 + \left(\frac{a_2}{P_2} f_2\right)^2 + \left(\frac{a_3}{P_3} f_3\right)^2 + \left(\frac{a_4}{P_4} f_4\right)^2 \right] \qquad (I.12)$$

$$= P^* \sum_{i=1}^{4} \left(\frac{a_i}{P_i} f_i \right)^2 \qquad (I.12.1)$$

Term (III)

Term (III) can remain in matrix form as the memory space required is small or it can be written as

$$\underline{f}^T \underline{Q} \underline{f} = \sum_{i=1}^{5} \sum_{j=1}^{5} \bar{f}_i \bar{f}_j Q_{ij} \qquad (I.13)$$

Term (IV)

Matrix multiplication leads here to

$$2\underline{f}^T \underline{Q} \underline{S} \underline{f} = 2P^* (\bar{f}_1 Q_1 + \bar{f}_2 Q_2 + \bar{f}_3 Q_3 + \bar{f}_4 Q_4 + \bar{f}_5 Q_5) \left(\frac{a_1}{P_1} f_1 + \frac{a_2}{P_2} f_2 + \frac{a_3}{P_3} f_3 + \frac{a_4}{P_4} f_4\right) \qquad (I.14)$$

$$= 2P^* \sum_{i=1}^{5} \bar{f}_i Q_i \sum_{j=1}^{4} \frac{a_j}{P_j} f_j \qquad (I.14.1)$$

with

$$Q_i = AQ_{i1} + BQ_{i2} + CQ_{i3} + DQ_{i4} + EQ_{i5} \quad \text{for } i = 1 \text{ to } 5 \qquad (I.14.2)$$

Term (V)

After some rearranging we can write for term (V),

$$\underline{f}^T \underline{S}^T \underline{Q} \underline{S} \underline{f} = P^{*2} \bar{Q} \sum_{i=1}^{4} \sum_{j=1}^{4} f_i f_j \frac{a_i a_j}{P_i P_j} \qquad (I.15)$$

with $\bar{Q} = \left[AQ_1 + BQ_2 + CQ_3 + DQ_4 + EQ_5\right]$ (I.15.1)

combining the five terms (I.11) to (I.15) yields an equation which can easily be realised in a mini computer:

$$Q_{FF} = \sum_{i=1}^{4} \frac{f_i^2}{P_i} - P^* \sum_{i=1}^{4} \left(\frac{a_i}{P_i} f_i\right)^2 + \sum_{i=1}^{5} \sum_{j=1}^{4} \bar{f}_j \bar{f}_j Q_{ij} - \qquad (I.16)$$

$$-2 P^* \sum_{i=1}^{5} \left(\bar{f}_i Q_i\right) \sum_{j=1}^{4} \left(\frac{a_j}{P_j} f_j\right) + P^{*2} \bar{Q} \sum_{i=1}^{4} \sum_{j=1}^{4} f_i f_j \frac{a_i a_j}{P_i P_j}$$

with Q_i from (I.14.2) and $\bar{Q}$ from (I.15.1)

In equation (I.16) quantities P^*, a_i, $\bar{Q}$, Q_i and A, B, C, D and E (in $\bar{Q}$ and Q_i) pertain to the model point in question, whereas elements f_i and $\bar{f}_i$ differ for the X, Y and Z co-ordinate of each point. Elements f_i and $\bar{f}_i$ are partial differentials of the equations for the model co-ordinates, expressions for f_i and $\bar{f}_i$ are listed below.

Equation (I.16), although mathematically less elegant than the original equation for Q_{FF} (I.1), can easily be programmed and requires minimum memory space.

Elements of vectors $\underline{f}$ and $\underline{\bar{f}}$

Partial differentials of the equation for the Z model co-ordinate (7.8.1.3):

$$Z = \frac{b}{\left[\frac{x'}{f'} - \frac{x''}{f''}\right]} = \frac{b}{V} \qquad \text{(I.17)}$$

where $V = \frac{x'}{f'} - \frac{x''}{f''}$

and x', f', x" and f" are rectified model co-ordinates (7.4.2 and 7.4.3).

The general form of the derivative of (I.17) is

$$\frac{\partial Z}{\partial \alpha} = - \frac{b}{V^2}\left[\frac{\frac{\partial x'}{\partial \alpha}f'' - x'\frac{\partial f'}{\partial \alpha}}{f'^2} - \frac{\frac{\partial x''}{\partial \alpha}f'' - x''\frac{\partial f''}{\partial \alpha}}{f''^2}\right] \qquad \text{(I.18)}$$

with $\alpha = \varkappa'$, φ', $\varkappa''$, φ'', ω'', $\bar{x}'$, $\bar{y}'$, $\bar{x}''$, $\bar{y}''$, ($\bar{f}'$ and $\bar{f}''$)

(although $\bar{f}'$ and $\bar{f}''$ are treated as error free in the adjustment, their differentials are also listed here).

$$\bar{f}_{z_1} = \frac{\partial Z}{\partial \varkappa'} = - \frac{b}{V^2}\left[\frac{(a_{12}\bar{x}' - a_{11}\bar{y}')\, f' - x'(a_{32}\bar{x}' - a_{31}\bar{y}')}{f'^2}\right] \qquad \text{(I.18.1)}$$

$$\bar{f}_{z_2} = \frac{\partial Z}{\partial \varphi'} = - \frac{b}{V^2}\left[\frac{(-\cos \varkappa' \sin \varphi'\bar{x}' + \sin \varkappa' \sin \varphi'\bar{y}' - \cos \varphi'\bar{f}')f' - x'^2}{f'^2}\right] \qquad \text{(I.18.2}$$

$$\bar{f}_{z_3} = \frac{\partial Z}{\partial \varkappa''} = - \frac{b}{V^2}\left[\frac{(b_{12}\bar{x}'' - b_{11}\bar{y}'')\, f'' - x''(b_{32}\bar{x}'' - b_{31}\bar{y}'')}{f''^2}\right] \qquad \text{(I.18.3)}$$

$$\bar{f}_{z_4} = \frac{\partial Z}{\partial \varphi''} = \frac{b}{V^2}\left[\frac{(-\cos \varkappa'' \sin \varphi''\bar{x}'' + \sin \varkappa'' \sin \varphi''\bar{y}'' - \cos \varphi''\bar{f}'')f'' - x''^2 \cos \omega''}{f''^2}\right]$$

(I.18.4

$$f_{z_5} = \frac{\partial Z}{\partial \omega''} = \frac{b}{V^2} \frac{x''y''}{f''^2} \tag{I.18.5}$$

$$f_{z_1} = \frac{\partial Z}{\partial \bar{x}'} = -\frac{b}{V^2} \frac{a_{11}f' - a_{31}x'}{f'^2} \tag{I.18.6}$$

$$f_{z_2} = \frac{\partial Z}{\partial \bar{y}'} = -\frac{b}{V^2} \frac{a_{12}f' - a_{32}x'}{f'^2} \tag{I.18.7}$$

$$f_{z_3} = \frac{\partial Z}{\partial \bar{x}''} = \frac{b}{V^2} \frac{b_{11}f'' - b_{31}x''}{f''^2} \tag{I.18.8}$$

$$f_{z_4} = \frac{\partial Z}{\partial \bar{y}''} = \frac{b}{V^2} \frac{b_{12}f'' - b_{32}x''}{f''^2} \tag{I.18.9}$$

$$\frac{\partial Z}{\partial f'} = -\frac{b}{V^2} \frac{a_{13}f' - a_{33}x'}{f'^2} \tag{I.18.10}$$

$$\frac{\partial Z}{\partial f''} = \frac{b}{V^2} \frac{b_{13}f'' - b_{33}x''}{f''^2} \tag{I.18.11}$$

The equivalent equations for the X model co-ordinate are from (7.8.1.4):

$$X = Z \frac{x'}{f'} \tag{I.19}$$

The general form of the partial derivatives of (I.19) is

$$\frac{\partial X}{\partial \alpha} = \frac{1}{f'^2} \left[\left(\frac{\partial Z}{\partial \alpha} x' + Z \frac{\partial x'}{\partial \alpha} \right) f' - Z x' \frac{\partial f'}{\partial \alpha} \right] \tag{I.20}$$

with α as in (I.18).

$$\bar{f}_{x_1} = \frac{\partial X}{\partial \varkappa'} = \frac{1}{f'^2}\left\{\left[\frac{\partial Z}{\partial \varkappa'}\, x' + Z(a_{12}\bar{x}' - a_{11}\bar{y}')\right] f' - Z\, x'(a_{32}\bar{x}' - a_{31}y')\right\} \quad \text{(I.20.1)}$$

$$\bar{f}_{x_2} = \frac{\partial X}{\partial \varphi'} = \frac{1}{f'^2}\left\{\left[\frac{\partial Z}{\partial \varphi'}\, x' + (-\cos\varkappa'\sin\varphi'\bar{x}' + \sin\varkappa'\sin\varphi'\bar{y}' - \cos\varphi' f')Z\right] f' - \right.$$

$$\left. - Z\, x'^2\right\} \quad \text{(I.20.2)}$$

$$\bar{f}_{x_3} = \frac{\partial X}{\partial \varkappa''} = \frac{x'}{f'}\,\frac{\partial Z}{\partial \varkappa''} \quad \text{(I.20.3)}$$

$$\bar{f}_{x_4} = \frac{\partial X}{\partial \varphi''} = \frac{x'}{f'}\,\frac{\partial Z}{\partial \varphi''} \quad \text{(I.20.4)}$$

$$\bar{f}_{x_5} = \frac{\partial X}{\partial \omega''} = \frac{x'}{f'}\,\frac{\partial Z}{\partial \omega''} \quad \text{(I.20.5)}$$

$$f_{x_1} = \frac{\partial X}{\partial \bar{x}'} = \frac{1}{f'^2}\left[\left(\frac{\partial Z}{\partial \bar{x}'}\, x' + Z\, a_{11}\right)f' - Z\, x'\, a_{31}\right] \quad \text{(I.20.6)}$$

$$f_{x_2} = \frac{\partial X}{\partial \bar{y}'} = \frac{1}{f'^2}\left[\left(\frac{\partial Z}{\partial \bar{y}'}\, x' + Z\, a_{12}\right)f' - Z\, x'\, a_{32}\right] \quad \text{(I.20.7)}$$

$$f_{x_3} = \frac{\partial X}{\partial \bar{x}''} = \frac{x'}{f'}\,\frac{\partial Z}{\partial \bar{x}''} \quad \text{(I.20.8)}$$

$$f_{x_4} = \frac{\partial X}{\partial \bar{y}''} = \frac{x'}{f'}\,\frac{\partial Z}{\partial \bar{y}''} \quad \text{(I.20.9)}$$

$$\frac{\partial X}{\partial f'} = \frac{1}{f'^2}\left[\left(\frac{\partial Z}{\partial f'} x' + Z\, a_{13}\right) f' - Z\, x'\, a_{33}\right] \tag{I.20.10}$$

$$\frac{\partial X}{\partial f''} = \frac{x'}{f'}\,\frac{\partial Z}{\partial f''} \tag{I.20.11}$$

And finally for the Y model co-ordinate we have with (7.8.1.5)

$$Y = Z\,\frac{y'}{f'} \tag{I.21}$$

The general form of the partial derivatives of (I.20) is

$$\frac{\partial Y}{\partial \alpha} = \frac{1}{f'^2}\left[\left(\frac{\partial Z}{\partial \alpha} y' + Z\,\frac{\partial y'}{\partial \alpha}\right) f' - Z\, y'\,\frac{\partial f'}{\partial \alpha}\right] \tag{I.22}$$

with α as above

$$\bar{f}_{y_1} = \frac{\partial Y}{\partial \varkappa'} = \frac{1}{f'^2}\left\{\left[\frac{\partial Z}{\partial \varkappa'} y' + Z(a_{22}\bar{x}' - a_{21}\bar{y}')\right] f' - Zy'(a_{32}\bar{x}' - a_{31}\bar{y}')\right\} \tag{I.22.1}$$

$$\bar{f}_{y_2} = \frac{\partial Y}{\partial \varphi'} = \frac{y'}{f'^2}\left(\frac{\partial Z}{\partial \varphi'} f' - Z\, x'\right) \tag{I.22.2}$$

$$\bar{f}_{y_3} = \frac{\partial Y}{\partial \varkappa''} = \frac{y'}{f'}\,\frac{\partial Z}{\partial \varkappa''} \tag{I.22.3}$$

$$\bar{f}_{y_4} = \frac{\partial Y}{\partial \varphi''} = \frac{y'}{f'}\,\frac{\partial Z}{\partial \varphi''} \tag{I.22.4}$$

$$\bar{f}_{y_5} = \frac{\partial Y}{\partial \omega'} = \frac{y'}{f'}\,\frac{\partial Z}{\partial \omega'} \tag{I.22.5}$$

$$f_{y_1} = \frac{\partial Y}{\partial \bar{x}'} = \frac{1}{f'^2}\left[\left(\frac{\partial Z}{\partial x'}\, y' + Z\, a_{21}\right) f' - Z\, y'\, a_{31}\right] \qquad \text{(I.22.6)}$$

$$f_{y_2} = \frac{\partial Y}{\partial \bar{y}'} = \frac{1}{f'^2}\left[\left(\frac{\partial Z}{\partial y'}\, y' + Z\, a_{22}\right) f' - Z\, y'\, a_{32}\right] \qquad \text{(I.22.7)}$$

$$f_{y_3} = \frac{\partial Y}{\partial \bar{x}''} = \frac{y'}{f'}\,\frac{\partial Z}{\partial \bar{x}''} \qquad \text{(I.22.8)}$$

$$f_{y_4} = \frac{\partial Y}{\partial \bar{y}''} = \frac{y'}{f'}\,\frac{\partial Z}{\partial \bar{y}''} \qquad \text{(I.22.9)}$$

$$\frac{\partial Y}{\partial \bar{f}'} = \frac{1}{f'^2}\left[\left(\frac{\partial Z}{\partial \bar{f}'}\, y' + Z\, a_{23}\right) f' - Z\, y'\, a_{33}\right] \qquad \text{(I.22.10)}$$

$$\frac{\partial Y}{\partial \bar{f}''} = \frac{y'}{f'}\,\frac{\partial Z}{\partial \bar{f}''} \qquad \text{(I.22.11)}$$

APPENDIX II

DERIVATION OF A CONDITION EQUATION FOR A MEASURED CONTROL DISTANCE IN OBJECT SPACE

To introduce an analytical equivalent to the "height pole" (Adams, 1978) that is a known distance in the Z-direction of the object space as a restraining condition into the relative orientation adjustment, a condition equation for such a distance must be formulated. This condition equation must influence the orientation angles in such a way that in the adjustment the finally evaluated model co-ordinates agree with the measured control distance. The condition equation for a control distance between any two object points is derived as follows:

A distance in space between points P_i and P_j has the form

$$d^2 = (X_j-X_i)^2 + (Y_j-Y_i)^2 + (Z_j-Z_i)^2 \qquad \text{(II.1)}$$

The X, Y and Z values in (II.1) are model co-ordinates and thus functions of the rectified plate co-ordinates. From (7.8.1.3) to (7.8.1.5) we have

$$X_i = Z_i \frac{x'_i}{f'_i}$$

$$Y_i = Z_i \frac{y'_i}{f'_i}$$

and $$Z_i = \frac{b}{\left[\frac{x'_i}{f'_i} - \frac{x''_i}{f''_i}\right]} = \frac{b}{V_i}$$

The rectified plate co-ordinates x'_i, y'_i, f'_i, x''_i, y''_i and f''_i are in turn functions of the observed image co-ordinates, the principal distances and the orientation angles (7.4.2 and 7.4.3):

$$d = f\ (\ \varkappa', \varphi', \varkappa'', \varphi'', \omega'', \bar{x}'_i, \bar{y}'_i, \bar{x}'_j, \bar{y}'_j, \bar{x}''_i, \bar{y}''_i, \bar{x}''_j, \bar{y}''_j,)$$

substituting the equations for X, Y and Z in (II.1) we obtain

$$\left[(Z_j \frac{x'_j}{f'_j} - Z_i \frac{x'_i}{f'_i})^2 + (Z_j \frac{y'_j}{f'_j} - Z_i \frac{y'_i}{f'_i})^2 + (Z_j - Z_i)^2\right]^{\frac{1}{2}} - d = 0 \qquad \text{(II.2)}$$

or

$$\left\{ Z_i^2 \left[(\frac{x'_i}{f'_i})^2 + (\frac{y'_i}{f'_i})^2 + 1\right] + Z_j^2 \left[(\frac{x'_j}{f'_j})^2 + (\frac{y'_j}{f'_j})^2 + 1\right] - \right.$$

$$\left. - 2 Z_i Z_j \left[\frac{x_i x_j}{f'_i f'_j} + \frac{y_i y_j}{f'_i f'_j} + 1\right] \right\}^{\frac{1}{2}} - d = 0 \qquad \text{(II.3)}$$

and further substituting Z we have

$$\Phi = b \left[\frac{x'^2_i + y'^2_i + f'^2_i}{(V_i f'_i)^2} + \frac{x'^2_j + y'^2_j + f'^2_j}{(V_j f'_j)^2} - 2 \frac{x'_i x'_j + y'_i y'_j + f'_i f'_j}{V_i V_j f'_i f'_j}\right]^{\frac{1}{2}} - d = 0 \qquad \text{(II.4)}$$

we abbreviate

$$\Phi = b \left[\frac{R}{(V_i f'_i)^2} + \frac{S}{(V_j f'_j)^2} - 2 \frac{T}{V_i V_j f'_i f'_j}\right]^{\frac{1}{2}} - d = 0 \qquad \text{(II.5)}$$

with the auxiliary variables

$$R = x'^2_i + y'^2_i + f'^2_i$$

$$S = x'^2_j + y'^2_j + f'^2_j \qquad \text{(II.5.1}$$

$$T = x'_i x'_j + y'_i y'_j + f'_i f'_j$$

and d = measured control distance

The condition equation Φ is not linear and must be differentiated with respect to the unknowns $\varkappa'$, φ', $\varkappa''$, φ'' and ω'' and the observations $\bar{x}'_i$, $\bar{y}'_i$, $\bar{x}''_i$, $\bar{y}''_i$, $\bar{x}'_j$, $\bar{y}'_j$, $\bar{x}''_j$ and $\bar{y}''$.

The final linearised condition equation introduced into the least squares adjustment is then

$$\frac{\partial\Phi}{\partial\varkappa'}\,d\varkappa' + \frac{\partial\Phi}{\partial\varphi'}\,d\varphi' + \frac{\partial\Phi}{\partial\varkappa''}\,d\varkappa'' + \frac{\partial\Phi}{\partial\varphi''}\,d\varphi'' + \frac{\partial\Phi}{\partial\omega''}\,d\omega'' +$$

$$+ \frac{\partial\Phi}{\partial\bar{x}'_i}\,v_{\bar{x}'_i} + \frac{\partial\Phi}{\partial\bar{y}'_i}\,v_{\bar{y}'_i} + \frac{\partial\Phi}{\partial\bar{x}''_i}\,v_{\bar{x}''_i} + \frac{\partial\Phi}{\partial\bar{y}''_i}\,v_{\bar{y}''_i} + \frac{\partial\Phi}{\partial\bar{x}'_j}\,v_{\bar{x}'_j} +$$

$$+ \frac{\partial\Phi}{\partial\bar{y}'_j}\,v_{\bar{y}'_j} + \frac{\partial\Phi}{\partial\bar{x}''_j}\,v_{\bar{x}''_j} + \frac{\partial\Phi}{\partial\bar{y}''_j}\,v_{\bar{y}''_j} + d_o - d = 0 \qquad \text{(II.6)}$$

in which symbol "d" for the differential is used for the corrections to the unknowns and symbol "v" for the corrections to the observations. The measured distance d is assumed to be without error. A provisional value for the distance is evaluated with:

$$d_o = b\left[\frac{R}{(V_i f'_i)^2} + \frac{S}{(V_j f'_j)^2} - 2\,\frac{T}{V_i V_j f'_i f'_j}\right]^{\frac{1}{2}}\Bigg|_o \qquad \text{(II.7)}$$

The thirteen partial derivatives in (II.6) can be derived from the general equation

$$\frac{\partial \Phi}{\partial \alpha} = \frac{b}{2P} \left[\frac{\partial R/\partial\alpha \, (V_i f_i')^2 - 2 R V_i \left(\partial V_i/\partial\alpha \, f_i' + V_i \, \partial f_i'/\partial\alpha \right)}{(V_i f_i')^4} + \right.$$

$$+ \frac{\partial S/\partial\alpha \, (V_j f_j')^2 - 2 S V_j \left(\partial V_j/\partial\alpha \, f_j' + V_j \, \partial f_j'/\partial\alpha \right)}{(V_j f_j')^4} -$$

$$\left. - \frac{\partial T/\partial\alpha \, (V_i V_j f_i' f_j') - T \left[\partial V_i/\partial\alpha \, V_j f_i' f_j' + V_i \partial V_j/\partial\alpha \, f_i' f_j' + V_i V_j \partial f_i'/\partial\alpha \, f_j' + V_i V_j f_i' \partial f_j/\partial\alpha \right]}{(V_i V_j f_i' f_j')^2} \right]$$

(II.8)

or

$$\frac{\partial \Phi}{\partial \alpha} = \frac{b}{2P} \left[\frac{\frac{\partial R}{\partial\alpha} - 2R \left(\frac{\partial V}{\partial\alpha} i / V_i + \frac{\partial f_i'}{\partial\alpha} / f' \right)}{(V_i f_i')^2} + \right.$$

$$+ \frac{\frac{\partial S}{\partial\alpha} - 2S \left(\frac{\partial V}{\partial\alpha} j / V_j + \frac{\partial f_j'}{\partial\alpha} / f_j' \right)}{(V_j f_j')^2} -$$

$$\left. - 2 \frac{\frac{\partial T}{\partial\alpha} - T \left(\frac{\partial V}{\partial\alpha} i / V_i + \frac{\partial f_i'}{\partial\alpha} / f_i' + \frac{\partial V}{\partial\alpha} j / V_j + \frac{\partial f_j'}{\partial\alpha} / f_j' \right)}{V_i V_j f_i' f_j'} \right] \qquad \text{(II.9)}$$

with $$P = \left[\frac{R}{(V_i f_i')^2} + \frac{S}{(V_j f_j')^2} - 2 \frac{T}{V_i V_j f_i' f_j'} \right]^{\frac{1}{2}}$$

and $$\alpha = \varkappa', \varphi', \varkappa'', \varphi'', \omega'', \bar{x}_i', \bar{y}_i', \bar{x}_i'', \bar{y}_i'', \bar{x}_j', \bar{y}_j', \bar{x}_j'', \bar{y}_j'' .$$

Equations for the rectified co-ordinates x', y', f', for the rotation matrix $\underline{R}$ and for the partial derivatives of $\underline{R}$ are given by (7.4.2 and 7.4.3), (7.4.2.2 and 7.4.3.2) and (3.1.15 and 3.1.16) respectively.

The individual partial derivatives of the auxiliary variables R, S, T, V_i and V_j as well as the rectified principal distances f'_i and f'_j as they occur in equations (II.8) and (II.9) are listed in Table II-1.

The complete linearised form of the condition equation for a control distance (7.10.3) can now be formulated by substituting the partial derivatives listed in Table II-1 into the thirteen partial derivatives of type (II.9). These in turn are substituted into (II.6) to form the final equation.

Equation (II.6) with all substitutions is very elaborate and therefore not quoted in full. (The full formula contains close to 800 symbols for variables, observations and constants; in spite of this large number of values the equation is relatively easy to program. (See computer program in Appendix IV))

	∂R	∂S	∂T	∂V_i	∂V_j	$\partial f_i'$	$\partial f_j'$
$\partial\kappa'$	$2\left[x_i'(a_{12}\bar{x}_i'-a_{11}\bar{y}_i')+ +y_i'(a_{22}\bar{x}_i'-a_{21}\bar{y}_I')+ +f_i'(a_{32}\bar{x}_i'-a_{31}\bar{y}_i')\right]$	$2\left[x_j'(a_{12}\bar{x}_j'-a_{11}\bar{y}_j')+ +\bar{y}_j'(a_{22}\bar{x}_j'-a_{21}y_j')+ +f_j'(a_{32}\bar{y}_j'-a_{31}\bar{y}_j')\right]$	*	$\frac{(a_{12}\bar{x}_i'-a_{11}\bar{y}_i')f_i'-(a_{32}\bar{x}_i'-a_{31}\bar{y}_i')x_i'}{f_i'^2}$	$\frac{(a_{12}\bar{x}_j'-a_{11}\bar{y}_j')f_j'-(a_{32}\bar{x}_j'-a_{31}\bar{y}_j')x_j'}{f_j'^2}$	$a_{32}\bar{x}_i'-a_{31}\bar{y}_i'$	$a_{32}\bar{x}_j'-a_{31}\bar{y}_j'$
$\partial\phi'$	0	0	0	$-1-\frac{x_i'^2}{f_i'^2}$	$-1-\frac{x_j'^2}{f_j'^2}$	x_i'	x_j'
$\partial\kappa''$	0	0	0	$\frac{(b_{12}\bar{x}_i''-b_{11}\bar{y}_i'')f_i''-(b_{32}\bar{x}_i''-b_{31}\bar{y}_i'')x_i''}{f_i''^2}$	$-\frac{(b_{12}\bar{x}_j''-b_{11}\bar{y}_j'')f_j''-(b_{32}\bar{x}_j''b_{31}\bar{y}_j'')y_j''}{f_j''^2}$	0	0
$\partial\phi''$	0	0	0	$\frac{C_i+(x_i''^2\cos\omega'')}{f_i''^2}$	$\frac{C_j+(x_j''^2\cos\omega'')}{f_j''^2}$	0	0
$\partial\omega''$	0	0	0	$-\frac{x_i''y_i''}{f_i''^2}$	$-\frac{x_j''y_j''}{f_j''^2}$	0	0
$\partial\bar{x}_i'$	$2\left(x_i'a_{11}+y_i'a_{21}+f_i'a_{31}\right)$	0	$\frac{1}{2}\frac{\partial S}{\partial\bar{x}_j'}$	$\frac{a_{11}f_i'-a_{31}x_i'}{f_i'^2}$	0	a_{31}	0
$\partial\bar{y}_i'$	$2\left(x_i'a_{12}+y_i'a_{32}+f_i'a_{32}\right)$	0	$\frac{1}{2}\frac{\partial S}{\partial\bar{y}_j'}$	$\frac{a_{12}f_i'-a_{32}x_i'}{f_i'^2}$	0	a_{32}	0
$\partial\bar{x}_i''$	0	0	0	$-\frac{b_{11}f_i''-b_{31}x_i''}{f_i''^2}$	0	0	0
$\partial\bar{y}_i''$	0	0	0	$-\frac{b_{12}f_i''-b_{32}x_i''}{f_i''^2}$	0	0	0
$\partial\bar{x}_j''$	0	$2\left(x_j'a_{11}+y_j'a_{21}+f_j'a_{31}\right)$	$\frac{1}{2}\frac{\partial R}{\partial\bar{x}_i'}$	0	$\frac{a_{11}f_j'-a_{31}x_j'}{f_j'^2}$	0	a_{31}
$\partial\bar{y}_j'$	0	$2\left(x_j'a_{12}+y_j'a_{22}+f_ja_{32}\right)$	$\frac{1}{2}\frac{\partial R}{\partial\bar{y}_i'}$	0	$\frac{a_{12}f_j'-a_{32}x_j'}{f_j'^2}$	0	a_{32}
$\partial\bar{x}_j''$	0	0	0	0	$-\frac{b_{11}f_j''-b_{31}x_j''}{f_j''^2}$	0	0
$\partial\bar{y}_j''$	0	0	0	0	$-\frac{b_{12}f_j''-b_{32}x_j''}{f_j''^2}$	0	0

Table II-1

$$\frac{\partial T}{\partial\kappa} = (a_{12}\bar{x}_i'-a_{11}\bar{y}_i')x_j'+(a_{22}x_i'-a_{21}\bar{y}_i')y_j'+(a_{32}\bar{x}_i'-a_{31}\bar{y}_i')f_j'$$
$$+(a_{12}\bar{x}_j'-a_{11}\bar{y}_j')x_j'+(a_{22}\bar{x}_j'-a_{21}\bar{y}_j')y_i'+(a_{32}\bar{x}_j'-a_{31}\bar{y}_j')f_i'$$

$C_i = (\cos\kappa''\sin\phi''\bar{x}_i''-\sin\kappa''\sin\phi''\bar{y}_i''+\cos\phi''\bar{f}_i'')f_i''$

$C_j = (\cos\kappa''\sin\phi''\bar{x}_j''\sin\kappa''\sin\phi''\bar{y}_j+\cos\phi''\bar{f}_j'')f_j''$

APPENDIX III

DERIVATION OF AN ALGORITHM FOR THE INCORPORATION OF A CONTROL DISTANCE CONDITION EQUATION INTO THE RELATIVE ORIENTATION ADJUSTMENT

The introduction of additional condition equations for control distances (Chapter 7.10) modifies the equation system (3.2.4)

$$\underline{Bv} + \underline{Ax} + \underline{w} = \underline{0}$$

in such a way that it is no longer possible to make use of the memory-saving quasi-parametric adjustment for the relative orientation.

Throughout this thesis algorithms are designed to permit the application of mini computers with limited memory space to all necessary numerical solutions.

With this objective in view, an abbreviated matrix algorithm for the addition of condition equations is developed.

The inclusion of a control distance condition equation changes the normal equation system of the relative orientation adjustment and the matrix of observation coefficients $\underline{B}$ becomes:

$$\underline{\tilde{B}} = \begin{array}{c} \begin{array}{cccccccc|cccc|cccc|cccc} 1 & 2 & 3 & 4 & 5 & 6 & 7 & 8 & 4k-3 & 4k-2 & 4k-1 & 4k & ..4\ell-3 & 4\ell-2 & 4\ell-1 & 4\ell & ..4n-3 & 4n-2 & 4n-1 & 4n \end{array} \\ \left[\begin{array}{cccccccc|cccc|cccc|cccc} B & 0 & B & 0 & & & & & & & & & & & & & & & & \\ & & & & B & B & B & B & & & & & & & & & & & & \\ & & & & & & & & B & B & B & B & & & & & & & & \\ & & & & & & & & & & & & B & B & B & B & & & & \\ & & & & & & & & & & & & & & & & B & B & B & B \\ & & & & & & & & B & B & B & B & B & B & B & B & & & & \end{array}\right] \end{array} \begin{array}{c} 1 \\ 2 \\ k \\ \ell \\ n \\ n+1 \end{array} \qquad \text{(III.1)}$$

Values shown against the margin of the matrix indicate column and row numbers (= point numbers) and symbol B indicates a non-zero element in the matrix. All other elements of $\underline{\bar{B}}$ are zero elements. The control distance is measured between points ℓ and k. Row n+1 contains the distance equation. This row prohibits the use of the quasi-parametric case, which becomes obvious when forming $\underline{\bar{B}}\ \underline{P}^{-1}\ \underline{\bar{B}}^T$.

If we formulate $(\underline{\bar{B}}\ \underline{P}^{-1}\ \underline{\bar{B}}^T)$ we obtain:

$$\underline{\bar{N}} = \left[\begin{array}{ccccccc|c} [B_1^2] & & & & & & & \\ & [B_2^2] & & & & & & \\ & & [B_k^2] & & & & & [B_k B_{n+1}] \\ & & & & [B_\ell^2] & & & [B_\ell B_{n+1}] \\ & & & & & & [B_n^2] & \\ \hline & & [B_k B_{n+1}] & & [B_\ell B_{n+1}] & & & [B_{n+1}^2] \end{array}\right] \quad \text{(III.}$$

To simplify the derivation, weights are included into the B terms and $|B_j^2|$ stands for

$$[B_j^2] = \frac{B_{j,1}}{\sqrt{P_{j,1}}} + \frac{B_{j,2}}{\sqrt{P_{j,2}}} + \frac{B_{j,3}}{\sqrt{P_{j,3}}} + \frac{B_{j,4}}{\sqrt{P_{j,4}}} \qquad \text{(III.2.1}$$

Matrix $\underline{\bar{N}}$ is no longer a principal diagonal matrix thus excluding the quasi-parametric case as a solution method.

---

(1) The symbol [ ] indicates summation.

If we introduce submatrices and vectors as indicated in (III.2) one can write for $\bar{\underline{N}}$:

$$\bar{\underline{N}} = \left[\begin{array}{c|c} \underline{R} & \underline{u}^T \\ \hline \underline{u} & r \end{array}\right] \tag{III.3}$$

The inverse of $\bar{\underline{N}}$ can be found by means of the "Bordering method" as described by Faddeev, Faddeeva, 1963.

$$\bar{\underline{Q}} = \bar{\underline{N}}^{-} = \left[\begin{array}{c|c} \underline{R}^{-1} + \dfrac{\underline{R}^{-1}\,\underline{u}^T\underline{u}\underline{R}^{-1}}{\alpha} & -\dfrac{\underline{R}^{-1}\,\underline{u}^T}{\alpha} \\ \hline -\dfrac{\underline{u}\,\underline{R}^{-1}}{\alpha} & \dfrac{1}{\alpha} \end{array}\right] \tag{III.4}$$

with $\alpha = r - \underline{u}\,\underline{R}^{-1}\,\underline{u}^T$ (III.5)

and substituting the elements of (III.2) into (III.4) the inverse of $\bar{\underline{N}}$ becomes:

$$\bar{\underline{Q}} = \left[\begin{array}{cccc|c} \frac{1}{[B_1^2]} & & & & \\ & \frac{1}{[B_2^2]} & & & \\ & & \frac{1}{[B_k^2]} + \frac{1}{\alpha}\frac{[B_kB_{n+1}]^2}{[B_k^2]} & \frac{1}{\alpha}\frac{[B_kB_{n+1}]\,[B_\ell B_{n+1}]}{[B_k^2]\,[B_\ell^2]} & -\frac{1}{\alpha}\frac{[B_kB_{n+1}]}{[B_k^2]} \\ & & \frac{1}{\alpha}\frac{[B_kB_{n+1}]\,[B_\ell B_{n+1}]}{[B_k^2]\,[B_\ell^2]} & \frac{1}{[B_\ell^2]} + \frac{1}{\alpha}\frac{[B_\ell B_{n+1}]^2}{[B_\ell^2]} & -\frac{1}{\alpha}\frac{[B_\ell B_{n+1}]}{[B_\ell^2]} \\ \hline & & -\frac{1}{\alpha}\frac{[B_kB_{n+1}]}{[B_k^2]} & -\frac{1}{\alpha}\frac{[B_\ell B_{n+1}]}{[B_\ell^2]} & \frac{1}{[B_n^2]} \\ & & & & \frac{1}{\alpha} \end{array}\right] \tag{III.6}$$

$$\alpha = [B_{n+1}^2] - \frac{[B_kB_{n+1}]^2}{[B_k^2]} - \frac{[B_\ell B_{n+1}]^2}{[B_\ell^2]} \tag{III.7}$$

We can split matrix $\underline{\bar{Q}}$ into matrices $\underline{\hat{Q}}$ and $\underline{\tilde{Q}}$, where $\underline{\hat{Q}}$ contains the elements of the original matrix $(\underline{B}\ \underline{P}^{-1}\underline{B}^T)^{-1}$ of the relative orientation adjustment without the condition equation for a control distance with an added border of zero elements. $\underline{\tilde{Q}}$ contains those elements of $\underline{\bar{Q}}$ which result from the addition of the condition equation

$$\underline{\hat{Q}} = (\underline{B}\ \underline{P}^{-1}\ \underline{B}^T)^{-1} + \text{"zero border"} \tag{III.8.1}$$

$$\underline{\bar{Q}} = \underline{\hat{Q}} + \frac{1}{\alpha}\,\underline{\tilde{Q}} \tag{III.8.2}$$

with

$$\underline{\hat{Q}} = \left[\begin{array}{ccccc|c} \frac{1}{[B_1^2]} & & & & & 0 \\ & \frac{1}{[B_2^2]} & & & & 0 \\ & & \frac{1}{[B_k^2]} & & & 0 \\ & & & \frac{1}{[B_\ell^2]} & & 0 \\ & & & & \frac{1}{[B_n^2]} & 0 \\ \hline 0 & 0 & 0 & 0 & 0 & 0 \end{array}\right] \tag{III.9}$$

and

$$\underline{\tilde{Q}} = \left[\begin{array}{ccc} 0 & 0 & \\ 0 & 0 & \\ & & \frac{[B_kB_{n+1}]^2}{[B_k^2]^2} \quad \frac{[B_kB_{n+1}]\ [B_\ell B_{n+1}]}{[B_k^2]\ [B_\ell^2]} \quad -\frac{[B_kB_{n+1}]}{[B_k^2]} \\ & & \frac{[B_kB_{n+1}]\ [B_\ell B_{n+1}]}{[B_k^2]\ [B_\ell^2]} \quad \frac{[B_\ell B_{n+1}]^2}{[B_\ell^2]^2} \quad -\frac{[B_\ell B_{n+1}]}{[B_\ell^2]} \\ & & -\frac{[B_kB_{n+1}]}{[B_k^2]} \quad -\frac{[B_\ell B_{n+1}]}{[B_\ell^2]} \quad 1 \end{array}\right] \tag{III.10}$$

The solution vector is then

$$\underline{x} = -(\underline{A}^T (\hat{\underline{Q}} + \frac{1}{\alpha} \tilde{\underline{Q}})\underline{A})^{-1} \underline{A}^T (\hat{\underline{Q}} + \frac{1}{\alpha} \tilde{\underline{Q}})\underline{w} \qquad \text{(III.11)}$$

$$\underline{x} = -(\underline{A}^T \hat{\underline{Q}} \underline{A} + \frac{1}{\alpha} \underline{A}^T \tilde{\underline{Q}} \underline{A})^{-1} (\underline{A}^T \hat{\underline{Q}} \underline{w} + \frac{1}{\alpha} \underline{A}^T \tilde{\underline{Q}} \underline{w}) \qquad \text{(III.11.1)}$$

In (III.11.1) matrices $\underline{A}^T \hat{\underline{Q}} \underline{A}$ and $\underline{A}^T \hat{\underline{Q}} \underline{w}$ can be formulated as in the quasi-parametric case. They are in fact the matrices as found in the relative orientation adjustment without restraints:

$$\underline{A}^T \hat{\underline{Q}} \underline{A} = \underline{A}^T \underline{P}^* \underline{A} \qquad \text{(III.12)}$$

and

$$\underline{A}^T \hat{\underline{Q}} \underline{w} = \underline{A}^T \underline{P}^* \underline{w} \qquad \text{(III.13)}$$

Matrices $\frac{1}{\alpha} (\underline{A}^T \tilde{\underline{Q}} \underline{A})$ and $\frac{1}{\alpha} (\underline{A}^T \tilde{\underline{Q}} \underline{w})$ contain the contribution of the distance condition and if a memory-saving technique can be found to formulate these two matrices directly the combined case can be avoided and one can revert to the convenient quasi-paramatric case. Inspection of the $\tilde{Q}$ matrix shows that it only contains non-zero elements in rows and columns k, ℓ and n+1.

$\underline{A}^T \tilde{\underline{Q}} \underline{A}$ therefore becomes simply

$$\underline{A}^T \tilde{\underline{Q}}\underline{A} = \begin{bmatrix} A_{k,1} & A_{\ell,1} & A_{n+1,1} \\ A_{k,2} & A_{\ell,2} & A_{n+1,2} \\ A_{k,3} & A_{\ell,3} & A_{n+1,3} \\ A_{k,4} & A_{\ell,4} & A_{n+1,4} \\ A_{k,5} & A_{\ell,5} & A_{n+1,5} \end{bmatrix} \begin{bmatrix} \tilde{Q}_{k,k} & \tilde{Q}_{k,\ell} & \tilde{Q}_{k,n+1} \\ \tilde{Q}_{\ell,k} & \tilde{Q}_{\ell,\ell} & \tilde{Q}_{\ell,n+1} \\ \tilde{Q}_{n+1,k} & \tilde{Q}_{n+1,\ell} & \tilde{Q}_{n+1,n+1} \end{bmatrix} \begin{bmatrix} A_{k,1} \cdots & A_{k,5} \\ A_{\ell,1} \cdots & A_{\ell,5} \\ A_{n+1,1} \cdots & A_{n+1,5} \end{bmatrix} \qquad \text{(III.1}$$

$$\tilde{Q}_{k,k} = \left[\frac{\left[B_k B_{n+1}\right]^2}{\left[B_k^2\right]^2}\right] \qquad \text{(III.14.1)}$$

$$\tilde{Q}_{k,\ell} = \tilde{Q}_{\ell,k} = \frac{\left[B_k B_{n+1}\right]}{\left[B_k^2\right]} \frac{\left[B_\ell B_{n+1}\right]}{\left[B_\ell^2\right]} \qquad \text{(III.14.2)}$$

$$\tilde{Q}_{\ell,\ell} = \frac{\left[B_\ell B_{n+1}\right]^2}{\left[B_\ell^2\right]^2} \qquad \text{(III.14.3)}$$

$$\tilde{Q}_{k,n+1} = \tilde{Q}_{n+1,\ell} = -\frac{\left[B_k B_{n+1}\right]}{\left[B_k^2\right]} \qquad \text{(III.14.4)}$$

$$\tilde{Q}_{\ell,n+1} = \tilde{Q}_{n+1,\ell} = -\frac{\left[B_\ell B_{n+1}\right]}{\left[B_\ell^2\right]} \qquad \text{(III.14.5)}$$

$$\tilde{Q}_{n+1,n+1} = 1 \qquad \text{(III.14.6)}$$

and with α as in (III.7).

The matrix $\underline{A}^T \underline{\tilde{Q}w}$ can be determined in a similar way:

$$\underline{A}^T \underline{\tilde{Q}w} = \begin{bmatrix} A_{k,1} & A_{\ell,1} & A_{n+1,1} \\ A_{k,2} & A_{\ell,2} & A_{n+1,2} \\ A_{k,3} & A_{\ell,3} & A_{n+1,3} \\ A_{k,4} & A_{\ell,4} & A_{n+1,4} \\ A_{k,5} & A_{\ell,5} & A_{n+1,k} \end{bmatrix} \begin{bmatrix} \tilde{Q}_{k,k} & \tilde{Q}_{k,l} & \tilde{Q}_{k,n+1} \\ \tilde{Q}_{\ell,k} & \tilde{Q}_{\ell,\ell} & \tilde{Q}_{\ell,n+1} \\ \tilde{Q}_{n+1,k} & \tilde{Q}_{n+1,\ell} & \tilde{Q}_{n+1,n+1} \end{bmatrix} \begin{bmatrix} w_k \\ w_\ell \\ w_{n+1} \end{bmatrix} \qquad \text{(III.15)}$$

The terms B_k and B_ℓ in the $\tilde{Q}$ elements of (III.14) and (III.15) are the coefficients of $v_{x'_k}$, $v_{y'_k}$, $v_{x''_k}$, $v_{y''_k}$ and $v_{x'_\ell}$, $v_{y'_\ell}$, $v_{x''_\ell}$, $v_{y''_\ell}$ as in (7.4.10) in the original relative orientation adjustment without restraints, while the B_{n+1} terms are the coefficients of the same corrections v in the additional condition equation.

The solution vector $\underline{x}$ can now be determined by adding the matrices $\frac{1}{\alpha}\,(\underline{A}^T\tilde{\underline{Q}}\,\underline{A})$ and $\frac{1}{\alpha}\,(\underline{A}^T\tilde{\underline{Q}}\,\underline{w})$ to the original matrices $\underline{A}^T\,\underline{P}^*\,\underline{A}$ and $\underline{A}^T\,\underline{P}^*\,\underline{w}$ as in (III.12). In this method it is not necessary to formulate the full $\underline{B}$ and $\underline{B}^T$ matrices at any stage of the calculation procedure and the quasi-parametric approach can be maintained in principle. It remains to determine the correction vector $\underline{v}$ in a similarly abbreviated technique. The equation for the corrections is given by (3.2.9) and (3.2.12).

$$\underline{v} = -\,\underline{P}\,\underline{B}^T\bar{\underline{Q}}\,(\underline{A}\,x + \underline{w})$$

as in (III.2.1) $\underline{P}$ is incorporated into $\underline{B}^T$ and we have

$$\underline{v} = -\,\underline{B}^T\bar{\underline{Q}}\,(\underline{A}\,\underline{x} + \underline{w}) \qquad \text{(III.16)}$$

and with (III.8)

$$\underline{v} = -\,\underline{B}^T\hat{\underline{Q}}\,(\underline{A}\,\underline{x} + \underline{w}) - \frac{1}{\alpha}\,\underline{B}^T\tilde{\underline{Q}}\,(\underline{A}\,\underline{x} + \underline{w}) \qquad \text{(III.17)}$$

Again corrections $\underline{v}$ can be evaluated as in the adjustment and the contribution of the distance condition can be determined separately from $\underline{B}^T\tilde{\underline{Q}}\,(\underline{A}\,\underline{x} + \underline{w})$.

Once more the zero rows and columns can be eliminated and $\underline{B}^T\tilde{\underline{Q}}$ can be written in full as:

$$\underline{B}^T\tilde{\underline{Q}} = \begin{bmatrix} B_{k,4k-3} & 0 & B_{n+1,4k-3} \\ B_{k,4k-2} & 0 & B_{n+1,4k-2} \\ B_{k,4k-1} & 0 & B_{n+1,4k-1} \\ B_{k,4k} & 0 & B_{n+1,4k} \\ 0 & B_{\ell,4\ell-3} & B_{n+1,4\ell-3} \\ 0 & B_{\ell,4\ell-2} & B_{n+1,4\ell-2} \\ 0 & B_{\ell,4\ell-1} & B_{n+1,4\ell-1} \\ 0 & B_{\ell,4\ell} & B_{n+1,4\ell} \end{bmatrix} \begin{bmatrix} \tilde{Q}_{k,k} & \tilde{Q}_{k,\ell} & \tilde{Q}_{k,n+1} \\ \tilde{Q}_{\ell,k} & \tilde{Q}_{\ell,\ell} & \tilde{Q}_{\ell,n+1} \\ \tilde{Q}_{n+1,k} & \tilde{Q}_{n+1,\ell} & \tilde{Q}_{n+1,n+1} \end{bmatrix} \qquad \text{(III.18)}$$

When multiplying $\underline{B}^T\tilde{\underline{Q}}$ by $(\underline{A}\ \underline{x} + \underline{w})$ only the three elements of $(\underline{A}\ \underline{x} + \underline{w})$ in rows k,ℓ and $n+1$ are involved and we replace $(\underline{A}\ \underline{x} + \underline{w})$ by

$$(\underline{A}\ \underline{x} + \underline{w}) \rightarrow \begin{bmatrix} (\underline{A}\ \underline{x} + \underline{w})_k \\ (\underline{A}\ \underline{x} + \underline{w})_\ell \\ (\underline{A}\ \underline{x} + \underline{w})_{n+1} \end{bmatrix} \qquad \text{(III.19)}$$

The final corrections can now easily be found by multiplying $B^T\tilde{\underline{Q}}$ by the three elements of $(\underline{A}\ \underline{x} + \underline{w})$ and the correction $\bar{v}$ for the eight plate co-ordinates associated with the two end points of the control distance can be determined directly from:

$$\bar{v}_{\bar{x}'_k} = v_{\bar{x}'_k} - \frac{1}{\alpha P_{\bar{x}'_k}} \left\{ \left(B_{k,4k-3}\, \tilde{Q}_{k,k} + B_{n+1,4k-3}\, \tilde{Q}_{k,n+1} \right) (\underline{A}\,\underline{x} + \underline{w}) + \right.$$

$$+ \left(B_{k,4k-3}\, \tilde{Q}_{k,\ell} + B_{n+1,4k-3}\, \tilde{Q}_{\ell,n+1} \right) (\underline{A}\,\underline{x} + \underline{w}) +$$

$$\left. + \left(B_{k,4k-3}\, \tilde{Q}_{k,n+1} - B_{n+1,4k-3} \right) (A\,x + w)_{n+1} \right\} \quad \text{(III.20.1)}$$

Weights are reintroduced in the above equation.

The equations for the remaining three corrections for co-ordinates of point P_k are found by replacing

for $\bar{v}_{\bar{y}'_k}$: $P_{\bar{x}'_k}$ by $P_{\bar{y}'_k}$; $B_{k,4k-3}$ by $B_{k,4k-2}$; $B_{n+1,4k-3}$ by $B_{n+1,4k-2}$ (III.20.2)

for $\bar{v}_{\bar{x}''_k}$: " by $P_{\bar{x}''_k}$; " by $B_{k,4k-1}$; " by $B_{n+1,4k-1}$ (III.20.3)

for $\bar{v}_{\bar{y}''_k}$: " by $P_{\bar{y}''_k}$; " by $B_{k,4k}$; " by $B_{n+1,4k}$ (III.20.4)

For the equivalent corrections for point P_ℓ all "k" indices in (III.20.1) to (III.20.4) are replaced by "ℓ".

Although the derivation of the formulae may seem somewhat elaborate, programming of the derived formulae is easy and the considerable memory-saving achieved merits the complete derivation.

We can now summarise the calculation procedure required for the addition of one (or more) additional distance condition to the relative orientation adjustment:

1) Matrices $\underline{A}^T \underline{P}^* \underline{A}$ and $\underline{A}^T \underline{P}^* \underline{w}$ are formed as for the adjustment without restraints.

2) The linearised condition equation for a distance between points P_k and P_ℓ is formulated as in Appendix II. The five coefficients of the unknowns in this equation are arranged in a row vector $\underline{A}_{n+1}$.

3) Applying the coefficients of the corrections in the condition equation to equations (III.14.1) to (III.14.6) the $\tilde{Q}$ matrix is formed and α is determined from (III.7).

4) The reduced $\underline{A}$ matrix is formulated as in (III.14) and $\underline{A}^T\tilde{\underline{Q}}\,\underline{A}$ is evaluated and added to $\underline{A}^T\underline{P}^*\underline{A}$:

$$\underline{A}^T\underline{P}^*\underline{A} + \underline{A}^T\tilde{\underline{Q}}\,\underline{A}$$

This matrix is inverted.(1)

5) The abbreviated $\underline{w}$ is formulated as in (III.15) and $\underline{A}^T\tilde{\underline{Q}}\,\underline{w}$ is evaluated and added to $\underline{A}^T\underline{P}^*\underline{w}$

6) The solution vector is then found from

$$\underline{x} = -(\underline{A}^T\underline{P}^*\underline{A} + \frac{1}{\alpha}\underline{A}^T\tilde{\underline{Q}}\,\underline{A})^{-1}(\underline{A}^T\underline{P}^*\underline{w} + \frac{1}{\alpha}\underline{A}^T\tilde{\underline{Q}}\,\underline{w})$$

7) Corrections v are evaluated as in the original adjustment and additions (III.20) are applied to find corrections $\bar{v}$.

8) Checks and error analysis are executed as usual.

---

(1) Because of the zero border of $\hat{Q}$ (III.8.1) $\underline{A}^T\underline{P}^*\underline{A}$ is equal to $\underline{A}^T\hat{\underline{Q}}\,\underline{A}$.

This technique can also be applied to more than one control distance provided none of the end points of the control distances are common to any two distances. In that case steps 2 to 5 are repeated for each new control distance and the resulting $\underline{A}^T\underline{Q}\,\underline{A}$ and $\underline{A}^T\underline{Q}\,\underline{w}$ matrices are added to the original matrices.

If the combined case of adjustment is applied instead of the method here described, matrix system (3.2.4) can contain any reasonable number of condition equations between any two points of the object space.

APPENDIX IV

Program documentation

Least Squares Adjustment of Relative Orientation

PROGRAM:	Relative Orientation	INSTALLATION:	Tektronix 4051 with 32K memory
AUTHOR:	H. Rüther	LANGUAGE:	Tektronix BASIC
DATE:	1982		

Type: Main program with subroutines. (The program is stored in four separate files owing to memory limitations. Program sections are called up by the main program.)

Auxiliary Equipment: Line printer, file manager for flexible disks

Objective: To determine orientation angles and model co-ordinates in a photogrammetric relative orientation based on the coplanarity condition

THEORY

The relative orientation of a stereo pair of photographic images is established by means of the coplanarity conditions in the form

$$y' - \frac{f'}{f''} y'' = 0$$

The quasi-parametric case of the least squares theory is employed.

Details of the functional model of the relative orientations are given in Chapter 7.

Provision is made for the introduction of a control distance for the correction of possible convergency errors (Chapter 7.10 and Appendices II and III).

INPUT: DATA is input in two forms:

i) Separate DATA files (BASIC)

The DATA statements on files must be in the form:

100 DATA "Project name", number of points, base length

110 DATA (plate co-ordinates) left $\bar{x}'_i$, left $\bar{y}'_i$, right $\bar{x}''_i$, right $\bar{x}''_i$

120 DATA $\bar{x}'_{i+1}$, $\bar{y}'_{i+1}$, $\bar{x}''_{i+1}$, $\bar{y}''_{i+1}$

say 200 DATA left P.D., right P.D., 0,0

Points are automatically numbered from 1 to n.

ii) Keyboard entry

The following questions will appear on the screen once the program run is initiated:

1. "DATA from disk file?" Enter: file name of file on which the data are stored.

2. "Do you require a matrix assessment?" Enter: yes/no

If affirmative, condition numbers will be evaluated after inversion of the normal equation matrix.

3. "Are the right place co-ordinates parallax readings?"

Enter: yes/no

If the stereo pair is observed on a stereo comparator, the plate co-ordinates of the right image are x- and y- parallax readings and must be added to the corresponding left image co-ordinates. This addition is executed if "yes" is entered.

4. "Is a distance in model space known?" Enter: yes/no

If affirmative, a convergency error correction will be applied. The point numbers of the end points of the control distances and the measured length is to be entered later.

5. "Do you require distances from model co-ordinates?"

Enter: yes/no

If affirmative, distances and directions between model points will be printed out at the end of the run. An affirmative answer requires additional DATA lines at the end of the DATA file in which the numbers of points are listed between which distances are required, for example

DATA 1,5,0,3,6,0,.....5,8,1

a "1" after the two point numbers indicates termination of this routine.

6. "Are fiducial marks observed?" Enter: yes/no

If affirmative, intersections of the fiducial mark connection lines are evaluated for both plates. In this case two DATA lines must be added to the DATA file after the first DATA line (containing project name, point number and base length). These

two DATA lines must contain the left and right plates fiducial mark co-ordinates measured in the same system as the plate co-ordinates in the sequence: top, right, bottom, left, as seen on the positive image.

101 DATA $\bar{x}'_T, \bar{y}'_T, \bar{x}'_R, \bar{y}'_R, \bar{x}'_B, \bar{y}'_B, \bar{x}'_L, \bar{y}'_L,$ (left image)

102 DATA $\bar{x}''_T, \bar{y}''_T, \bar{x}''_R, \bar{y}''_R, \bar{x}''_B, \bar{y}''_B, \bar{x}''_L, \bar{y}''_L,$ (right image)

If the answer is negative the principal point position in the comparator co-ordinate system is assumed to be $\bar{x}_o$ = zero and $\bar{y}_o$ = zero for both images. Should the principal point co-ordinates differ from zero and their values are known, then these can be introduced directly into the program section I by changing lines 470 to 500 to the known co-ordinate values.

470 E(1) = $\bar{x}'_o$ left principal point

480 E(2) = $\bar{y}'_o$ left principal point

490 E(3) = $\bar{x}'_o$ right principal point

500 E(4) = $\bar{y}'_o$ right principal point

Also, the GO TO statement in line 510 must be eliminated in this case.

7. "Do you want to enter provisional orientation angles?"

Enter: yes/no

If affirmative, program execution will be interrupted after the printout of the observed image co-ordinates and the provisional values for the five orientation angles can be entered via the keyboard.

8. "How many points to be excluded?"

This option can be employed if image co-ordinates of points of suspected poor quality are to be excluded from the adjustment. These points then play no role in the determination of the

orientation angles, although their model co-ordinates will be evaluated. If all points are to be used in the adjustment values, "zero" is entered.

At the end of the run the option is offered to evaluate the model co-ordinates of further points which can be entered in the form of image co-ordinates from disk files as in i), or as individual points directly via the keyboard.

Note: Input and output units of all quantities are "mm" with the exception of base length and plate co-ordinates which are in units of "m".

OUTPUT:

i) Project name, base length, principal distances, observed image co-ordinates and parallax readings where applicable.

ii) Intermediate results for the unknown orientation angles at each iteration step.
(If a control distance was introduced, then the coefficients of the distance condition equation and the discrepancy term v are printed out as well as the intermediate results of further iterations necessitated by the added condition.)

iii) Corrections v to observed plate co-ordinates and adjusted plate co-ordinates, $\underline{v}^T\underline{P}\underline{v}$ and variance factors, check for $\underline{v}^T\underline{P}\underline{v}$. Note that the $\underline{v}^T\underline{P}\underline{v}$ check compares the sum of all quasi-corrections and weights $\underline{V}^{*T}\underline{P}^*\underline{V}^*$ with $\underline{v}^T\underline{P}\underline{v}$. These quantities are not expected to agree if a control distance condition is added owing to the way in which the bordering method is employed (Appendixes II and III).

iv) Rectified image co-ordinates and global check. (In the global

check the rectified image co-ordinates are evaluated from the most probable values for the orientation angles and the adjusted image co-ordinates. The rectified co-ordinates are introduced into the coplanarity condition

$$y' - \frac{f'}{f''} y'' = 0$$

which should be satisfied within the numerical accuracy of the computer system employed.

v) Model co-ordinates and their standard deviations.

vi) If required, distances between model points.

LIMITATIONS:

i) To obtain the co-ordinate of the principal point, fiducial marks or fiducial mark equivalents must be measured in the same system as the plate co-ordinates, or the principal point position must be determined by some other means.

ii) Not more than 30 points can be adjusted in a Tektronix 4051 with a Tektronix core memory of 32K.

iii) There is some limitation of the size of the orientation angles. It is impossible to stipulate numerical threshhold values up to which convergence can be guaranteed; there are too many possible permutations of the five angles. The program has been successfully tested for situations in which the values for $\varkappa'$, φ', $\varkappa''$, φ'' and ω'' varied between 0° and 15°. Convergence was also achieved with one of the five angles being close to 40° while the remaining four were less than 5°.

Note: Some of the subroutine addresses in the following program

listing seemingly direct program executions to non-existing program lines. It must be borne in mind here that the program had to be broken up into two main sections and two subsections which are stored on different files and appended to form the complete program - line numbers change when a program is appended and this must be taken into consideration when directing the program to subroutines or other addresses. Table V-1 shows a flowchart of the relative orientation adjustment, which is followed by a program listing.

BASIC PROGRAM FOR RELATIVE ORIENTATION ADJUSTMENT

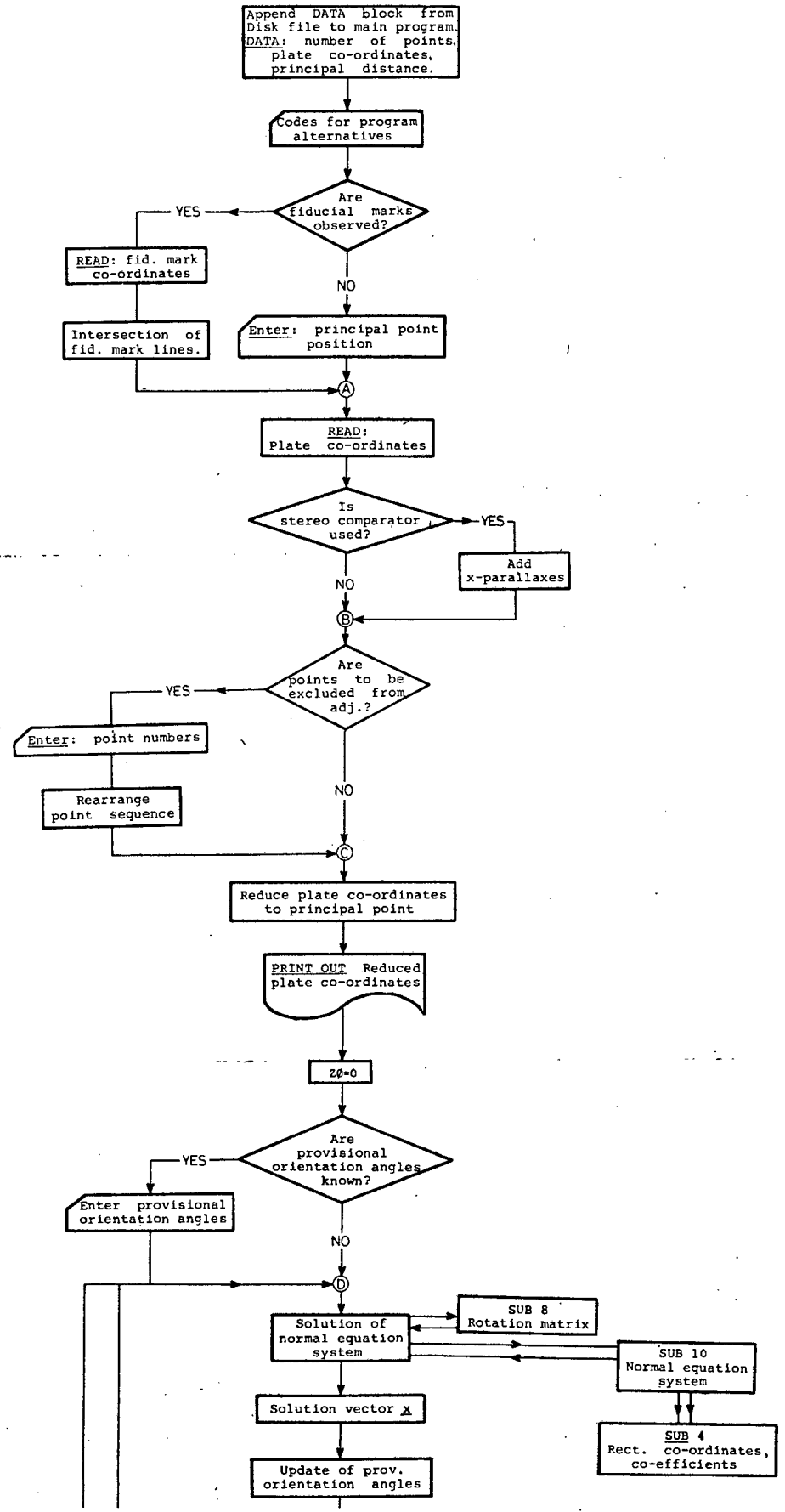

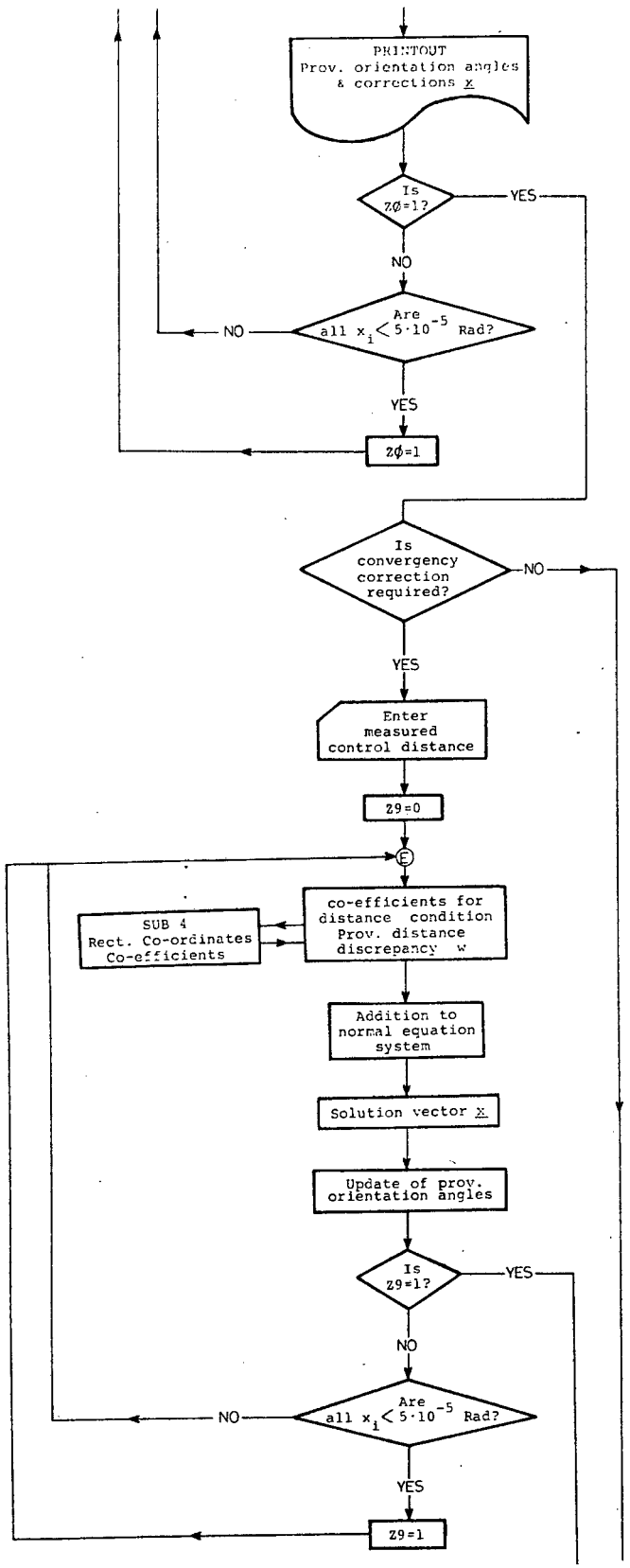
PRINTOUT
Prov. orientation angles
& corrections x
Is
ZØ=1?
YES
NO
Are
all $x_i < 5 \cdot 10^{-5}$ Rad?
NO
YES
ZØ=1
Is
convergency
correction
required?
NO
YES
Enter
measured
control distance
Z9=0
E
SUB 4
Rect. Co-ordinates
Co-efficients
co-efficients for
distance condition
Prov. distance
discrepancy w
Addition to
normal equation
system
Solution vector x
Update of prov.
orientation angles
Is
Z9=1?
YES
NO
Are
all $x_i < 5 \cdot 10^{-5}$ Rad?
NO
YES
Z9=1

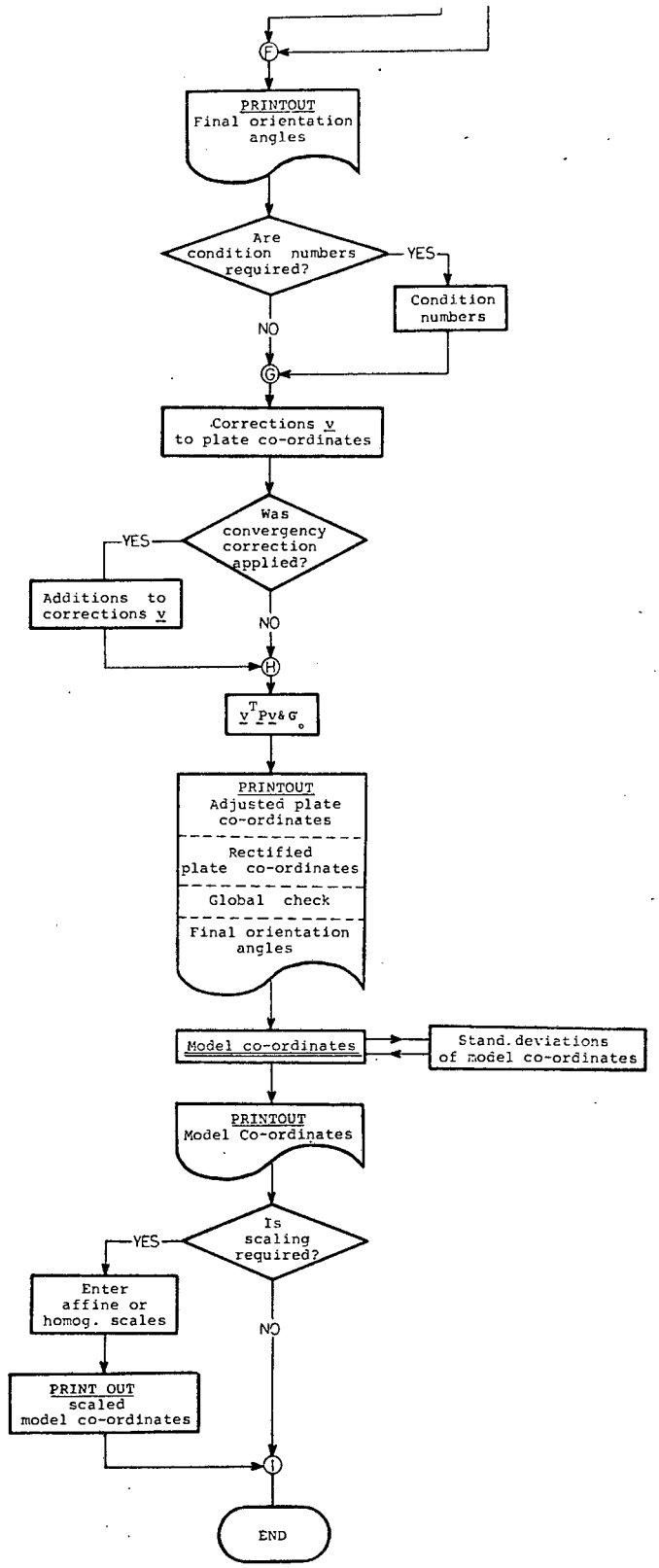
F
PRINTOUT
Final orientation angles
Are condition numbers required?
YES
Condition numbers
NO
G
Corrections v to plate co-ordinates
Was convergency correction applied?
YES
Additions to corrections v
NO
H
$v^T Pv \& \sigma_o$
PRINTOUT
Adjusted plate co-ordinates
Rectified plate co-ordinates
Global check
Final orientation angles
Model co-ordinates
Stand. deviations of model co-ordinates
PRINTOUT
Model Co-ordinates
Is scaling required?
YES
Enter affine or homog. scales
NO
PRINT OUT
scaled model co-ordinates
I
END

Printout of

Tektronix BASIC Program

for

Relative Orientation Adjustment with Distance Condition Equation and Matrix Assessment by means of Condition Numbers

Least Squares Adjustment of Relative Orientation

Part I

```
4 RUN 100
8 PRINT "BASE LENGTH "
9 INPUT B0
10 RUN 770
100 REM
110 INIT
120 REM.............RELATIVE ORIENTATION--ITERATION-CONDITION NO
130 REM .....................................DATA X,Y LEFT-PX,PY RIGHT
140 PRINT "DATA FROM DISK-FILE G_G_G_";
150 INPUT Z$
160 APPEND Z$;9000
170 I8=1
180 PAGE
190 REM ********************************DATA  HEADING - NO OF PNTS - BASE
200 READ C$,N,B0
210 DIM Z(N+1,4),K(7),N1(5,5),L(N+1),X(N,2),Y(N,2),U(5),W(5),S(3),Q(2,1)
220 DIM C(3),O(N),B(4),A(5),P(N),V1(4),Z8(N+1,2),N2(5,1)
230 DIM P1(N,4),D(5),D2(5),D3(5,5),E(4),A$(35),B$(7),D$(3)
240 PRINT "DO YOU REQUIRE A MATRIX ASSESSMENT "
250 INPUT D$
260 Q9=LEN(D$)-2
270 PRINT "IS A DISTANCE IN MODEL SPACE KNOWN "
280 INPUT D$
290 T7=LEN(D$)-2
300 PRINT "ARE THE RIGHT PLATE CO-ORD. PARRALAX READING "
310 INPUT D$
320 V9=LEN(D$)-2
330 PRINT "DO YOU REQUIRE DISTANCES FROM MODEL CO-ORD. "
340 INPUT D$
350 W0=LEN(D$)-2
360 PRINT " ARE FIDUCIAL MARKS OBSERVED  "
370 INPUT D$
380 V8=LEN(D$)-2
390 PRINT "DO YOU WANT TO ENTER PROVISIONAL ORIENTATION ANGLES "
400 INPUT D$
410 V7=LEN(D$)-2
420 REM FIDUCIALS IN DATA STATEMENT IN TOP-RIGHT-BOTTEM-LEFT  SEQUENCE
430 IF V8=0 THEN 470
440 GOSUB 1440
450 GO TO 510
460 REM *****************  CONSTANTS TO BE SUBTRACTED FROM X' Y' X'' Y''
470 E(1)=85.878
480 E(2)=60.16
490 E(3)=85.978
500 E(4)=60.173
510 PRINT @3: USING 520:"RELATIVE ORIENTATION AND MODEL CO-ORDINATES"
520 IMAGEP 35XFA/35X43("_")/ L
530 K=0
540 REM ************************************* READ PLATE CO-ORDINATES
550 GOSUB 1310
560 IF V9=1 THEN 580
570 Z8=0
580 L=0
590 H1=0
600 REM ************************************ EXCLUSION OF UNWANTED PNTS
610 PRINT "HOW MANY POINTS TO BE EXCLUDED"
620 INPUT H1
630 IF H1=0 THEN 680
640 FOR I=1 TO H1
650 PRINT "WHICH POINT TO BE EXCLUDED"
```

```
660 INPUT L(I)
670 NEXT I
680 GOSUB 1230
690 IF H1=0 THEN 910
700 FOR I1=1 TO H1
710 U6=L(I1)-I1+1
720 U1=X(U6,1)
730 U2=X(U6,2)
740 U3=Y(U6,1)
750 U4=Y(U6,2)
760 U5=0(U6)
770 FOR I=L(I1)+1-I1 TO N-I1
780 X(I,1)=X(I+1,1)
790 X(I,2)=X(I+1,2)
800 Y(I,1)=Y(I+1,1)
810 Y(I,2)=Y(I+1,2)
820 0(I)=I+I1
830 NEXT I
840 U7=N+1-I1
850 X(U7,1)=U1
860 X(U7,2)=U2
870 Y(U7,1)=U3
880 Y(U7,2)=U4
890 0(U7)=U5
900 NEXT I1
910 A$="KAPPA' PHI'   KAPPA''PHI''  OMEGA''"
920 U=0
930 PRINT @3: USING 940:I8,C$
940 IMAGE5X3D ,4X,FA/L
950 PRINT @3: USING 960:"BASE:",B0,"P.D. LEFT:",K(6),"P.D. RIGHT:",K(7)
960 IMAGE27XFA4D.3D,2(6X,FA4D.2D)/L/L
970 PRINT @3: USING 1000:"OBSERVED PLATE CO-ORDINATES"
980 PRINT @3: USING 990:"PT","X'","Y'","Z'","PX","PY","X''","Y''","Z''"
990 IMAGE 9XFA6XFA8XFA8XFA13XFA8XFA13XFA7XFA7XFA/L
1000 IMAGE44X,F A/L
1010 REM ************************************ PRINTOUT OF PLATE CO-ORD.
1020 FOR I=1 TO N-H1
1030 PRI @3: USI 1040:I,0(I),X(I,1),X(I,2),K(6),Z8(0(I),1),Z8(0(I),2)
1040 IMAGE7D 4D 3(6D.3D) 5X 2(6D.3D) 5X S
1050 PRINT @3: USING 1060:Y(I,1),Y(I,2),K(7)
1060 IMAGE3(6D.3D)
1070 NEXT I
1080 IF I=N+1 THEN 1170
1090 PRINT @3: USING 1100:"POINTS EXCLUDED FROM RELATIVE ORIENTATION"
1100 IMAGE/L,3XFA/L
1110 FOR I=N TO N-H1+1 STEP -1
1120 I0=2*N-H1+1-I
1130 PRINT @3: USING 1040:I0,0(I),X(I,1),X(I,2),K(6),Z8(I,1),Z8(I,2)
1140 PRINT @3: USING 1060:Y(I,1),Y(I,2),K(7)
1150 NEXT I
1170 P1=1
1180 P0=0
1190 Z4=0
1200 GO TO 1590
1220 REM ********************************************** SUB Z INTO X&Y
1230 FOR I=1 TO N
1240 X(I,1)=Z(I,1)
1250 X(I,2)=Z(I,2)
1260 Y(1,1)=Z(I,3)
1270 Y(I,2)=Z(I,4)
```

```
1280 NEXT I
1290 RETURN
1300 REM ********* SUB READ PLATE CO-ORD AND FD'S**CORRECTION FOR SHIFT
1310 FOR I=1 TO N+1
1320 READ Z(I,1),Z(I,2),Z8(I,1),Z8(I,2)
1330 Z(I,3)=Z(I,1)*V9-Z8(I,1)*SGN(V9-0.5)-E(3)
1340 Z(I,4)=Z(I,2)*V9-Z8(I,2)*SGN(V9-0.5)-E(4)
1350 IF I<N+1 THEN 1380
1360 K(6)=Z(N+1,1)
1370 K(7)=Z(N+1,2)
1380 Z(I,1)=Z(I,1)-E(1)
1390 Z(I,2)=Z(I,2)-E(2)
1400 IF I>N THEN 1420
1410 O(I)=I
1420 NEXT I
1430 RETURN
1440 REM ***************************** SUB FIDUCIAL MARK INTERSECTION
1450 FOR I=1 TO 4
1460 READ Z(I,1),Z(I,2),Z(I;3),Z(I,4)
1470 NEXT I
1480 FOR I=1 TO 2
1490 FOR J=1 TO 4
1500 Z(5,J)=Z(2*I,J)-Z(2*I-1,J)
1510 NEXT J
1520 Q(1,1)=-Z(5,2)/Z(5,1)*Z(2*I-1,1)+Z(2*I-1,2)
1530 Q(2;1)=-Z(5,4)/Z(5,3)*Z(2*I-1,3)+Z(2*I-1,4)
1540 J=Z(5,2)/Z(5,1)-Z(5,4)/Z(5,3)
1550 E(2*I-1)=(Q(2,1)-Q(1,1))/J
1560 E(2*I)=(Z(5,2)/Z(5,1)*Q(2,1)-Z(5,4)/Z(5,3)*Q(1,1))/J
1570 NEXT I
1580 RETURN
1590 DELETE 110,1580
1595 OO=MEMORY
1600 APPEND "REL/RELATIVE2";100
1630 RUN 100
9000 REM
```

```
100 PRINT @3: USING 120:18,C$
110 K9=0
120 IMAGEF3(/L)5X3D ,4XFA2(/L)
130 M1=0
140 Z0=0
150 S1=0
160 U=0
170 FOR I=1 TO 5
180 K(I)=0
190 IF V7=0 THEN 240
200 B$=SEG(A$,7*I-6,7)
210 PRINT " PROV. ";B$," IN DEG."
220 INPUT K(I)
230 K(I)=K(I)/180*PI
240 NEXT I
250 Z1=-1
260 Z1=Z1+1
270 PRINT @3: USING 280:"   ITERATION",Z1
280 IMAGE/LFA60/L23X"KAPPA'    PHI'     KAPPA''    PHI''    OMEGA''"
290 PRINT @3: USING 300:"PROV. UNKNOWNS  ",K(1),K(2),K(3),K(4),K(5)
300 IMAGE3XFA5(50.4D)
310 GOSUB 3520
320 GOSUB 3760
330 N1=INV(N1)
340 U=N1 MPY N2
350 K4=DET
360 GOSUB 3920
370 IF Z0=1 THEN 440
380 REM ****************************************** ITERATION CRITERION
390 FOR I=1 TO 5
400 IF ABS(U(I))>5.0E-5 THEN 430
410 NEXT I
420 Z0=1
430 GO TO 260
440 IF T7=1 THEN 470
450 GOSUB 3440
460 GO TO 500
470 PRI @3: USI 3460:"INTERM. ROTATION ANGLES IN RADIANS","IN DEGREES"
480 PRINT @3: USING 3490:
490 PRI @3: USI 3500:K(1),K(2),K(3),K(4),K(5),W(1),W(2),W(3),W(4),W(5)
500 S0=0
510 IF T7=0 THEN 690
520 APPEND "REL/SUB/DISTCON";4000
530 Z9=0
540 GO TO 580
550 GOSUB 3520
560 PRINT @3: USING 300:"PROV. UNKNOWNS  ",K(1),K(2),K(3),K(4),K(5)
570 GOSUB 3760
580 GOSUB 4000
590 N1=INV(N1)
600 K4=DET
610 U=N1 MPY N2
620 GOSUB 3920
630 IF Z9=1 THEN 690
640 FOR I=1 TO 5
650 IF ABS(U(I))>5.0E-5 THEN 550
660 NEXT I
670 Z9=1
680 GO TO 550
690 IF Q9=0 THEN 780
```

```
700 DELETE 4001,5660
710 OO=MEMORY
720 APPEND "REL/SUB/MATASS";4000
730 GOSUB 3490
740 DELETE 4001,5660
750 OO=MEMORY
760 APPEND "REL/SUB/DISTCON1";4000
770 REM ************************************* ADJUSTED OBSERVATIONS
780 PRINT @3: USING 790:I8,C$,"ADJUSTED OBSERVATIONS"
790 IMAGEP2(L)5X3D ,4XFA (/L)33XFA/L
800 PRINT @3: USING 810:"XO","VX","X","YO","VY","Y","PX","PY"
810 IMAGE15XFA8XFA8XFA14XFA8XFA8XFA15XFA9XFA/L
820 R6=0
830 FOR I=1 TO N-H1
840 GOSUB 2210
850 V=-(A(1)*U(1)+A(2)*U(2)+A(3)*U(3)+A(4)*U(4)+A(5)*U(5)+L(I))
860 S1=S1+V↑2*P(I)
870 FOR J=1 TO 4
880 V1(J)=V*B(J)*P(I)/P1(I,J)
890 SO=SO+V1(J)↑2*P1(I,J)
900 REM
910 NEXT J
920 IF T7=0 THEN 950
930 IF I<>M5(1) AND I<>M5(2) THEN 950
940 GOSUB 5460
950 M1=X(I,1)
960 M2=X(I,2)
970 M3=Y(I,1)
980 M4=Y(I,2)
990 R6=R6+V1(1)+V1(2)+V1(3)+V1(4)
1000 X(I,1)=M1+V1(1)
1010 X(I,2)=M2+V1(2)
1020 Y(I,1)=M3+V1(3)
1030 Y(I,2)=M4+V1(4)
1040 R5=P1(I,2)
1050 PRI @3: USI 1060:O(I),M1,V1(1),X(I,1),M2,V1(2),X(I,2),P1(I,1),R5
1060 IMAGE8D.,6D.3D5D.4D6D.3D5X6D.3D5D.4D6D.3D"  L"X2(8D.2D)
1070 PRI @3: USI 1080:M3,V1(3),Y(I,1),M4,V1(4),Y(I,2),P1(I,3),P1(I,4)
1080 IMAGE9X6D.3D5D.4D6D.3D5X6D.3D5D.4D6D.3D"  R"X2(8D.2D)
1090 NEXT I
1100 REM ********************************************* RECTIFIED CO-ORD.
1110 PRINT @3: USING 1120:"RECTIFIED CO-ORDINATES"
1120 IMAGELL 32XFA/L
1130 PRINT @3: USING 1140:"X'","Y'","Z'","X''","Y''","Z''","CHECK"
1140 IMAGE15XFA8XFA8XFA13XFA7XFA7XFA7XFA/L
1150 IMAGE8D.  3(6D.3D)5X3(6D.3D)8D.3D
1160 FOR I=1 TO N
1170 GOSUB 2210
1180 XO=X2*Y3-X3*Y2
1190 PRINT @3,32: USING 1150:O(I),X1,X2,X3,Y1,Y2,Y3,XO
1200 IF I<>N-H1 THEN 1220
1210 PRINT @3:
1220 NEXT I
1230 MO=SQR(SO/(N-H1+T7-5))
1240 PRINT @3: USING 1250:S1,MO,SO
1250 IMAGE2(/L)3X"PVV:"5D.6D8X"MO:"5D.4D10X"CHECK PVV:"5D.6D
1260 FOR I=1 TO 5
1270 D(I)=MO*180/PI*SQR(N1(I,I))
1280 NEXT I
1290 GOSUB 3440
```

```
1300 PRINT @3: USING 1310:"M.S.E. OF UNKNOWNS IN DEGREES","KAPPA'      "
1310 IMAGE2(/L)67XFA/L67XFA"PHI'     KAPPA''    PHI''    OMEGA''"/62XS
1320 PRINT @3: USING 1330:D
1330 IMAGEX5(5D.4D)2(/L)
1340 REM ****************************************** MODEL CO-ORDINATES
1350 DELETE 1,1090
1360 FOR I7=1 TO N
1370 O(I7)=I7
1380 NEXT I7
1390 R5=0
1400 I9=999
1410 PRINT @3: USING 1420:I8,C$,"MODEL CO-ORDINATES","BASE",BO
1420 IMAGE 2(/L)5X3D ,4XFA2(/L)26XFA10XFA8D.4D/L
1430 PRINT @3: USING 1450:" X "," Y "," Z "," MX "," MY "," MZ "
1440 PRINT @3: USING 1450:"(M)","(M)","(M)","(MM)","(MM)","(MM)"
1450 IMAGE24X3(FA7X)4X3(FA4X)
1460 DELETE Z
1470 DIM Z(N+1,4)
1480 FOR I=1 TO N-H1
1490 GOSUB 2210
1500 GOSUB 2460
1510 PRINT @3: USING 1520:O(I),X6,Y6,Z6,G5(2)*1000,G5(3)*1000,G5(1)*1000
1520 IMAGE10X80.3(5D.4D)5X3(6D.1D)
1530 Z(I,1)=X6
1540 Z(I,2)=Y6
1550 Z(I,3)=Z6
1560 Z(I,4)=O(I)
1570 NEXT I
1580 DELETE Z8,A$,N1
1590 PRINT "ENTER 0 IF YOU DO NOT WANT TO CALCULATE ADDITIONAL POINTS "
1600 PRI "ENTER 1 IF YOU WANT TO CALCULATE INDIVID. ADDITIONAL POINTS "
1610 PRI "ENTER 2 IF YOU WANT TO CALC. ADDITIONAL POINTS FROM FILE DATA"
1620 INPUT D9
1630 DELETE G,G1,G4,G6,N1
1640 IF D9=0 THEN 1910
1650 PRINT "WHICH FILE"
1660 INPUT A$
1670 PRINT @3: USING 1680:A$,"X","Y","Z"
1680 IMAGEP2(/L)16XFA     (/L)24X3(FA9.X)
1690 IF D9<2 THEN 1710
1700 OPEN "A$";4,"R",F$
1710 FOR I=1 TO 200
1720 IF D9<2 THEN 1760
1730 READ #4:X(1,1),X(1,2),Y(1,1),Y(1,2)
1740 GO TO 1770
1750 PRINT "ENTER LEFT AND RIGHT PLATE CO-ORDINATS OF NEW POINT"
1760 INPUT X(1,1),X(1,2),Y(1,1),Y(1,2)
1770 X(I,1)=X(I,1)-E(1)
1780 X(I,2)=X(I,2)-E(2)
1790 Y(I,1)=Y(I,1)-E(3)
1800 Y(I,2)=Y(I,2)-E(4)
1810 K9=1
1820 GOSUB 2210
1830 GOSUB 2460
1840 G5(1)=(G2(1,2)+G3(1,2))/2
1850 G5(2)=(G2(1,3)+G3(1,3))/2
1860 G5(3)=(G2(1,4)+G3(1,4))/2
1870 PRINT @3: USING 1960:I,G5(1),G5(2),G5(3)
1880 IF X(1,1)=999 THEN 1900
1890 NEXT I
```

```
1900 CLOSE
1910 IF W0=0 THEN 2190
1920 PRINT @3: USING 1930:"DISTANCES AND DIRECTIONS FROM MODEL CO-ORD."
1930 IMAGE4(/L),21XFA/21X43("-")2(/L)
1940 PRI @3: USI 1950:"FROM-TO","DX","DY","DZ","HORIZ.","SPACE","HORIZ."
1950 IMAGE8XFA4XFA6XFA6XFA6XFA4XFA3XFA5
1960 PRINT @3: USING 1970:"VERT.","DISTANCE","ANGLE"
1970 IMAGE3XFA/47XFA11XFA
1980 READ 01,02,T6
1990 FOR I=1 TO N
2000 IF Z(I,4)=01 THEN 2020
2010 NEXT I
2020 03=I
2030 FOR I=1 TO N
2040 IF Z(I,4)=02 THEN 2060
2050 NEXT I
2060 04=I
2070 05=Z(04,1)-Z(03,1)
2080 06=Z(04,2)-Z(03,2)
2090 07=Z(04,3)-Z(03,3)
2100 08=SQR(05↑2+07↑2)
2110 09=SQR(08↑2+06↑2)
2120 SET DEGREES
2130 T4=180-SGN(07+1.0E-90)*90-ATN(05/(07+1.0E-90))
2140 T5=ATN(06/08)
2150 SET RADIANS
2160 PRINT @3: USING 2170:01,02,05,06,07,08,09,T4,T5
2170 IMAGE11D,"-",3D,3(4D.3D), X,2(5D.3D), X,2(4D.3D)
2180 IF T6=0 THEN 1980
2190 END
2200 REM *********  SUB RECTIFIED AND COEFFICIENTS
2210 X1=A1*X(I,1)+A2*X(I,2)+A3*K(6)
2220 X2=A4*X(I,1)+A5*X(I,2)+A6*K(6)
2230 X3=A7*X(I,1)+A8*X(I,2)+A9*K(6)
2240 Y1=B1*Y(I,1)+B2*Y(I,2)+B3*K(7)
2250 Y2=B4*Y(I,1)+B5*Y(I,2)+B6*K(7)
2260 Y3=B7*Y(I,1)+B8*Y(I,2)+B9*K(7)
2270 IF K9=0 THEN 2290
2280 RETURN
2290 L(I)=-(X3*Y2/Y3-X2)
2300 C0=Y2/Y3
2310 C1=X3/Y3
2320 B(1)=A4-C0*A7
2330 B(2)=A5-C0*A8
2340 B(3)=C0*C1*B7-C1*B4
2350 B(4)=C0*C1*B8-C1*B5
2360 REM ************************************************ QUASI WEIGHTS
2370 P(I)=B(1)↑2/P1(I,1)+B(2)↑2/P1(I,2)+B(3)↑2/P1(I,3)+B(4)↑2/P1(I,4)
2380 P(I)=1/P(I)
2390 A(1)=(A5-C0*A8)*X(I,1)-(A4-C0*A7)*X(I,2)
2400 A(2)=-X1*Y2/Y3
2410 A(3)=-C1*((B5-B8*C0)*Y(I,1)-(B4-B7*C0)*Y(I,2))
2420 A(4)=C1*(-S(3)+C0*C(3))*Y1
2430 A(5)=-X3*(1+(Y2/Y3)↑2)
2440 RETURN
2450 REM ********************************************* SUB MODEL CO-ORD.
2460 Z6=B0/(X1/X3-Y1/Y3)
2470 IF R5>0 THEN 2490
2480 GOSUB 2720
2490 X6=Z6*X1/X3
```

```
2500 X9=Z6*Y1/Y3+B0
2510 Y6=Z6*X2/X3
2520 Y9=Z6*Y2/Y3
2530 X6=(X6+X9)/2
2540 X9=(X9+Y9)/2
2550 IF R5=0 THEN 2710
2560 G2(1,1)=SQR(X1↑2+X2↑2+X3↑2)
2570 G3(1,1)=SQR(Y1↑2+Y2↑2+Y3↑2)
2580 G2(1,2)=X1/G2(1,1)
2590 G2(1,3)=X2/G2(1,1)
2600 G2(1,4)=X3/G2(1,1)
2610 G3(1,2)=Y1/G3(1,1)
2620 G3(1,3)=Y2/G3(1,1)
2630 G3(1,4)=Y3/G3(1,1)
2640 G2(1,5)=G2(1,2)*G3(1,2)+G2(1,3)*G3(1,3)+G2(1,4)*G3(1,4)
2650 G5(1)=-B0*(G2(1,5)*G3(1,2)-G2(1,2))/(1-G2(1,5)↑2)
2660 G5(2)=B0*(G2(1,5)*G2(1,2)-G3(1,2))/(1-G2(1,5)↑2)
2670 FOR I9=1 TO 3
2680 G2(1,I9+1)=G2(1,I9+1)*G5(1)
2690 G3(1,I9+1)=G3(1,I9+1)*G5(2)+B0*(I9=1)
2700 NEXT I9
2710 RETURN
2720 REM ************************************SUB M.S.E. OF MODEL CO-ORD.
2730 SET RADIANS
2740 G9=1
2750 DELETE L1
2760 DIM G(5,1),G2(1,5),G3(1,5),G4(1,1),G5(3),G6(5,1),L1(5,1),L2(1,5)
2770 DIM L3(1,5),L5(4),L0(1,4),L5(4),L6(1,1),L4(1,5),L7(1,1)
2780 G1=B0/(X1/X3-Y1/Y3)↑2
2790 G7=A2*X(I,1)-A1*X(I,2)
2800 G8=A8*X(I,1)-A7*X(I,2)
2810 G(1,1)=-G1/X3↑2*(G7*X3-G8*X1)
2820 G(2,1)=G1*(X1↑2+X3↑2)/X3↑2
2830 G(3,1)=G1/Y3↑2*((B2*Y(I,1)-B1*Y(I,2))*Y3-(B8*Y(I,1)-B7*Y(I,2))*Y1)
2840 G(4,1)=-COS(K(3))*SIN(K(4))*Y(I,1)+SIN(K(3))*SIN(K(4))*Y(I,2)
2850 G(4,1)=G(4,1)-COS(K(4))*K(7)
2860 G(4,1)=G1*(G(4,1)*Y3-COS(K(5))*Y1↑2)/Y3↑2
2870 G(5,1)=G1*Y1*Y2/Y3↑2
2880 L0(1,1)=-(A1*X3-A7*X1)/X3↑2*G1
2890 L0(1,2)=-(A2*X3-A8*X1)/X3↑2*G1
2900 L0(1,3)=(B1*Y3-B8*Y1)/Y3↑2*G1
2910 L0(1,4)=(B2*Y3-B8*Y1)/Y3↑2*G1
2920 FOR I5=1 TO 4
2930 L4(1,I5)=L0(1,I5)
2940 NEXT I5
2950 G6=G
2960 GOSUB 3200
2970 G9=G9+1
2980 G(1,1)=((G6(1,1)*X1+G7*Z6)*X3-Z6*X1*G8)/X3↑2
2990 G(2,1)=((G6(2,1)*X1-Z6*X3)*X3-Z6*X1↑2)/X3↑2
3000 G(3,1)=G6(3,1)*X1/X3
3010 G(4,1)=G6(4,1)*X1/X3
3020 G(5,1)=G6(5,1)*X1/X3
3030 L0(1,1)=((L4(1,1)*X1+Z6*A1)*X3-Z6*X1*A7)/X3↑2
3040 L0(1,2)=((L4(1,2)*X1+Z6*A2)*X3-Z6*X1*A8)/X3↑2
3050 L0(1,3)=L4(1,3)*X1/X3
3060 L0(1,3)=L4(1,4)*X1/X3
3070 GOSUB 3200
3080 G9=G9+1
3090 G(1,1)=((G6(1,1)*X2+Z6*(A5*X(I,1)-A4*X(I,2)))*X3-Z6*X2*G8)/X3↑2
```

```
3100 G(2,1)=(G6(2,1)*X3-Z6*X1)*X2/X3↑2
3110 G(3,1)=G6(3,1)*X2/X3
3120 G(4,1)=G6(4,1)*X2/X3
3130 G(5,1)=G6(5,1)*X2/X3
3140 L0(1,1)=((L4(1,1)*X2+Z6*A4)*X3-Z6*X2*A7)/X3↑2
3150 L0(1,2)=((L4(1,2)*X2+Z6*A5)*X3-Z6*X2*A8)/X3↑2
3160 L0(1,3)=L4(1,3)*X2/X3
3170 L0(1,4)=L4(1,4)*X2/X3
3180 GOSUB 3200
3190 RETURN
3200 REM ************************************************************ SUB QFF
3210 FOR I5=1 TO 5
3220 L1(I5,1)=A(I5)
3230 NEXT I5
3240 G2=TRN(G)
3250 L2=TRN(L1)
3260 L4=L2 MPY N1
3270 L7=L4 MPY L1
3280 L5=0
3290 FOR I5=1 TO 4
3300 L5(1)=L5(1)+L0(1,I5)↑2
3310 L5(2)=L5(2)+(B(I5)*L0(1,I5))↑2
3320 L5(3)=L5(3)+B(I5)*L0(1,I5)
3330 FOR J=1 TO 4
3340 L5(4)=L5(4)+L0(1,I5)*L0(1,J)*B(I5)*B(J)
3350 NEXT J
3360 NEXT I5
3370 L6=L4 MPY G
3380 G3=G2 MPY N1
3390 G4=G3 MPY G
3400 G5(G9)=-P(I)*L5(2)+G4(1,1)-2*P(I)*L6(1,1)*L5(3)+P(I)↑2*L5(4)
3410 G5(G9)=M0*SQR(G5(G9)+L5(1))
3420 IMAGE5(6D.2D)
3430 RETURN
3440 REM ************************************************************ SUB PRINT
3450 PRI @3: USI 3460:"FINAL ROTATION ANGLES IN RADIANS","IN DEGREES"
3460 IMAGE2(/L)3XFA32XFA/3X32("-")32X10("-")/
3470 PRINT @3: USING 3490:
3480 PRI @3: USI 3500:K(1),K(2),K(3),K(4),K(5),W(1),W(2),W(3),W(4),W(5)
3490 IMAGE2(5X"KAPPA'"5X"PHI'"5X"KAPPA''    PHI''    OMEGA''"10X)
3500 IMAGE2(X5(5D.4D)11X)/2(3X48"="11X)
3510 RETURN
3520 REM ************************************    ROTATION MATRIX
3530 A1=COS(K(1))*COS(K(2))
3540 A2=-SIN(K(1))*COS(K(2))
3550 A3=-SIN(K(2))
3560 A4=SIN(K(1))
3570 A5=COS(K(1))
3580 A6=0
3590 A7=COS(K(1))*SIN(K(2))
3600 A8=-SIN(K(1))*SIN(K(2))
3610 A9=COS(K(2))
3620 FOR L1=1 TO 3
3630 S(L1)=SIN(K(2+L1))
3640 C(L1)=COS(K(2+L1))
3650 NEXT L1
3660 B1=C(1)*C(2)
3670 B2=-S(1)*C(2)
3680 B3=-S(2)
3690 B4=C(1)*S(2)*S(3)+S(1)*C(3)
```

```
3700 B5=-S(1)*S(2)*S(3)+C(1)*C(3)
3710 B6=C(2)*S(3)
3720 B7=C(1)*S(2)*C(3)-S(1)*S(3)
3730 B8=-S(1)*S(2)*C(3)-C(1)*S(3)
3740 B9=C(2)*C(3)
3750 RETURN
3760 REM ************************************ NORMAL EQUATION & FREE TERM
3770 N1=0
3780 N2=0
3790 FOR I=1 TO N-H1
3800 GOSUB 2210
3810 FOR KO=1 TO 5
3820 FOR J=KO TO 5
3830 N1(KO,J)=N1(KO,J)+A(KO)*A(J)*P(I)
3840 N1(J,KO)=N1(KO,J)
3850 NEXT J
3860 NEXT KO
3870 FOR J=1 TO 5
3880 N2(J,1)=N2(J,1)-L(I)*A(J)*P(I)
3890 NEXT J
3900 NEXT I
3910 RETURN
3920 REM ****************************   UPDATING OF X FOR ITERATION
3930 FOR I=1 TO 5
3940 K(I)=K(I)+U(I)
3950 W(I)=K(I)*180/PI
3960 NEXT I
3970 PRINT @3: USING 3980:"COR. TO UNKNOWNS",U(1),U(2),U(3),U(4),U(5)
3980 IMAGE3X,16A,5(5D.4D),/,L
3990 RETURN
4000 REM
```

Subroutine

Distance Condition Equation

```
100 REM..... CONDITION EQUATION FOR A DISTANCE IN MODELSPACE
110 DIM G(5,5),M5(6),R1(4,3),R3(7),R4(6,2),R7(4,5),R8(3,5),R9(5,3)
120 DELETE Z
130 DIM N8(5,3),Z(13,7)
140 R7=0
150 IF Z4>0 THEN 180
160 PRINT "FROM POINT # ,TO POINT # , DISTANCE  ";
170 INPUT M5(1),M5(2),M5(3)
180 FOR J=1 TO 2
190 I=M5(J)
200 GOSUB 2200
210 I=2*J-1
220 R1(I,1)=X1
230 R1(I,2)=X2
240 R1(I,3)=X3
250 R1(I+1,1)=Y1
260 R1(I+1,2)=Y2
270 R1(I+1,3)=Y3
280 NEXT J
290 FOR J=1 TO 2
300 I=M5(J)
310 GOSUB 2200
320 I=2*J-1
330 R3(J)=R1(I,1)↑2+R1(I,2)↑2+R1(I,3)↑2
340 R3(J+3)=R1(I,1)/R1(I,3)-R1(2*J,1)/R1(2*J,3)
350 R3(J+5)=R1(I,3)
360 I=3*J
370 I0=M5(J)
380 R4(I-2,1)=A2*X(I0,1)-A1*X(I0,2)
390 R4(I-1,1)=A5*X(I0,1)-A4*X(I0,2)
400 R4(I,1)=A8*X(I0,1)-A7*X(I0,2)
410 R4(I-2,2)=B2*Y(I0,1)-B1*Y(I0,2)
420 R4(I-1,2)=B5*Y(I0,1)-B4*Y(I0,2)
430 R4(I,2)=B8*Y(I0,1)-B7*Y(I0,2)
440 FOR I=1 TO 4
450 R7(J,I)=B(I)
460 R8(J,I)=A(I)
470 NEXT I
480 R8(J,5)=A(5)
490 R7(J,5)=1/P(M5(J))
500 NEXT J
510 R3(3)=R1(1,1)*R1(3,1)+R1(1,2)*R1(3,2)+R1(1,3)*R1(3,3)
520 Z=0
530 FOR J=1 TO 2
540 I=3*J
550 I0=2*J-1
560 Z(1,J)=(R1(I0,1)*R4(I-2,1)+R1(I0,2)*R4(I-1,1)+R1(I0,3)*R4(I,1))*2
570 Z(1,J+3)=(R4(I-2,1)*R1(I0,3)-R4(I,1)*R1(I0,1))/R1(I0,3)↑2
580 Z(1,J+5)=R4(I,1)
590 Z(2,J+3)=-(1*(R1(I0,1)/R1(I0,3))↑2)
600 Z(2,J+5)=R1(I0,1)
610 Z(3,J+3)=-(R4(I-2,2)*R1(2*J,3)-R4(I,2)*R1(2*J,1))/R1(2*J,3)↑2
620 R5=M5(J)
630 Z(4,J+3)=COS(K(3))*SIN(K(4))*Y(R5,1)
640 Z(4,J+3)=Z(4,J+3)-SIN(K(3))*SIN(K(4))*Y(R5,2)+COS(K(4))*K(7)
650 Z(4,J+3)=(Z(4,J+3)*R1(2*J,3)+COS(K(5))*R1(2*J,1)↑2)/R1(2*J,3)↑2
660 Z(5,J+3)=-R1(2*J,1)*R1(2*J,2)/R1(2*J,3)↑2
670 Z(2+4*J,J)=2*(A1*R1(I0,1)+A4*R1(I0,2)+A7*R1(I0,3))
680 Z(2+4*J,J+3)=(A1*R1(I0,3)-A7*R1(I0,1))/R1(I0,3)↑2
690 Z(2+4*J,J+5)=A7
```

```
700 Z(3+4*J,J)=2*(A2*R1(IO,1)+A5*R1(IO,2)+A8*R1(IO,3))
710 Z(3+4*J,J+3)=(A2*R1(IO,3)-A8*R1(IO,1))/R1(IO,3)↑2
720 Z(3+4*J,J+5)=A8
730 Z(4+4*J,J+3)=-(B1*R1(2*J,3)-B7*R1(2*J,1))/R1(2*J,3)↑2
740 Z(5+4*J,J+3)=-(B2*R1(2*J,3)-B8*R1(2*J,1))/R1(2*J,3)↑2
750 NEXT J
760 FOR J=1 TO 6
770 Z(1,3)=Z(1,3)+R1(1+(J>3)*2,J-3*(J>3))*R4(J+3-6*(J>3),1)
780 NEXT J
790 FOR J=1 TO 2
800 Z(5+J,3)=Z(9+J,2)/2
810 Z(9+J,3)=Z(5+J,1)/2
820 NEXT J
830 REM..................... COEFFICIENTS OF X INTO R8 AND V INTO R7
840 U9=R3(2)/(R3(5)*R3(7))↑2+R3(1)/(R3(4)*R3(6))↑2
850 U9=SQR(U9-2*R3(3)/R3(4)/R3(5)/R3(6)/R3(7))
860 FOR I=1 TO 13
870 R5=Z(I,5)/R3(5)+Z(I,7)/R3(7)
880 R6=Z(I,4)/R3(4)+Z(I,6)/R3(6)
890 J1=(Z(I,2)-2*R3(2)*R5)/(R3(5)*R3(7))↑2
900 J1=J1+(Z(I,1)-2*R3(1)*R6)/(R3(4)*R3(6))↑2
910 J1=J1-2*(Z(I,3)-R3(3)*(R5+R6))/R3(4)/R3(5)/R3(6)/R3(7)
920 J1=J1*B0*1000/2/U9
930 IF I>5 THEN 960
940 R8(3,I)=J1
950 GO TO 1000
960 IF I>9 THEN 990
970 R7(3,I-5)=J1
980 GO TO 1000
990 R7(4,I-9)=J1
1000 NEXT I
1010 L(N-H1+1)=(B0*U9-M5(3))*1000
1020 IF Z4>0 THEN 1050
1030 PRINT @3: USING 1040:M5(1),M5(2),"MEASURED LENGTH :",M5(3)
1040 IMAGEPLL"CONDITION EQUATION FOR DISTANCE"3D"-"3D10XFA6D.3D/38"-"LL
1050 PRI @3: USI 1060:"X1' ","Y1' ","X2' ","Y2' ","X1''","Y1''","X2''"
1060 IMAGE(/L)4X7(FA4X)"Y2''"S
1070 PRI @3: USI 1080:"KAPPA'","PHI'","KAPPA''","PHI''","OMEGA''","W"
1080 IMAGE6XFA4XFA4XFA2XFA5XFA4XFA(/L)
1090 REM
1100 FOR I=1 TO 8
1110 PRINT @3: USING 1120:R7(3+(I>4),I-4*(I>4))
1120 IMAGE4D.3DS
1130 NEXT I
1140 PRI @3: USI 1150:R8(3,1),R8(3,2),R8(3,3),R8(3,4),R8(3,5),L(N-H1+1)
1150 IMAGE3X5(6D.2D)6D.3D2(/L)
1160 Z1=Z1+1
1170 PRINT @3: USING 1180:"   ITERATION",Z1
1180 IMAGE/LFA6D/L23X"KAPPA'     PHI'     KAPPA''    PHI''    OMEGA'''
1190 REM..................... ADDITION TO ORIGINAL NORMAL EQUATION
1200 DIM R1(3,3)
1210 R5=0
1220 R6=0
1230 FOR I=1 TO 4
1240 R7(3,5)=R7(3,5)+R7(3,I)↑2/P1(M5(1),I)+R7(4,I)↑2/P1(M5(2),I)
1250 R5=R5+R7(1,I)*R7(3,I)/P1(M5(1),I)
1260 R6=R6+R7(2,I)*R7(4,I)/P1(M5(2),I)
1270 NEXT I
1280 A0=R7(3,5)-R5↑2/R7(1,5)-R6↑2/R7(2,5)
1290 R1(1,1)=(R5/R7(1,5))↑2
```

```
1300 R1(2,2)=(R6/R7(2,5))↑2
1310 R1(3,3)=1
1320 R1(1,2)=R5*R6/R7(1,5)/R7(2,5)
1330 R1(1,3)=-R5/R7(1,5)
1340 R1(2,3)=-R6/R7(2,5)
1350 R1(2,1)=R1(1,2)
1360 R1(3,1)=R1(1,3)
1370 R1(3,2)=R1(2,3)
1380 N8=TRN(R8)
1390 R9=N8 MPY R1
1400 G=R9 MPY R8
1410 FOR I=1 TO 5
1420 FOR J=1 TO 5
1430 N1(I,J)=N1(I,J)+G(I,J)/A0
1440 NEXT J
1450 NEXT I
1460 DIM G(3),N8(5)
1470 G(1)=L(M5(1))
1480 G(2)=L(M5(2))
1490 G(3)=L(N-H1+1)
1500 N8=R9 MPY G
1510 FOR I=1 TO 5
1520 N2(I,1)=N2(I,1)-N8(I)/A0
1530 NEXT I
1540 Z4=Z4+1
1550 RETURN
1560 REM..................................... SUB CORRECTIONS TO V'S
1570 G=0
1580 G=R8 MPY U
1590 G(1)=G(1)+L(M5(1))
1600 G(2)=G(2)+L(M5(2))
1610 G(3)=G(3)+L(N-H1+1)
1620 J4=1+(I=M5(2))
1630 FOR J=1 TO 4
1640 S0=S0-V1(J)↑2*P1(I,J)
1650 V=0
1660 FOR I1=1 TO 3
1670 V=V+(R7(J4,J)*R1(J4,I1)+R7(2+J4,J)*R1(3,I1))*G(I1)
1680 NEXT I1
1690 V1(J)=V1(J)-V/A0/P1(I,J)
1700 S0=S0+V1(J)↑2*P1(I,J)
1710 NEXT J
1720 RETURN
```

Subroutine

Evaluation of Various Condition Numbers

for Matrix of Normal Equation Coefficients

```
100 DIM D3(5,5),D4(8),D2(5),Z9(5,5)
110 K5=0
120 PRINT @3: USING 180:I8,C$,"ASSESSMENT OF MATRIX-CONDITION"
130 PRINT @3: USING 140:"NORMAL EQUATIONS"
140 IMAGE2(/L)3XFA/3X16("=")(/L)
150 K6=DET
160 PRINT @3: USING 170:Q
170 IMAGE5(5(10D.4D)/)
180 IMAGEP,3(/L),5X3D ,4X,FA,2(/L)3XFA/ 3X30("=")
190 PRINT @3: USING 200:"DETERMINANT",K4,"VARIANCE CO-VARIANCE MATRIX"
200 IMAGE3(/L)3XFA2E3(/L)3XFA/L3X27("=")/L
210 PRINT @3: USING 220:"KAPPA'","PHI'","KAPPA''","PHI''","OMEGA''"
220 IMAGE14XFA7XFA7XFA6XFA6XFA
230 FOR I=1 TO 5
240 B$=SEG(A$,7*(I-1)+1,7)
250 PRINT @3: USING 260:B$,N1(I,1),N1(I,2),N1(I,3),N1(I,4),N1(I,5)
260 IMAGE3XFAX5(2E2X)
270 NEXT I
280 PRI @3: USI 290:"(INVERSE* NORMAL) DEVIATION FROM IDENTITY MATRIX"
290 IMAGE3(/L)FA/L
300 D3=N1 MPY Q
310 GOSUB 1340
320 PRI @3: USI 290:"(NORMAL* INVERSE) DEVIATION FROM IDENTITY MATRIX"
330 D3=Q MPY N1
340 GOSUB 1340
350 GOSUB 370
360 GO TO 650
370 REM ************************************************SUB CONDITION NO
380 D3=Q
390 GOSUB 940
400 Z8=K8
410 PRINT @3: USING 1510:K4,K4/D4(6),K8,K4/(K8/SQR(5))↑5
420 PRINT @3: USING 1520:K4/D4(8),D6
430 D7=D6
440 GOSUB 1390
450 K1=D3(5,5)
460 D3=N1
470 GOSUB 940
480 PRINT @3: USING 490:
490 IMAGE2(/L)"INVERS"2(/L)
500 Z0=K8
510 PRINT @3: USING 1510:1/K4,1/K4/D4(6),K8,1/K4/(K8/SQR(5))↑5
520 PRINT @3: USING 1520:1/K4/D4(8),D6
530 D8=D6
540 GOSUB 1390
550 K2=D3(5,5)
560 K3=K1*K2
570 PRI @3: USI 580:"HIGHEST VALUE IN N-MATRIX",K1,K2,"  CONDITION",K3
580 IMAGELL3XFA13D.3D/17X"IN Q-MATRIX"13D.3D7XFAX"NUMBER"9D.4D
590 D9=D7*D8
600 PRINT @3: USING 610:"MAXIMUM EIGENVALUE OF N-MATRIX",D7,D8,D9,1/D9
610 IMAGE2(/L)3XFA8D.3D/25X"Q-MATRIX"8D.3D9X"CONDITION NUMBER"2(9D.4D)
620 PRINT @3: USING 630:Z8*Z0/5
630 IMAGE2(/L)38X"TURING'S FIRST  CONDITION NUMBER"9 D.3D
640 RETURN
650 PRINT @3: USING 660:"NORMALIZED VARIANCE CO-VARIANCE MATRIX"
660 IMAGEP2(/L)3XFA2(/L)
670 GO TO 690
680 PRINT @3: USING 660:"NORMALIZED NORMAL EQUATION MATRIX"
690 PRINT @3: USING 700:"KAPPA'","PHI'","KAPPA''","PHI''","OMEGA''"
```

```
700 IMAGE15XFA5XFA5XFA4XFA4XFA
710 FOR I=1 TO 5
720 FOR KO=1 TO 5
730 IF K5=2 THEN 760
740 Z9(I,KO)=N1(I,KO)/(SQR(N1(I,I))*SQR(N1(KO,KO)))
750 GO TO 770
760 Z9(I,KO)=F(I,KO)/(SQR(F(I,I))*SQR(F(KO,KO)))
770 NEXT KO
780 NEXT I
790 FOR I=1 TO 5
800 B$=SEG(A$,7*(I-1)+1,7)
810 PRINT @3: USING 820:B$,Z9(I,1),Z9(I,2),Z9(I,3),Z9(I,4),Z9(I,5)
820 IMAGE3XFA 5(60.30)
830 NEXT I
840 Q=INV(Z9)
850 K4=DET
860 GOSUB 380
870 IF K5=2 THEN 910
880 K5=2
890 GO TO 680
900 PRINT Q
910 Q=Q1
920 DELETE Q1,D4,D2,D3,K5,K8,K6,D,D6,D7,D1,K1,K2,K3
930 END
940 REM ************************************************* MAX EIGENVALUE
950 DIM D(5)
960 FOR I=1 TO 5
970 D(I)=I
980 NEXT I
990 D1=0
1000 D2=D3 MPY D
1010 D4(1)=0
1020 D5=0
1030 FOR I=1 TO 5
1040 D4(1)=D4(1)+D(I)*D(I)
1050 D5=D5+D(I)*D2(I)
1060 NEXT I
1070 D6=D5/D4(1)
1080 D=D2
1090 IF ABS(D4(1))<1.0E+50 AND ABS(D4(1))>1.0E-50 THEN 1140
1100 K8=SQR(D(1)↑2+D(2)↑2+D(3)↑2+D(4)↑2+D(5)↑2)
1110 FOR I=1 TO 5
1120 D(I)=D(I)/K8
1130 NEXT I
1140 IF ABS(D6-D1)<=ABS(D1*1.0E-4) THEN 1180
1150 D1=D6
1160 GO TO 1000
1170 GOSUB 1540
1180 D4=0
1190 D4(8)=1
1200 FOR I=1 TO 5
1210 FOR J=1 TO 5
1220 D4(I)=D4(I)+D3(I,J)↑2
1230 NEXT J
1240 D4(8)=D4(8)*D3(I,I)
1250 NEXT I
1260 D4(6)=1
1270 FOR I=1 TO 5
1280 D4(6)=D4(6)*SQR(D4(I))
1290 D4(7)=D4(7)+D4(I)
```

```
1300 NEXT I
1310 K8=SQR(D4(7))
1320 RETURN
1330 REM ********************************************* MAX DIFF. IN INVERS
1340 FOR I=1 TO 5
1350 D3(I,I)=D3(I,I)-1
1360 NEXT I
1370 PRINT @3: USING 1380:D3
1380 IMAGE5(5(2E2X)/)
1390 D3=ABS(D3)
1400 FOR J=1 TO 5
1410 FOR I=1 TO 4
1420 D3(J,I+1)=D3(J,I) MAX D3(J,I+1)
1430 NEXT I
1440 NEXT J
1450 FOR J=1 TO 4
1460 D3(J+1,I)=D3(J,5) MAX D3(J+1,5)
1470 NEXT J
1480 PRINT @3: USING 1490:D3(5,5)
1490 IMAGE/L"MAX VALUE IN MATRIX :"4X2E2(/L)
1500 RETURN
1510 IMAGE 2(/L)"DET",12X4E/"HADAM."9X4E/"EUC.NORM"7X4E/"EUC.COND."6X4E
1520 IMAGE"FRIEDRICH"6X4E/"MAX EIGENVAL."2X4E
1530 LIST
1540 Z9=-1
1550 D3=Z9*D3
1560 FOR I=1 TO 5
1570 D3(I,I)=D3(I,I)+D6
1580 NEXT I
1590 D3=INV(D3)
1600 K8=DET
1610 PRINT K8
1620 RETURN
```